Spring 2008

Geological sequestration of carbon dioxide by hydrous carbonate formation in steelmaking slag

C. Hank Rawlins

GEOLOGICAL SEQUESTRATION OF CARBON DIOXIDE BY HYDROUS CARBONATE FORMATION IN STEELMAKING SLAG

by

CHARLES HENRY RAWLINS

A DISSERTATION

Presented to the Faculty of the Graduate School of the

MISSOURI UNIVERSITY OF SCIENCE AND TECHNOLOGY

In Partial Fulfillment of the Requirements for the Degree

DOCTOR OF PHILOSOPHY IN METALLURGICAL ENGINEERING

2008

Approved by

Kent D. Peaslee, Advisor
Simon N. Lekakh
Von L. Richards
Jeffrey D. Smith
David J. Wronkiewicz

PUBLICATION DISSERTATION OPTION

This dissertation consists of six articles submitted for publication as follows. Each article is prepared according to the respective style of the publication. Pages 64-86 have been published in the Proceedings of AISTech 2006, Volume II. Pages 87-112 have been published in Metallurgical and Materials Transactions B. Pages 113-136 have been accepted for publication in Metallurgical and Materials Transactions B. Pages 137-166 are intended for submission in Hydrometallurgy. Pages 167-182 have been published in the Proceedings of the 2008 SME Annual Meeting and Exhibit. Pages 183-206 have been accepted for publication in AIST Transactions. The introduction, experimental work and analysis, and appendices sections are completed in dissertation format.

ABSTRACT

The formation of carbonate solids from the alkaline earth oxide phases in steelmaking slag was investigated in dry and aqueous conditions as a vehicle for carbon dioxide sequestration. The goal of this research was to determine the process conditions that would increase the kinetics of the carbonate formation process under hydrous conditions, enabling direct removal of carbon dioxide from steelmaking offgas.

The rate controlling mechanisms of leaching and carbonation in industrial slags exposed to carbon dioxide were investigated using a thermogravimetric reactor, batch aqueous reactor, and a two-stage aqueous reactor. In addition, detailed chemical and physical slag properties at the macro- and micro-scale levels were measured using XRF, XRD, SEM/EDS, TGA, and grindability methods.

The carbonate formation rate is primarily governed by particle size. Slag grinding will increase the reaction surface area, and is itself carbon dioxide sequestration net positive. The grinding cost can be recouped by recovering liberated steel particles. The critical (economic) grind size for BOF and EAF slag is 100-150 μm, and for LMF slag is 350-400 μm. Aqueous processing proceeds much faster than dry processing due to separate leaching and carbonation processes in the latter. In a batch reactor, the precipitated calcium carbonate product layer may inhibit further reaction by reducing the diffusion rate of the reacting species. A continuous (two-stage) system allows separate leaching and carbonation reactions to take place thus overcoming product layer blinding, however, the water requirement is greatly increased.

Leaching occurs faster than carbonation, and both processes are described accurately by the shrinking core model after correction for particle surface area. A minimum pH of 8.5 is critical to realize fast carbonation rates, while carbonic anhydrase enzyme will catalyze the reaction at a pH>10.33. The best results achieved in this project show 47% of the theoretical amount of carbonation can be achieved at 24 hours in a reactor using 100 μm slag particles. This amount is equal to 0.5% and 2.4% of the carbon dioxide emitted by integrated and mini-mills, respectively.

ACKNOWLEDGMENTS

This material is based upon work sponsored by the U.S. Department of Energy, in cooperation with the American Iron and Steel Institute (AISI) and its participating companies under Agreement DE-FC36-97ID13554. Any opinions, finding, and conclusions or recommendations expressed in the material are those of the authors and do not necessarily reflect the views of the Department of Energy. Financial support was also provided by the Missouri University of Science and Technology in the form of a GAANN Fellowship.

Support from the project corporate sponsors – ArcelorMittal, Dofasco, Gallatin Steel, Hylsa, Ipsco, Nucor, Praxair, Timken, and US Steel – in the form of guidance, data, samples, and analysis is greatly appreciated.

I am most thankful for the devoted support of my lovely bride, Kristi, through her words of encouragement, prayers, and maintaining our home-life focused on the Lord. My two sons Connor and Nathanael are a constant source of joy and I am thankful for all their distractions.

I would like to thank my advisory committee for their assistance with this work. Kent Peaslee and Von Richards have kept me on track daily and Jeff Smith and David Wronkiewicz have provided guidance at just the right times. Simon Lekakh has been a tireless laborer in this project and his assistance has been invaluable. From all of you I have watched and learned; and, I hope this training will make me a better researcher and teacher.

Ryan Spoering and Josh Noll deserve special recognition for turning my PowerPoint ideas into physical reality, and helping me remember the fun side of work.

TABLE OF CONTENTS

LIST OF ILLUSTRATIONS

PAPER 5

PAPER 6

LIST OF TABLES

SECTION

1. INTRODUCTION

1.1. PROJECT PURPOSE AND METHODOLOGY

The objective of this project is to develop and demonstrate a process for sequestering CO_2 generated from steel production by forming carbonates with the alkaline earth components in slag, generating a higher value slag co-product. The net project result is the design of reactor operating parameters that can be used to treat steelmaking offgas rich in CO_2 with raw or minimally processed slag. To achieve this result, the core research focus is to improve the process kinetics of the hydrous carbonate formation reaction, enabling direct removal of CO_2 from steelmaking exhaust. The net plant CO_2 emissions will be reduced by the amount sequestered in the carbonate formation, and the resulting slag product increases in value due to immediate stabilization allowing direct use in a wider range of construction or other applications.

A comprehensive literature and intellectual property review was completed as part of American Iron and Steel Institute (AISI) project contract TRP9955 and published in January 2006 as completion of Work Plan Task 3.0 of this contract. Section 1.0 of this dissertation serves as an abridgement of the full literature review and covers published information pertaining to slag production and characterization, carbonate mineral sequestration, and CO_2 capture in slag directly related to the dissertation topic. The literature review was used to define the thermodynamic and kinetic test boundary parameters, compare thermodynamic, kinetic, and characterization results, and generate ideas for the CO_2/slag reactor design.

1.2. SLAG PRODUCTION, HANDLING, AND USES

1.2.1. Slag Production. Slag is a co-product from iron and steel making. The American Society for Testing and Materials (ASTM) defines steelmaking slag in their publication D5106-03, as “the nonmetallic product, consisting essentially of calcium silicates and ferrites combined with fused and mineralogically combined oxides of iron,

aluminum, manganese, calcium, and magnesium, that is developed simultaneously with steel in basic oxygen, electric arc, or open hearth furnaces".[1]

Slag is produced during each discrete state of iron and steel making, and the corresponding slag produced has its own chemical and physical character. For example, the slag from blast furnace ironmaking is high in silica and lime, while low in iron oxide content. However, slag from steelmaking has a higher lime and iron oxide content. Slag produced during iron or steel refining operations (i.e., hot metal desulphurization and dephosphorization or steelmaking ladle metallurgy) has high phosphorus, sulfur, and impurity contents removed from the melt. Generally, each type of slag is differentiated for treatment and end use due to its chemical and physical nature. This project will focus on steelmaking slag produced from basic oxygen furnace (BOF), electric arc furnace (EAF), and ladle metallurgy furnace (LMF) operations. While open-hearth slag piles are being actively processed, this type of steelmaking is not producing significant amounts of new slag to include in this study. In this dissertation, the term "slag" will refer to that produced from BOF, EAF, or LMF operations only.

Slag production can be stated per heat or per year. The National Slag Association estimates that per metric ton of steel produced, BOF operations generate 75-150 kilograms of slag (150-300 lbs/st), while EAF operations generate less at 65-80 kilograms (130-160 lbs/st).[2] This corresponds to the net 10-15% of crude steel output that van Oss[3] uses in his estimates, and 100-200 kg/t (200-400 lbs/st) per Ionescu et al[4]. In comparison, van Oss[3] estimates the production of blast furnace slag at 25-120% of the hot metal produced per ton, depending on the overall ore grade.

Annual slag production tonnage and value is tracked by the U.S. Geological Service in their minerals commodity and yearbook reports.[5] Production tonnage in the U.S. has grown about 3.2% per year during the 1993-2003 period, with the value ($/t) growing about 5.5% during that time. The estimated production tonnage for 2004 is eight million tonnes. Most of this growth occurred from 2000-2003, during which the tonnage and value grew 69.2% and 75.0%, respectively. This greatly outpaced the rate of construction sand and gravel, which grew at 3.6% in tonnage and 11.1% in value during the 2000-2003 time period.[6] Actual per ton price ranges from $0.50 where natural aggregates are abundant, to $11.00 where construction demand is high with little or no

local natural aggregate. In 2002, the U.S. Geological Service began tracking U.S. output compared to world output. U.S. output ranks at approximately 10% of the world production, and is directly correlated to steel production.

1.2.2. Slag Handling. Slag handling is not well documented, mostly because it is not a process requiring a high degree of technology. After cooling to ambient temperature, slag is processed similar to bulk aggregate (sizing, separation, and transport). Other than storage requirements to achieve stabilization, limited literature exists detailing the physical handling of slag from the furnace to end-use. Steel producers have not documented the process in detail, as the most common business approach is to subcontract slag handling and processing to a specialist handling company.

Physical handling of slag is carried out similar to gravel aggregate. One slag processor (MultiServ^{TM}) lists the handling steps on their website.[7] In their business model the contractor takes possession of the slag as it is tapped from the furnace (under furnace removal) into transport pots. The contractor transports the slag to a pour pit or pad where it is dumped and allowed to cool naturally or by spray quenching. The cooled slag is dug out of the pit with a front loader and brought to the processing station.

Slag processing typically consists of crushing, screening, and magnetic separation.[7,8] Magnetic separation may be followed by screening. The oversized material may be crushed and sent back through the process again. Magnetic recovered material is sold back to the steel mill for furnace feed. van Oss[3] estimates that up to 50% of the slag volume is recovered as magnetic (entrained metal) for return to the furnace. The non-magnetic material is graded by size, and stockpiled for sale.

The end use destination will dictate storage time in the stockpile. This is because slag must go through an ageing period to reach stabilization. During aging, CaO/MgO phases in the slag react with water and carbon dioxide from the air to form hydroxides and carbonates. Formation of these compounds results in a volume change or “swelling” of the slag. Stabilization in a stockpile prevents end use *in-situ* swelling or leaching.

Slag swelling is a concern when the slag is used as construction aggregate. Crawford and Burns document the case of an office building on the Canadian side of the international bridge at Sault Ste. Marie, Michigan that experienced wall buckling and floor heave due to swelling of steel slag foundation fill.[9] This was open hearth slag that

generated 9% vertical lift on the building floor slab upon *in-situ* swelling. To prevent *in-situ* swelling, many state governments now require steelmaking slag to be aged before use. For example, the Missouri Department of Transportation requires slag used in asphaltic concrete to be aged for at least three months after crushing and screening[10], while the Pennsylvania Department of Transportation requires slag to be tested for expansion after six months stockpile curing.[11]

An additional problem that may occur with the use of raw slag is leaching of alkaline earth metals materials into the surface water. While testing on slag shows the leachate reporting to the surface water is non-hazardous[12], it may be perceived as a problem by the public. For example, slag used in the Cleveland airport runway produced a "milky white, sulfuric runoff".[13] While analysis showed that free lime leaching into the surface water precipitated calcium carbonate (milky white), which is stable and non-hazardous, the perception led to a project delay and negative publicity for the use of slag in construction.

1.2.3. Uses for Slag. The National Slag Association (NSA) employs promotional and research efforts to identify and develop innovative applications for steel slag's unique chemical and/or physical properties. The key uses the NSA have identified are as a source of iron and flux materials into blast furnace operations, high quality mineral aggregate, Portland cement, unconfined construction applications, soil conditioning, and environmental pH neutralization of abandoned mines and contaminated sites.[2,14] In 2003, the U.S. Geological survey listed the breakdown of use which supports these same categories.[3] High quality mineral aggregate (asphaltic concrete, road bases, and surfaces) account for more than 63% of the steel slag sold. The next largest use is unconfined construction (fill), which accounts for approximately 12-13%, followed by clinker feed at 5.4%. Other uses include railroad ballast, roofing, mineral wool, soil conditioning, recycling into iron making, and environmental pH neutralization of acid mine drainage.

1.3. PHYSICAL PROPERTIES OF SLAG

Steel slag's unique physical properties result from both its chemical composition and its production method. Comparison to standard construction aggregates show a

higher bulk density and specific gravity, higher hardness/toughness, coarser surface texture, and darker color.

1.3.1. Density and Hardness. The bulk density and specific gravity of steelmaking slag is higher than blast furnace slag and natural aggregates due to the increased content of iron and manganese. Specific gravity values for steel slag averages 3.1-3.7 for BOF and 3.2-3.8 for EAF, in comparison to 2.1-2.5 for air cooled blast furnace slag and 2.85 for dolomite.[15-18] The resultant bulk density values are 1770-2500 kg/m^3 (156.1 lbs/ft^3), in comparison to 1440-1600 kg/m^3 (89.9-99.9 lbs/ft^3) for dolomite.[11,16] Beaver Valley Slag, a slag processing subcontractor, lists as-sold bulk densities of steel slag from 1410-1930 kg/m^3 (88.0-120.5 lbs/ft^3) depending upon the degree of compaction.[19] Estimated Moh's hardness for steel slag is 6-7 compared to 3-4 for dolomite.[17] Crushing work index and grinding work index provide comparison values for crushing (breakage down to 1-2 cm) and grinding (breakage below 1-2 cm) operations, respectively. The crushing work index for dolomite is 12.8, which is the same for slag.[16] However, the grinding work index (ball mill) for dolomite is 13.9 versus 17.2 for slag.[16] Work index has the units of kWh/ton, and a comparison shows it takes about 24% more energy to grind steel slag compared to dolomite.

1.3.2. Mechanical Swelling. Mechanical swelling of steel slag results from hydration and carbonation of compounds present in the matrix. Quantification of slag expansion was undertaken by Tsuchiya et al. in 1980 by studying the expansion characteristics of slag during the water immersion test.[20] Their test method measured the rate and total volume of expansion of four LD slags. Employing a constant-temperature-water-immersion test with molds used for measuring California Bearing ratio, data was obtained on expansion with time. Expansion ratios of 2-13% were achieved at one year, with the ultimate expansion reaching 2.0-35.9% (time not given). A comparison between the final expansion ratio and the chemical composition suggests a proportional relationship with the amount of free lime (f-CaO). It is assumed that primarily hydrates were formed (as opposed to carbonates), since the slags were subjected to water immersion testing in a closed mold and not exposed to atmospheric carbon dioxide. No characterization was undertaken on the final aged slags. A second round of tests was conducted on the highest expanding slag where the slag was allowed to field age at zero,

one, three, and six months before undergoing the immersion test. Field aging had the effect of significantly reducing the ultimate expansion ratio of the slag. Qualitatively, their results show that the processes occurring in the field aging and water immersion are different. It is suggested that the free lime in field aging is subject to competing hydration and carbonation reactions from the H_2O and CO_2 in the air. Tsuchiya et al. found that most free lime in LD slag is present in unassimilated lumps, not distributed in solid solution.[21] The free lime lumps are several mm in diameter at a population of one per cm^3, and are observed as white to brown color in a blackish slag matrix.

In 1997 Kandhal and Hoffman published the results from a 1982 feasibility study of using cured steel slag fine aggregate in hot mix asphalt mixtures.[11] They noted that for raw slag, the un-slaked lime will hydrate, causing large volume expansions in a few weeks, while the magnesium oxide hydrates more slowly causing volume changes that may occur after several years. As a result, the Pennsylvania Testing Method (PTM) 130 was produced to better characterize expansion characteristics of steel slag. This method was used to generate ASTM D4792-00 Standard Test Method for Potential Expansion of Aggregates from Hydration Reactions.[22] Their research focused on the use of fine steel slag for hot-mix asphalt. Because the asphalt binder coats the aggregate particles and seals of the hydration route, this application serves as a better use for steel slag than unbound aggregate.

The testing time range for Tsuchiya et al. and Kandhal et al. was significantly different (>400 days vs. 14 days). However, a comparison of data from both sources at 14 days gives an average expansion on uncured slag of 0.7% for Tsuchiya and 1.9% for Kandhal. The difference lies in both the sample source (Tsuchiya was LD slag and Kandhal was unspecified), and that the Kandhal testing allowed the second half of the testing to have contact with air. The higher expansion rate may be a result of carbonation expansion taking place in addition to hydration expansion. Insufficient data was available from Tsuchiya to compare the cured slag expansion. The literature sources reviewed have stated several times that the primary constituents in slag that lead to swelling are free lime (CaO) and free magnesia (MgO). However, in the slag mechanical swelling studies reviewed[11,20], no characterization work was undertaken to compare the phases before and

after the swelling test. The volume increase contribution of free oxides alone versus other phases could not be determined.

1.4. CHEMICAL PROPERTIES OF SLAG

The final chemical composition of steel slag is a result of the fluxing agent used during steelmaking, the charge composition (hot metal and scrap), and refining agents. The primary fluxing agents are limestone (standard and dolomitic), lime (standard and dolomitic), dolomite, and fluorspar. Refining agents include aluminum, ferromanganese, ferrosilicon, and calcium-silicate, all used to remove oxygen, sulfur, phosphorus, and other impurities in the molten steel. Most of the fluxing agent and impurities will report to the slag phase for removal from the furnace.

1.4.1. Elemental Content of Slag and TCLP. A study in 2000 by Proctor et al. measured the elemental breakdown of slag samples from 58 active mills with BF, BOF, and/or EAF production.[12] This study represents approximately 47% of North American steel production. Data from this study for BOF and EAF production is shown in Table 1.1.

The primary elements indicated are Al, Ca, Fe, Mg, Mn, and Si, which are expected from standard steelmaking processes. Fluxing agent serves as the source for Ca and Mg, deoxidizer additions account for Al and Si, and oxidation/entrapment in the slag accounts for Fe and Mn. Using the average values for the primary elements in BOF slag, we find that their oxides (and complex combinations of oxides) account for 93.5% of the slag mass. The secondary elements of importance are C, Cr, P, and S, which are present as oxides, or carbonates, sulfates, and phosphates with the primary elements. These are the impurities removed by steelmaking, which report to the slag.

In addition to slag characterization, Proctor et al. sought to determine the potential for slag to leach chemicals into the soil or groundwater.[12] Water leachate tests using EPA method 131149 were performed for toxicity characterization leaching potential (TCLP) on each critical metal in the slag. The elements C, S, Mg, Ca, and P are considered major elements in the earth's crust, and essential human nutrients, and were excluded from the analysis. Analysis of the leachate testing showed a pH of 11.8 for both BOF and EAF slag. Comparison to the TCLP regulatory standards was made for As, Ba, Cd, Cr-VI, Cr

(total), Pb, Hg, Se, and Ag. None of these elements exceeded U.S. EPA standard limit, and most were at least one order of magnitude below. This indicates that in acidic-soil conditions the metals present in steel slag do not leach to any appreciable degree and steelmaking slag should not be considered hazardous waste.

Table 1.1. Elemental Chemical Composition of Slag by Furnace Type[12]

	Average Conc. (mg/kg)		Concentration Range (min – max, mg/kg)	
Metal	BOF	EAF	BOF	EAF
Al	23841	35009	100 – 108800	14100 - 71600
Sb	3.3	4	3 - 8.8	1.1 - 18
As	ND	1.9	ND	0.5 - 5.8
Ba	75	557	24 – 260	160 - 1800
Be	0.5	1.1	5 – 5	0.6 - 6.3
Cd	2.5	7.6	8 – 15	0.1 - 19
Ca	280135	250653	206900 – 367200	172300 - 324400
C	2600	2936	500 – 5800	100 - 12100
Cr (tot)	1271	3046	440 – 2000	320 - 6200
Cr (VI)	ND	1.2	ND	1 - 9.1
Co	3.8	4.8	2 – 12	2.5 - 11
Cu	30	178	12 – 120	62 - 540
Fe	184300	190211	115700 – 229000	32700 - 312000
Pb	50	27.5	2.4 – 330	4.5 - 220
Mg	55318	54460	28700 – 72000	23600 - 91500
Mn	32853	39400	12900 – 65700	18900 - 63800
Hg	0.1	0.04	0.1 - 0.1	0.1 - 0.7
Mo	11	30	0.8 – 73	1.6 - 81
Ni	4.9	30	2.1 – 10	5.2 - 310
P	3197	1781	470 – 5720	580 - 4290
Se	15	18	7.7 – 25	7.5 - 36
Si	59653	74524	30900 – 114100	39900 - 152700
Ag	9.1	8.4	2.3 – 100	1.3 - 100
S	1112	1891	440 – 5000	600 - 3310
Tl	7.2	11	11 – 11	11 - 11
Sn	6.5	10	2.7 – 26	3.2 - 34
V	992	513	430 – 1700	170 - 1500
Zn	46	165	8.5 – 150	31 - 690

Note: Oxygen values are not reported.

1.4.2. Compound Content of Slag. Steel slag rarely contains free elements and and at ambient conditions these will be present as compounds. Typically, these compounds are oxides, carbonates, or sulfates. Several sources provide a chemical compound breakdown of steel slag, as summarized in Table 1.2.

Table 1.2. Steel Slag Chemistry – Compound Basis (Wt. Percent)

	NSA[23]	Emery[15]	BVS[24]		Noureldin[17]	Sorrentino[25]
Type	Steel	BOF	Steel (high Si)	Steel (high Fe)	Steel	Steel
CaO	42.9	41.3	35.3	37.7	34	50.03
FeO/Fe_2O_3	25.0	20.0	9.6	30.8	23	22.67
SiO_2	14.9	15.6	31.4	17.9	16	15.22
MgO	8.1	6.9	6.2	5.8	8	6.59
MnO	5.0	8.9	1.9	4.8	10	2.38
Al_2O_3	5.0	2.2	8.9	2.7	3	1.68
P_2O_5	0.8	NR	NR	NR	NR	2.06
S*	0.08	- -	1.9	0.52	NR	NR
TiO_2	NR	0.5	0.46	0.39	1	0.7
Na_2O	NR	NR	0.03	0.05	NR	NR
K_2O	NR	NR	0.48	0.28	NR	NR
free CaO	NR	3.3	NR	NR	3	10.40

* Sulfur exists principally as calcium sulfate

A range of reported data exists, but the major compounds contain Ca, Mg, Fe, Si, Mn, and Al. These elements plus oxygen account for >97% of the slag mass. The data from the National Slag Association represents a U.S. average, while that from Emery, Beaver Valley Slag, and Noureldin represent an approximation for their geographic regions. The data from Tsuchiya lists analysis from an individual source. Geiseler[18] compared the amount of free CaO between BOF and EAF slag, estimating <10% and <3%, respectively, which corresponds with the data listed in Table 1.2. Little differentiation exists in literature to characterize BOF versus EAF, and for the purposes of this project unless specified the compositions stated are for steel slag without segregation by furnace type.

1.5. SLAG MINERALOGY

A variety of minerals has been observed in steelmaking slags. Table 1.3 contains a listing of the predominant minerals from published work. This table includes work from Corus RD&T (Ceramic Research Centre)[26], Emery[15], Monaco and Wu[27], Suito[28], Bradaskja[29], Luxán[30], and Sorrention.[25] The work by Corus utilized DTA and high temperature XRD to characterize the solidification sequence of steelmaking slag (type not specified). Emery's findings were based on literature review, while the work by Monaco and Wu was based on K-OBM slag. The LD converter slag studied by Suito et al. is listed in Table 1.3; however, their data on phosphorus enriched synthetic slags is not included. Bradaskja et al. studied minerals in EAF and VOD slags. Only the predominant minerals from EAF slag are listed. Luxán et al. carried out a study of EAF black slags in Spain, which are defined as a lime content <40% resulting from the cold loading of scrap.

Table 1.3. Predominant Minerals Found in Steel Slag, by Source

Mineral*	Monaco[27]	Corus[26]	Emery[15]	Suito[28]	Bradaskja[29]	Luxán[30]	Sorrentino[25]
Lime	X	X	X				X
Periclase	X	X	X		X		
Hatrurite	X	X	X				X
Larnite	X	X	X	X	X	X	X
Srebrodolskite	X	X	X	X			
Brownmillerite	X				X		
Wustite	X	X	X	X	X		X
Calcium Ferrite	X		X	X			X
Gehlenite						X	
Bredigite						X	
Magnetite						X	
Magnesioferrite						X	
Manganese Oxides						X	

*Note: Table 1.4 lists the chemical formula for each mineral.

Good agreement exists between researchers on the predominate minerals observed. These are alkaline earth metal oxides (lime and periclase), calcium-silicates (hatrurite and larnite), iron oxide (wustite and magnetite), and calcium-ferrites (calcium ferrite and dicalcium ferrite). Many other species are present, all of them solid solutions

or complex combinations of the oxides of calcium, magnesium, iron, aluminum, and silicon. This work focuses on the predominant minerals listed and not an exhaustive analysis of all species contained. Table 1.4 shows that most of these minerals are complex combinations of simple oxides. Based on their properties, the combinations containing iron and manganese oxides lead to the high density of the slag composite.

Table 1.4. Properties of Minerals Found in Steel Slag

Chemical Formula	Name	Density (g/cm^3)	Molar Volume (cm^3)
CaO	Lime	3.35[31]	16.76
MgO	Periclase	3.58[31]	11.25
$3CaO \cdot SiO_2$	Hatrurite	3.15[32]	72.4
β-$2CaO \cdot SiO_2$	Larnite	3.34	51.60[33]
$2CaO \cdot Fe_2O_3$	Srebrodolskite	4.04	67.18[33]
$4CaO \cdot Al_2O_3 \cdot Fe_2O_3$	Brownmillerite	3.73[32]	130.3
$Fe_{0.947}O$	Wustite	5.87[31]	12.25
$CaO \cdot Fe_2O_3$	Calcium Ferrite	5.08[31]	42.47
$2CaO \cdot Al_2O_3 \cdot SiO_2$	Gehlenite	3.04	90.24[33]
α'-$2CaO \cdot SiO_2$	Bredigite	3.40[34]	50.69
Fe_3O_4	Magnetite	5.20[31]	44.52
$MgO \cdot Fe_2O_3$	Magnesioferrite	4.49	44.57[33]
Mn_3O_4	Hausmannite	4.86[31]	17.30
MnO_2	Pryolusite	5.03[31]	49.89

While a wide range of minerals has been observed, the focus of this project is the minerals that will sequester carbon dioxide. Several minerals in steelmaking slag are meta-stable, meaning that under dry vacuum conditions they will stay in their present state. However, exposure of these minerals to ambient atmospheric conditions will lead to their eventual spontaneous reaction with water and carbon dioxide in air to form more stable compounds. Of the minerals listed in Tables 1.3 and 1.4, those containing calcium and magnesium are meta-stable in the raw slag, and will sequester carbon dioxide under ambient atmospheric conditions by dissolution and subsequent formation of more stable compounds. A thermodynamic analysis provides insight to the mechanism of these reactions.

1.6 THERMODYNAMICS OF SLAG STABILIZATION

Stabilization is the process that the slag minerals go through to transform from the meta-stable to most stable state. The basis of this study is the naturally occurring process that involves exposure of the raw slag to ambient atmospheric conditions (temperature, pressure, gas phase composition, and humidity). Under these conditions, specific minerals in the slag will react spontaneously (e.g., exothermic reaction). As the slag is exposed to both water and carbon dioxide, competition exists between hydroxide and carbonate formation of each compound. A thermodynamic review determines both the heat released in each reaction, and the final stable state of each compound (hydroxide or carbonate).

The key minerals identified for carbon dioxide sequestration are the free oxides and silicates of calcium and magnesium. These minerals form both hydroxides and carbonates, and their respective Gibbs free energy of formation at ambient conditions (G°) determines the final stable state. The subsequent analysis concerns spontaneous reactions to form hydroxides and carbonates at ambient temperature of 25°C (77°F). An increase in temperature pushes the system away from forming hydroxides/carbonates, and ultimately, a temperature will be reached in which the reaction goes backwards (decomposition). Hydroxide formation will be studied discretely and as a step in the formation of carbonate, while carbonate formation will be studied in both dry and wet processes.

1.6.1. Hydroxide Formation. The reaction of water with alkaline earth metal oxides and silicates in the slag leads to the formation of hydroxides. Water can be sequestered from air (ambient humidity) or liquid (submersion), and the concentration available partially governs the rate of the reaction. Reaction thermodynamics provides the state of the equilibrium products and any heat produced. The literature provides this information for CaO, MgO, $2CaO{\bullet}SiO_2$, and $3CaO{\bullet}SiO_2$ at standard conditions (298 K, 1 atm.).

Equations 1-4 show the formation of the respective hydroxide from each compound, while Table 1.5 provides the heat released ($\Delta H°_r$), Gibbs free energy ($\Delta G°_r$), and volume change (ΔV) of each respective reaction.

$$CaO + H_2O \rightarrow Ca(OH)_2 \quad (1)$$

$$MgO + H_2O \rightarrow Mg(OH)_2 \quad (2)$$

$$\tfrac{1}{2}[2CaO \cdot SiO_2] + 2.15H_2O \rightarrow \tfrac{1}{2}[1.7CaO \cdot SiO_2 \cdot 4H_2O] + 0.15Ca(OH)_2 \quad [35](3)$$

$$\tfrac{1}{3}[3CaO \cdot SiO_2] + 1.77H_2O \rightarrow \tfrac{1}{3}[1.7CaO \cdot SiO_2 \cdot 4H_2O] + 0.43Ca(OH)_2 \quad [35](4)$$

Table 1.5. Formation of Hydroxides from Steelmaking Slag Oxides and Silicates

Eq.	Product Formula	Product Name	$\Delta H°_r$ (kJ/mole)	$\Delta G°_r$ (kJ/mole)	Molar Vol. (cm^3) (each)	ΔVol. (%) (total)
1	$Ca(OH)_2$	Portlandite	-65.2	-57.9	33.08[31]	97%
2	$Mg(OH)_2$	Brucite	-37.3	-27.3	24.63[31]	119%
3	$0.5(1.7CaO{\cdot}SiO_2{\cdot}4H_2O)$ $0.15Ca(OH)_2$	C-S-H Portlandite	-19.1[35,36]	-7.9[33,35,36]	108[35] 42.98	127%
4	$0.3(1.7CaO{\cdot}SiO_2{\cdot}4H_2O)$ $0.43Ca(OH)_2$	C-S-H Portlandite	-40.7[35,36]	-28.2[35-37]	108[35] 42.98	113%

Free lime and magnesia readily react with water at ambient conditions to form calcium hydroxide (portlandite) and magnesium hydroxide (brucite), respectively, as shown in Equations 1 and 2. These reactions have been extensively studied, as they are widely used industrial minerals. Thermochemical data for their respective reactions can be obtained from FactSage, Ver. 5.4.[31] Their reaction with water is spontaneous and exothermic, with lime as the stronger reactant. Calcium hydroxide begins to decompose at 325°C (617°F), but has a quoted dehydration temperature of 518°C (964°F).[38,39] Magnesium hydroxide begins to decompose at a slightly lower temperature of 200°C

(392°F) as reported by Butt et al.[40] and has a quoted dehydration temperature of 285°C (545°F).[38] The reactions of these oxides with water lead to a substantial volume change (97% and 119%, respectively), which is why they are listed as key compounds in slag swelling studies.

The hydration of calcium silicates has been studied extensively in cement chemistry. Dicalcium silicate and tricalcium silicate together account for approximately 75% of ordinary Portland cement (OPC) by weight.[41] The hydration of dicalcium silicate and tricalcium silicate is documented by Tennis and Jennings[32], Bentz[35], and Fuji and Kondo.[36] Their work provides the reactions listed in Equation 3 and 4. Their hydration route is similar in that they both form calcium silicate hydrate and calcium hydroxide (in varying ratios). More than 30 crystalline phases of calcium silicate hydrate (C-S-H) are known. The preparation of C-S-H from dicalcium silicate and tricalcium silicate forms a C-S-H gel, which may vary in composition. The hydrate reaction path for these minerals used by Bentz and Tennis and Jennings has been adopted for cement modeling and studied to provide thermochemical data. A ratio of 1.7:1 CaO to SiO_2 is adopted by the researchers listed; however, the amount of water varies. Thermochemical data for heat of formation and molar volume are obtained from Bentz, and data for free energy of formation is obtained from Fujii and Kondo. Fujii and Kondo use 2.62 moles of water for C-S-H, as opposed to four moles by Bentz, which provides different listed heats of formation. However, normalizing both to the same hydration level (4 moles) gives the same heat of formation for C-S-H (-3288 kJ/mole for Fujii and -3283 kJ/mole for Bentz). The hydration of tricalcium silicate is the strongest listed, providing nearly twice as much heat as the slaking of lime. Both dicalcium silicate and tricalcium silicate will spontaneously react with water at ambient conditions. The change in volume by the hydration provides a significant volume increase (127% and 113%, respectively), indicating that they are a significant contributor to slag swelling.

1.6.2. Carbonate Formation. Formation of carbonates in slag can occur either dry (from non-hydrated minerals) or wet (from hydrated minerals). The ambient conditions (amount of water and length of time present) will determine if the slag forms carbonates from the dry state, or if hydroxides are formed as an intermediate step.

Carbonates of calcium and magnesium oxide will form directly if no water is present. Dry carbonation of lime occurs to form calcium carbonate as shown in Equation 5.

$$CaO + CO_2 \rightarrow CaCO_3 \quad (5)$$

This reaction is significantly more exothermic than the hydroxide formation, and with a lower free energy, this is a more stable compound. The dissociation (calcining) temperature of calcium carbonate depends on the partial pressure of CO_2 (pCO_2) in the surrounding atmosphere. It can range as low as 650°C (1202°F) at pCO_2 near zero, to 898°C (1648°F) for pCO_2 at unity.[42] Cement kilns normally operate in the 950-1100°C (1742-2012°F) range to increase the decomposition rate.

Dry carbonation of magnesia occurs to form magnesium carbonate (magnesite) as shown in Equation 6.

$$MgO + CO_2 \rightarrow MgCO_3 \quad (6)$$

As with calcium carbonate formation, the magnesium carbonate dry reaction is significantly more exothermic than the corresponding hydroxide formation. Butt et al., reports the dissociation temperature of magnesium carbonate at 320°C (608°F) and pCO_2 near zero to 410°C (770°F) and pCO_2 near unity.[40]

An alternate dry reaction may occur utilizing both CaO and MgO to reform dolomite ($CaMg(CO_3)_2$) as shown in Equation 7.

$$CaO + MgO + CO_2 \rightarrow CaMg(CO_3)_2 \quad (7)$$

Dolomite has a free energy of formation that is an average of CaO and MgO conversion. Dolomite formation requires the intimate association of CaO, MgO, and CO_3^{2-} molecules, and as slag is a heterogeneous mixture, the formation of dolomite may be more difficult to achieve than the respective single carbonate compounds (even with solid-state diffusion). Dolomite in its pure state has a dissociation temperature of

approximately 600°C (1112°F), which is expected, as it is a combination of calcium and magnesium carbonate.[43]

The dry formation of carbonates from dicalcium silicate and tricalcium silicate are given by Goto et al.[44] Respectively, they will form carbonates according to the reactions shown in Equations 8 and 9.

$$\tfrac{1}{2}[CaO \cdot SiO_2] + CO_2 \rightarrow CaCO_3 + \tfrac{1}{2} SiO_2 \quad (8)$$

$$\tfrac{1}{3}[3CaO \cdot SiO_2] + CO_2 \rightarrow CaCO_3 + \tfrac{1}{3} SiO_2 \quad (9)$$

Both reactions are exothermic and readily produce more stable compounds than their respective hydroxide formations at atmospheric ambient conditions. Table 1.6 summarizes the data from Equations 5-9 on dry carbonate formation.

Table 1.6. Summary Data from Dry Carbonation Calculations

Eq.	Product Formula	Product Name	$\Delta H°_r$ (kJ/mole)	$\Delta G°_r$ (kJ/mole)	Molar Vol. (cm^3) (each)	ΔVol. (%) (total)	CO_2 Seq. Pot. (kg/kg)
5	$CaCO_3$	Calcite Aragonite	-178.8 -178.8	-131.0 -129.9	36.89[31] 34.15[31]	120% 104%	0.78 0.78
6	$MgCO_3$	Magnesite	-116.7	-64.5	28.03[31]	149%	1.09
7	$CaMg(CO_3)_2$	Dolomite	-151.1	-100.8	64.36[31]	130%	0.91
8	$CaCO_3$ $0.5SiO_2$	Calcite Quartz	-116.2	-66.2	36.89 22.68[31]	87%	0.51
9	$CaCO_3$ $0.3SiO_2$	Calcite Quartz	-140.3	-90.1	36.89 22.68[31]	77%	0.58

In each of these reactions, the formation of carbonate compounds results in a significant volume increase compared to the oxidized states. The carbonates of CaO and MgO are larger in volume than their respective hydrates, indicating that hydration followed by carbonation will lead to continued swelling in the slag. The total molar volume increase represented by dry carbonation of the silicates, shows a significant volume change (77-87%), but the final molar volume is less than that of the hydrates.

This indicates that swelling will occur with the silicates upon hydration, but this will be followed by subsequent shrinkage upon carbonate formation.

While a thermodynamic analysis shows dry carbonation of the preceding compounds is possible, the reactions are dependent on the availability (partial pressure) of CO_2, which is low at atmospheric ambient conditions (pCO_2~33.4 Pa ($3.30x10^{-4}$ atm)). Research in Finland (Zevenhoven et al.[45]) is concentrating on dry mineral carbonation primarily with magnesium oxides and silicates. They concluded that a catalyst will be required (and possibly elevated temperature and pressure) to achieve reaction rates for dry carbonation in a reasonable time. The highest reaction rates occurred in the presence of humid (water saturated) gas. Hydrates should form more readily due to the higher availability of water in normal ambient air. The partial pressure of water vapor in air ranges from pH_2O=3141 Pa ($3.10x10^{-2}$ atm) for saturated air at standard conditions to pH_2O=0.1 MPa (1.0 atm) when rain falls on the slag. It is anticipated that hydrates will form more readily, due to availability of water then convert to the more stable carbonate compounds.

In Equations 5-9, oxides and silicates in the slag are combining with ambient CO_2 to form more stable carbonates. The CO_2 sequestration potential for each compound indicates the mass of CO_2 captured per mass of reactant (kg CO_2/kg reactant). The CO_2 sequestration potentials for each compound are listed in Table 1.6. The oxides have a higher sequestration potential than the silicates. The CO_2 sequestration potential is directly proportional to the volume increase associated with carbonation.

1.6.3. Hydrous Carbonate Formation. While dry carbonation can take place, the most likely scenario for the hydroxide and carbonation reactions to take place concurrently or in series, which would be the case for slag exposed to ambient air with water vapor and CO_2. Single step hydroxide and carbonate formation have been covered, so conversion of hydroxides to carbonates links these into series. Equations 10-14 show the hydroxide to carbonate formation for $Ca(OH)_2$, $Mg(OH)_2$, $Ca(OH)_2$+$Mg(OH)_2$, 2C-S-H, and 3C-S-H, respectively. Table 1.7 summarizes the resultant enthalpy, free energy, and volume change data from these reactions, respectively.

$$Ca(OH)_2 + CO_2 \rightarrow CaCO_3 + H_2O \quad (10)$$

$$Mg(OH)_2 + CO_2 \rightarrow MgCO_3 + H_2O \quad (11)$$

$$\tfrac{1}{2}Ca(OH)_2 + \tfrac{1}{2}Mg(OH)_2 + CO_2 \rightarrow \tfrac{1}{2}CaMg(CO_3)_2 + H_2O \quad (12)$$

$$\tfrac{1}{2}\left[1.7CaO \cdot SiO_2 \cdot 4H_2O\right] + 0.15Ca(OH)_2 + CO_2 \rightarrow CaCO_3 + \tfrac{1}{2}SiO_2 + 2.15H_2O \quad (13)$$

$$\tfrac{1}{3}\left[1.7CaO \cdot SiO_2 \cdot 4H_2O\right] + 0.43Ca(OH)_2 + CO_2 \rightarrow CaCO_3 + \tfrac{1}{3}SiO_2 + 1.77H_2O \quad (14)$$

Table 1.7. Sequential Carbonate Formation from Hydrates in Steel Slag Components

Eq	Product Formula	$\Delta H°_r$ (kJ/mole)	$\Delta G°_r$ (kJ/mole)	Molar Vol. (cm^3)	ΔVol. (%) (overall)	ΔVol. (%) (hydrate)	CO_2 Seq. Pot. (kg/kg)
10	$CaCO_3$	-112.7	-71.4	36.89	120%	12%	59%
11	$MgCO_3$	-79.3	-37.2	28.03	149%	14%	75%
12	$0.5CaMg(CO_3)_2$	-99.8	-58.2	64.36	130%	12%	66%
13	$CaCO_3$ $0.5SiO_2$	-94.3	-59.1	73.78 22.68	87%	-18%	35%
14	$CaCO_3$ $0.33SiO_2$	-100.7	-63.6	110.67 22.68	77%	-12%	41%

As shown by the free energy data in Table 1.7 for Equations 10-14, all hydroxide species will react to form carbonate at atmospheric ambient conditions. The heat released equals the heat of dry carbonation minus the heat of hydration. The carbonate compounds of these oxides and silicates are more stable than the hydroxides, and the hydroxides will convert to the more stable forms at equilibrium. Carbonate conversion from oxides produces a small volume increase to additional slag swelling. The conversion of the silicate hydrates to carbonates leads to a volume decrease. The competing increase and decrease of hydration and carbonation of the various components, will lead to cracking of

the slag during the stabilization period. The cracking will produce smaller slag particles (proportional to the amount of oxides and silicates available to react with water and carbon dioxide), and open new surfaces for reaction in the slag matrix, thus increasing the overall slag stabilization rate. This is the phenomena observed by Tsuchiya et al.[20] in their slag swelling study. The CO_2 sequestration potential is lower for the hydroxide compounds compared to dry carbonation due to the extra mass of water in each hydroxide.

1.7. CO_2 CAPTURE AND SEQUESTRATION

1.7.1. Implications of CO_2 Control in the Steel Industry. The driving factors for CO_2 sequestration are extremely complex and involve political, economic, and scientific factors. There is uncertainty or disagreement about almost every aspect of the anthropogenic greenhouse gas theory, and it is extremely unlikely that anyone in government, or indeed possibly in science, is able to command a comprehensive view of the whole situation.[46] Regardless of personal, corporate, or governmental views of the anthropogenic greenhouse gas theory, a binding agreement for the industrial countries was put forward at the world summit in Kyoto, Japan in 1997. This agreement, called the Kyoto Protocol, proposes that the industrial nations cut their collective emissions of specific gases (CO_2, CH_4, NO_x, SF_6, hydrofluorocarbons, and perfluorocarbons) by an average of 5.2% below the 1990 levels by 2012. The Kyoto Protocol is supported by 156 countries since it came into force in February 2005.

The industries working in the countries that have signed the Kyoto Protocol have the responsibility to work within the scope of their respective legislation in reducing emissions of the gases listed. The iron and steel industry is highly reliant on carbon based fuels both directly (coke for iron oxide reduction) and indirectly (EAF use of electricity from coal burning power plant). The emission of CO_2 has been targeted most heavily by the supporting countries, with the net result that the iron and steel industries will need to make changes in operation and methodology to meet this cutback. Long-term changes may require the development of carbon-free steelmaking, both in the production of steel and generation of the energy, but that is many years in the future. Short-term goals can be achieved by reducing the carbon intensity of iron and steel making. These include

injecting hydrogen rich fuel in the blast furnace (natural gas instead of coke), alternative ironmaking technologies (DRI, ITmk3™, COREX, etc.), maximizing scrap recovery and use in steelmaking, and optimizing energy use in all areas of ferrous processing. Medium-term goals for the iron and steel industry should include greater industrial symbiosis, such as limestone replacement by slag cement clinker, and the use of byproduct gas and heat for power generation and industrial heating.[46] Permanent sequestration of CO_2 from industrial sources is being investigated as a medium to long term option, and if developed properly may provide a commercially favorable route.

1.7.2. Geological Methods for Sequestration. Geological sequestration of carbon dioxide is actively being researched as a long-term disposal scenario. The two significant geological bodies available to capture CO_2 permanently from the atmosphere are the oceans and mineral deposits in the earth's crust.

Natural precipitation of projected CO_2 emissions in marine sediments in ocean bodies would result in an estimated sequestration of 70-80% of the carbon dioxide; however, the process may take several centuries to 1500 years to complete.[47,48] Injection of liquefied carbon dioxide into deep ocean zones to reduce the time required for natural equilibrium is an active research area. Alternatively, liquefied CO_2 can be injected into subterranean formations, as researched by the Pacific Northwest National Laboratory.[49] While these methods greatly speed up the reaction of carbon dioxide with seawater or geologic formations, they both require technologies for capture, liquefaction, transport, and injection. To date these methods have shown to be prohibitively expensive for common industrial use, mainly due to transport of the liquefied carbon dioxide to a proper disposal site.

Solid based CO_2 sequestration holds great potential for industrial operations, as a wide variety of minerals are available to form permanent carbonate sinks. The distribution of the mineral body in relation to the locality of the CO_2 generation source will be the primary cost hurdle. The design of a system that can accomplish a reaction of the mineral with gaseous CO_2 will simplify the unit process by eliminating gas based capture and liquefaction systems. Transport of the CO_2 to the mineral body or of the prepared mineral to the CO_2 source becomes the driving economic factor, providing the reaction rate is sufficiently fast.

Three classes of mineral carbonate disposal strategies have been proposed.[47] The first approach mimics the natural weathering process whereupon mineral alkalinity neutralizes carbonic acid species (e.g., $H_2CO_{3(aq)}$ and HCO_3^-). Natural carbonate weathering generates bicarbonate that goes into surface or ground water solutions, eventually reporting to the ocean as the final geological sink. Natural silicate weathering extracts alkalinity (e.g., Ca^{2+} or Mg^{2+}) into surface water, which in turn combines with bicarbonate (HCO_3^-) in the ocean to precipitating solid carbonates (e.g., $CaCO_3$ or $MgCO_3$). A strategy to accelerate the two steps of this process provides a permanent ocean-based disposal of bicarbonate salts. The second strategy is similar, but the carbonate or bicarbonate brines are injected into an underground reservoir, as opposed to ocean disposal. The third strategy involves the formation of solid carbonates for surface or underground disposal. The latter strategy is most similar to the current research involving slag-CO_2 sequestration.

1.7.3. Minerals for Solid Carbonate Sequestration. The most common minerals studied for solid carbonate sequestration are based on the alkali or alkaline earth metals. Respectively, the base ions are monovalent sodium and potassium, or divalent calcium and magnesium. Table 1.8 lists many of the potential minerals readily available for solid carbonate sequestration.

Since the desired disposal form of this study is a solid carbonate, the source of alkaline ions cannot be a carbonate (which produces CO_2 during dissolution), but will most likely be a silicate mineral rich in magnesium or calcium, thus the bicarbonate forming minerals listed in Lackner are precluded from Table 1.8. Significant sources of magnesium and calcium silicates are available on all continents, some of which are feasible for use in industrial systems.[47] Magnesium ions can be extracted from serpentine or olivine rock, and periodite deposits containing these minerals are widespread. Total estimates are several hundred thousand GT. Simple oxide minerals, such as lime, periclase, or their hydroxides are only locally available in natural mineral form and can only be used where these compounds are synthetically produced. Weathering of feldspars is a natural phenomenon that captures CO_2, but extraction of sodium and potassium from these minerals has not been widely studied.

Table 1.8. List of Potential Minerals for Solid Carbonate Sequestration (from Lackner[47])

Mineral	Chemical Formula	Resource Size (1000 Gt)	Chemical Preprocess	Disposal Form
Lime	CaO	Synthetic	None	$CaCO_3$
Brucite	$Mg(OH)_2$	Small/Synthetic	None	$MgCO_3$
Calcium hydroxide	$Ca(OH)_2$	Synthetic	None	$CaCO_3$
Periclase	MgO	Small	None	$MgCO_3$
Wollastonite	$CaSiO_3$	Small	None	$CaCO_3$
Peridotite	Olivine + Pyroxene		Extraction of MgO or $Mg(OH)_2$	$MgCO_3$
Serpentine	$Mg_3Si_2O_5(OH)_4$	100,000	Acid dissolution leading to MgO or $Mg(OH)_2$	$MgCO_3$
Olivine	$(Mg,Fe)_2SiO_4$	100,000	Acid dissolution leading to MgO or $Mg(OH)_2$	$MgCO_3$
Forsterite	Mg_2SiO_4	Pure deposits are very small	Acid dissolution leading to MgO or $Mg(OH)_2$	$MgCO_3$
Potassium feldspar	$KAlSi_3O_8$	Very large	Dissolution in water or brine	K_2CO_3
Sodium feldspar	$NaAlSi_3O_8$	Very large	Extraction of sodium alkalinity	Na_2CO_3

1.7.4. Solid Carbonate Capture Chemistry. Carbon sequestration on a geologic scale requires neutralization of carbonic acid. Divalent metal oxides or hydroxides (such as Mg^{2+} or Ca^{2+}) would react with carbonic acid as shown in Equations 15-18 as given by Lackner.[47]

$$MeO + H_2CO_3 \rightarrow MeCO_3 + H_2O \quad (15)$$

$$Me(OH)_2 + H_2CO_3 \rightarrow MeCO_3 + 2H_2O \quad (16)$$

$$MeO + 2H_2CO_3 \rightarrow Me(HCO_3)_2 + H_2O \quad (17)$$

$$Me(OH)_2 + 2H_2CO_3 \rightarrow Me(HCO_3)_2 + 2H_2O \quad (18)$$

While these equations show the thermodynamic possibility of carbonate capture with metal oxides and hydroxides, the availability of these minerals are very limited. A

more appropriate route would be direct carbonate formation from the silicates as shown in Equations 19-20 from Lackner.[47]

$$(MeO)(SiO_2)_m + H_2CO_3 \rightarrow MeCO_3 + H_2O + m(SiO_2) \quad (19)$$

$$(MeO)(SiO_2)_m + 2H_2CO_3 \rightarrow Me(HCO_3)_2 + H_2O + m(SiO_2) \quad (20)$$

The formation of a bicarbonate salt in solution allows for the use of carbonate minerals as shown in Equation 21.

$$MeCO_3 + H_2CO_3 \rightarrow Me(HCO_3)_2 \quad (21)$$

This reaction produces a bicarbonate salt requiring aqueous or oceanic disposal, which is counter to the goal of this research to bind CO_2 into a solid slag product. Lackner states that it is easier to transform carbonates into bicarbonates than it is to drive silicic acid out of its minerals, and that in forming bicarbonates from silicates, only half as much silicate is required compared to carbonate formation only.[47] The first statement is not supported thermodynamically as, for example, the formation of the carbonate from forsterite (Mg_2SiO_4) is exothermic with a ΔG of -230.2 kJ/mole, while bicarbonate formation from magnesium carbonate is endothermic at +221.2 kJ/mole. His observations also suggest that bicarbonates may represent a more convenient form of sequestration. The ocean is large enough to accept the bicarbonates formed, but the practical and environmental logistics of this route are not well defined. Solid carbonate formation, however, provides a specific and well-defined capture method not subject to the same geologic intrusion. The environmental impact from solid disposal is confined to the smallest possible region.

Mineral carbonate formation is a thermodynamically stable route for disposal of carbon dioxide that under most natural atmospheric conditions occurs very slowly. Carbon dioxide can be released through a reaction of these carbonate phases with a strong acid, such as sulfuric; however, under natural conditions even that produced from burning

sulfur rich coal is insufficient to free sequestered carbon dioxide. Atmospheric carbonic acid (CO_2 plus rainwater) reacts with carbonate rocks to release CO_2; however, because this is a weak acid the rates are relatively slow. Alternatively, carbon dioxide may be released through natural calcination, which may take place upon mineral heating through volcanic action. The amount of carbon dioxide released through this method on a global scale will be very limited. The thermodynamic stability of solid carbonates minimizes the need for long-term monitoring and continued maintenance of the disposal site.[47]

1.7.5. Formation of Carbonate from Natural Minerals. Several methods are currently being researched to produce a viable large-scale industrial solid carbonate disposal method. These methods primarily focus on the silicate minerals, with magnesium ores favored more than calcium ores, as magnesium silicates are usually more reactive than the calcium silicates. Some work has been done on simple oxides, but they are less naturally abundant. Cement chemistry can provide valuable insight to mineral carbonation, as can a study of biological carbonate forming processes. The information discussed in this section focuses mainly on the carbonation of natural minerals, which are minerals obtained from natural geologic occurrences for the primary purpose of reaction with carbon dioxide. Carbonation of "derived" minerals (industrial co-products such as slags and ash) will be covered in the section on carbonate formation in steelmaking slag. The methods researched for carbonation of virgin minerals have a direct impact on work to do the same with slags, as the chemical reactions are the same.

A consortium managed by the National Energy Technology Laboratory has done the largest amount of work with solid mineral sequestration. This group, comprised of Los Alamos National Laboratory, Arizona State University, and Albany Research Centre (ARC), has researched the applications of silicate-based minerals for permanent carbon dioxide sequestration. Other groups at the University of Ohio, University of Pennsylvania, and Helsinki University of Technology have added to this research.

Butt et al. at Los Alamos National Laboratory have carried out extensive research on carbon dioxide disposal in carbonate minerals.[39,40,50,51] Their initial research focused on calcium and magnesium silicate minerals. The reactions are exothermic, therefore chemically stable; however, the main constraint for cost implementation is the reaction

speed. Two approaches were researched to improve the reaction rate: solid-gas reaction at high-temperature and reactions in aqueous solutions.

The focus of solid-gas reactions was to determine the maximum temperature for stable formation of the carbonate from silicate. Calculations of the maximum carbonation temperature for several common minerals (where CO_2=0.1 MPa), are shown in Table 1.9. The reaction products are the alkaline earth metal carbonate plus silicate/aluminate/water.

Table 1.9. Thermodynamics of Mineral Carbonation Reactions (from Lackner[39])

Mineral	Formula	T_{deh} °C	T_{max} °C	ΔH kJ/mole	ΔQ kJ/mole
Lime	CaO	-	888	-167	87
Periclase	MgO	-	407	-115	34
Portlandite	$Ca(OH)_2$	518	888	-68	114
Brucite	$Mg(OH)_2$	265	407	-37	46
Wollastonite	$CaSiO_3$	-	281	-87	37
Clinoenstatite (Pyroxene)	$MgSiO_3$	-	201	-81	23
Forsterite (Olivine)	$½Mg_2SiO_4$	-	242	-88	24
Diopside (Pyroxene)	$½CaMg(SiO_3)_2$	-	164	-71	19
Grossular (Garnet)	$⅓1/3Ca_3Al_2Si_3O_{12}$	-	192	-67	28
Anorthite (Feldspar)	$CaAl_2Si_2O_8$	-	165	-81	39
Pyrope (Garnet)	$⅓Mg_3Al_2Si_3O_{12}$	-	260	-92	40
Talc	$⅓Mg_3Si_4O_{10}(OH)_2$	439	201	-44	64
Tremolite (Ampibole)	$1/7Ca_2Mg_5Si_8O_{22}(OH)_2$	566	164	-37	72
Chrysotile (Serpentine)	$⅓Mg_3Si_2O_5(OH)_4$	535	407	-35	78

The temperature T_{max} is the maximum carbonation temperature for pCO_2=101 kPa (1 atm). The temperature T_{deh} refers to the dehydroxylation temperature at pH_2O=101 kPa (1 atm). The enthalpy of reaction, ΔH, is normalized for one mole of CO_2 at the temperature T_{max}. The heat, ΔQ, is the energy required to heat the original mineral and the CO_2 to the higher of T_{max} or T_{deh}, from 25°C (77°F). They state in most cases that the energy released from carbonation exceeds that required to heat the reactants to T_{max}; so, theoretically, the reaction can be made self-sustaining. Grinding followed by direct carbonation in a rotary kiln or fluidized bed is recommended to achieve minimal cost.

While this data proves useful in comparison to the thermodynamic phase stability diagram calculated for slag phases, Lackner et al., do not provide reaction rates for the direct carbonation reaction in their initial work.[39]

Following their initial study, Lackner et al. performed experiments primarily on magnesium-based ores.[39] This is because two to two and one-half tons of magnesium-based rock is required to bind one ton of CO_2, as opposed to seven tons of calcium-based rock. The results of the consortium are extensive, and the key quantitative results are presented in Table 1.10. Also included in this table are results from Park et al.[52], Kutcha et al.[53,54], and Zevenhoven et al.[45] that are directly comparable.

Table 1.10. Process Conditions Investigated for Carbonate Formation from Minerals

Mineral Treatment	Particle Size (μm)	pCO_2 (atm.)	Temp. (°C)	Time (hr)	% Carb.	Note	Ref.
Serpentine	100	336	500	2	25%		36,63
$Mg(OH)_2$ extracted by HCl from Serpentine	-	49.3	550	0.5	90%+	1	63
$Mg(OH)_2$	28.7	0.76 52	25 375 565	12	2% 16% 90%	2	64
Serpentine heated to 600°C and He cooled	-	115-185	150	1	70-85%	3	65-68
Olivine, aqueous with $NaHCO_3$ and NaCl	37	150	185	1	30-50%	4	68
Olivine/Serpentine, aqueous with $NaHCO_3$ and NaCl	25	115-185	155-185	-	99%	5	69-74,88
Olivine with $NaHCO_3$ and NaCl	75 10 dry 10 wet	150	155	1	47% 82% 100%	6	71
Olivine	37 75	170	200	-	72% 67%	7	74
Olivine, Serpentine, and Magnesia	125 dry 125 wet	1-25 15-25	350 200	24	<1% -	8	75
Olivine, pretreated	<150 <37	-	-	-	11% 92%	9	76,80
Serpentine Serpentine Serpentine 1000°C pre-treat	50 50 50	1 14.8 1	200 200 200	3 3 3	<1% <1% <1%	10	46
Wollastonite	- 2-4	1 150	25 185	600 -	- 70%	11	77-78

Note 1: The rate of direct $Mg(OH)_2$ carbonation was found to be most rapid very near the dissociation temperature, as shown in Figure 1.1.

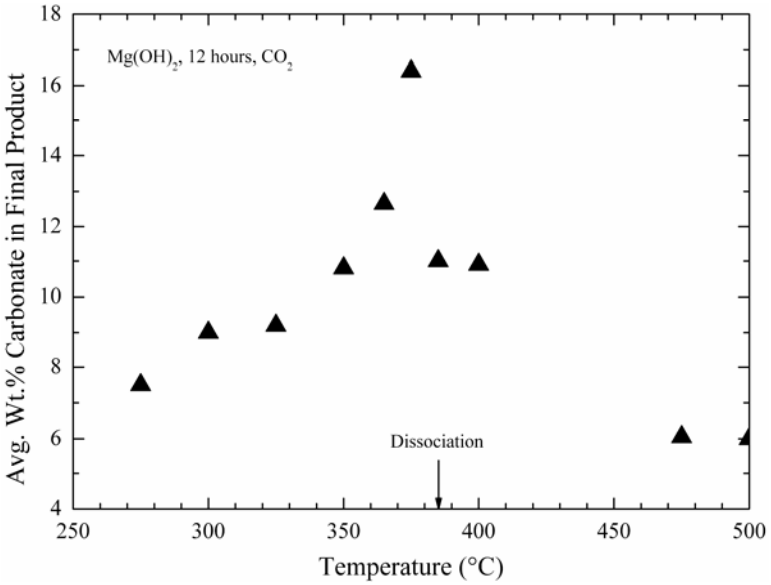

Figure 1.1. $Mg(OH)_2$ conversion to carbonate as a function of temperature at pCO_2=77.5 kPa (0.765 atm), from Butt et al.[40]

Note 2: Overall, the efficiency of carbonation at atmospheric pressure is relatively slow due to the formation of a product (carbonate) barrier that inhibits outward diffusion of water and inward diffusion of CO_2. The kinetics of both dehydroxylation and simultaneous dehydroxylation-carbonation obey the contracting-sphere model.[51] Water is required to provide a reasonable reaction rate, and that kinetics of carbonation are better in a low velocity CO_2 stream compared to a higher velocity of CO_2.

Note 3: During dehydroxylation the $Mg(OH)_2$ crystal structure contracts by 50% perpendicular to and 5% parallel to its lamella, respectively.[55] The resultant distortion induces high levels of interlamellar and intralamellar strain, which facilitates cracking and the formation of MgO nanostructures with very high surface areas near 100-200 m^2/g.

Note 4: Slurry stirred at 1000-2000 rpm. Mechanical stirring was found to be effective at exfoliating the SiO_2-rich surface layer, thus exposing fresh olivine for carbonation.

Note 5: Stirred autoclave with 15-30 wt.% solids. The rate controlling parameters for the direct carbonation of olivine and serpentine are chemical kinetics and diffusion through the product layer, respectively. The rate constant for direct conversion of olivine is of the order of 10^{-7} cm/s, while the diffusivity coefficient in serpentine is of the order of 10^{-10} cm^2/s. The diffusivity value is much lower than that of CO_2 into water ($2x10^{-5}$ cm^2/s), but similar to helium into silica ($2.4\text{-}5.5x10^{-10}$ cm^2/s), suggesting the pores are not filled with water and/or the process is controlled by the diffusion of other components.

Note 6: Uses a stirred autoclave containing15 wt.% solids. Pre-treatment involves dry and wet attrition grinding to <10 μm. Activation mechanisms are size reduction to increase surface area (wet grinding) and destruction of the crystal lattice to form an amorphous material (dry grinding).

Note 7: Uses a high-pressure high-temperature (HPHT) loop reactor with 100% flow recycle. The turbulent environment results in high particle-to-particle interaction, therefore continually exposing fresh surfaces to reaction.

Note 8: Dry tests showed negligible carbonation. Wet carbonation took place at 2-10 wt.% solids, with $NaHCO_3$ and NaCl additives. Quantitative results are not given

Note 9: Pretreatments studied include particle comminution, magnetic separation, acid treatment, and HCl extraction. Acid pre-treatment was conducted with HNO_3, H_2SO_4, HCl, and a combination of orthophosphoric acid, oxalic acid, and EDTA. Sulfuric acid proved the most effective acid for chemical activation.

Note 10: Separate tests were conducting with 1 wt.% NaCl, $NaHCO_3$, or Al_2O_3 mixed into the $Mg(OH)_2$, and 500 PPM SO_2 mixed into the gas phase with no discernable effect of these materials on carbonation rate was observed.

Note 11: Carbonation of wollastonite at ambient pressure/temperature found to be too slow for further investigation.

1.7.6. Formation of Carbonates from Oxides or Cement Minerals. The simple oxides of calcium and magnesium are more effective for sequestering carbon dioxide than their respective silicates, however due to their high reactivity they are rarely found

in nature. Small amounts of CaO or MgO are found in slag, and work by researchers in Spain on the natural form of these minerals is valuable for better understanding sequestration of carbon dioxide in slag.

Abanades et al. have done extensive research on the use of CaO as a sorbent to capture CO_2 from industrial combustion processes, primarily for large-scale power generation systems.[56-62] His work is partially funded by the European Coal and Steel Community (7220-PR-125). This work has focused on the characteristics of CaO to serve as a regenerative sorbent in a fluidized bed capture system. The reaction of carbon dioxide with lime is very simple and proceeds exothermically as detailed previously. The equilibrium limit in terms of CO_2 capture efficiency from gas phase in a lime carbonation-calcination reaction is shown by the reaction in Equation 22, where T is expressed in K.[57] This equation was developed from data by Baker.[63]

$$C_{CO_2,eq} = \frac{1.462x10^{11}}{T}\exp(\frac{-19130}{T}) \qquad (22)$$

The work by Abanades et al. has focused on a reactor operating at 650°C (1202°F) and atmospheric pressure. Using coal combustion flue gases at 12-15 vol.% CO_2 (similar to steelmaking offgas), initial capture efficiencies higher than 90% have been exhibited. Although the initial capture rates of CO_2 are high, the regenerative performance of CaO as a sorbent decreases rapidly after cycling several times through the carbonation-calcination process. This effect is shown in Figure 1.2.

The sharp decline in activity for carbonate conversion is due to limited diffusion of the CO_2 through the carbonate product layer and pore closure combined with grain growth, which leads to internal sintering and overall shrinkage of the original CaO particle.[61] The latter factors reduce the effective contact area for CaO-CO_2 reaction within the fluidized bed. While data from Abanades et al. work is useful in slag-offgas reactor and in understanding the carbonation kinetics of calcium oxide, it is not focused on a permanent solid carbonate disposal method, but a solid sorbent to compete with liquid sorbent (amine) systems.

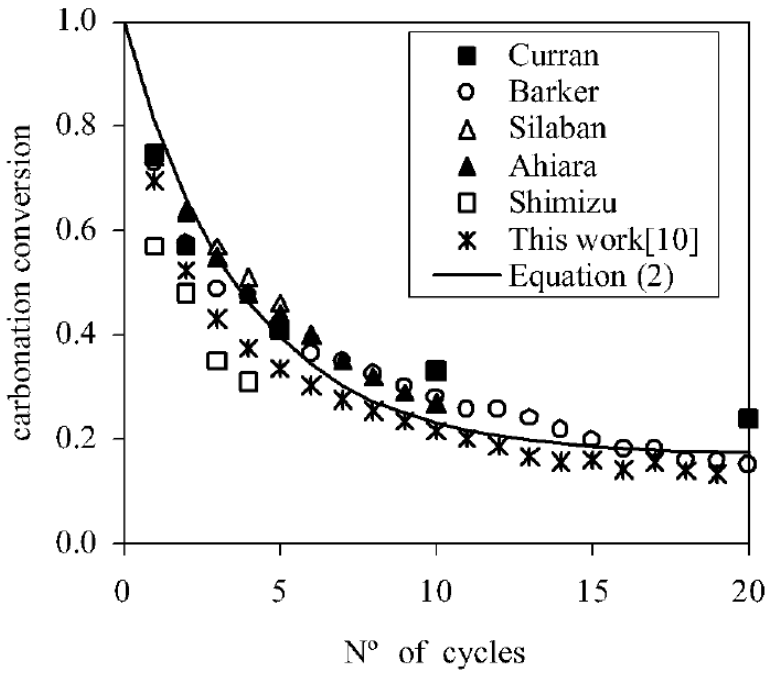

Figure 1.2. The decay in CO_2 sorbent capture capacity with the number of carbonation/calcination cycles (from Abanades[60])

Fernandez et al. from the University of Barcelona studied the carbonation of MgO slurries at atmospheric pressure.[64] Calcined magnesite (89.3% MgO) was mixed with water to form a slurry through which CO_2 was passed. The reactivity was directly related to the specific surface area of the MgO. A specific surface area of 43.1 m^2/g yielded 90% MgO conversion in 50 minutes, while 210 minutes was required to reach the same yield with a specific surface area of 1.8 m^2/g. Specific surface area could be controlled by time and temperature during calcining, with an increase in both reducing the specific surface area (due to internal sintering). Decreasing particle size or increasing pCO_2, solid-liquid ratio, CO_2, and temperature were all beneficial in speeding up the reaction rate. The kinetic relation expressed by Equation 23 was found to be valid for MgO slurry carbonation for the first 10 minutes.

$$1-(1-X_{MgO})^{\frac{1}{3}} = kt \tag{23}$$

X_{MgO} is the fraction carbonated; k is the rate constant (min^{-1}), and t is time (min). A plot of the rate constant versus temperature yields an activation energy of 29.1 kJ/mol. Studies of the reaction mechanisms indicate that the process is mixing controlled and chemical reaction controlled, with reaction of the magnesium carbonate on the particle surface with CO_2 to form magnesium bicarbonate as the rate-determining step.

Cement chemistry can provide valuable insight to slag carbonation, as it has many of the same mineral phases. Cement and slag both contain calcium silicates, calcium aluminates, and calcium ferrites. While cement chemists are primarily concerned with the hydraulic activity of these phases, work has been undertaken to understand long-term carbonate formation and the corresponding structural and physical changes that take place.

Berger et al. studied the carbonation of calcium silicates and calcium aluminates in their research of cement chemistry.[65-70] Even though this work was undertaken for accelerated curing of cement, the chemistry involved pertains directly to geological CO_2 sequestration. Initial work tested the compressive strength of pure cement minerals carbonated after hydration. Pure Ca_3SiO_5, β-Ca_2SiO_4, $Ca_3Al_2O_6$, and $C_{12}Al_{14}O_{33}$, were mixed with water at 92 wt.% solids for five minutes then compacted to 5.86 MPa (57.8 atm) in a cylinder and exposed to CO_2 at 0.39 MPa (3.8 atm) for five minutes. The Ca_3SiO_5 and β-Ca_2SiO_4 minerals produced an appreciable temperature rise upon reaction and the resultant strength was similar to standard cement. The aluminate samples showed no appreciable temperature rise or increase in strength from carbonation.

The carbonation of tricalcium and β-dicalcium silicate was studied further to understand the process chemistry. Powdered Ca_3SiO_5 (3300 cm^2/g) and β-Ca_2SiO_4 (4500 cm^2/g) were mixed with 12.5 wt.% water and subjected to pCO_2~0.1 MPa (1 atm) for varying times. X-ray diffraction and ignition loss measurements showed the initial chemical reaction occurring for the silicate followed Equation 24.

$$\begin{aligned} &nCaO \cdot SiO_2 + yH_2O + (n-x)CO_2 \\ &\rightarrow xCaO \cdot SiO_2 \cdot yH_2O + (n-x)CaCO_3 \end{aligned} \qquad (24)$$

This initial reaction takes place with CO_2 accelerating the hydration of the silicate to form C-S-H gel and $CaCO_3$. The stoichiometry of the gel is similar to that formed in conventional cement hydration. However, the gel carbonates rapidly to eliminate lime and produce calcite and silicate gel, yielding an overall reaction shown by Equation 25.

$$nCaO \cdot SiO_2 + nCO_2 + zH_2O \rightarrow SiO_2 \cdot zH_2O + nCaCO_3 \quad (25)$$

The carbonation reaction kinetics of β-Ca_2SiO_4 and Ca_3SiO_5 powders were determined as a function of material parameters and process conditions. Both silicates follow a decreasing-volume diffusion-controlled kinetic model expressed in Equation 26.

$$\left[1-(1-\alpha)^{\frac{1}{3}}\right]^2 = K_T' t \quad (26)$$

In this equation, α is the degree of carbonation, K'_T is the apparent rate constant, and t is the time of reaction (hours). A plot of $\log[1-(1-\alpha)^{1/3}]^2$ versus log(t) yields a straight line with slope approximately equal to 1.0. Substituting the temperature dependency of K_T' as an Arrhenius equation provides a direct relationship for the degree of carbonation, as shown in Equation 27.

$$\alpha = 1-\left\{1-\left[K_o' \exp^{\frac{-E_a}{RT}} A^2 t\right]^{\frac{1}{2}}\right\}^3 \quad (27)$$

K_o' is the pre-exponential term in the Arrhenius relationship times the diffusion coefficient; E_a is the activation energy; R is the gas constant; T is the temperature (K), and A is the average particle surface area (assumed monodispersed size). The values for the reaction parameters for both silicates are shown in Table 1.11.

Table 1.11. Reaction Parameters for Calcium Silicate Carbonation (from Goodbrake[69])

Phase	K_o' (h^{-1})	E_a (kcal/mol)	ΔH_f (kcal/mol)
Ca_3SiO_5	$3.44x10^4$	9.8	-83
β-Ca_2SiO_4	$2.39x10^9$	16.9	-44

These values were obtained from Arrhenius plots for both silicates. The reaction conditions were fixed at 0.1 MPa (0.99 atm) CO_2 at 100% relative humidity.

The carbonation mechanism for anhydrous powders is best described by Equation 24. A small amount of C-S-H gel forms, which rapidly loses CaO and water to form amorphous silica. The carbonation heats of formation are shown in Table 1.10 and are strongly exothermic. Both silicates form aragonite during carbonation, as long as the water stays in the vapor phase. If water condenses on the sample, they will form calcite initially, which transforms to aragonite as the sample dries.

Several other processes are worth mentioning in brief for their value in comparison with geological sequestration. Golomb at the University of Massachusetts Lowell investigated the formation of a stabilized limestone-CO_2 emulsion for carbonate sequestration into seawater.[71] Finely ground calcium carbonate (10-20 μm) is mixed with liquid or supercritical CO_2 in water to form a stable emulsion. The $CaCO_3$-coated CO_2-globules are stable and settle in water, thus allowing dissemination into the ocean. Lackner mentions that citric acid and EDTA are two chelating agents shown to break apart serpentine mineral; however, this method has not been researched in detail.[47] TecEco, a company in Australia envisions the use of forsterite and serpentine minerals as feedstock for making a magnesium oxide based cement (Eco-cement) that would sequester CO_2 from the air as it cures.[72] The company fails, however, to properly credit the CO_2 released through calcining, and at best (even with a solar powered Tec-Kiln), this process provides a zero sum for total carbonate sequestration.

1.7.7. Biomimetic Processes. Several biological processes form calcium carbonate from (dissolved) calcium oxide. These processes (e.g., shellfish exoskeletons) use a natural catalyst, carbonic anhydrase enzyme, to increase the formation rate compared to a geologic process. The use of purified carbonic anhydrase to mimic the

biological process (biomimetic) for industrial scale carbon dioxide sequestration has been proposed by Bond, Medina, and Simsek-Ege.[73-76] Carbonic anhydrase, a zinc metalloenzyme, increases the hydration of CO_2 to form carbonic acid, which is defined as the rate-limiting step of the fixation of carbon dioxide into calcium carbonate in aqueous solution. The overall objective of their research is to develop an industrial CO_2 scrubber using carbonic anhydrase to catalyze the rate of CO_2 hydration for subsequent fixation into stable mineral carbonates. Bovine carbonic anhydrase (BCA) was tested in a laboratory scale exhaust-seawater contactor and found to reduce the time for calcium carbonate precipitation from 20 minutes to less than 10 seconds. This process was repeated 15 times using the same catalyst (BCA immobilized on alginate beads), and exhibited less than 1% loss in experimental yield. BCA was also found to be stable to 70°C and resistant to SO_x and NO_x inhibition at levels expected in normal power plant exhaust gas.

1.8. CARBONATE FORMATION IN STEELMAKING SLAG

Steelmaking slag can be considered a mineral source, thus research in geological CO_2 sequestration is directly applicable for understanding the mechanisms involved with slag-CO_2 sequestration. Steel slag, however, is a derived synthetic mineral, in that it contains a mixture of minerals found in nature, but it is not naturally produced. Because slag is an industrial co-product it is subject to environmental regulations and controls not imposed on natural minerals containing the same phases. The high content of CaO, MgO, and SiO_2 in slag leads to the formation of silicates, which are similar to those minerals studied under geological sequestration (i.e., olivine, serpentine, and wollastonite). The high iron oxide content in slag however produces phases not commonly studied in geological CO_2 sequestration, and gives rise to unique work with steelmaking slags.

Several researcher groups are investigating the carbonation of steelmaking slag for use as an industrial sequestration reagent. This research has focused on a wide variety of carbonation routes from aqueous dissolution to supercritical carbon dioxide exposure to steam-CO_2 reactors. All of these processes use steelmaking slag as a direct sequestering agent, however additional work is undertaken to produce an end-product

product from the stabilized slag, such as blocks, construction material, or waste containment.

Huijgen and Comans at the Energy Research Centre of the Netherlands (ECN) have done the largest amount of recent research on the use of steelmaking slag for mineral-based CO_2 sequestration.[77-81] Their literature review covers much of the background geological sequestration research described earlier, including mineral selection, thermodynamics, pre-treatment and processing methods, and kinetics.[77] They selected steel slag as a research focus due to its high theoretical sequestration capacity (0.25 kg CO_2/kg slag), and it was compared to wollastonite. In their research, slag or wollastonite was mixed with water and reacted with CO_2 in a batch autoclave reactor. A summary of their finding is presented in Table 1.12.

Table 1.12. Summary of Slag Carbonation Results from Huijgen and Comans[77-81]

Material	Particle Size (μm)	pCO_2 (atm.)	Temp. (°C)	Time (hr)	Carbonation Amount
Steel Slag	<2000	0.99-28.6	25-225	2-30	25%
	<38	0.99-28.6	25-225	2-30	70%
	<106	15.1	50	30	48%
	<106	15.1	175	30	70%
	<38	9.9	200	15	80%
	<106	19.7	25	-	115 g CO_2/kg
Wollastonite	<106	19.7	25	-	10 g CO_2/kg

Several notes listed in their conclusion are applicable to the current research. They found that the percent conversion (to carbonate) is inversely proportional to the square root of the particle size (volume based mean diameter). As Ca-conversion was not affected by the stirring rate in the reactor, they concluded that Ca-diffusion through the matrix is the rate-limiting step. A fit of the data to an Arrhenius equation yielded an activation energy of 3.6 kJ/mol, which is consistent with solid-state diffusion control. Reaction time and CO_2 partial pressure had milder effects on Ca-conversion, compared to temperature.

Scanning electron microscopy analysis of the carbonated steel slag helps reveal the rate determining mechanism. Figure 1.3 shows a back-scattered electron (BSE) image of a polished steel slag sample after carbonation. The core of the particle is calcium silicate and calcium ferrite, two common slag phases. During carbonation, calcium diffuses outward from the calcium silicate phase leaving a Ca-depleted SiO_2 phase behind. Calcium on the rim of the particle reacts to form $CaCO_3$. The calcium carbonate rim and silica phases both provide a hindrance for further carbonation by limiting the diffusion rate of calcium to the surface.

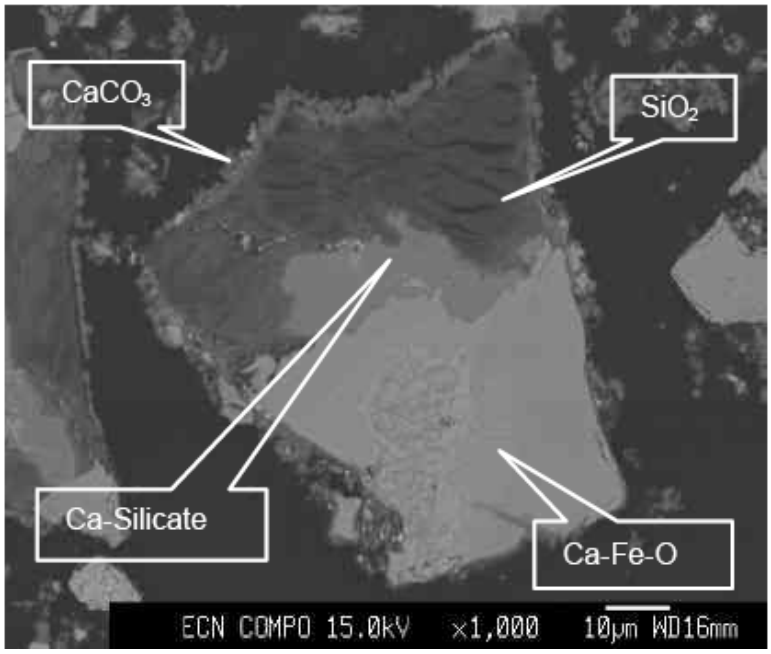

Figure 1.3. BSE image of carbonated steel slag particle (from Huijgen[79])

A comparison of wollastonite with steel slag shows the latter to have a higher reactivity to sequester CO_2. Figure 1.4 shows the comparison of steel slag and wollastonite for a range of temperatures. Peak reactivity was achieved at ~200°C (392°F), in which steel slag and wollastonite reached 170 and 135 g CO_2 per kg, respectively. A decrease in reactivity above 200°C (392°F) was due to the lowering of CO_2 solubility in water, making the delivery of CO_2 to the particle surface the limiting factor. The peak

values obtained for slag are 68% of the stated theoretical maximum (0.17 kg versus 0.25 kg).

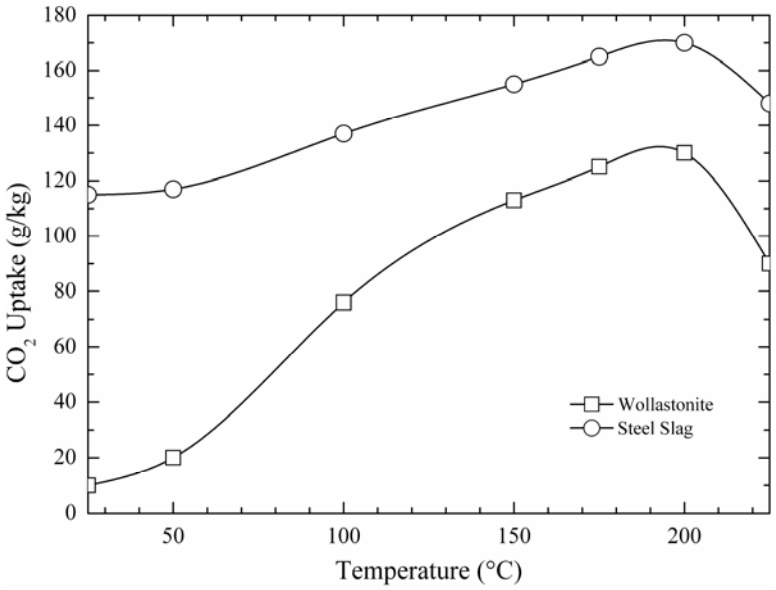

Figure 1.4. Carbon dioxide uptake of Wollastonite versus steel slag in a batch autoclave (d<106 μm, pCO_2=2.0 MPa), data from Comans[78]

Teir et al. at the Helsinki University of Technology have investigated the carbonation of blast furnace and steelmaking slags as an extension of their work with precipitated calcium carbonate formation from primary silicate ores.[82] They investigated acetic acid extraction of Ca^{2+} ions for precipitation of calcium carbonate in a slurry crystallizer. Blast furnace slag showed 97% Ca^{2+} in 20 minutes at 60°C compared to 38% extraction achieved with wollastonite under the same conditions. Further work is planned with this process.

Stolaroff et al. proposed formation of dilute aqueous alkali-metal solutions from steel slag or concrete that can be used to extract CO_2 from ambient air.[83-86] Steel slag at three different size fractions (45-74 μm, 74-300 μm, and 300-600 μm) was leached with de-ionized water and a pH buffer at ambient temperature to measure the amount of Ca^{2+} extracted. The initial rate and extend of calcium dissolution is higher for smaller particle sizes and lower pH. Approximately 50% of the Ca^{2+} is leached within the first minute,

and 80% within the first hour. A process reaching near terminal concentration of Ca^{2+} may be reached in a few hours.

Their recommendation for industrial scale-up uses the slag in a water spray bed, as shown in Figure 1.5. In this method, water spray leaches Ca^{2+} from slag piles. The leachate is collected and pumped back through the sprayers in a closed system. As the leachate droplets fall through the air, CO_2 is captured from the atmosphere to precipitate $CaCO_3$, which deposits on the slag. Calculations of CO_2 absorption rate show that a 0.8 mm droplet falling from 10 m height will utilize 84% of the Ca^{2+} in solution in forming carbonate. A 140,000 tons per year slag processing system, including water use, pumping energy, and material flow, is estimated to exhibit a CO_2 sequestration rate of 32,000 tons per year at an average cost of \$8/ton-CO_2.

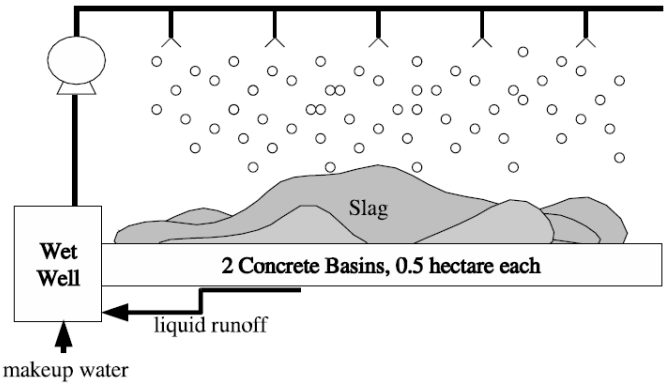

Figure 1.5. Spray bed for carbonation of steel slag (from Stolaroff[85])

Hills et al. have studied the accelerated carbonation of stainless steel slag and other materials for the purpose of rapid stabilization to prevent leaching of heavy metals during disposal.[87-91] The primary mineral phase in the slags tested was composed of calcium silicate. Carbonation was carried out with pCO_2 of 3.0 atmospheres for 24 hours. The slag was mixed with water in varying ratios, and the maximum carbonation (20% weight gain) was achieved with 12.5 wt.% water in solids. No carbonation occurs at 0% water, and increasing the water above 12.5 wt.% decreases the carbonation. Comparison of the results with industrial materials (pulverized fly ash, municipal solid waste

incineration ash, de-inking ash, and ordinary Portland cement) shows a directly proportional trend of carbonation weight gain with weight percent CaO in material. X-ray diffraction revealed that the carbonation reaction took place by γ-Ca_2SiO_4 conversion to calcite (this is a falling slag). Further testing showed that grinding prior to carbonation led to 10 times the compressive strength achieved, but this was not correlated to the amount of CO_2 captured.

A second set of tests was conducted on the stainless steel slag only, using the optimum conditions found earlier. The bulk slag was graded into three size fractions (<40 mm, 4-8 mm, and <125 μm), which were then ground for five minutes. The samples were mixed with 12.5 wt.% water and exposed to the same pCO_2 atmosphere for one hour. The theoretical maximum uptake capacity is given by Equation 28, which factors in the original slag composition. This equation does not include the MgO fraction, which averaged 9.8% in this slag.

$$CO_2\% = 0.785(CaO \cdot 0.7SO_3) + 1.09Na_2O + 0.93K_2O \quad (28)$$

The theoretical carbon dioxide capacity calculated was 45-50% depending upon the size fraction, compared to an actual measured capacity of ~18%, showing that one-hour reaction time was insufficient to reach carbonation equilibrium.

The carbonation reaction steps and mechanisms have been studied extensively for cementitious materials, which can be applied directly for the same process in slags.[91] CO_2 from the air permeates through the solid, which is the diffusion controlled rate-limiting step. The presence of water solvates CO_2 and a high surface area favors transport of the CO_2 to the solid surface. CO_2 hydrates to H_2CO_3, which then may ionize to H^+, HCO_3^-, and CO_3^{2-} depending upon the pH of the solution. The pH after the reaction drops approximately three units, typically from eleven to eight. The cementitious phases Ca_3SiO_5 and Ca_2SiO_4 are dissolved. The calcium silicate grains are covered by a calcium-silicate-hydrate gel, which quickly dissolves releasing Ca^{2+} and SiO_4^{4-} ions. The nucleation of calcium carbonate and calcium silicate hydrate is promoted by slightly increased temperatures and high surface area. While vaterite and aragonite may

precipitate, ultimately all the carbonate converts to calcite. A calcium silicate hydrate gel forms and is progressively decalcified converting to silica hydrate and $CaCO_3$.

Several key factors are found to influence the carbonation process of cementitious materials. Increasing the Ca content and Ca/Si ratio favor effective carbonation. Ferrite and Ca_3AlO_6 promote the formation of ettringite ($Ca_6(Al,Cr,Fe,Mn,Si)_2(SO_4)_3(OH)_{12}$-$26H_2O$), which readily decomposes to calcium carbonate in the presence of CO_2. The heavy metals Pb, Cd, and Ni increase the susceptibility of carbonation of cementitious materials by 40%, while organics will adversely affect carbonation. Water is necessary to promote carbonation, but too much blocks the pores and limits the reaction. Higher microporosity, surface area, and permeability all enhance carbonation rate. The rate of carbonation is directly proportional to the concentration of CO_2 in the gas phase. Carbonation peaks at 50-70% relative humidity and 60˚C (140°F). Above or below these ranges carbonation is less favorable.

Different methods of carbonation have been tried in the search for a commercially favorable route. Exposing solids to dry CO_2 under pressure leads to dehydration, causing water starvation of the carbonation reaction. At low pressure, a dynamic system is favored to a static system as the flowing CO_2 helps remove the water vapor produced by the reaction. At elevated pressures larger amounts of CO_2 are introduced throughout the sample before pore closure occurs, aiding carbonation. Vacuum carbonation using a desiccant showed a higher amount of carbonation. This is due to diminished resistance of water transport from the carbonating solid leaving an open pore network. Supercritical carbon dioxide penetrates into fine pores displacing water and replacing structurally bound water with CO_2. A system to treat Galligu, a calcium sulfide containing waste product from soap manufacturing, through an accelerated carbonation process uses a cement binder and gaseous CO_2 in an enclosed rotary kiln. This system is commercially from Forkers, Ltd.[91]

Isoo et al. has developed a process to make large blocks from steelmaking slag that are used as growth sites for marine life.[92-94] Dephosphorization slag (56.8% CaO and 13.8% SiO_2) was ground to a median diameter of 0.61 mm. Exposure to the atmosphere led to the formation of 0.9% $Ca(OH)_2$ and 2.5% $CaCO_3$ after one month. The slag was placed in large (1m x 1m x 1.2m) molds and reacted with CO_2 saturated with water vapor

at one atmosphere pressure for 12 days. The main carbonate product was calcite, and approximately 6% by weight CO_2 was reacted (~20% of theoretical amount). Blocks weighing 2.4 tons (1 m^3) contain about 130-160 kg CO_2.

1.9. CONCLUSIONS

The production and uses of steelmaking slag were analyzed to estimate the impact of implementing slag-based carbon dioxide sequestration. This data, along with the chemical analysis and mineralogy of slag, can be used to provide the sequestration potential (kg CO_2 captured per ton of slag) for slag compared to naturally occurring minerals. Significant mineralogical and thermodynamic analysis has been done with naturally occurring minerals, which can be directly applied to steelmaking slag. Large-scale sequestration into natural formations is being actively studied by several research consortia around the world. They have analyzed carbonate formation in MgO- and CaO-based minerals in a variety of reactor conditions, and found that the carbonate product layer is the primary factor in retarding the reaction kinetics. Pre-treatment methods and reactor conditions have been investigated to minimize the product layer effect. Pre-treatment methods focus on increasing the surface area through heat/quench, acid leaching, or grinding, while reactor conditions include increased pressure and temperature, or high-shear reactors to exfoliate the product layer. From these methods, only grinding and increased temperature (as available from steelmaking offgas sensible heat) are deemed feasible for use in a slag-CO_2 sequestration system. Aqueous-based reactors have been shown to have a much higher reaction rate compared with dry reactors, even at high temperatures. Chemical or biological catalysts, such as $NaHCO_3$, NaCl, or carbonic anhydrase enzyme, are available for use in aqueous reactors, and can be applied to a slag sequestration system. Steelmaking slags have somewhat different composition, morphology, and mineralogy compared with natural minerals, which will affect the reaction kinetics of CO_2 sequestration. However, data from the literature review was used as a starting point for understanding slag characterization, as well as reactor design.

2. EXPERIMENTAL WORK AND ANALYSIS

Investigative work and experimental research for this project was conducted in a stepwise manner to complete the key tasks identified. These items included industrial site application surveys, slag characterization, bench evaluation of kinetic factors, and bench-scale prototype reactor design. Figure 2.1 is a flowchart showing how these tasks are related. The following sections each provide a summary of the methods and results for each respective research task. Further details and relevant background material are contained in the appendices as appropriate.

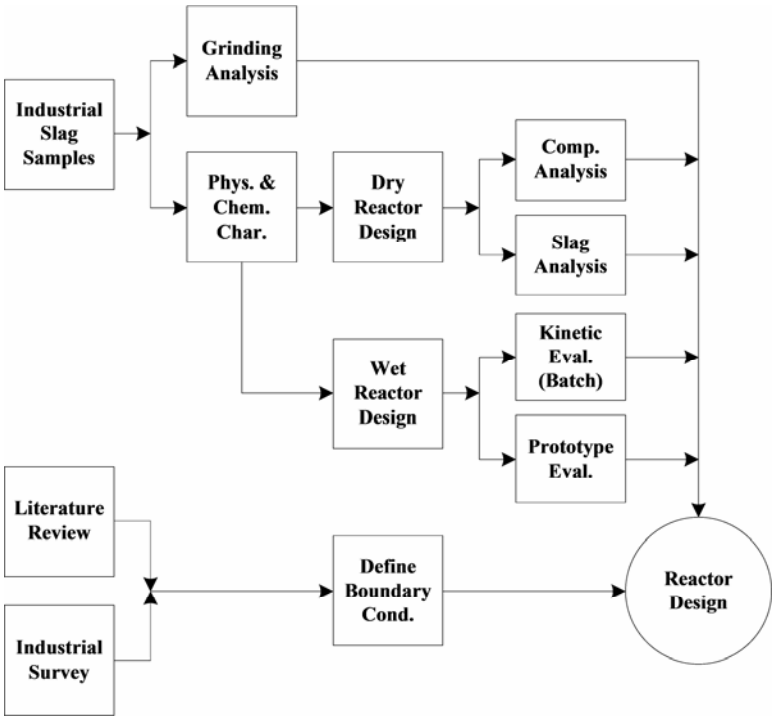

Figure 2.1. Flow scheme of research work conducted

2.1. INDUSTRIAL SURVEY

Initially, six steelmaking plants were visited to gather process data and slag samples and to compile survey feedback from project participants. The purpose of the survey was to provide practical operating parameters and determine the steelmaking

offgas and slag production parameters. This data was used to identify the process boundary conditions for a slag-CO_2 sequestration reactor.

Offgas composition and CO_2 emission results from the surveys were analyzed in comparison to literature review data and published in the Proceedings of AISTech 2006, Volume II and Steel Time International.[95,96] Paper 1 of this dissertation is comprised of the AISTech 2006 paper.

Developed through discussions with project participants, a concept for capturing CO_2 from steelmaking offgas using slag is illustrated in Figure 2.2. The proposed reactor would be installed after the baghouse, which generally allows for retrofit accessibility and prevents contact between the slag and furnace dust.

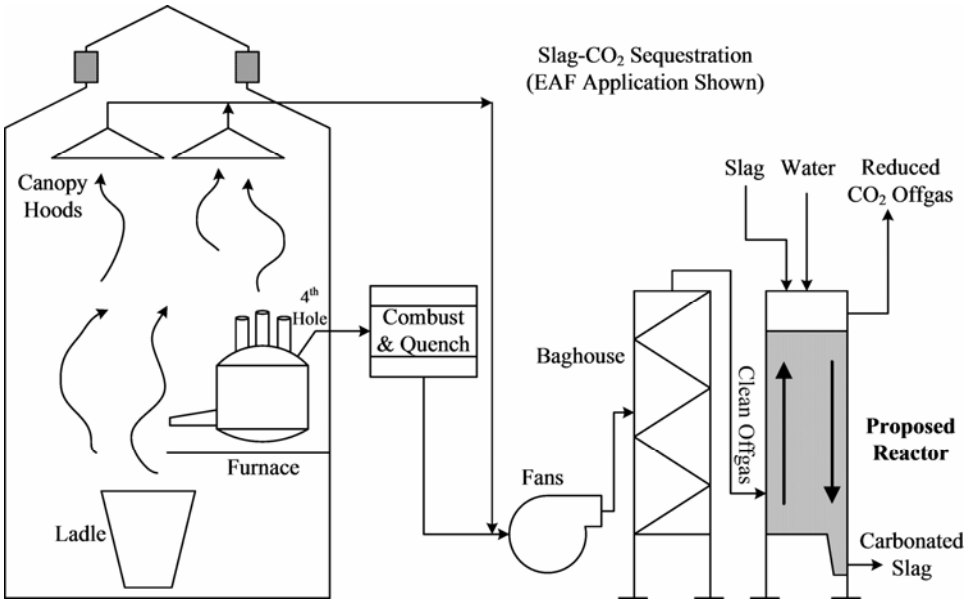

Figure 2.2. Schematic of process for capturing carbon dioxide from steelmaking offgas using slag (EAF application shown)

The proposed reactor is designed to contact granulated slag and cleaned offgas. Based on survey data, the boundary operating conditions for the incoming offgas stream at the exit of the baghouse (stack discharge) are listed in Table 2.1. The granulated slag will come from the processing stockpiles and will be at ambient temperature and pressure.

Table 2.1. Process Boundary Conditions for Slag-CO_2 Sequestration Reactor

Pressure	Direct after baghouse, ~ 1atm.
Temperature	Max. allowable to increase reaction rate 150°C (typical baghouse limit) 220-350°C (thermodynamic limit by phase)
Gas Composition	<15 vol.% CO_2 (remainder N_2 and O_2) 4-5% CO_2 average CO, SO_x, and NO_x in PPM amounts

2.2. SLAG CHARACTERIZATION

Detailed chemical and physical slag characterization was undertaken as a necessary starting point to understanding the nature of the industrial slag samples as a baseline for thermodynamic and kinetic analysis.

2.2.1. Chemical Characterization. Slag chemical characterization involved elemental and phase identification. Elemental analysis of the first nine industrial samples (A1α-E2α) was conducted at ArecelorMital. Carbon and sulfur were measured using a LECO C/S analyzer. Thirteen metals (oxides) were measured using x-ray fluorescence (XRF). In the XRF analysis, each slag was milled to pass an 80-mesh screen and fused into a bead with flux of 75% $Li_2B_4O_7$ and 15% La_2O_3. Elemental analysis of the last four samples (E1β,γ-E2β,γ) was performed by Nucor Hickman using the XRF standards for their slag. A summary of the elemental analysis is presented in Table 2.2. Detailed results from all samples are listed in Appendix A.

X-ray diffraction (XRD) phase analysis was used to identify the phase components of the slag samples. This was done at Missouri S&T using a Scintag, Inc. PadX x-ray diffractometer with a copper source. Powdered slag samples were analyzed from 10-70 degrees two theta at 0.03 deg/min. Steelmaking slag exhibits a high background noise level due to the glassy (amorphous) and free metal (steel) content. Table 2.3 lists the primary phases identified in each slag sample. Quantification of several of the phases was not completed because ICSD card data for some of the more complex phases could not be found. All primary phases listed in Table 2.3 are oxides or combinations of oxides. Much like similar studies in the literature, iron oxide and calcium disilicate were found in almost all slag samples.

Table 2.2. Elemental Composition of Industrial Slags as Determined by XRF (wt.%)

Elements (as oxides)	EAF (8 samples)		BOF (2 samples)		LMF (3 samples)	
	Avg.	Range	Avg.	Range	Avg.	Range
CaO	32.44	27.3-35.9	40.71	40.5-40.9	49.43	47-51.3
MgO	11.20	9.4-12.8	12.90	12-13.8	6.23	4.3-10
FeO	26.85	20.2-31.6	21.68	21.6-21.7	5.61	5-6.3
SiO_2	13.95	8.7-19.4	11.65	10.4-12.9	12.96	4.5-28.3
Al_2O_3	8.29	5.6-11.8	5.93	5.2-6.6	21.26	4.9-32.3
MnO	5.37	3.4-7.1	4.59	4.5-4.7	1.06	0.8-1.3
TiO_2	0.47	0.4-0.5	0.58	0.5-0.7	0.34	0.3-0.4
ZrO_2	0.07	0-0.2	0.18	0.1-0.3	0.20	0.2-0.2
Cr_2O_3	1.48	0.8-2.5	0.36	0.3-0.4	0.25	0.2-0.2
K_2O	0.05	0.1-0.1	B.L.	0-0	0.01	0-0
Na_2O	B.L.	0-0	B.L.	0-0	0.01	0-0
S	0.34	0.1-0.9	0.11	0.1-0.1	1.33	1-1.6
P	0.30	0.2-0.6	0.43	0.4-0.5	0.08	0-0.2
C	0.23	0.1-0.3	0.53	0.4-0.7	0.38	0.4-0.4
Sr	B.L.	0-0	B.L.	0-0	B.L.	0-0
F	0.65	0.3-0.9	0.33	0.3-0.3	1.66	1.7-1.7

B.L. = Below Limit

The reactivity of the oxide phases in Table 2.3 with respect to CO_2 partial pressure and temperature is determined by the phase stability diagram shown in Figure 3 of the paper published in the Proceedings of AISTech 2006, Volume II. The partial pressure of CO_2 in the reacting offgas limits the temperature at which the reactor may operate. The limiting phase is $MgFe_2O_4$, which is stable to 227°C at 5% CO_2 and 267°C at 11% CO_2. Assuming Ca_2SiO_4 is the most prevalent phase in slag, the stability limit increases to 267°C and 352°C at 5% and 11% CO_2, respectively.

Phase distribution was determined by scanning electron microscopy (SEM) and electron diffraction spectroscopy (EDS) analysis. Figure 2.3 shows an EDS elemental map for slag E1α. The sample was mounted in Spurr resin, polished to 0.5 μm in non-aqueous suspension, and carbon coated. The image in Figure 2.3 shows primary metal particles distributed throughout the slag in discrete shapes. Spectrum analysis shows these regions to be composed of Fe and Mn (not oxides). The matrix of the slag is composed of a calcium-silicon-iron oxide mix. Slags E1β, E2α, and E2β were analyzed in

the same manner, and their respective EDS elemental maps and spectra are provided in Appendix A.

Table 2.3. Primary Phases Identified from XRD Analysis of Steelmaking Slag

		EAF	EAF	LMF	BOF	BOF	EAF	EAF	EAF
Formula	Phase	A1α	A1β	A1γ	B1α	C1α	D1α	E1α	E2α
Oxide									
FeO	Iron Oxide	X	X				X	X	X
MgO	Periclase			X					
CaO	Calcium Oxide					X			
Silicate									
$Ca_2(SiO_4)$	Larnite	X			X	X			
$Ca_2(SiO_4)$	Larnite		X						
$Ca_2(SiO_4)$	Dicalcium Silicate			X					X
$Ca_2(SiO_4)$	Dicalcium Silicate						X		
$Ca_5MgSi_3O_{12}$	C_5MS_3							X	
Ca_3SiO_5	Tricalcium Silicate							X	
$Ca_2Al_2SiO_7$	Gehlenite				X				
Aluminate									
$Ca_{12}Al_{14}O_{33}$	$C_{12}A_7$			X	X	X	X		
$(Fe_{0.855}Al_{0.145})$ $\cdot(Al_{0.855}Fe_{0.145})$	Hercynite							X	
Ferrite									
$(MgO)_{0.432}$ $\cdot(FeO)_{0.568}$	Magnesium Iron Oxide				X	X	X		

Several key conclusions were obtained from SEM/EDS analyses that were used in subsequent testing. Fe-rich material is present in EAF slag as particles (10-100μm), stringers, globules, and dendrites. Grinding below 100μm should liberate these metallic particles for separation and recovery. Manganese is associated with the iron dendrite particles; and, it should be recovered with the metallic fraction. Lime (CaO) is dispersed throughout EAF and LMF slags to form the matrix material. Grinding to 100μm to recover metallic particles should expose sufficient matrix material to enable full exposure of CaO for CO_2 sequestration. Aluminum and silicon are associated with the matrix

material in EAF and LMF slag, but not present in the iron particles. Magnesium oxide is present in LMF slag as large (100-500μm) blocks. Grinding to 100μm should expose all MgO material for sequestration.

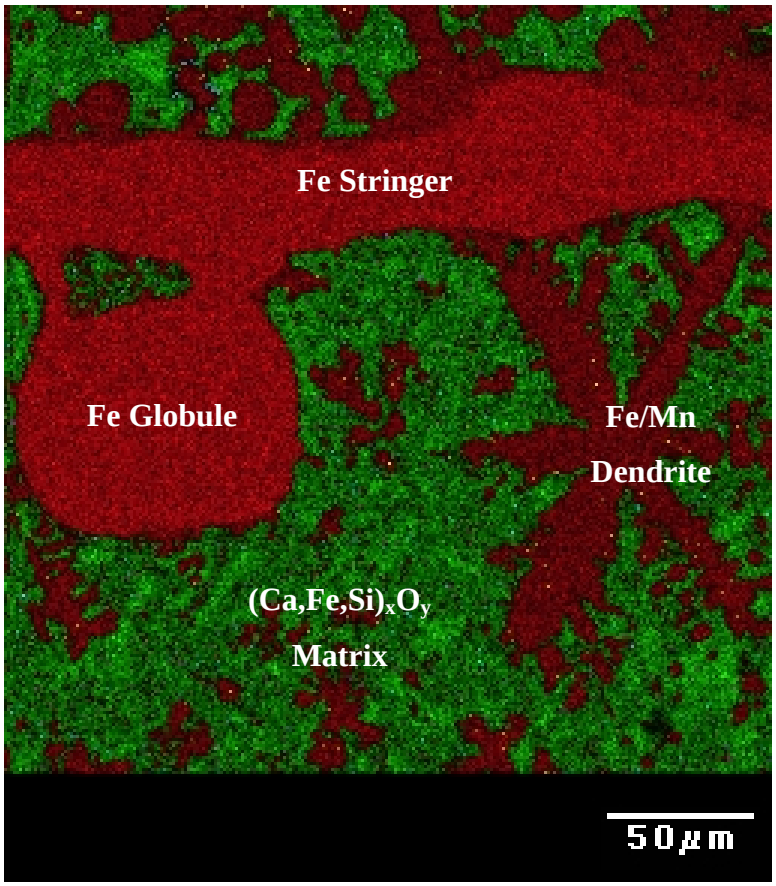

Figure 2.3. EDS elemental map for slag E1α showing stringers, globules, and dendrites of primary metal in a matrix rich in CaO and SiO_2

2.2.2. Characterization of Physical Properties. Physical property characterization was undertaken to quantify the slag samples properties for the surface area analysis, grindability test, and metal liberation analysis. Surface area analysis requires the true density, while the grindability test and liberation analysis require the bulk density and particle size distribution. Table 2.4 summarizes the slag samples' physical properties. Evaporable moisture content and bulk density were determined according to the ASTM specification listed, and true density was measured by inert gas

pycnometry on slag samples ground to <106 μm. Loss on ignition testing was done in an air atmosphere furnace.

Table 2.4. Physical Properties of Steelmaking Slag Samples

Sample	Evap. Moisture (wt.%) ASTM C566-97	Bulk Density (kg/m^3) ASTM C29M-97	True Density (kg/m^3) By Pycnometry	Loss on Ignition @ 990°C (Δwt.%)
A1α	0.00%	2014	4052	-1.7%
A1β	1.14%	1941	3881	-1.4%
A1γ	2.59%	1778	2900	3.3%
B1α	2.52%	2019	3614	0.8%
C1α	4.25%	2138	3548	0.3%
D1α	1.56%	2180	3697	-1.1%
E1α	1.44%	1795	3760	-1.7%
E2α	0.41%	1650	3822	-1.7%
E1β-1	0.02%	1438	3021	-3.2%
E1γ-1	0.81%	2167	3906	-1.2%
E2β-1	0.00%	1849	3069	-1.9%
E2γ-1	1.03%	1874	3665	-0.7%
Average Values				
EAF	0.91%	1945.9	3826.2	-1.35%
BOF	3.38%	2078.7	3580.9	0.57%
LMF	0.87%	1688.1	2996.7	-0.58%

Evaporable moisture content tests showed most of the slags were very dry in the as-received condition. Slag C1α (BOF) was not received in the raw state and its higher moisture content reflected the fact that it had been stockpiled for several weeks. True density values show that slag is denser than silica (2650 kg/m^3) mainly due to its high iron content. On average, EAF and BOF slags are denser than LMF slag, also due to iron content. Loss on ignition (LOI) data (to determine bound water or carbon dioxide) was inconclusive because most of the samples gained weight due to oxidation of the free metal content that oxidized upon heating. LOI analysis was not repeated in an inert atmosphere furnace.

Slag particle size distribution (PSD) was measured using a series of nested 8" U.S. series mesh sieves. A sub-sample from each slag was obtained using a riffle splitter and analyzed on a vibratory shaker according to ASTM D448-03a/D692-00 and ASTM

D1073-01 methods for coarse (>9.5 mm) and fine (<9.5 mm) fractions. A summary of PSD results for nine slag samples is shown in Figure 2.4.

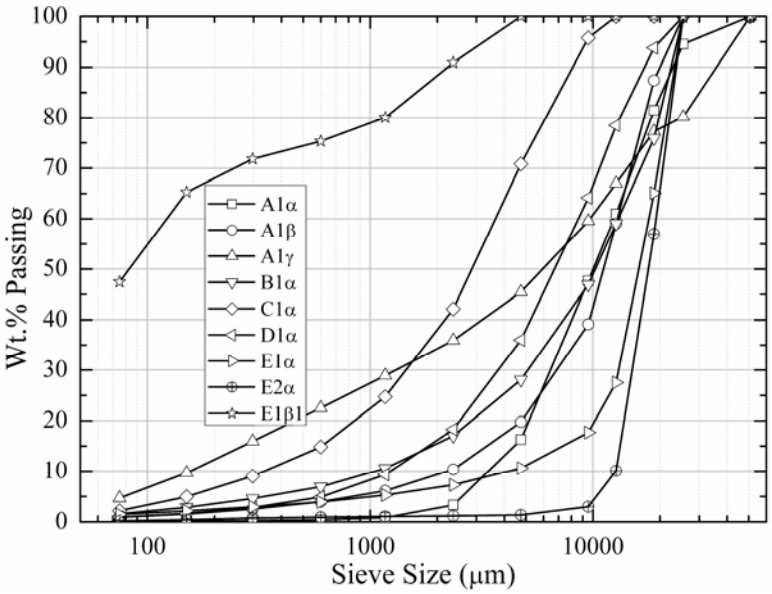

Figure 2.4. Particle size distributions of steelmaking slag samples

Most of the 80% passing (P_{80}) values lie between 10-20 mm and all particles were smaller than 50.4 mm (2”). The fines (<100 μm) values were all less than 5%. The primary exception to this observation is slag E1β1, which is a falling LMF slag that self-comminuted upon cooling. It had a P_{80} of ~1.1 mm and a fines value of 55%. Most of the subsequent testing procedures required grinding and sizing of the slag samples, which was done on an as-needed basis.

2.3. THERMOGRAVIMETRIC ANALYSIS

The first major testing area investigated in an effort to determine the carbonation kinetics of steelmaking slag used a purpose built apparatus for thermogravimetric analysis (TGA) designed by Dr. Simon Lekakh of the Department of Materials Science & Engineering at Missouri S&T, and I carried out the experimental work and data analysis. This device was built to measure the reaction kinetics between a CO_2 containing gas stream and solid slag particles. The TGA-based method could determine the necessary

parameters for fluidized-bed or rotary-kiln reactors in which steelmaking offgas and granulated slag are in direct contact. A schematic of the device and operating details are given in Paper 1.

One hundred and fifty one tests were completed using the TGA reactor. Ninety of these tests were debugged the furnace, sample holder, and procedure for optimization of distributed gas flow, heat distribution, gas humidification, powder preparation, gas composition, and data acquisition. Initial tests were conducted using single particles of hi-cal lime suspended by a platinum wire in the gas stream. While this method provided initial data on temperature and gas humidification effects, it was not applicable to powdered materials such as ground slag or standard powder reagents.

A new method was devised in which powdered material (e.g., reagent powders or slag ground to <106 μm) were pressed into 3.81 cm (1.50”) discs using a Carver press. The thickness of the discs averaged one centimeter. Each disc was then placed into a 316SS sample holder that encouraged reaction only on the top face of the disc. The press fixture, sample holder, and disc are shown in Figure 2.5.

The pressed disc was placed in the sample holder and suspended from a digital balance in the tube furnace of the TGA. A measured gas stream was introduced at the bottom of the tube furnace and flowed upward to make contact with the disc. A thermocouple introduced at ~0.6 cm (0.25”) above the disc surface was used to control the furnace temperature. The gas stream could be introduced dry or humidified using a heated bubbling column. Figure 2.6 is a schematic of the gas flow path in relation to the sample holder and sample disc.

The schematic in Figure 2.6 shows the sample holder suspended in the tube furnace with a gap of approximately 1 centimeter on each side for gas flow. This figure also shows a CaO disc that is exposed to a humidified CO_2 stream. The water vapor absorbs into the CaO disc to form a gel in which CO_2 solvates, allowing aqueous carbonation to take place. Ideally, the disk was subject to a 1-D reaction front (from the top down). However, no method was used to seal the disk in the holder, so some gas migrated between the sample and the holder, allowing a reaction to take place along the sample sides.

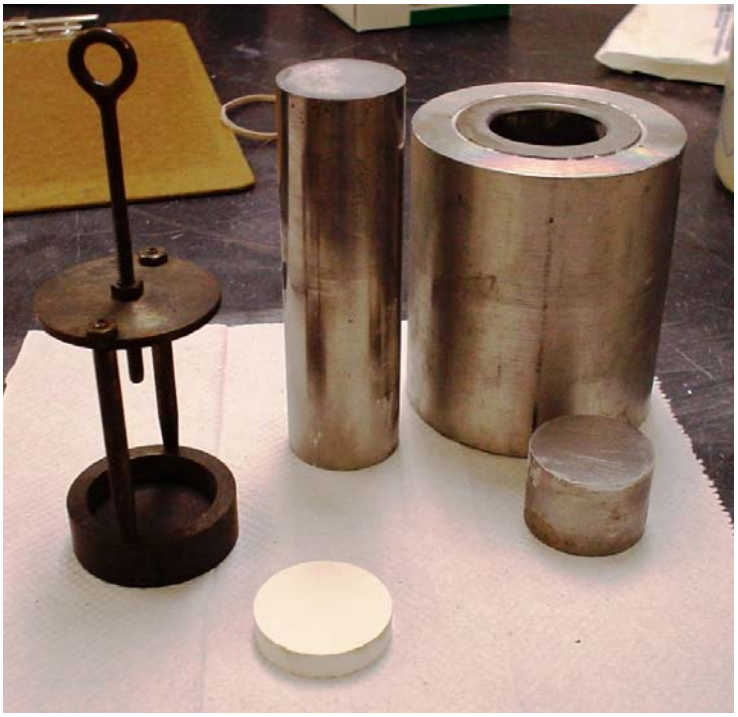

Figure 2.5. Sample holder (left), pressed sample disc of CaO (middle bottom), and Carver press ram with cylinder (back right) used to make samples for TGA reactor

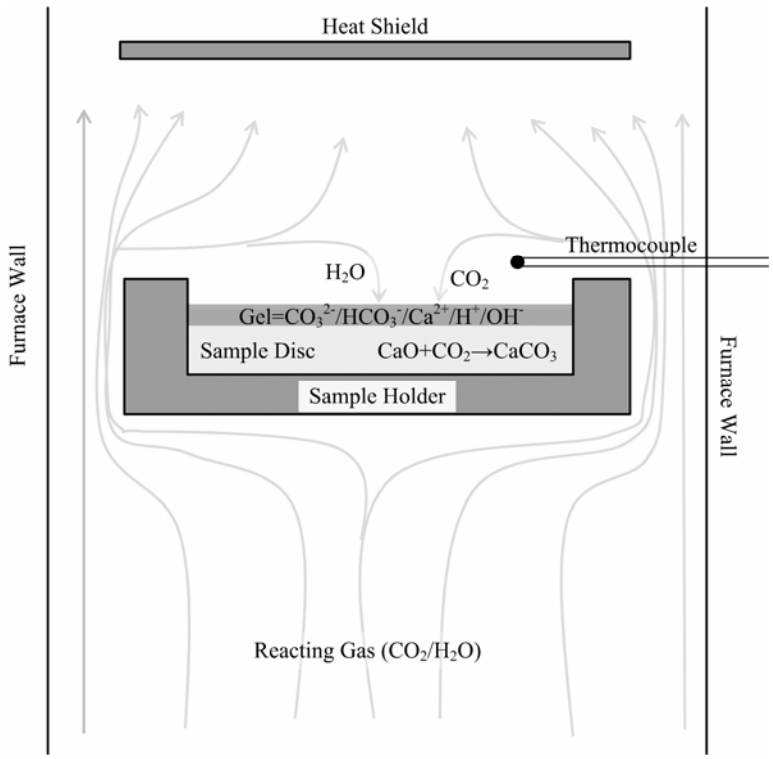

Figure 2.6. Placement of disc sample in flow stream of TGA reactor

The initial results of hi-cal lime testing in dry and humidified streams at a range of temperatures are shown in Figure 5 of Paper 1. As the composition of hi-cal lime particles varied, further tests were undertaken with reagent grade CaO in order to form a baseline for comparing the slag results. Figure 2.7 summarizes the results of testing calcined reagent grade CaO in anaerobic grade CO_2. All tests were conducted under atmospheric pressure. The amount of carbonation was calculated as a function of weight gain in relation to CO_2 uptake only. Differentiation between H_2O and CO_2 uptake was measured by TGA decomposition analysis of the samples after the reaction tests were completed.

All tests showed similarly shaped reaction curves with initial rapid carbonation rates (weight gains) that leveled off at longer times. This leveling off is most evident in the 100°C and 300°C dry data in Figure 2.7a. More than 95% of the carbonation took place in the first 15 minutes and very little occurred after six hours. At 300°C in humidified CO_2, approximately 50% of the carbonation took place in the first 15 minutes and the remainder over the six-hour test period. A dramatic increase was shown at 500°C in both dry and humidified CO_2, which had the highest carbonation amounts and rapid reaction rates at six hours. Long-term tests conducted over a period of several weeks at 500°C show that the reaction still progresses even at 10 days with humidified gas resulting in 60% carbonation, as compared to 45% in dry gas.

The shape of the reaction curve is a result of two mechanisms. The initial rapid carbonation rate is caused by the chemical reaction between CO_2 and the initial unreacted surface layer of CaO particles. As a $CaCO_3$ product layer develops, it swells to block off the inter-particle path to CaO deeper in the disk and forms a dense barrier through which diffusion of the reacting species must take place to continue the reaction. These two mechanisms are elucidated in Appendix B, in which log-log plots show a linear relationship between time and carbonation. Arrhenius analysis at 0.3% and 3% carbonation revealed the activation energy of the chemical and diffusion mechanisms as 41.6 kJ/mole and 121.5 kJ/mole, respectively, for the dry CO_2 case and 38.1 kJ/mole and 63.9 kJ/mole, respectively, for the humidified CO_2 case. The addition of water vapor to the gaseous CO_2 stream reduces the activation energy for both the formation of $CaCO_3$ from CaO and the diffusion of CO_2 through the $CaCO_3$ product layer.

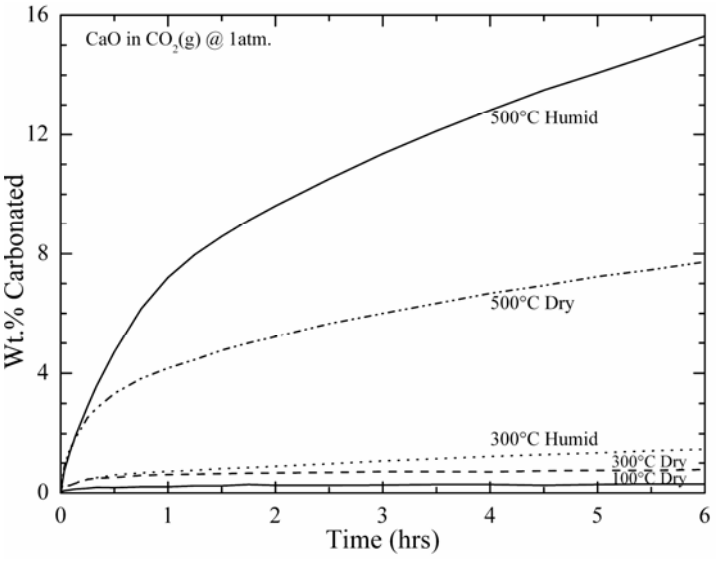

(a)

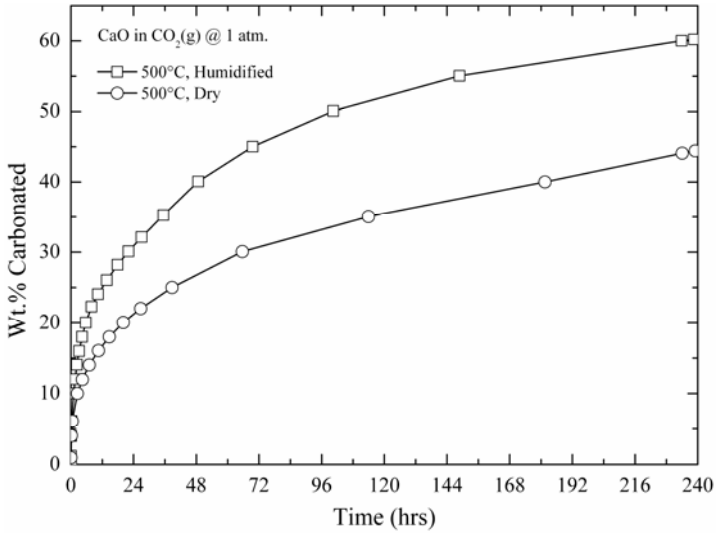

(b)

Figure 2.7. Carbonation rate of CaO in dry and humidified CO_2 gas: (a) At 6 hours from 100-500°C and (b) after 10 days at 500°C

While temperature and water vapor both increased the carbonation rate of CaO in this system, the overall carbonation magnitude was still quite low for both lime and slag. Figure 2.8 compares several slag samples analyzed with the TGA reactor to CaO and slag tests in an aqueous based system.

Slags E2β1, E2α, and B2α represent the highest CaO containing LMF, EAF, and BOF slags, respectively. Each slag was ground to pass 106 μm and pressed into a disc for

the TGA reactor test. At 500°C in humidified CO_2, these three slags achieved 4.2%, 5.3%, and 5.5% carbonation, respectively at 24 hours reaction time. In comparison, aqueous testing of slag E2β1 (detailed in Paper 2) yielded 12.8% carbonation at 16 hours reaction time. Extrapolation to 24 hours shows that aqueous testing with slag should yield ~15% carbonation, which is three times that achieved under the best conditions in the TGA reactor. Reagent grade CaO shows the same type of improvement with aqueous processing resulting in 31% carbonation at 24 hours in 500°C humidified CO_2 compared to the 95% achieved through aqueous processing. Finally, synthetic dicalcium silicate (Ca_2SiO_4) tested in the TGA reactor was compared to the same material tested using the aqueous processing method. At 24 hours processing time <0.5%, carbonation was achieved in the TGA reactor (500°C, humidified CO_2), while 74% carbonation was achieved in the aqueous system. Based on these results, the primary focus of experimental testing for the reactor design shifted to the aqueous based system and testing with the TGA reactor system was discontinued. Even though a gas-solid based processing scheme may lead to a simpler industrial scale reactor design than will slurry reactor processing, the kinetic reaction rate in the gas-solid system is too slow to provide adequate efficiency for effective scale-up.

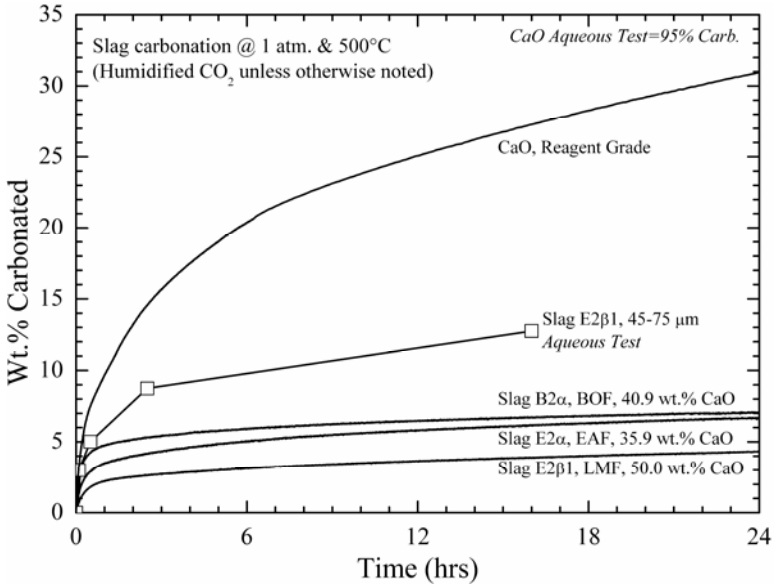

Figure 2.8. Summary of TGA reactor tests on steelmaking slags compared to CaO and aqueous test results

2.4. AQUEOUS PROCESSING

Slag carbonation in an aqueous-based system was undertaken in parallel with the TGA reactor tests. Initial results from aqueous processing exhibited more favorable reaction kinetics than gas-solid processing, so the remainder of the project focused on the design of a gas-liquid-solid reactor. Both leaching and carbonation kinetic parameters were investigated, and the methods, results, analysis, and modeling were published in two Metallurgical and Materials Transactions B papers, which comprise Paper 2 and 3 of this dissertation.[97,98]

Paper 2 covers the results from batch leaching and carbonation testing of the slag samples. These tests were primarily conducted by Dr. Simon N. Lekakh, whom I assisted with sample analysis and data interpretation. Batch reactor tests were conducted at ambient temperature and pressure. The specific surface area of slag particles was increased by leaching or carbonization. Selective dissolution of the Ca-bearing phase resulted in increased surface roughness, while carbonation produced overlapping plates of $CaCO_3$ product layer to create a highly irregular surface. Both Ca-leaching and carbonation were analyzed using the shrinking core model. The experimental data for both processes fit this model well after correction for effective particle size based on the measured surface area. Analysis of Ca-leaching showed linear proportionality to particle size during the initial stage, which supported a chemical reaction controlled model (CaO dissolution). The later stage of leaching is controlled by diffusion of the Ca^{2+} ions through the resulting porous surface layer, as shown by square-root proportionality of reaction time to particle size. Carbonate conversion is heavily dependent on particle size and the reaction is limited by product layer diffusion. The effective diffusivity of the product layer decreased by an order of magnitude from $5x10^{-9}$ cm^2/s at the start of precipitation to $5x10^{-10}$ cm^2/s as the product layer formed and its density increased. Carbonate conversion proceeded more slowly than leaching conversion, and both processes were inhibited by the calcium carbonate product layer.

Paper 3 describes modeling a two-stage reactor system using METSIM Ver. 5.4, commercial process simulation software. The modeling was primarily conducted by Dr. Lekakh and Dr. David G.C. Robertson (Department of Materials Science & Engineering, Missouri S&T), whom I assisted with data analysis and interpretation. The kinetic

leaching and carbonation parameters obtained from the batch tests were used to create the model. Several operating scenarios of a two-stage system were modeled using water/slag contact in Reactor 1 and leachate/CO_2 contact in Reactor 2. These scenarios included batch versus continuous processing and fresh water input versus water recirculation. Fresh water addition to Reactor 1 allowed the highest leaching efficiency and resulted in excellent carbonization in Reactor 2, but a continuous system has a high water demand. Recirculation of the spent leachate minimized the fresh water addition, but inhibited the leaching process by producing a calcium carbonate product layer on the slag particles in Reactor 1. Increasing the slag surface area, slag/solution ratio, or reactor residence time partially overcame product layer blinding. Optimal residence times were defined for different process parameters and slag particle sizes.

While aqueous processing allowed detailed kinetic analysis, bench scale prototype testing, and scale-up modeling of a two-stage reactor, the hydrous carbonation rate of slag was found to be insufficient to make an industrial reactor feasible. The batch tests showed that 10-15% carbonation could be achieved at 24 hours (~3x better than gas-solid results), but modeling showed that up to 20 days processing in a two-stage aqueous reactor was required to double that amount to 30%. Several pre-treatment and processing factors that increased the carbonation rate and amount were found in the literature review (see Table 1.10). These factors included increased temperature and pCO_2 to improve diffusion rates, high shear processing to abrade away the product layer, particle pre-processing (i.e., acid leaching, heat and quench, or high pressure grinding) to increase the particle surface area, and addition of $NaHCO_3$ and NaCl to the aqueous phase to catalyze the reaction. Increasing the temperature and pressure would require batch autoclave processing, which would greatly add to the cost and complication of industrial scale-up. Particle pre-processing was accomplished in the current test program by grinding of the slag to produce a specific size fraction for testing. The $NaHCO_3$ or NaCl catalyzing mechanism was not well understood by previous researchers, so the magnitude of their improvements was inconsistent.

2.5. BIOMIMETIC PROCESSING

One unique area that has not been investigated with slag or mineral sequestration is biomimetic processing. A biomimetic catalyst (carbonic anhydrase enzyme) has been shown to improve the rate of calcium carbonate precipitation by two orders of magnitude.[99] The carbonic anhydrase mechanism and effect on carbonate chemistry are described in Paper 4. Carbonic anhydrase was investigated in the current project as an aid to improve the aqueous processing rate of slag-CO_2 sequestration. Aqueous leaching and carbonation tests conducted on steelmaking slags showed the rates of these processes and the effects of carbonic anhydrase enzyme. A paper containing the methods, results, and analysis has been written for Hydrometallurgy and is contained in Paper 4. The results are summarized below.

The amount of calcium leached is a strong function of particle surface area, which is a more important factor than calcium oxide content. BOF slag exhibited a calcium-leaching rate of approximately five times that of LMF slag, though it had 80% of the calcium content. The higher leaching rate occurs because BOF slag had 8.7 times the specific surface area in the raw state. EAF showed an increase in calcium leached similar to that of LMF slag. Carbonic anhydrase did not affect the leaching rate. A low amount of magnesium was leached for all slags, and BOF/EAF slags showed negligible amounts of iron leached. The specific surface area increased from 15-40 times from leaching and BOF particles exhibited the most extensive leaching depth. All leaching curves exhibited similar trends. The extent of calcium leaching as a function of time and particle size can be expressed by a simple mathematical relationship.

Carbonic anhydrase catalyzed the reaction between calcium oxide and carbon dioxide in water, resulting in a 50% decrease in neutralization time. A 66.6 nM concentration of BCA reduced the neutralization time to near the theoretical rate. Similar reductions in neutralization time were also observed for all three slags. Carbonic anhydrase modified the structure of the precipitating layer on the slag particles from an overlapping block structure to a dendritic morphology with smaller particles by increasing the nucleation rate of the precipitating particles at the expense of the particle growth.

The rate of carbonation is a strong function of pH. Time controlled tests in which the pH dropped to ~six resulted in a decreased amount of carbonate produced for a given time. Comparison of the results to the carbonate speciation predominance diagram in Figure 2.9 (for 25°C and 1 atm.), shows that the carbonate (CO_3^{2-}) ion has negligible concentration at low pH, so carbon dioxide would be taken from any calcium carbonate present to maintain equilibrium with aqueous carbon dioxide. This decrease in carbonation amount with time was accelerated by carbonic anhydrase because it accelerates the reversible hydration of carbon dioxide. Thus, it will accelerate the system towards equilibrium from whichever side. If the pH drops to a level at which carbonate dissolution would be necessary to reach equilibrium, the enzyme will accelerate that dissolution.

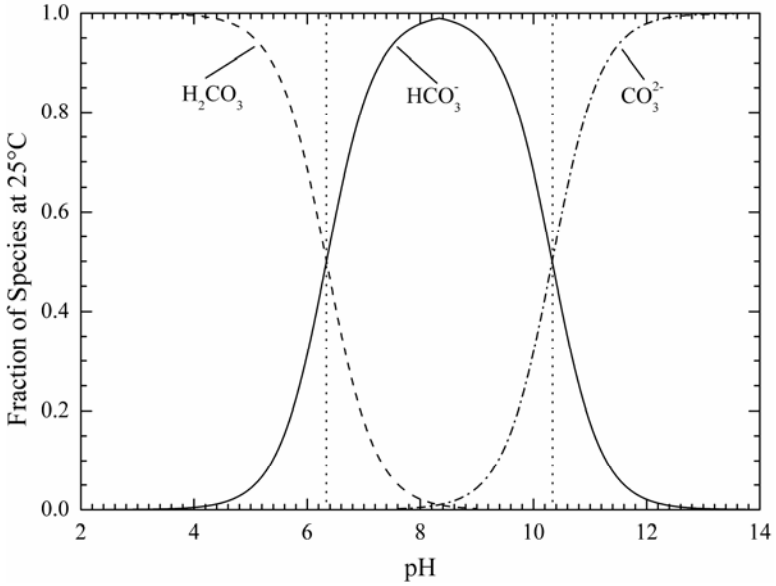

Figure 2.9. Carbonate species predominance diagram based on solution pH

Tests in which the pH was maintained at greater than 8.5 (with a buffer) exhibited the highest rates of carbonation, even compared to all previous testing, as shown in Figure 2.10. The carbonate ion is present at pH>8.5 and dominant at pH>10.33. As pH increases, so does calcium carbonate formation rate, but even at >8.5 pH the resultant carbonation rate was 16 wt.% at 13.25 minutes (BOF slag at 100 μm particle size).

Extrapolation of the curve fit for carbonation shows that 47 wt.% carbonation would be achieved by BOF slag at 100 μm particle size at 24 hours in a batch reactor. As the leaching rate was found to be ~50% faster than the carbonation rate, a further increase in carbonation can be realized by using carbonic anhydrase, assuming the pH is at >10.33.

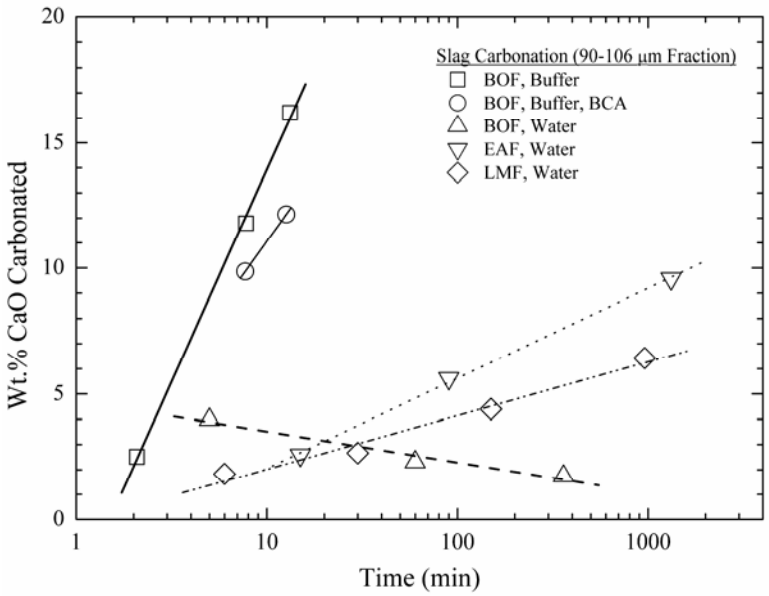

Figure 2.10. Comparison of time controlled and pH controlled slag carbonation results

According to the carbonation results, as long as the system pH stays above 8.5, the slag system can process 151 kg carbon dioxide per ton of slag in a 24-hour period, which is 47% of the slag theoretical calcium carbonate capacity. On a per hour basis, the amount of carbon dioxide sequestered is 0.4% of that emitted per ton of steel produced for BOF production. As a first-order approximation, assuming the carbonation rate is proportional to leaching activity, the pH-controlled process should sequester 1.8% of the carbon dioxide emitted from EAF steelmaking. Under the same conditions, LMF slag can add another 0.1% and 0.6% to the sequestration amounts for BOF and EAF mills, respectively. BOF and EAF slags will achieve approximately 50% stabilization in 24 hours, while LMF slag should reach the same amount in five days.

2.6. COMMINUTION ANALYSIS

In the aqueous processing study of slag-CO_2 sequestration, carbonate conversion was shown to be strongly dependent upon particle size. Reducing the particle size through grinding exposes more surface area for leaching or carbonation and removes the product layer to expose fresh Ca and Mg bearing phases. Raw slag contains particles up to several inches in diameter but the results of the carbonation modeling show that to achieve efficient CO_2 sequestration the particles may need to be reduced to <100 μm through grinding. Because mineral comminution is energy intensive, there are concerns that slag grinding may nullify the CO_2 sequestration benefit in both direct cost and indirect CO_2 generation (e.g., CO_2 emitted from the electric generation source). To characterize the comminution energy for steelmaking slag, a separate study was conducted to measure slag grindability using the Bond Work Index method. Details of the test method and results were published in the Proceedings of the 2008 SME Annual Meeting and Exhibit[100], which is listed in Paper 5.

The grindability study was conducted on BOF, EAF, and LMF slags in a batch ball mill at 106 μm grind size. The resulting Work Index values ranged from 13.8-24.9 kWh/st, with an average for all slags of 19.9 kWh/st. BOF slag exhibited the highest Work Index at 22.2 kW/st, followed by EAF and LMF slags at 20.2 kWh/st and 16.8 kWh/st, respectively. In comparison, dolomite and silica have Work Index values of 13.9 kWh/st and 23.8 kWh/st, respectively.

The Work Index and slag physical properties were used to determine the energy consumption of a slag comminution system. A dry comminution system using a cone crusher, ball mill, and vibrating screen were modeled using METSIM software for three slag types across a range of grind sizes (P_{80}). The method and analysis of this model are contained in a paper accepted for publication by AIST Transactions, which is reproduced in Paper 6 of this dissertation.[101]

All slags showed increasing comminution power consumption with decreasing P_{80}, and increased sharply below 200 μm. The crushing power requirement ranged from 1-7% of the total power and the remaining power (93-99%) consumed by ball mill grinding. Comminution optimization, therefore, should focus on the grinding process. On a normalized mass throughput basis (kWh/tonne), the decreasing order of power

consumption was BOF, EAF, and LMF slag. At a 50 μm grind size, these three slags consumed 43.5 kWh/tonne, 40 kWh/tonne, and 34 kWh/tonne, respectively, which dropped to 8 kWh/tonne, 8 kWh/tonne, and 7.5 kWh/tonne, respectively, at a P_{80} of 1000 μm.

The amount of CO_2 generated at the power supply source was calculated by applying an emission factor (kg/kWh) obtained from the U.S. Environmental Protection Agency to the grinding power consumption. The amount of CO_2 captured by the slag at each grind size was calculated using the two-stage reactor sequestration model detailed in Paper 3. The resulting CO_2 balance for each slag is represented graphically, such as in Figure 2.11. For EAF slag, this graph shows the amount of CO_2 captured, the amount of CO_2 emitted by the electric supply source (as a negative sequestration value), and the net CO_2 sequestered. Similar graphs are shown for BOF and LMF slags in Paper 6.

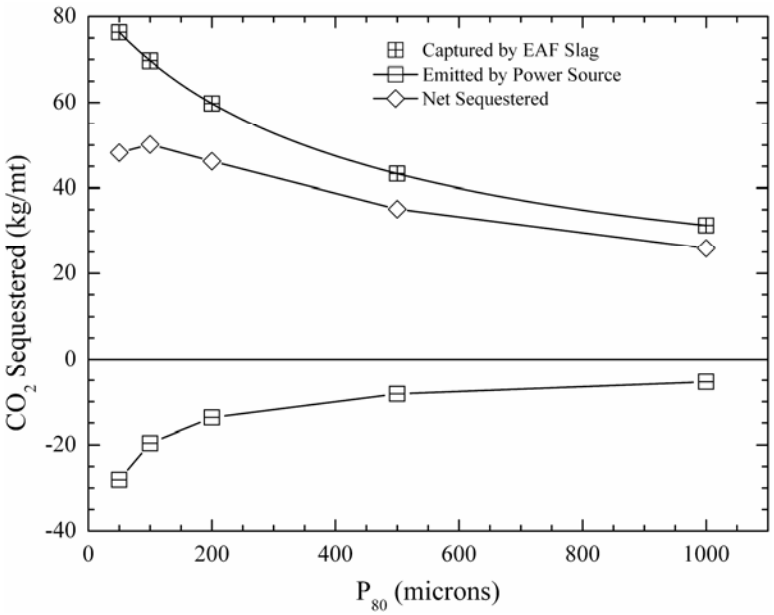

Figure 2.11. Net carbon dioxide sequestered (slag capture-power source emission) for EAF slag versus grind size (P_{80})

All slags showed net positive CO_2 sequestration benefits based on slag-CO_2 capture and CO_2 generation at the power supply source. While the peak net sequestration

values are ~20% of the theoretical values due to the low kinetic reaction rate, the net amount of CO_2 sequestered is positive, indicating that slag grinding has positive environmental value.

2.7. METAL LIBERATION ANALYSIS

Recovery of metal (steel) from the slag was investigated as a means of offsetting the cost of slag grinding. Slag is typically processed at steel mills by large-scale crushing, screening, and magnetic separation. Large particles (>1.25 cm) of metal are recovered by the slag processor and sold back to the mill. The processed slag, however, still has a significant metallic content, but the metal is distributed in small particles throughout the slag. When the slag is ground for CO_2 sequestration processing, the metal particles are liberated and can be recovered by magnetic separation. The quantity and distribution of the particles are not well documented, so size-by-size recovery of the metallic particles was undertaken using grindability tests.

The procedures for separating of the magnetic content and quantifying the magnetic fraction are detailed in the Paper 5, which was published in the Proceedings of the 2008 SME Annual Meeting and Exhibit.[100] All slag fractions >106 μm ranged from 14-21 wt.% magnetic content, while the <106 μm fraction had less than 4 wt% magnetic material. Overall >91% of the magnetic particles were >106 μm, confirming that grinding to this size should be sufficient to liberate most of the metallic fraction from the slag. EAF slag had the lowest amount of material >106 μm (86.6%), due to fine steel droplet break-up caused during slag foaming. LMF slag had the largest amount >106 μm (95.6%), and is produced using a less turbulent process than the supersonic jets used to produce EAF or BOF slag. The lower turbulence leads to the generation and entrainment of fewer fine steel droplets in the slag. EAF and BOF slags have over twice the amount of magnetic material available for recovery than LMF slag.

The grade of the magnetic fraction after crushing was quite good (89 wt.% of the material was reported as metallic). However, the grade of the magnetic fraction after grinding was lower in metal content (68 wt.% of the material was reported as magnetic). The lower grade was caused by the higher surface area of the fine material, which leads to a higher amount of oxidized iron, in addition to incomplete liberation of the metal from

the slag. Based on the average amount of material recovered through magnetic separation during grinding, the overall amount of metallic material recoverable from ground slag is estimated to be 5 wt.% of the total slag ground. Similar analysis yields the overall amount of metallic material recoverable from crushed slag of 1.2 wt.%.

The amount of recoverable metal was factored by slag type into an overall valuation model for the slag grinding process. Input from power consumption, net CO_2 sequestration, and metal recovery for each slag type were multiplied by their respective commodity prices, then summed to give the operating cost. Equipment capital costs were not factored into this analysis. The results of the model are given in the AIST Transactions paper in Paper 6.[101] The valuation analysis resulted in peak curves for all slags. EAF and BOF slags exhibited sharp maximum net values ($7.25/tonne and $6.25/tonne) at 110 μm and 120 μm, respectively, with rapid value decreases at larger or smaller sizes due to increased grinding cost or decreased metal recovery. LMF slag exhibited much less sensitivity to grind size, only varying ~3% from its peak value ($5.75/tonne) at a size of 370 μm over most of the studied range. In terms of the overall valuation, metal recovery is the most significant factor. The magnitude of its value is 3-10 times the magnitude of power consumption. Carbon dioxide credit/value is not a primary factor in direct economic valuation of the process.

PAPER

1. Sequestration of CO_2 from Steelmaking Offgas by Carbonate Formation with Slag

C. Hank Rawlins, Von L. Richards, Kent D. Peaslee, Simon N. Lekakh

Missouri University of Science and Technology
Department of Materials Science and Engineering
Rolla, Missouri 65409
Tel.: 574-341-4714
E-mail: kpeaslee@mst.edu

Key Words: Steelmaking Slag, Offgas, Carbon Dioxide, Sequestration, Phase Stability, Reaction Kinetics

Published in the Proceedings of AISTech 2006, Volume II, and edited for this dissertation.

INTRODUCTION

The alkaline earth-containing phases in steelmaking slag can form carbonates thus sequestering carbon dioxide from the surrounding atmosphere. Work has been undertaken to improve the carbonate formation kinetics, enabling steelmakers to remove CO_2 from furnace offgas with slag, which in turn reduces the slag stabilization time. A study of basic oxygen furnace (BOF) and electric arc furnace (EAF) slags is reported in conjunction with their carbonate formation thermodynamics and capacities, yielding an overall slag CO_2 capture potential. Preliminary results are presented from bench-top "wet" and "dry" slag carbonation tests on industrial slags using a slurry reactor and large-scale thermogravimetric analysis (TGA).

CO_2 EMISSIONS IN STEELMAKING

In response to political demands, carbon dioxide has been targeted as a key industrial emission requiring regulation and control. As a key industrial sector relying on carbonaceous material for operation, the steel industry worldwide will be affected by these regulations. The regulation of carbon dioxide as an emission in the steel industry must be based on an understanding of the sources, amounts, and variations of the generation of this gas. Control methods can be put in place to target specific sources and sized to handle the amounts and variations involved. Carbon dioxide can be generated directly through iron or steel processes (blast furnace or BOF), or through indirect means (coke ovens or coal burning power plants providing electricity to EAF). Each of these sources requires a specific means for regulation and control, which also must be viewed in relation to the entire steelmaking route. A comparison of CO_2 emissions based on geographic regions and steelmaking technologies can be made from published data.

Stubbles provides trends of U.S. domestic steel industry energy use and CO_2 emissions.[1] Technological evolution has reduced the required energy per ton of steel from 47.4 GJ (45 million BTU) in 1950 to 17.9 GJ (17 million BTU) in 2000. Carbon dioxide emissions, stated in terms of carbon equivalent (CE) units (0.27 x tons CO_2), have only been tracked since 1990, but they exhibit a similar trend to the reduction in energy use.

Integrated mills produce more CO_2 than mini-mills because of their reliance on coke making and blast furnace ironmaking. In the year 2000, integrated mills produced 33.46 million tons of CO_2 (CE units), of which 64% (21.47 million tons) came from the production and use of coke. Mini-mills produced 13.65 million tons of CO_2 (CE units), of which 80% (10.86 million tons) came from electrical production at the power plant. On average the U.S. steel industry produced 0.42 carbon equivalent tons of CO_2 per ton of steel shipped in 2000.

Carbon dioxide emission data from the steel industries of several other countries are available from the literature. Afonin provides data for the steelmaking sector in Russia.[2] Based on 1998 data, the total CO_2 emissions from integrated steelmaking stands at 48.6 million tons carbon equivalent, which is 8.5% of all Russian CO_2 emissions. On an intensity basis, this equals 1.4 tons CE per ton of steel produced. Data from Birat et al. show that in 1989 the French integrated-steel industry produced a total of 26.3 million metric tons of CO_2 total at an intensity of 0.42 tons CE per ton steel.[3-6] This is comparable to the U.S. emission rates of 2000. By 1994, the CO_2 intensity had dropped in France to 0.40 tons CE per ton steel, which is approaching the theoretical limit. France reported an extremely low CO_2 emission rate of 0.03 tons CO_2 per ton of steel for EAF steelmaking with 100% scrap, due to their high reliance on nuclear power. Holappa reports data from Finnish ironmaking that can be used to estimate the carbon dioxide intensity for that region, which is approximately 0.53 tons CE per ton of steel for integrated steelmaking.[7] Data from Emi and Gielen show that the 2005 carbon intensity rate for Japanese integrated steelmaking is 0.46 tons CE per ton of steel.[8,9]

Anderson et al. reported the results of a study comparing the carbon dioxide emissions and energy requirements for 30 different steelmaking routes.[10] To the BF/BOF baseline of 89% hot metal/11% scrap, they have compared EAF steelmaking using standard and alternative iron sources/steelmaking routes at 80%, 50%, and 30% replacement of scrap. The carbon dioxide emission data from this publication in 2002 for a U.S. basis are shown in Figure 1. The highest CO_2 producer is the traditional BF-BOF route at 519 kg CE per ton of liquid steel. The lowest CO_2 producer is 100% scrap in an EAF at 119 kg CE per ton of liquid steel (CE/t LS). All other processes fall between these boundaries. As the amount of scrap blending is increased, the carbon dioxide production

decreases. Comparison of data from Goodfellow et al. on 100% scrap in an EAF shows that the indirect sources produce almost 70% of the CO_2 generated, with the largest fraction from electricity generation.[11,12] These authors showed that U.S. EAF production with 100% scrap produces 140 kg CE/t LS (compared with 119 kg CE from Anderson) due to the high fraction of electricity supplied from hydrocarbon combustion sources (69%). However, on the same basis, Canadian EAF's generate 89 kg CE due to the lower fraction of electrical supply from hydrocarbon fuel (32%), and French EAF's generate 46 kg CE due to an even lower reliance on hydrocarbon-based fuels (5%).

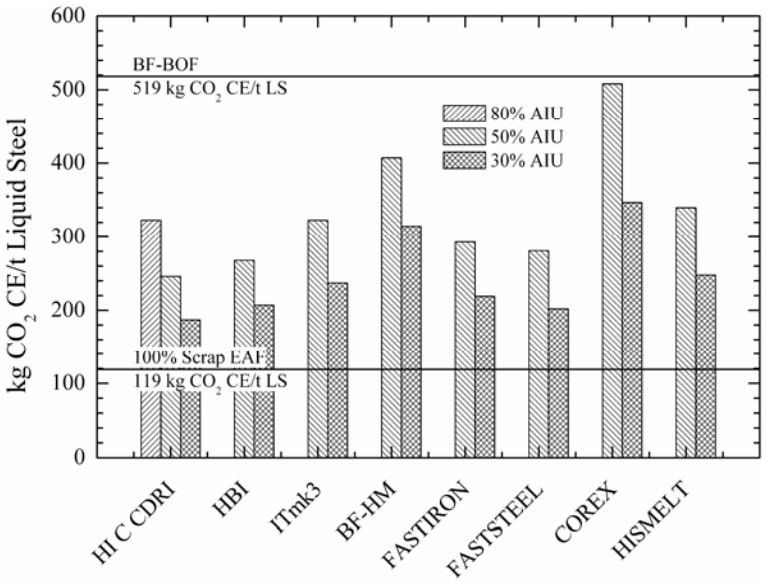

Figure 1 CO_2 emission amount (carbon equivalent tons per ton of liquid steel) for EAF steelmaking with 30%, 50%, and 80% addition of alternative iron units (AIU) to scrap, data from Anderson 2002[10]

The composition of steelmaking offgas changes during the stages of the steelmaking heat, such as charging, blowing, refining, and tapping. Knowledge of composition variation is necessary for feedback control and mitigation technologies. Evenson et al. reported on an expert system relying on feedback control from offgas analysis in EAF operations.[13] Sampling probes installed at the entrance to the fixed duct after the combustion gap and at the end of the water-cooled duct downstream of the

combustion chamber provide real time composition analysis. For an average of 30 heats, the concentration averages upstream and downstream, respectively, were 22.7±2.4% and 10.3±1% for CO_2, 21±2.5% and 0±0% for CO, 0.6±0.5% and 11.3±0.7% for O_2, and 8.1±1.2% and N/A for H_2. This data is reported for an upstream flow rate of 15900 Nm^3/hr (9358 SCFM) and a downstream flow rate of 68400 Nm^3/hr (40259 SCFM), yielding a dilution flow ratio of 4.3. Grant reports EAF offgas data from a U.S.-based shop (location not specified) in his work with post-combustion optimization.[14] The offgas composition profile at the inlet of the fixed duct just after the combustion gap (same upstream location as Evenson et al.) for a period of 15 heats shows that the CO_2 average is a little lower (~15%), the CO average is similar (~18%), the O_2 value is higher (~4%), and the H_2 average is similar (~6%). The high downstream O_2 value shows less combustion of the CO.

The current project has worked to establish an understanding of the CO_2 concentration in offgas for the design and placement of a sequestration system. The concentrations of CO_2, CO, H_2, and O_2 were measured using a water-cooled probe placed in the offgas ducting just after the combustion gap (pre-combustion) of a northeastern U.S. EAF shop. The data was analyzed for 10 heats, and the concentration of CO_2 in the offgas during the stages of one heat is shown in Figure 2. The carbon dioxide content approached zero during charging when the roof was moved to the side and the offgas did not flow through the duct. During the melting phase, CO_2 concentration averaged 20-25% from the combustion of natural gas in the oxy-fuel burners and other sources of carbon in the charge. The CO_2 concentration reached its highest peak of 30-35% during the oxygen blow from the combustion of dissolved carbon and carbon injected into the slag. The average CO_2 concentration across the entire heat is about 18%, which corresponds well with the values shown by Evenson and Grant.[13,14] Remarkable consistency was shown for the 10 heats with peak CO_2 concentrations averaging 30-35% and an overall average at 18-20%.

Combining the concentration data in Figure 2 with the temperature profile and operation of the offgas system yields the estimated CO_2 concentration at the discharge point (stack). The fourth-hole combustion zone operates at 1760°C and after dilution, the offgas is cooled to 450°C. Based on the heat capacity of air, and assuming full

combustion of CO to CO_2, the peak carbon dioxide concentration drops to 14-15% with an average to 6-7%. Further dilution and quenching is required to drop the offgas temperature to 90°C for discharge through the baghouse. The carbon dioxide concentration in the stack discharge is 10-11% peak and 4-5% average. A CO_2 capture and sequestration system will most likely be installed after the baghouse to prevent dust contamination. Therefore, the final discharge values must be considered for the design. These values are significantly higher when compared to the CO_2 concentration of 350-370 PPM in ambient air.

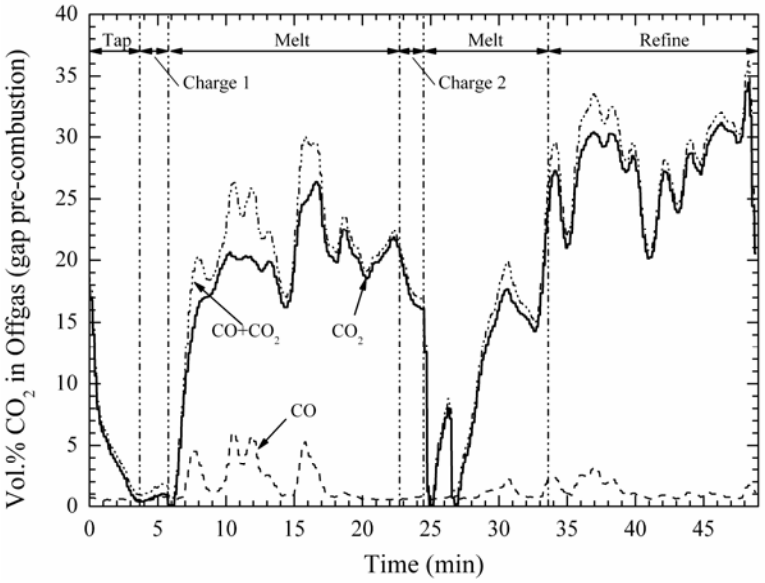

Figure 2 CO_2 concentration (volume %) measured in the offgas collection system at the 4th hole gap prior to combustion during stages of a heat (data from NE U.S. EAF shop)

Analysis of the steelmaking process shows that energy conservation provides the most cost effective method for reduction of CO_2 emissions. Energy conservation minimizes the direct CO_2 sources (less combustion of carbon) and indirect sources (reduction in electricity). The U.S. has focused on energy reduction as a primary goal, which will, in turn, reduce CO_2 emissions. These reductions will mostly be realized from indirect sources as the U.S. relies heavily on hydrocarbon fuels for electrical generation (69%). In Stubbles' analysis of the history of energy reduction in the U.S. steel industry,

he found that the drive towards near net shape final products has provided the largest energy savings. Continuous casting and thin slab casting have reduced energy consumption from 36.9 GJ/t to 21.1 GJ/t (35 million BTU/t to 20 million BTU/t). The move towards strip casting and closure of inefficient facilities should drop the industry amount to 14.8 GJ/t (14 million BTU/t) by 2010.[1] In addition, the data from Anderson et al. clearly shows that steel production from scrap provides the lowest amount of CO_2 emissions and energy requirement.

Alternative iron and steel making technologies will also provide reductions in carbon dioxide emissions, primarily through energy reduction, but also through operational changes. Europe and Japan have undertaken proactive research initiatives for the purpose of reducing carbon dioxide emissions, and in some cases, to develop carbon-free steelmaking. Most of the research involves the use of new technologies to replace or augment the traditional blast furnace ironmaking. Emi lists injection of pulverized coal, plastic, and LNG, as well as increased blast temperatures and decreased moisture, as current technologies to reduce CO_2 emissions by up to 23% in Japanese iron making.[8] Alternative iron technologies, such as ITmk3® and HIsmelt®, may provide further 20-25% reduction but are still in development. Birat lists several carbon-free technologies being proposed, but they are many years from large-scale commercial development.[7] These technologies include hydrogen reduction and direct electrolytic production of iron. Both technologies require a source of electricity that is not hydrocarbon-based, in order to provide a net reduction in CO_2 emissions. In all cases, recycling is being researched as the most powerful method of reducing CO_2 emissions for the material community as a whole. This includes use of the steel scrap in the EAF and use of the slag to offset the limestone used in cement production.

Sequestration technologies provide direct reduction in CO_2 emissions and will be effective at specific source point mitigation where further energy or technological changes cannot be made. At the present time, most sequestration technologies provide a negative cost impact to the steel producer. If CO_2 regulations develop to the point where emission credits are bought and sold, then the cost-benefit of installing a sequestration technology versus paying an emission penalty will be weighed. The current research project seeks to develop a cost-effective sequestration technology using slag, which is

available in plentiful amounts at the steel plants, to permanently sequester carbon dioxide. A side benefit is that the formation of carbonates in slag will render the slag immune to *in-situ* swelling or leaching, thus stabilizing it for immediate commercial use.

SLAG CHARACTERIZATION

The potential of steelmaking slag to react with CO_2 to form permanent carbonate minerals (sequestration) is derived from slag's high concentration of alkaline earth metal oxides. Two alkaline earth metal oxides in sufficient quantity to sequester CO_2 are CaO and MgO. These oxides report to the slag from the fluxing agents used during steelmaking, which are primarily standard and dolomitic lime or limestone. Table 1 shows the composition of nine slags surveyed in this project. Six sites are represented (A1, B1, C1, D1, E1, and E2), with multiple EAF slag samples taken at some sites. In addition, at site A1 an LMF sample was taken for comparison.

The sequestration potential of a slag can be determined from the formation reactions with carbon dioxide at ambient conditions (1 atm, 25°C). Both CaO and MgO exhibit a negative ΔG°_{f} in the reaction with CO_2, and thus they readily form carbonates. The other major phases (SiO_2, FeO/Fe_2O_3, Al_2O_3, and MnO) are inert to spontaneous reactions with carbon dioxide, and thus they are precluded from the sequestration potential. Both K_2O and Na_2O will readily form carbonates, but neither is present in sufficient quantities to be significant. Both CaO and MgO react with CO_2 in a 1:1 molar combination to form $CaCO_3$ and $MgCO_3$, respectively. On a weight basis, 1000 kg of CaO will capture 785 kg of CO_2, which can be expressed as 214 kg CE units. Using the same basis, 1000 kg of MgO will capture 1092 kg of CO_2, or 298 kg CE units. Using the average values for CaO and MgO of 34.41% and 11.71%, respectively, from Table 1, 1000 kg of steelmaking slag has the potential to sequester 398 kg of CO_2, or 109 kg CE units. The National Slag Association estimates that per metric ton of steel produced, BOF operations generate 75-150 kilograms of slag, while EAF operations generate less at 65-80 kilograms.[15] Combining this with the carbon emission values from Anderson et al. of 519 kg CE/t LS for BF-BOF steelmaking and 119 kg CE/t LS for 100% scrap EAF will yield the overall effective yield potential. At these values, the slag produced per ton of

liquid steel can sequester 2.4% of BF-BOF and 3.3% of EAF carbon dioxide emissions. Segregating the slag types in Table 1 (EAF or BOF) and using the average values for their respective processes yields an average carbon equivalent sequestration potential of 2.7% for BF-BOF and 3.2% for EAF.

Table 1 Composition of nine steelmaking slags surveyed in this project

	A1α	A1β	A1γ	B1α	C1α	D1α	D1β	E1α	E2α	Avg.*
Type	EAF	EAF	(LMF)	BOF	BOF	EAF	EAF	EAF	EAF	-
CaO	27.34	31.22	47.02	40.90	40.53	33.02	34.49	31.91	35.86	34.41
SiO_2	14.84	13.86	6.07	12.89	10.42	12.43	15.08	17.32	9.93	13.35
FeO	30.05	24.96	5.02	21.72	21.65	27.93	25.76	20.20	27.98	25.03
MgO	10.55	11.61	10.03	11.98	13.81	10.98	11.76	12.85	10.13	11.71
Al_2O_3	7.02	8.61	26.55	5.22	6.65	8.74	5.56	6.79	9.22	7.23
MnO	6.51	6.07	1.04	4.67	4.50	3.98	4.85	7.07	4.29	5.24
TiO_2	0.39	0.42	0.41	0.68	0.47	0.50	0.55	0.49	0.49	0.50
ZrO_2	<0.01	0.03	0.20	0.08	0.28	<0.01	<0.01	0.16	0.02	0.08
Cr_2O_3	2.48	1.98	0.25	0.31	0.42	0.87	0.78	1.62	0.95	1.18
K_2O	0.05	<0.01	<0.01	0.01	<0.01	<0.01	<0.01	<0.01	<0.01	0.02
Na_2O	<0.1	<0.1	<0.1	<0.1	<0.1	<0.1	<0.1	<0.1	<0.1	0.10
S	0.16	0.27	1.35	0.12	0.11	0.21	0.08	0.22	0.30	0.18
P	0.16	0.16	0.02	0.42	0.45	0.25	0.32	0.18	0.28	0.28
C	0.11	0.26	0.38	0.67	0.40	0.22	<0.1	0.32	<0.1	0.27
Sr	<0.01	<0.01	<0.01	<0.01	<0.01	<0.01	0.01	<0.01	<0.01	<0.01
F	0.33	0.54	1.66	0.33	0.33	0.87	0.75	0.86	0.55	0.57

* The average of all slags except A1γ, which is from the LMF at an EAF mill

These estimates are based on full conversion to carbonate at ambient temperature and pressure, assuming pure CaO and MgO in the slag reacting with an atmosphere carbon dioxide at unity partial pressure (pCO_2=1.0). These estimates represent the thermodynamic potential. A system designed for reacting slag with offgas CO_2 will deviate from most all of these assumptions. The offgas stack temperature for the data in Figure 2 is 90°C, but in some plants this may increase to 150°C. The total gas pressure will be at ambient conditions (1 atm.), but the partial pressure of CO_2 will be in the range of 4-11% (pCO_2=0.04-0.11 atm). Steelmaking slag contains only a few percent of free lime or magnesia, and thus these compounds cannot be considered in the pure state.

Predominately the CaO and MgO will form silicate, aluminate, or ferrite phases. The results of XRF analysis showed that the slags listed in Table 2 contain dicalcium silicate and larnite (Ca_2SiO_4), akermanite ($Ca_2MgSi_2O_7$), C_5MS_3 ($Ca_5MgSi_3O_{12}$), $C_{12}A_7$ ($Ca_{12}Al_{14}O_{33}$), clinoenstatite ($MgSiO_3$), magnesio-wustite ($MgFeO_2$), hatrurite (Ca_3SiO_5), periclase (MgO), and lime (CaO). Small amounts of free alumina, wustite, and silica have been found, but these do not contribute to carbon dioxide sequestration.

The ability of specific phases in steelmaking slag to sequester carbon dioxide into stable carbonates under non-ideal conditions can be expressed in the phase stability diagram shown in Figure 3. Each line shown, generated from data in FactSage™ 5.4, represents the reaction of a slag phase to form a carbonate versus temperature and equilibrium partial pressure of carbon dioxide (pCO_2). For example, the bottom line labeled "CaO" represents the reaction $CaO+CO_2 \rightarrow CaCO_3$. The top line similarly represents the reaction $MgSiO_3+CO_2 \rightarrow MgCO_3+SiO_2$. Above each line the carbonate is stable (i.e., reaction proceeds to the right), and correspondingly below each line the oxide is stable (i.e., reaction proceeds to the left). As the temperature increases (right to left), the carbonate stability region for each phase shrinks. Therefore, at high temperature the carbonates will decompose to form oxides. The concentration of CO_2 in the atmosphere surrounding the slag also affects the carbonate stability. As pCO_2 increases, the carbonate becomes more stable, thus requiring a higher temperature to calcine the material. For example, magnesite ($MgCO_3$) decomposes to magnesia (MgO) at 210°C in ambient air (pCO_2=350 PPM), but if it is placed in a pure CO_2 atmosphere (pCO_2=1), then it does not decompose until 389°C.

The sequestration of carbon dioxide by slag operates opposite to calcining. When calcining limestone, carbon dioxide is driven off in the clinker by the application of heat. To capture CO_2 in lime or in other slag phases lower temperatures favor thermodynamic stability. At ambient conditions (25°C, pCO_2=350 PPM), all phases listed in Figure 3 are stable as carbonates, and thus the slag will spontaneously react to sequester CO_2. However, the major hurdle to slag sequestration is that the reaction kinetics are extremely slow. Some states require steelmaking slag to stabilize in stockpiles for three to six months prior to use.[16,17] The limiting rate step in slag carbonation is the diffusion of the CO_2 into the slag particles. The CO_2 diffusion rate can be improved by increasing the

reaction temperature. However, an upper boundary is set by the phase stability of carbonate formation. The gray shaded region in Figure 3 shows the pCO_2 operating region exhibited by the stack offgas, as calculated from Figure 2 data. The lower limit is 350 PPM, which is the approximate ambient CO_2 concentration. The upper limit is 11%, with an average of 4%. As pCO_2 increases, the allowable reaction temperature for carbonate formation also increases. Thus, considering a slag containing clinoenstatite ($MgSiO_3$), under ambient CO_2 concentration, the carbonate formation reaction can proceed up to 74°C. However, exposing slag to offgas at 11% carbon dioxide increases the allowable reaction temperature to 168°C. An analysis of the slag phases is critical to the sequestration system design to determine the maximum allowable temperature to allow carbonate formation while enhancing reaction kinetics.

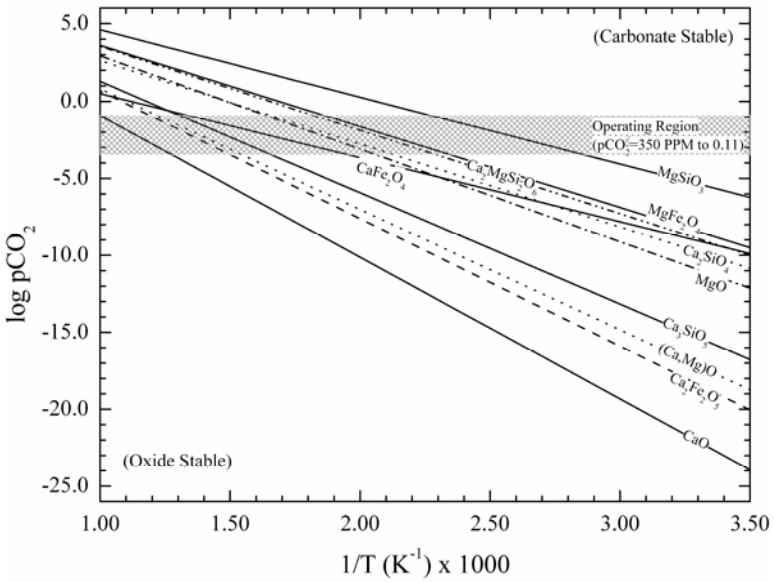

Figure 3 Carbonate stability diagram for alkaline earth metal oxide phases found in steelmaking slag (data generated from FactSage™ 5.4)

The objective of the current project is to develop and demonstrate a process for sequestering CO_2 from steelmaking offgas by forming carbonates with the alkaline earth oxide-containing phases in slag. To achieve this result, the process kinetics of the carbonate formation reaction must be improved to allow the design of a commercially

feasible reactor. This reactor will contact stack exhaust gas with fresh or minimally processed slag allowing rapid sequestration of the CO_2 and stabilization of the slag.

CARBONATE FORMATION IN STEELMAKING SLAG

Two different reactor design bases (“wet” and “dry”) are proposed for contacting slag and offgas. The first basis (“dry”) is a solid-gas contactor with either a plug flow or rotary design. In this system, the stack offgas would be directed through an atmospheric pressure-rated vessel containing slag particles. Only the sensible heat of the offgas would be used to provide a temperature increase of the system. After sufficient reaction time, the carbonated slag is dumped, and fresh slag is input to repeat the process. To allow continuous operation, a plug flow design would use two parallel contacting vessels, and thus while one is dumping/loading the other is reacting. A rotary design would be similar to a cement clinker, with slag particles flowing countercurrent to the offgas. The other basis (“wet”) of design allows for slurry contact, and thus the slag is mixed with water through which the offgas is bubbled. The slurry reactor would require continuous stirring, and thus it could be modeled after a mechanical flotation cell, which allows for intimate gas-solid contact in a water-dispersed system. While a slurry reactor is more complicated for operations, the water addition may be necessary to achieve sufficient reaction kinetics. Both design bases are being investigated in this project through bench-scale testing.

Investigation of the solid-gas contactor design basis is done with a large-scale thermogravimetric analyzer designed for this project. A drawing of the bench-scale TGA is shown in Figure 4. A traditional TGA apparatus is designed to handle samples of just a few grams, but due to the heterogeneous nature of slag, much bigger samples are required. The TGA for this project can handle a gross sample weight of 410g with a resolution of 0.001g. The central chamber is a vertically oriented tube furnace capable of operation to 1100°C. The furnace controller allows a programmable ramp rate (1-100°C/min) and hold time. Samples are suspended in the furnace from a digital balance, which records the sample weight. Samples for gas-solid contact are held in a 304SS mesh basket or by a platinum wire (single particle). Samples for decomposition analysis are

placed in an alumina crucible held by a platinum wire. The digital balance is protected from the furnace heat output through a tortuous path barrier, cross flow fan, and reflective radiation shield. The bottom entrance of the tube furnace contains a gas distribution device through which reaction gases are introduced. Up to three gases can be metered individually or in combination. The gases used in this project are Ar, CO_2, N_2, and air. In addition, the introduced gas can be humidified by bubbling through a heated water column. Weight and temperature data are collected to a computer through a portable data acquisition system.

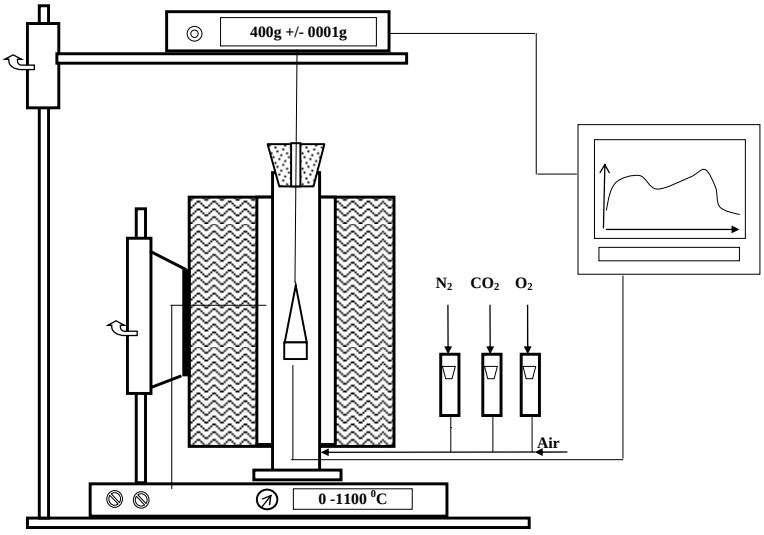

Figure 4 Bench-scale TGA used for slag-CO_2 reaction measurements of gas-solid carbonation kinetics

Baseline testing to determine the effect of temperature and humidity on the carbonation rate was conducted with “Hi-cal” lime obtained from a project sponsor. The “Hi-cal” lime has a composition of 95% CaO, 3% MgO, and 2% SiO_2. Single particles of lime, with an average 1.5 cm equivalent spherical diameter, were suspended into the TGA from a platinum wire holder. The first series of tests were conducted at 200°C, 300°C, 400°C, and 500°C with dry CO_2 (p=1 atm). A second series of tests was conducted at the same temperatures using CO_2 gas humidified through a bubbling column. In each test, the lime single-particle was suspended in the TGA furnace in an Ar

atmosphere while the temperature was ramped to the testing point. Once the temperature reached the desired test point, the particle was held in the Ar atmosphere for one hour. After one hour, the Ar was turned off and the desired CO_2 stream (dry or humidified) was introduced into the furnace chamber. The lime sample was allowed to react with CO_2 for approximately 5.5 hours, after which the Ar stream was reintroduced while the sample cooled to room temperature. A plot of weight percent carbonation versus time for each sample is shown in Figure 5.

Each dry sample exhibited an increase in weight with time as it was allowed to react with CO_2 at the test temperature. The total weight increase at 200°C in dry CO_2 at 5.5 hours was marginal (~1.25%). This corresponds to 2% carbonation. The percent carbonation is defined as the fraction of lime converted to calcium carbonate (assuming only $CaCO_3$ formed). Increasing the temperature to 300°C and 400°C showed incremental increases up to approximately a five weight percent increase for the latter temperature. A test temperature of 500°C in dry CO_2 showed a significant jump to a 13 weight percent increase, which is equivalent to 16.5% carbonation. Increasing the temperature alone has a significant impact on the reaction kinetics by increasing the diffusion rate of CO_2 into the lime particle.

Humidifying the CO_2 provided as significant of an impact as increasing the reaction temperature. The total weight increase at 200°C in humid CO_2 at 5.5 hours was approximately double (2.5%) of that exhibited with dry CO_2. The weight gain at 300°C in humid CO_2 was higher than that with dry CO_2, but not twice as much. The largest difference occurred in humid CO_2 at 400°C, which showed a weight gain of 15%, which is three times that shown for the dry CO_2 at the same temperature. The highest weight gain of 17% occurred at 500°C in humid CO_2, which corresponds to 21% carbonation of the lime sample. Humidification of the reaction gas has a catalytic effect in dramatically increasing the reaction rate between CO_2 and lime.

The catalytic effect of a humid CO_2 stream in reacting with alkaline earth metal oxide-based solids has been noted by several researchers. Both Lackner et al. and Zevenoven et al. noted in their work with serpentine ($Mg_3Si_2O_5(OH)_4$) that humidity greatly increased the percent conversion to carbonate with all other factors equal.[18,19] Hills et al. also reported in their work the importance of humidifying the CO_2 stream with

accelerated carbonation of slag and other cementitious wastes.[20,21] They propose that CO_2 from the air permeates through the solid, which is the diffusion controlled rate-limiting step. The presence of water forms a gel on the lime particle surface into which CO_2 solvates. CO_2 hydrates to H_2CO_3 in the surface gel, which is then ionized to H^+, HCO_3^-, and CO_3^{2-}. The pH in the water drops, thus assisting in the dissolution of the lime. The reaction rate in solution is much faster than between the gas and solid state. In the current project, temperature, humidification, and particle size will be evaluated for their effect on the reaction rate of the industrial slag.

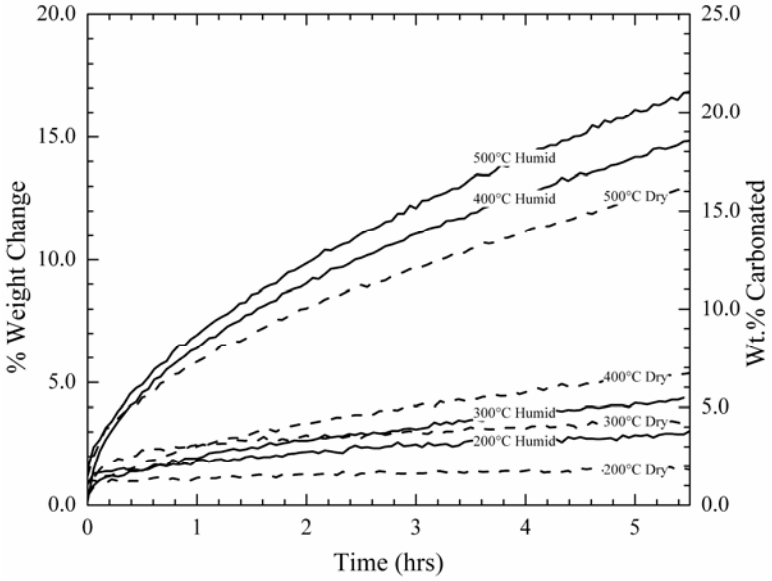

Figure 5 Carbonation rate of Hi-cal lime (95% CaO) in dry and humid CO_2 atmosphere (pCO_2=1) at 200°C, 300°C, 400°C, and 500°C

Investigation of the "wet" process, based on a water-solid-gas reactor design, was done with a bench-scale flotation cell using a two-liter chamber with an internally rotated impeller. The rate of the carbonation reaction was studied under intensive mixing as shown in Figure 6. The rate of slag reaction was compared with the rate of "Hi-cal" lime reaction under the same test conditions. For each test, 50 g of solid material was crushed and graded to <106 μm then mixed with two liters of tap water. Bottled CO_2 was injected into the slurry at a rate of 1460 cm^3/min for a total of two hours (lime only). Periodic

slurry samples of 3-5 g in size were taken, decanted through vacuum filtration, and then dried in an oven. Oven drying took place at 220°C for one hour, followed by calcium hydrate decomposition at 480°C for two hours and calcium carbonate decomposition at 920°C for two hours. These temperatures were chosen based on thermodynamic equilibrium of the CaO-CO_2-H_2O system as determined by FactSage 5.4. Parallel samples were taken and subjected to analysis in the TGA.

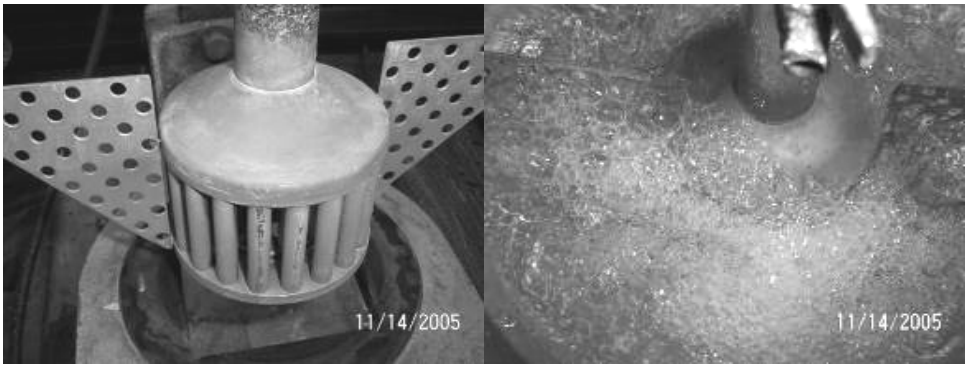

Figure 6 Bench-scale slurry mixer with internally rotated impeller (left) and mixing process with slag-CO_2-water (right)

Three types of materials were tested in the slurry reactor: “Hi-cal” lime, eight of the industrial slags in Table 1, and three synthetic slags produced from reagent grade material in an induction furnace. The compositions of the mixtures used to produce the three synthetic slags are shown in Table 2. The synthetic slag composition was selected to represent a low, medium, and high basicity in slag A, B, and C, respectively. Synthetic slags A and B exhibited a “falling” condition and self-disintegrated into a powder during cooling. This is a result of the $\beta \rightarrow \gamma$ polymorphic transformation of calcium disilicate. Slag C did not exhibit self-disintegration, and thus it was crushed after cooling to produce the same particle size as slags A and B. Each synthetic slag was screened to produce particles <106 μm.

The test results with “Hi-cal” lime are shown in Figure 7. Within the first two minutes, the pH rose from a background level of 5.8 in carbonated tap water to 12 after the addition of lime, indicating a relatively rapid dissolution of CaO and showing the gas-

liquid-solid mixing process was very efficient. A sample taken at this time showed 47% carbonation of the lime and full utilization of the CO_2. At six minutes, the pH stayed at 12 and the percent carbonation jumped to 84%. As the lime consumed the CO_2, the pH and CO_2 efficiency began to drop rapidly. By 20 minutes, both the pH and percent carbonation had stabilized, thus very little further CO_2 was consumed causing the CO_2 efficiency to drop rapidly. Samples taken at 120 minutes showed little change in the percent carbonation and pH, indicating the process had essentially reached completion.

Table 2 Mixture composition of synthetic slags used in slurry testing (by weight)

Component	Slag A	Slag B	Slag C
CaO	40%	49%	56%
FeO	15%	15%	15%
SiO_2	26%	20%	15%
MgO	10%	7%	5%
Al_2O_3	5%	5%	5%
MnO	4%	4%	4%

A similar procedure was used for the evaluation of the slag carbonation rate in the slurry reactor. However, based on the rapid reaction of lime in this process, testing with the slag materials was conducted for only 60 minutes. As an initial comparison of reactivity between the slags to lime, the change in pH with time is plotted in Figure 8.

Slag A1γ (LMF slag) and lime proved to have similar reactivity dropping to just a few percent more than the background pH in five minutes, and reaching the background pH in 30 minutes. Slags D1α, A1α, and A(synthetic), respectively, exhibited decreasing initial pH values, however they all dropped to the same baseline level in 30 minutes. These latter slags are less reactive compared with lime and slag A1γ, showing the CaO/MgO species to be more tightly bound in the slag.

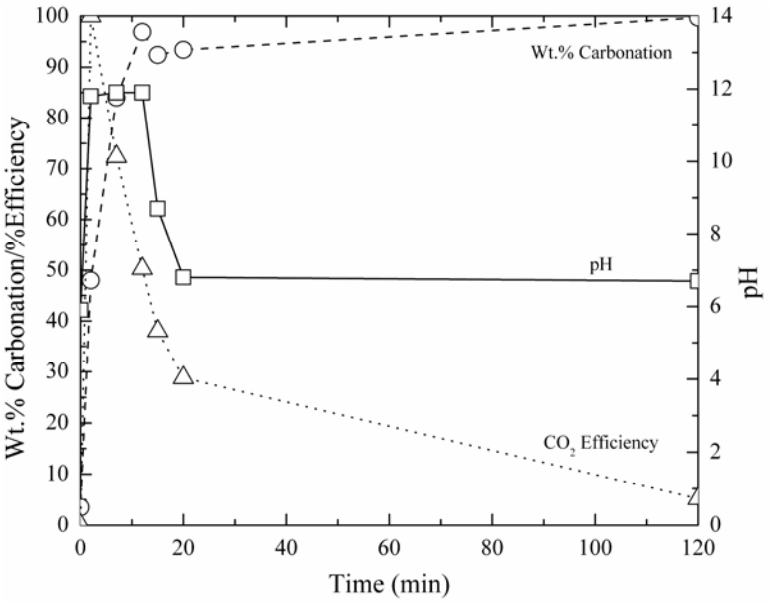

Figure 7 Reaction rate of CO_2 with lime (95% CaO) in gas-liquid-solid slurry reactor process

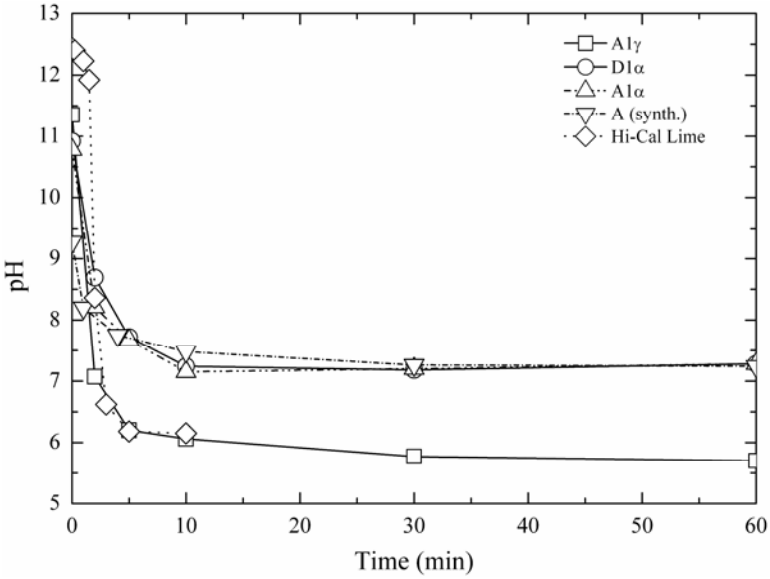

Figure 8 Change of slurry pH with time during reaction of slags and lime with carbon dioxide

The percent carbonation for eight of the steelmaking slags from Table 1 is shown in Figure 9. The results are presented as the percentage of weight loss from calcium carbonate decomposition and as the percent carbonization, calculated in reference to the

calcium concentration in each slag sample. The percent carbonation at 60 minutes varied from zero for slag A1α to a high of 57.5% for slag A1γ. Each sample either reached or approached stead-state carbonation within 10 minutes of starting the reaction indicating good efficiency of mixing and contact in the slurry reactor vessel. The lack of further carbonation after five minutes indicates that the slags become passivated in respect to reacting with CO_2 after reaching a steady state. Future analysis will focus on the analysis of the raw and passivated slag samples to determine the change in surface composition and morphology and the corresponding effect on the diffusion of CO_2 into the slag particle.

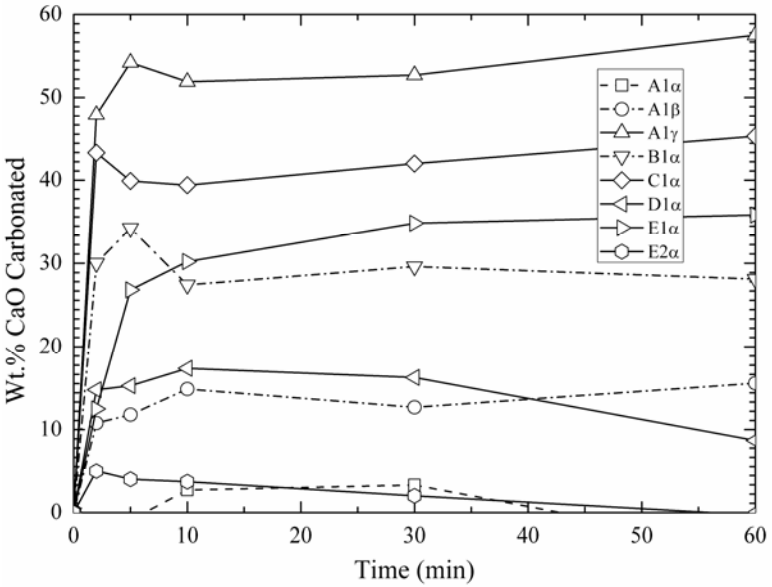

Figure 9 Percent carbonation versus time for eight industrial steelmaking slags in a slag-water-CO_2 slurry reactor

A correlation between the endpoint carbonation percent from Figure 9 and the amount of CaO in each slag is shown in Figure 10. As expected from the thermodynamic calculations, the amount of CaO is proportional to the slag reactivity with CO_2. Phase determination was not undertaken on the samples to determine the amount of free versus combined CaO (i.e., into silicates or ferrites). Two slag samples (A1α and E1α), however, showed no reactivity with CO_2 in the slurry reactor. Phase characterization of the slags

will be undertaken in future work to determine the effect of bulk and surface phase composition on carbonation reactivity.

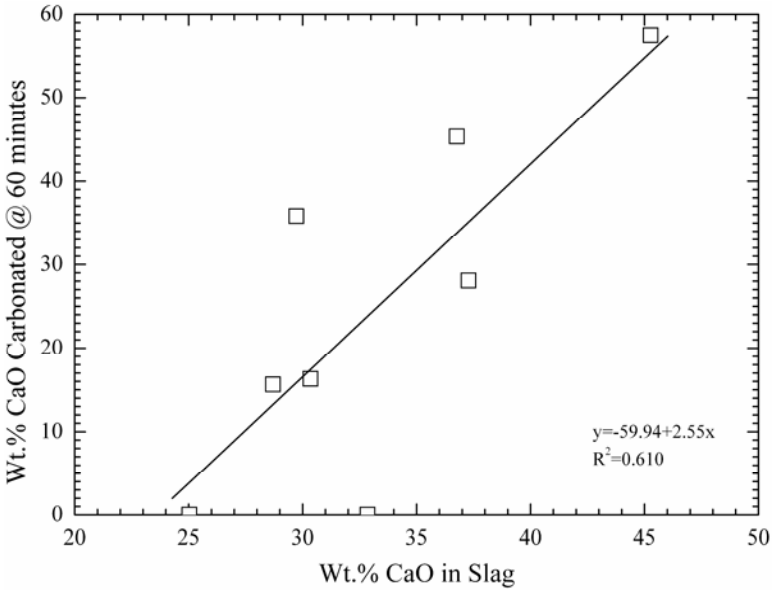

Figure 10 End-point carbonation percent from slurry reaction with CO_2 versus CaO content (weight %) in industrial steelmaking slags

SUMMARY

The results of bench-scale CO_2 sequestration tests by steelmaking slags are presented in this paper. In the “dry” process, the rate of reaction of solid lime or slag increases proportionally to the reactor temperature. However, an upper boundary condition exists, defined by a thermodynamic phase stability diagram that must be identified for each phase in the slag. Tests results showed that the addition of water vapor (humidification) to the CO_2 gas significantly accelerated the carbonation reaction of pure lime. The mechanism of this catalytic effect is possibly defined by the formation of intermediate calcium hydrate gel on the solid particle surface. A “wet” process, which includes the interaction between three phases (water-solid slag-CO_2 gas), has a much higher carbonation reaction rate when compared with the “dry” process. The percent of carbonation statistically correlated to the CaO contents of industrial slags. This data will

be used to determine the design parameters for a lab-scale reactor for CO_2 sequestration by steelmaking slags.

ACKNOWLEDGEMENTS

The authors gratefully acknowledge the support of the U.S. Department of Energy and the American Iron and Steel Institute (AISI) in their direction of this project, and of the individual corporate sponsors—DOFASCO, Gallatin Steel, Hylsa, IPSCO, Mittal Steel, Praxair, Nucor, Timken Company, and US Steel—for their input and support. This paper was prepared as an account of work sponsored by an agency of the United States Government in cooperation with the American Iron and Steel Institute (AISI) and its participating companies under Agreement DE-FC36-97ID13554. Neither the United States Government or AISI nor any agency or affiliate thereof, nor any of their employees, makes any warranty, express or implied, or assumes any legal liability or responsibility for the accuracy, completeness, or usefulness of any information, apparatus, product, or process disclosed, or represents that its use would not infringe privately owned rights. Reference herein to any specific commercial product, process, or service by trade name, trademark, manufacturer, or otherwise, does not necessarily constitute or imply endorsement, recommendation, or favoring by the United States Government, AISI or any agency thereof. The views and opinions of authors expressed herein do not necessarily state or reflect those of the United States Government, AISI or any agency thereof.

REFERENCES

1. J.R. Stubbles. “Carbon dioxide emissions from the U.S. steel industry.” In: *Proceedings of the International Symposium on Greenhouse Gases in the Metallurgical Industries: Policies, Abatement and Treatment; 26-29 August, 2001; Toronto, ON, Canada. Editor: C.A. Pickles.* Montreal, Quebec, Canada: Canadian Institute of Mining, Metallurgy, and Petroleum. pp. 103-116.
2. S.Z. Afonin, Y.S. Yusfin, P.I. Chernousev, and S.V. Murinets. “Energy conservation in ferrous metallurgy.” *Metallurgist*, Vol. 42, No. 7-8, 1999, pp. 292-296.

3. J.-P. Birat, M. Antoine, A. Dubs, H. Gaye, Y. de Lassat, R. Nicolle, and J.L. Roth. "Towards a carbon-free steel production route?" *La Revue de Metallurgie-CIT*, Vol. 90, No.3, 1993, pp. 411-421.
4. J.-P. Birat, J.-M. Delbecq, E. Hess, and D. Huin. "Slag, steel and greenhouse gases." *La Revue de Métallurgie-CIT*, Vol. 99, No.1, 2002, pp. 13-21.
5. J.-P. Birat, F. Hanrot, and G. Danloy. "CO_2 mitigation technologies in the steel industry: a benchmarking study based on process calculations." *Stahl und Eisen*, Vol. 123, No. 9, 2003, pp. 69-72.
6. J.-P. Birat. "CO_2 emissions and the steel industry's available responses to the greenhouse effect." In: *Proceedings of the 59th Ironmaking Conference; 26-29 March 2000; Pittsburgh, PA, U.S. Warrendale, PA, U.S.:* Association for Iron and Steel Technology; 2000. pp. 409-420.
7. L.E.K. Holappa. "Impact of energy and environment on the development of metallurgical processes." In: *Proceedings of the 2nd International Symposium on Metallurgical Processes for the Year 2000 and Beyond; 1994; San Diego, CA, U.S. Editor: H.Y. Sohn.* Warrendale, PA, U.S.: The Minerals, Metals, and Materials Society. pp. 641-660.
8. T. Emi. "Changing paradigm of metal separation technology for steel production." *Scandinavian Journal of Metallurgy*, Vol. 34, No. 2, 2005, pp. 79-88.
9. D. Gielen. "CO_2 removal in the iron and steel industry." *Energy Conversion and Management*, Vol. 44, No.7, 2003, pp. 1027-1037.
10. S.H. Anderson, G.E. Metius, and J. M. McClelland. "Future green steelmaking technologies." In: *Proceedings of the 60th Electric Furnace Conference; 10-13 November 2002; San Antonio, TX, U.S.* Warrendale, PA, U.S.: Association for Iron and Steel Technology; 2002. pp. 175-191.
11. H.D. Goodfellow, M. Thomson, L. Cibert, P. Morere, and E. Evenson. "Overview global warming issues and EAF production." In: *Proceedings of the 56th Electric Furnace Conference; 15-18 November 1998, New Orleans, LA, U.S.* Warrendale, PA, U.S.: Association for Iron and Steel Technology; 1998. pp. 623-627.
12. M.J. Thomson, E.J. Evenson, M.J. Kempe, and H.D. Goodfellow. "Control of greenhouse gas emissions from electric arc furnace steelmaking: evaluation methodology with case studies." *Ironmaking and Steelmaking*, Vol. 27, No. 4, 2000, pp. 273-279.
13. E.J. Evenson, H.D. Goodfellow, and M.J. Kempe. "EAF process optimization through offgas analysis and closed-loop process control at Deacero, Saltillo, Mexico." *Iron & Steelmaker*, Vol. 28, No. 5, 2001, pp. 53-58.
14. M.G. Grant. "Principles and strategy of EAF post-combustion." In: *Proceedings of the 58th Electric Furnace Conference; 12-15 November 2000; Orlando, FL, U.S.* Warrendale, PA, U.S.: Association for Iron and Steel Technology; 2000. pp. 15-28.
15. "Steel slag: A premier construction aggregate." West Lawn, PA, U.S.: National Slag Association. http://www.nationalslagassoc.org/PDF_files/SSPremAgg.PDF, June 2005.
16. Missouri (U.S.). Department of Transportation. "Section 1002: Aggregate for Asphaltic Concrete." Jefferson City, MO, U.S.: Missouri Department of Transportation, June 2005, http://www.modot.org/business/standards_and_specs/nov2004specbook/Sec1002.pdf.

17. P.S. Kandhal and G.L. Hoffman. “Evaluation of steel slag fine aggregate in hot-mix asphalt mixtures.” *Transportation Research Record*, No. 1583, 1997, pp. 28-36.
18. K.S. Lackner, D.P. Butt, C.H. Wendt. “Magnesite disposal of carbon dioxide.” In: *Proceedings of the 22nd International Technical Conference on Coal Utilization & Fuel Systems; 16-19 March 1997; Clearwater, FL,* United States. Editor, B.A. Sakkestad. Gaithersburg, MD: Coal Technology Association; 1997, pp. 419-430.
19. R. Zevenhoven, J. Kohlmann, A.B. Mukherjee. “Direct dry mineral carbonation for CO_2 emissions reduction in Finland.” In: *Proceedings of the 27th International Technical Conference on Coal Utilization & Fuel Systems; 4-7 March 2002; Clearwater, FL,* United States. Editor, B.A. Sakkestad. Gaithersburg, MD: Coal Technology Association; 2002, pp. 743-754.
20. D.C. Johnson, C.L. MacLeod, P.J. Carey, C.D. Hills. “Solidification of stainless steel slag by accelerated carbonation.” *Environmental Technology,* Vol. 24, No.6, 2003, pp. 671-678.
21. M. Fernández Bertos, S.J.R. Simons, C.D. Hills, P.J. Carey. “A review of accelerated carbonation technology in the treatment of cement-based materials and sequestration of CO_2.” *Journal of Hazardous Materials*, Vol. 112, No.3, 2004, pp. 193-205.

2. Kinetics of Aqueous Leaching and Carbonization of Steelmaking Slag

S.N. Lekakh, C.H. Rawlins, D.G.C. Robertson, V.L. Richards, K.D. Peaslee

Department of Materials Science and Engineering
Missouri University of Science and Technology
Rolla, Missouri, USA 65409
Email: kpeaslee@mst.edu

Published in Metallurgical and Materials Transactions B, and edited for this dissertation.

Sequestration of carbon dioxide by steelmaking slag was studied in an atmospheric three-phase system containing industrial slag particles, water, and CO_2 gas. Batch-type reactors were used to measure the rate of aqueous alkaline leaching and slag particle carbonization independently. Four sizes of slag particles were tested for Ca leaching rates in deionized water at a constant 7.5 pH in an argon atmosphere and for carbonate conversion by bubbling CO_2 through an aqueous suspension. Conversion data (fraction of Ca leached or converted to carbonate) were evaluated to determine the rate-limiting step based on the shrinking core model. For Ca-leaching, the initial controlling mechanism is chemical dissolution but as the porous layer develops diffusion becomes the rate limiting step. Carbonate conversion proceeded much more slowly than leaching conversion and was limited by diffusion through the product calcium carbonate layer. The calculated value of diffusivity was found to be $5x10^{-9}$ cm^2/sec, which decreased by an order of magnitude with increasing carbonization conversion due to changing product layer density. The experimental data fit the shrinking core model well after correction for the particle specific surface area.

I. INTRODUCTION

The U.S. produces 9-14 Mt of steelmaking slag annually, which represents approximately 10-15 wt. % of crude steel output.[1,2] Primary uses for steelmaking slag include high quality mineral aggregate, Portland cement, soil conditioning, and pH neutralization of abandoned mine drainage.[3,4] The key factor prescribing slag use is the alkaline-earth metal (e.g. Ca and Mg) oxides content, which contributes to overall basicity and cementitious strength. However, as-produced steelmaking slag is chemically unstable because these oxides readily form hydroxides and carbonates through reaction with atmospheric gases. Because both hydroxide and carbonate formation produce substantial mechanical swelling that leads to heave failure in confined construction applications, many states dictate stockpile aging for 3-6 months prior to commercial use.[5,6]

Forced carbonation of steelmaking slag is a method of circumventing lengthy stockpile stabilization and providing the benefit of carbon dioxide sequestration. The

conversion of CaO/MgO to carbonates serves to both stabilize the slag, and permanently capture and store the CO_2. Several research groups have started projects to determine the mechanisms involved in forced (accelerated) carbonation of steelmaking slag with the goal of using this material as a CO_2 sequestering agent. This work is an offshoot of a much larger-scale effort aimed at permanent geological sequestration of carbon dioxide with naturally occurring silicate or carbonate minerals.[7]

Huijgen and Comans measured the carbonation of steel slag in an autoclave reactor.[8-9] Particle size was found to have a strong effect on the extent of carbonation, while reactor temperature, reaction time, and CO_2 partial pressure had milder effects on Ca-conversion. Carbonation was unaffected by stirring rate in the reactor, so Huijgen and Comans concluded that Ca-diffusion through the product layer was the rate-limiting step. They concluded that their process can yield an 80% carbonation in relatively mild conditions (<38 μm, 200°C, 1.0 MPa pCO_2, 15 minutes). In comparison with naturally occurring wollastonite ($CaSiO_3$), steel slag was able to sequester 11 times more CO_2 at ambient temperature. Eloneva et al. investigated acetic acid leaching of slag for extraction of Ca^{2+} for use in producing precipitated calcium carbonate by reaction with CO_2 in a slurry crystallizer.[10] Leaching of the slag resulted in extraction of 97% of the calcium ions, as compared to 38% extraction from wollastonite under the same conditions. Stolaroff et al. investigated the use of steel slag to form a dilute aqueous alkali-metal solution from steel slag that can be used to extract CO_2 from ambient air.[11-12] The rate and extent of calcium dissolution was found to be inversely related to particle size and pH. Near terminal concentration of Ca^{2+} may be reached in a few hours. Carbonation kinetics were not studied in this work, but its authors suggest that Ca leaching and slag carbonation would occur simultaneously.

Extraction of CO_2 from steel manufacturing offgas using steelmaking slag is being studied in an effort to quantify the extent and rate of carbonate formation under near-atmospheric aqueous conditions.[13] The value of CO_2 sequestration arises from steelmaking slags total carbonation potential and ready availability as a co-product in steel production. A survey of industrial slags has found the CaO and MgO contents of BOF and EAF slags to average 30-50 wt.% and 10-12 wt.%, respectively.[13] Additionally, LMF slag contains 50-60 wt.% CaO and 10-12 wt.% MgO. The amount of slag produced

per ton of steel is estimated at 75-150 kg for BOF, 65-80 kg for EAF, and 15-20 kg for LMF.[14] Production of a ton of steel generates 519 kg CO_2 carbon equivalent (CE) for BOF and 119 kg CO_2 CE for EAF. Assuming full stoichiometric conversion of CaO and MgO to carbonate, steelmaking slag has the potential to sequester 6-11% of the CO_2 generated from BOF production and 35-45% of the CO_2 generated from EAF production.[14]

While slag may contain a considerable fraction of CaO and MgO, these compounds are rarely present in their pure forms. The alkaline-earth metal oxides are primarily locked into silicate, aluminate, or ferrite phases. While the carbonation of these phases is highly exothermic (e.g., $\Delta H°_r$=-116.2 kJ/mole for $CO_2+½Ca_2SiO_4 \rightarrow CaCO_3+½SiO_2$), the reaction rates are very slow. Methods investigated for increasing the reaction rate include fine grinding to increase surface area, increasing CO_2 partial pressure, increasing reactor temperature, and catalysis. The current study aims to quantify the reaction rate of steelmaking slag with CO_2 in aqueous systems operating at ambient pressure and temperature. The reaction rate of Ca leaching from slag into water and the direct carbonation of slag particles were investigated separately in an effort to understand the limiting mechanisms for the overall sequestration reaction.

II. EXPERIMENTAL

Batch-reactor experiments were conducted to measure the reaction rate of industrial EAF and LMF slags with carbon dioxide in an aqueous system. The effects of slag particle surface area and alkaline earth metal oxide content on the extent of carbonization (wt. % CaO converted to $CaCO_3$) were investigated. These two parameters were selected in order to determine the hydrometallurgical model that best fits aqueous-assisted carbonation of steelmaking slag.

Three industrial slag samples (18-22 kg each) were studied. Slag #1 was from an electric arc furnace (EAF), Slag #2 from an Al-killed ladle metallurgy furnace (LMF), and Slag #3 from a Si-killed LMF. As-received Slags #1 and #2 were gravel sized with most particles 2.5-7.5 cm diameter, while Slag #3 was a "falling slag" present as a fine powder. The slags were obtained within 24 hours of production and prior to on-site

crushing and magnetic separation to ensure minimal reaction with the local atmosphere. Each slag sample was stored in its own separate double sealed plastic bin with bulk desiccant.

A. Slag Characterization and Sample Preparation

Prior to beginning the reactor experiments, the chemical and physical characteristics of the slags were determined. X-ray fluorescence (XRF) spectroscopy was used to measure the elemental composition of each slag, with all components assumed present as oxides. X-ray diffraction (XRD) phase analysis (Scintag, Inc. PadX with a Cu source) was used to indicate the phase components of the slag samples.

To obtain fresh particle surfaces and sufficient amounts of slag particles across a range of size fractions, Slags #1 and #2 were crushed in a laboratory jaw crusher and then a roll crusher until small enough to pass a 6-mesh sieve size (3.35 mm). Slag #3 contained a high fraction of dicalcium silicate which self-comminuted upon cooling therefore was used in the raw condition. Particle size distribution (PSD) was obtained using a U.S. mesh series of 20 cm (8 in.) diameter sieves on a vibratory shaker with ~700 g samples produced by riffle splitting. After crushing and particle size analysis, five size fractions—45-75 µm, 150-250 µm, 420-590 µm, and 2300-3300 µm—were chosen for subsequent testing. Because the slag-CO_2 reaction may be governed by particle surface area, the specific surface area (m^2/g) was determined for several fractions of the crushed slag samples using BET gas sorption method (Quantachrome® Corp., NOVA® 1000). Reflected light (RL) microscopy and scanning electron microscopy (SEM) with energy dispersive spectrometry (EDS) were used to study the surface topology, structure, and composition throughout different testing stages.

B. Reaction Kinetics

Two sets of aqueous experiments were performed using the batch type reactors. The first set of tests involved a simple stirred batch reactor to measure the leaching rate of calcium from the different size fractions of the slags. The leaching procedure was adopted from the work of Stolaroff.[12] Each leaching test was done in a 500 ml glass flask filled with 300 ml double de-ionized water and pH buffer TES (2-[(2-hydroxy-1,1-

bis(hydroxymethyl)ethyl)amino]ethanesulfonic acid). The buffer was used to maintain the pH between 7.0-7.5. The buffered water was degassed by Ar bubbling and sealed under Ar positive pressure during the experiments. A quantity of slag (400 mg) was added such that the aqueous solution would be not saturated by Ca^{2+} in the case of complete leaching. At a predetermined time, a ten ml sample of the solution was taken from the reactor for each test and immediately filtered through 0.45 μm syringe filters to remove any suspended solids, leaving only the dissolved fraction of Ca^{2+}. ICP-OES spectrometry (PerkinElmer® Optima 2000™ DV) was used to measure the Ca^{2+} concentration in the samples.

The second set of experiments involved measuring the slag particles carbonization in aqueous conditions. Thirty grams of each of the four size fractions from the slag samples were mixed with 250 ml of de-ionized water in a 500 ml flask. Standard grade CO_2 was introduced into the mixture through a 1.0 mm glass capillary tube. Each sample was allowed to react for a designated period of time, after which the CO_2 flow was stopped. The slurry mixture was filtered through 11μm filter paper with a vacuum pump. The filtrand was dried at 180°C and analyzed for carbon content by the combustion/IR method (LECO® CS600) or thermogravimetric analysis (TGA) in an Ar atmosphere. Total weight loss up to ~600°C indicated the amount of hydroxide ($Ca(OH)_2$) formed. Weight loss above this temperature was associated with the amount of carbonate ($CaCO_3$) formed.

III. RESULTS

A. Slag Characterization

Table I lists the slag chemical compositions obtained by XRF, assuming all components to be oxides. EAF slag #1 contained 32.1% CaO while LMF slags #2 and #3 contained higher, but nearly equal, percentages of CaO plus an Al_2O_3/SiO_2 amount that reflected their respective steel deoxidation practices. XRD showed that the three slags listed in Table I contained primarily dicalcium silicate (Ca_2SiO_4) and tricalcium silicate (Ca_3SiO_5) with lesser amounts of akermanite ($Ca_2MgSi_2O_7$), $C_{12}A_7$ ($Ca_{12}Al_{14}O_{33}$), clinoenstatite ($MgSiO_3$), and magnesio-wustite ($MgFeO_2$). Only a minor amount of free

periclase (MgO) and lime (CaO) was present, showing that the alkaline earth metal oxides are primarily tied up as silicates, aluminates, and ferrites. Minor amounts of free alumina (Al_2O_3), wustite (FeO), and silica (SiO_2 quartz) were also found, but do not contribute to carbon dioxide sequestration.

Table I. Steelmaking Slag Composition (Wt Pct)

Sample	#1	#2	#3
Type	EAF	LMF Al-Killed	LMF Si-Killed
CaO	32.1	49.9	51.3
SiO_2	19.4	4.5	28.3
Al_2O_3	8.6	32.3	4.9
TiO_2	0.4	0.3	0.3
MgO	9.4	4.3	4.3
MnO	6.8	0.8	1.3
Fe_xO_y	26.4	6.3	5.5
SO_3	0.6	1.0	1.6

Figure 1 shows the particle size analysis of Slags #1 and #2 after crushing, along with Slag #3 in the raw state. Slags #1 and #2 have similar particle size distributions after crushing, but Slag #3 is much finer. The measured specific surface area (m^2/g) was compared with the calculated surface area for hypothetical smooth uniform spherical particles. The measured surface area of LMF slag particles was an order of magnitude larger than that calculated for uniform spheres, while the EAF slag particles had a surface area two orders of magnitude greater due to their internal and external porosity.

B. Reaction Kinetics

1. Ca Leaching

Figure 2 shows the effects of particle size, solution temperature, and slag composition on the aqueous extraction rate of Ca^{2+} from slag samples. The aqueous solution was maintained at a constant pH of 7.5 throughout each test. Figure 2a shows the amount of Ca^{2+} dissolved in 24 hours for four size fractions of Slag #2 (LMF slag with

49.9% CaO). The percentage of calcium dissolved was calculated from the concentration of Ca^{2+} in the solution and the total amount of Ca (as CaO) added to the batch reactor. The particle size (i.e., surface area) had a dominant influence on the amount of calcium leached.

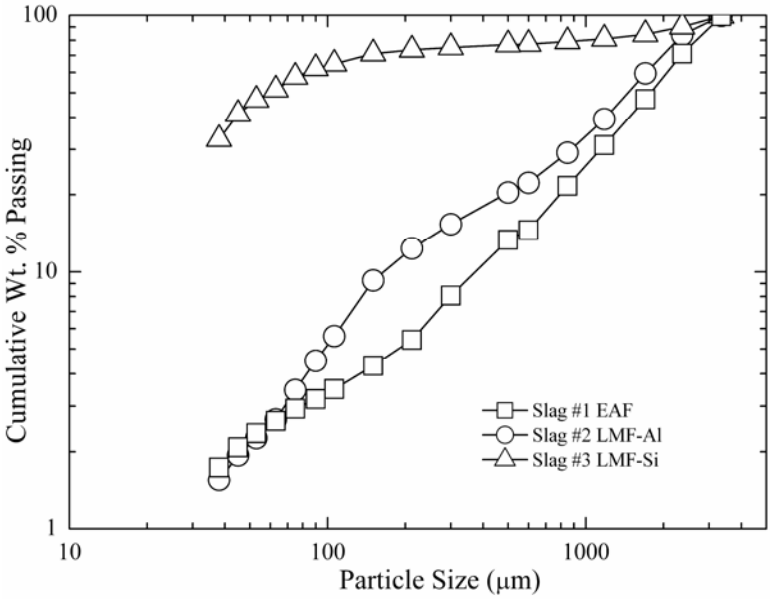

Fig. 1—Particle size analysis of Slags #1 and #2 after crushing and Slag #3 (as-received).

During the first hour, approximately 33% of the calcium was leached from the 45-75 μm fraction, while less than 5% of the calcium was leached from the 2300-3300 μm fraction at 24 hours. The effect of temperature on Ca leaching, as shown in Figure 2b, was more pronounced during the first few hours, but after three hours the leaching rate (% Ca dissolved/time) became similar for the two temperatures tested. Figure 2c provides a comparison of leaching different types of slags with the same size particles (150-200 μm) by showing the absolute value of Ca^{2+} (ppm) in solution versus time. EAF Slag #1 has less CaO than LMF Slag #2 (32.1% versus 49.9%), but a higher surface area. The leaching rate during the first 100 minutes was higher for Slag #1 due to the increased surface area, but the overall amount of calcium dissolved after 24 hours is significantly higher for Slag #2 due to the higher starting CaO concentration.

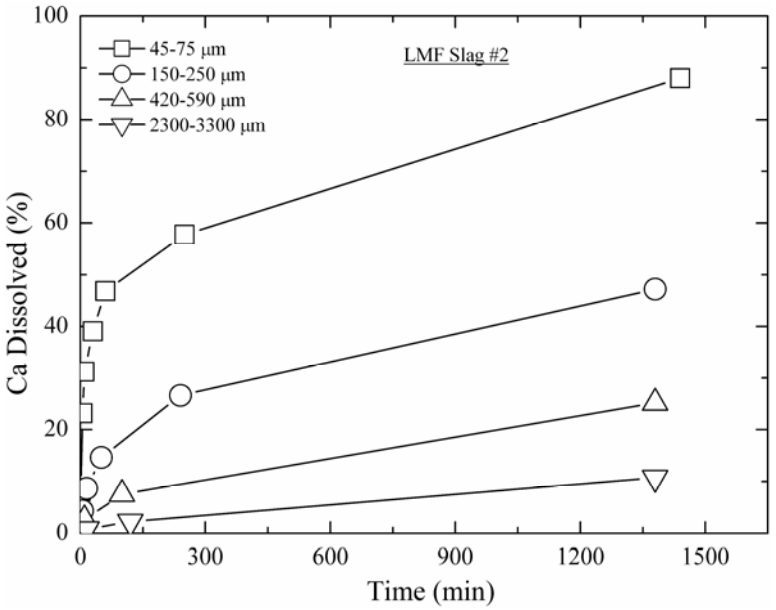

(a)

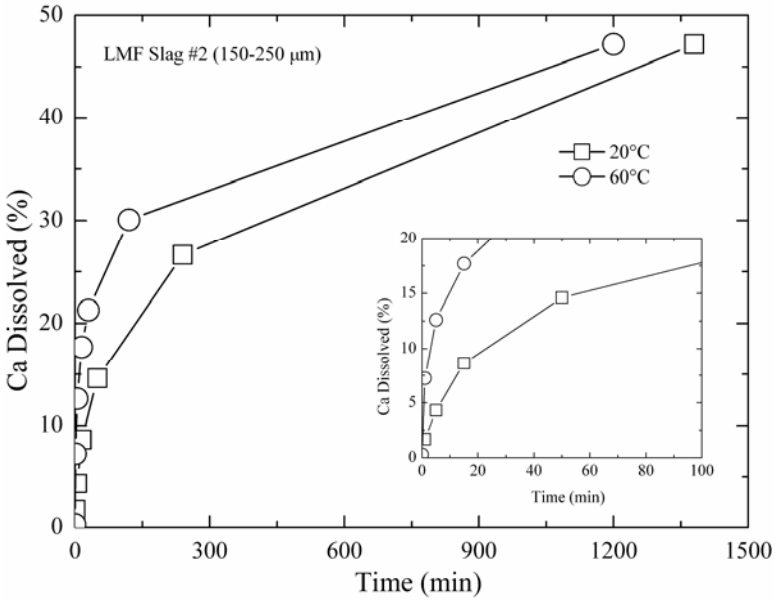

(b)

Fig. 2—Effect of (a) particle size, (b) temperature, and (c) CaO concentration in slag on the aqueous leaching rate of calcium.

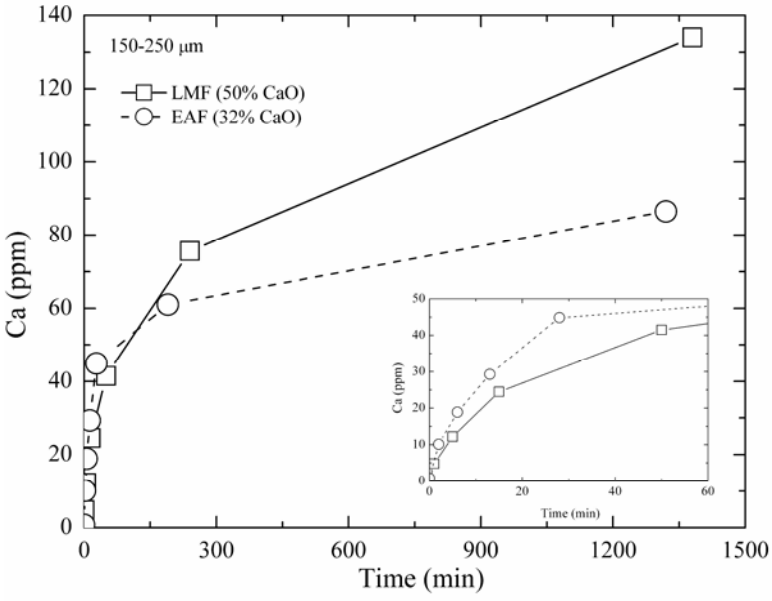

(c)

Fig. 2—Effect of (a) particle size, (b) temperature, and (c) CaO concentration in slag on the aqueous leaching rate of calcium (cont.).

The changes in particle morphology and composition during leaching were examined using SEM/EDS and XRD analysis. The leaching of Ca from a slag particle started at the slag surface and included internal pores connected to the particle's external surface. Figure 3 shows the porous layer remaining on the external surface (Figure 3a) and internal surface (Figure 3b) of Slag #1 after leaching. EDS analysis of the unreacted core and the surface after leaching showed that selective dissolution takes place. The concentration of Ca in the unreacted core is very high (44.5 wt.%), while the Ca at the surface after leaching is depleted (0.33 wt.%). Selective leaching of the Ca from the surface leaves behind an un-dissolved layer of mixed (Al,Fe,Mn,Mg) oxides in different phases than in the original slag. XRD analysis showed that the alumino-calcium-silicate phase was eliminated after 24 hours leaching.

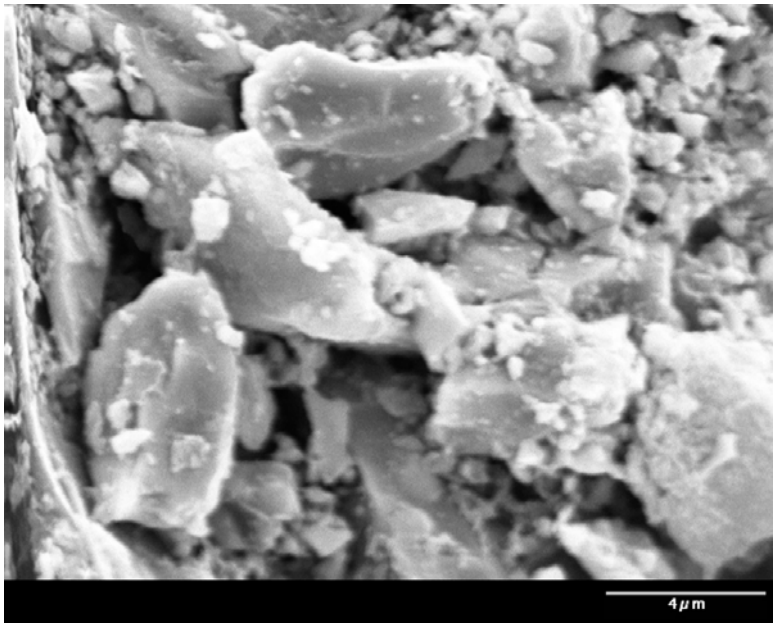

(a)

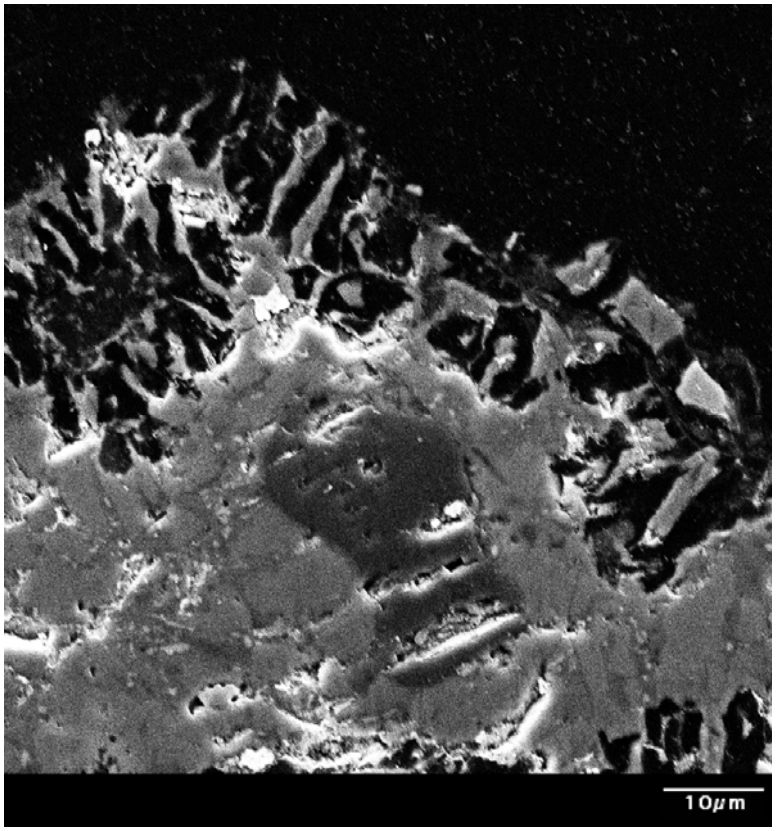

(b)

Fig. 3—(a) External surface and (b) cross-section images of Slag #1 after leaching.

2. Slag Carbonation

The degrees of carbonization versus time for the four size fractions of Slags #1 and #2 are presented in Figure 4. For both slags, the particle size predominantly influences the amount of carbonization. For the 0.06 mm, 0.2 mm, 0.5 mm, and 1.25 mm average particle sizes tested for Slag #1 (Figure 4a), the times to reach 6% carbonization were approximately 20 minutes, 800 minutes, 1500 minutes, and 4200 minutes, respectively. The data for Slag #2 (Figure 4b) showed the same relationship between particle size and degree of carbonization, but the overall carbonization amount is less than in Slag #1 for all particle sizes. Measuring the degree of carbonization is less precise than measuring the rate of Ca leaching due to the small amount of initial carbon present in the slag, and the lower precision of TGA carbon measurement compared to aqueous Ca ion measurement with the ICP.

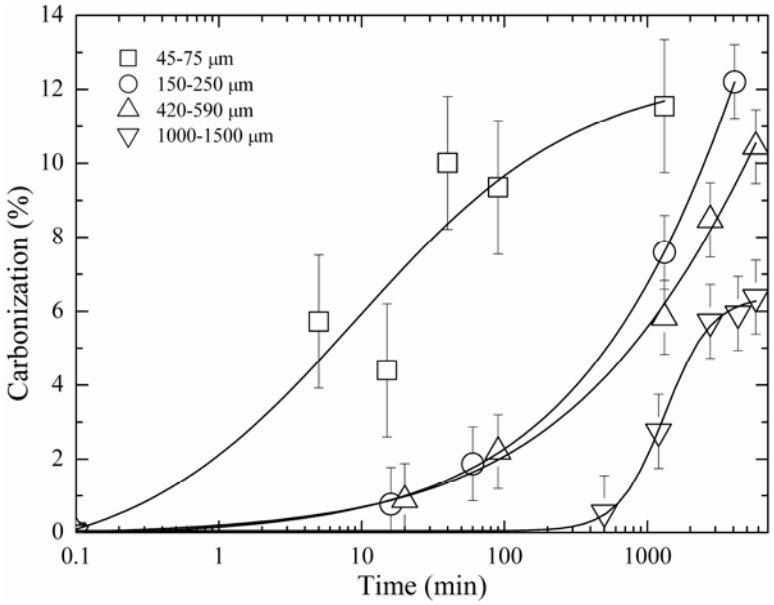

(a)

Fig.4—Degree of carbonization versus time for four size fractions of (a) Slag #1 and (b) Slag #2.

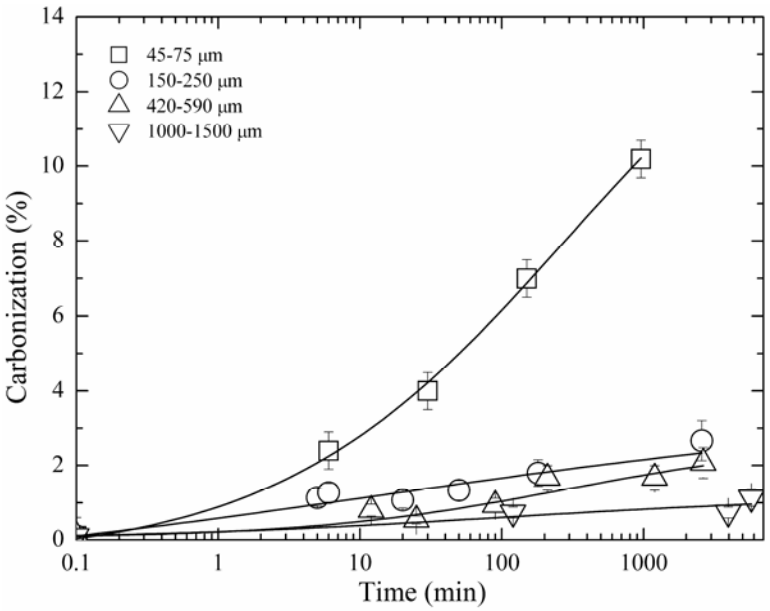

(b)

Fig.4—Degree of carbonization versus time for four size fractions of (a) Slag #1 and (b) Slag #2 (cont.).

Morphological analysis of the resultant carbonate layers is shown in Figure 5. Because they exhibit a highly porous structure, interconnected channels allow surface reactions to take place deep inside slag particles. A cross-sectional sample of a 0.5 mm particle from Slag #2 (Figure 5a) showed after 48 hours carbonization treatment, a 10-20 μm thick carbonate layer on the external surface (dark region) extending into the pores which are up to 100 μm diameter. SEM analysis revealed that the carbonate layer on the external surface of Slag #2 consisted of plate-like crystals in a random high-porosity structure with 1-3 μm openings (Figure 5b). According to EDS analysis, the plates were composed primarily of Ca, O, and C, indicating a calcium carbonate composition. Pores connected to the slag surface through channels were exposed by crushing prior to SEM analysis. The pore surfaces exhibited a reaction layer made of overlapping calcium carbonate plates packed very close together and thus having a high bulk density (Figure 5c).

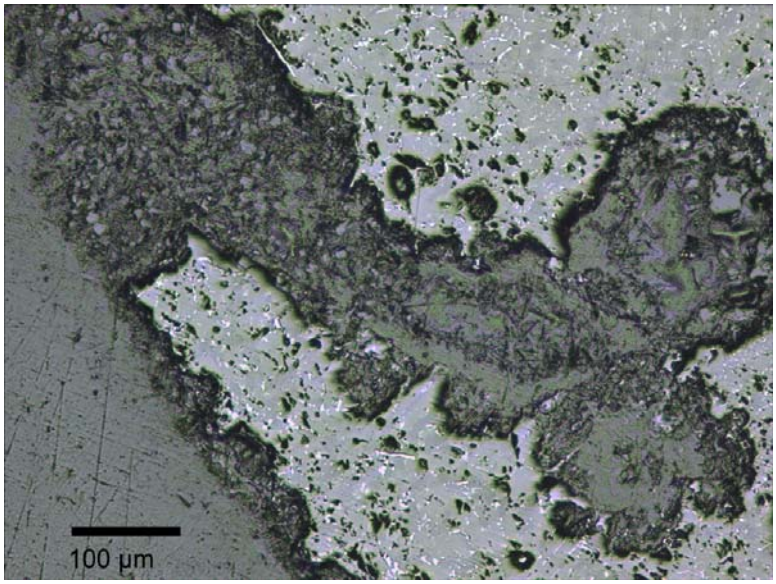

(a)

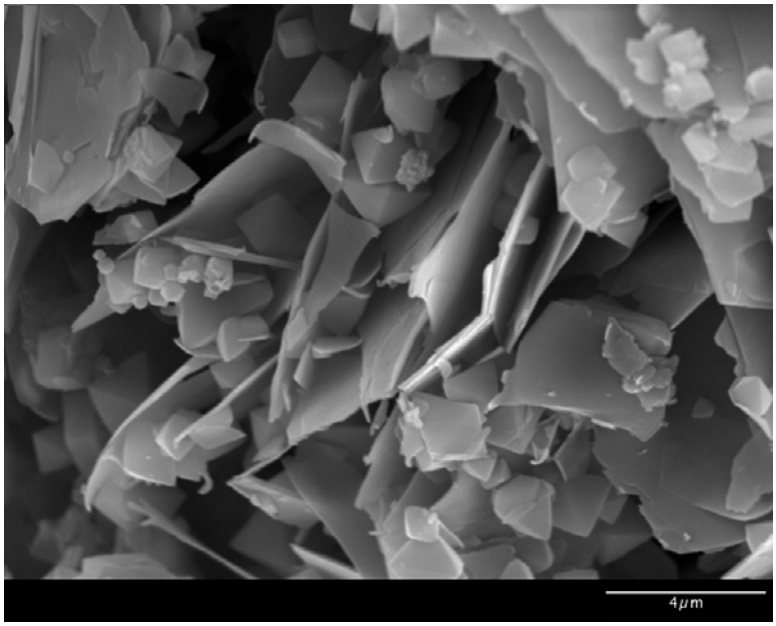

(b)

Fig. 5—Optical image of Slag #2 particle showing (a) the cross section of a pore, and SEM images of (b) the external surface carbonate layer and (c) the pore surface carbonate layer.

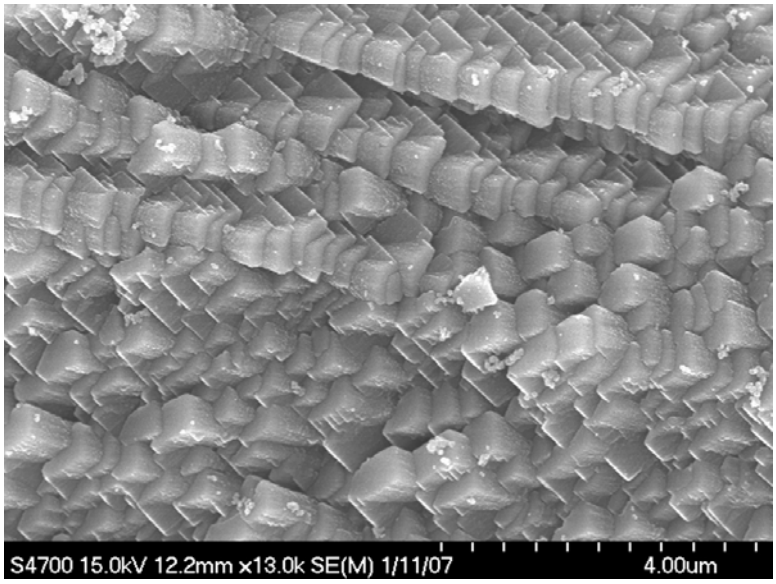

(c)

Fig. 5—Optical image of Slag #2 particle showing (a) the cross section of a pore, and SEM images of (b) the external surface carbonate layer and (c) the pore surface carbonate layer (cont.).

Two different types of reactions between steelmaking slag and water were experimentally tested. The first reaction involved simple leaching of Ca^{2+} ions from slag into nearly pure water with a constant pH and surrounded by an inert atmosphere. No hydrous CO_2 or other impurities were present to react with the calcium ions. In contrast, the second type of reaction allowed for the formation of calcium carbonate due to saturation of the aqueous solution with CO_2. The progress of both types of reactions changed the specific surface area of the solid slag particles, as shown in Table II. Leaching increased the specific surface area by increasing the surface porosity from selective dissolution of the Ca bearing-phases (Figure 3), while the carbonization reaction increased it by producing a highly irregular product layer (Figure 5).

IV. DISCUSSION

The shrinking core model is typically employed for analysis of particulate-based heterogeneous solid-fluid reactions for determination of the rate-limiting mechanism.

Han describes the fundamentals of this model.[15] Applying this model to slag carbonization reveals that the reaction steps must include (1) mass transport of the aqueous carbonic acid ions through the liquid boundary layer surrounding the particle, (2) diffusion of the reacting ions through the pores in the product layer ($CaCO_3$) accreted on the slag particle surface, and (3) reaction of calcium ions at the solid surface with aqueous carbonic acid ions (HCO^{3-} and CO_3^{2-}). The steps of Ca ion leaching-only process include (1) surface reaction of Ca bearing phases with water, (2) mass transport of the Ca^{2+} through the porous surface structure developed from selective leaching, and (3) mass transport of the calcium ion through the liquid boundary layer. According to the shrinking core model, which was originally developed for dense, spherical, uniformly sized particles, each reaction step possesses a specific time dependence that has a characteristic proportionality to the particle surface area and solution temperature. The measured effective diffusivity was approximately 10^{-9}-10^{-10} cm^2/s, while the diffusivity in the bulk liquid was approximately10^{-5} cm^2/s. Thus, mass transport through the liquid boundary layer was neglected as the rate-limiting step. The slurry was intensively mixed with magnetic stirring to maintain a uniform concentration in the bulk solution. Therefore, the chemical reaction between the solid and liquid-ionic species and/or diffusion through the pores in the product layer can be assumed to control the rate of the processes studied.

Table II. Specific Surface Area (m^2/g) of Slag after Aqueous Treatment

Slag (0.15-0.25 mm)	Condition		
	Initial	CO_2 Treated	Leached
EAF #1	1.13	12.6	5.42
LMF #2	0.092	4.4	N/A

When the diffusion of the reactants through the product layer is rate-limiting, Equation [1] gives the dependence of the molar transport of bulk fluid reactant A ($-dN_A/dt$, mol/sec) through the product layer at a radius r (cm) and effective diffusivity D_e

(cm^2/s).[15] The term C_A (mol/cm^3) is the concentration of the bulk reactant, which is a function of the radius. At the radius of the unreacted core C_A is zero, while at the outer radius of the product layer (in contact with surrounding fluid), C_{Ab} is the concentration of the reactant ions in the bulk fluid.

$$\frac{-dN_A}{dt} = (4\pi r^2)(-D_e \frac{dC_A}{dr}) \tag{1}$$

Solving for the reaction time t (sec), as shown in Equation [2], shows its dependence on the particle initial radius R (cm), the unreacted core radius r_c (cm), molar density of the solid ρ_B (mol/cm^3), and stoichiometric coefficient b.[15] Regarding particle size, the reaction time to a fixed level of completion is a function of the square of the particle radius.

$$t = \frac{\rho_B R^2}{6bD_e C_{Ab}}\left[1 - 3\left(\frac{r_c}{R}\right)^2 + 2\left(\frac{r_c}{R}\right)^3\right] \tag{2}$$

When the chemical reaction between the solid and liquid-ion species is rate-limiting, Equation [3] gives the relationship between surface area, molar transport of bulk fluid reactant A, rate constant k_r (cm/sec), and concentration of bulk reactant.

$$-\frac{1}{4(\pi)r^2}\frac{dN_A}{dt} = k_r C_A \tag{3}$$

Rearrangement and integration of Equation [3] provides the reaction time as a function of the parameters shown in Equation [4]. In terms of particle size, the reaction time is a function of the particle radius to the first power.

$$t = \frac{\rho_B}{bk_r C_{Ab}}(R - r_c) \tag{4}$$

To determine the rate-controlling step, the influences of particle size and solution temperature were analyzed. The effect of particle size on the time to reach the equivalent levels of Ca^{2+} in the solute (Figure 2) or the time to reach the equivalent levels of carbonization (Figure 4) was analyzed for the respective experiments. If the time has a squared dependence particle size, then the reaction is likely governed by product layer diffusion (Equation [2]), but if the time has a linear dependence on particle size, the reaction is governed by the chemical reaction (Equation [4]). The time dependence for both leaching and carbonization is analyzed based on calcium conversion, X_{Ca}, as a fraction of reacted calcium initially present in the slag.

A. Ca Leaching

Analysis of experimental data for Slag #2 (Figure 2a) showed that both chemical reaction and diffusion mechanisms were involved sequentially during Ca leaching from steelmaking slag. During the initial stage (i.e., to 0.07 conversion), the reaction time showed linear proportionality to particle size (Figure 6a), supporting a chemical reaction controlled model whereby solid CaO dissolves into Ca^{2+} ions in the water.

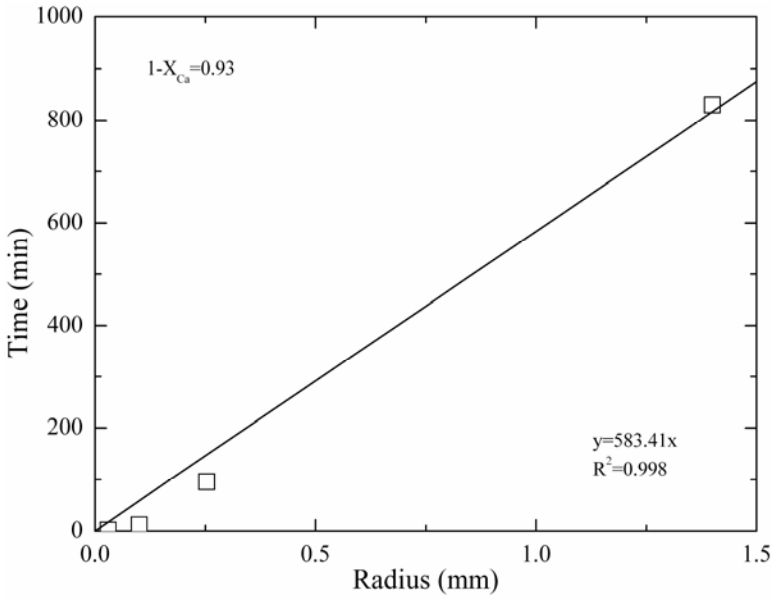

(a)

Fig. 6—Time dependence with particle size for Ca leaching from Slag #2 for (a) initial stage and (b) progressive stage.

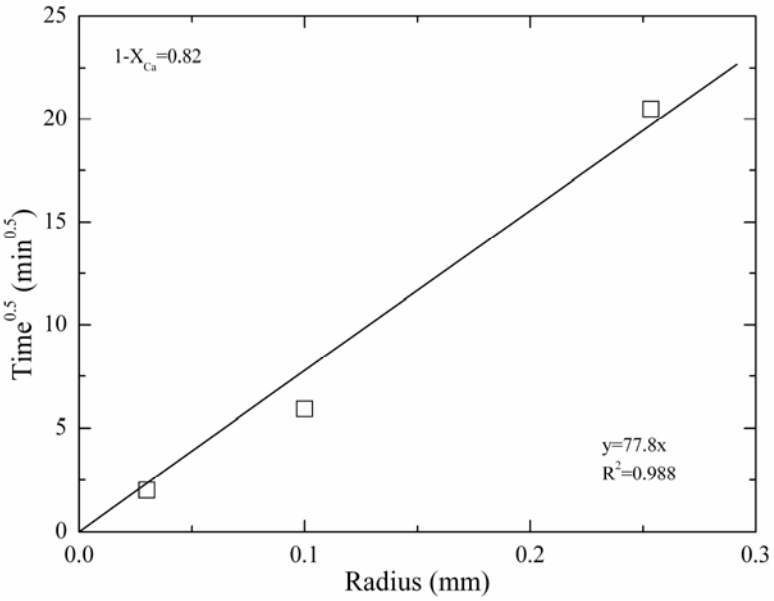

(b)

Fig. 6—Time dependence with particle size for Ca leaching from Slag #2 for (a) initial stage and (b) progressive stage (cont.).

As the dissolution reaction progressed to 0.18, conversion a porous surface structure developed, as shown in Figure 3, resulting in a tortuous path for the ions to travel. Subsequent diffusion through this structure became the rate-limiting step as shown by the square root proportionality of the reaction time to particle size (Figure 6b).

Comparison of the experimental data for Slag #2 (Figure 2a) with Equations [2] and [4] allows for direct correlation. Figure 7 shows a plot of the experimental data (45-75 μm particles) compared to the diffusion and reaction equations. A combination of the two equations shows that the experimental data fits well to a chemical reaction controlled mechanism up to ~0.3 conversion (60 minutes), which then switches to a combination of chemical reaction and porous diffusion layer control to the terminal conversion of 0.63.

Each reaction mechanism has a different sensitivity to solution temperature. In the case studied, increasing the temperature of the aqueous solution enhanced Ca leaching at the initial reaction time period (Figure 2b). While the rate of dissolution increased significantly with temperature during the initial period, the rate of leaching at the end of

the test did not differ greatly between 20°C and 60°C, because the solution temperature affects the rate of the chemical reaction more than the rate of diffusion.

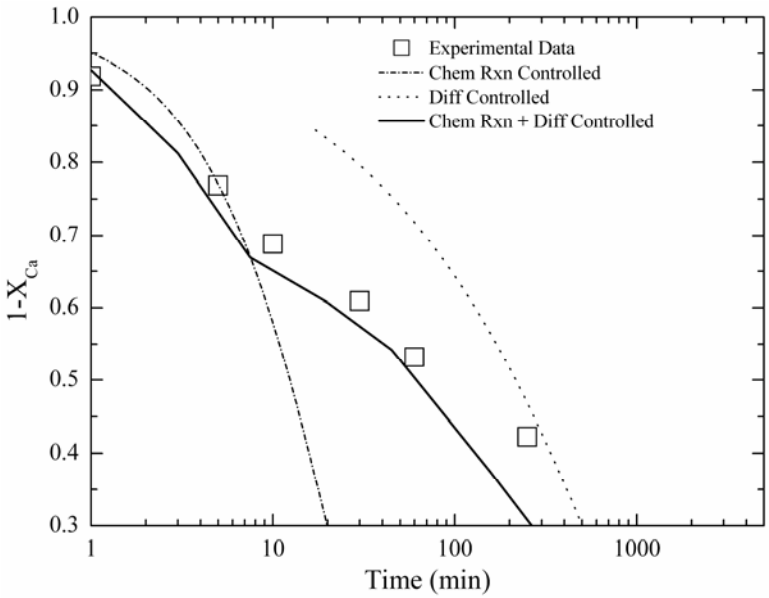

Fig. 7—Comparison of experimental data for Ca leaching from Slag #2 (45-75 μm particle size) with chemical and diffusion reaction control mechanisms.

As shown in Figure 2c, EAF Slag #1 showed higher Ca dissolution rate during the initial period, even with a lower Ca concentration in slag than did LMF Slag #2. This is inconsistent with a simple shrinking core model based on uniform smooth solid spheres. This model can be corrected by substituting an effective particle size based on the specific surface area. Slag #1 had ~10 times the surface area of Slag #2 for the same particle size. The much higher surface area led to an increased Ca dissolution rate during the initial period. However, rapid dissolution decreased the amount of Ca left in the slag, leaving less gradient to maintain the high dissolution rate. Slag #2 had 55% more Ca to start with, so it was able to maintain a higher gradient than was the bulk solution, resulting in higher total amount of Ca leached.

B. Slag Carbonization

The slag carbonization data was analyzed in a similar manner to determine the controlling reaction mechanism. Figure 8a shows the time required to achieve 0.02 conversion (carbonate reaction) for four particle sizes of Slag #1 and Slag #2. Conversion was heavily dependent on particle size and showed proportionality to the square root of time, indicating that product layer diffusion was the rate-controlling step. The layer of calcium carbonate formed on the surface (Figure 5) retarded the diffusion of carbonic acid ions to the slag particle surface. The different slopes exhibited by the two slags reflected the effect of true surface area. The effective diameters, calculated from specific surface measurements on assumption of uniform spherical particles, were used to recalculate the curves shown in Figure 8b, bringing both curves into congruence.

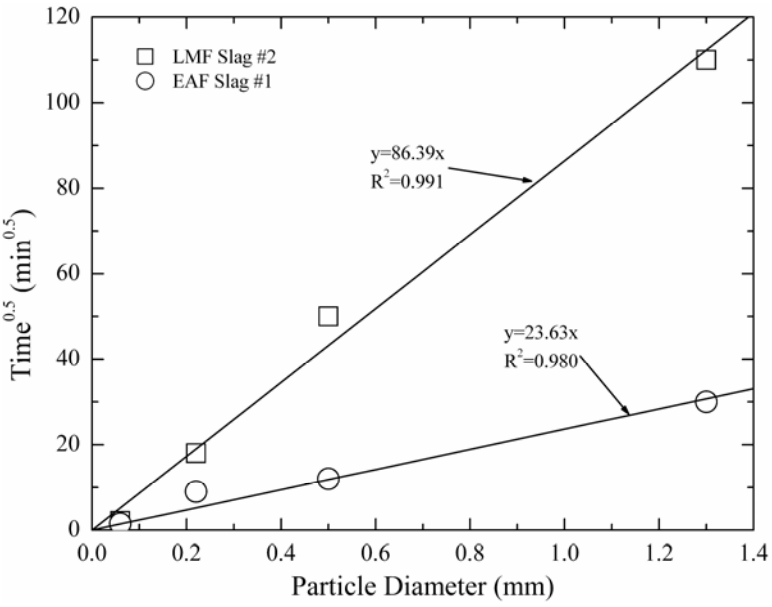

(a)

Fig. 8—Diffusion limiting model for slag carbonization reaction at 0.02 Ca conversion using (a) real particle diameter and (b) effective particle diameter.

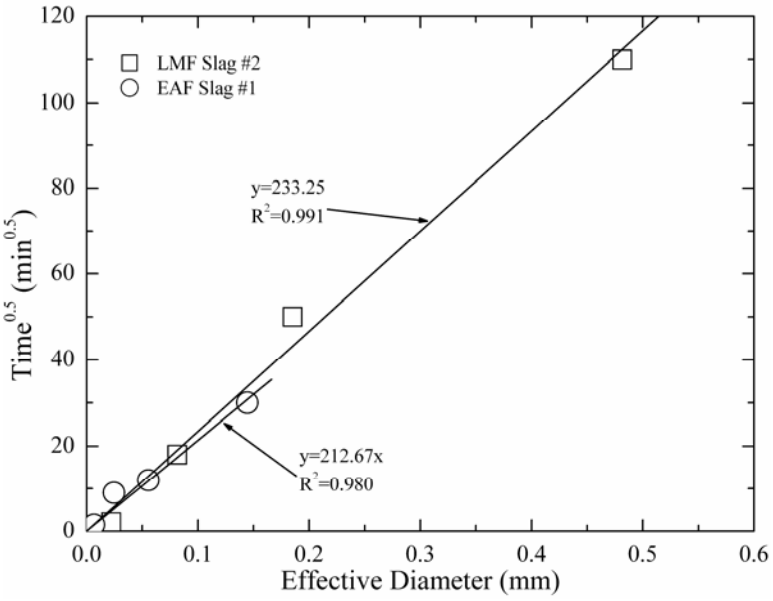

(b)

Fig. 8—Diffusion limiting model for slag carbonization reaction at 0.02 Ca conversion using (a) real particle diameter and (b) effective particle diameter (cont.).

According to the shrinking core model, if product layer diffusion is the limiting mechanism (Equation [2]), conversion should exhibit a dependence on the square root of reaction time. Figure 9a shows the experimental data for conversion of Slag #1 versus [time$^{0.5}$]. During the initial reaction period (i.e. to 0.03 conversion), the experimental results closely match the theoretical model. As the product layer increases in thickness, the reaction tends to decelerate. The changing density of carbonized layer (Figure 5a), which was not considered in this model, is a possible explanation for the decrease in reaction rate. Equation [2] was solved numerically by changing the effective diffusivity (i.e., increased product layer thickness) for the three conversion periods shown in Figure 9a (<0.03, 0.03-0.10, and >0.10) to allow the fraction converted to match the square root relationship. The experimental data were fit to the resulting equations to yield a diffusion coefficient, which changed from $5x10^{-9}$ cm^2sec^{-1} at the initial time-period to $5x10^{-10}$ cm^2sec^{-1} when carbonate layer was formed, as shown in Figure 9b.

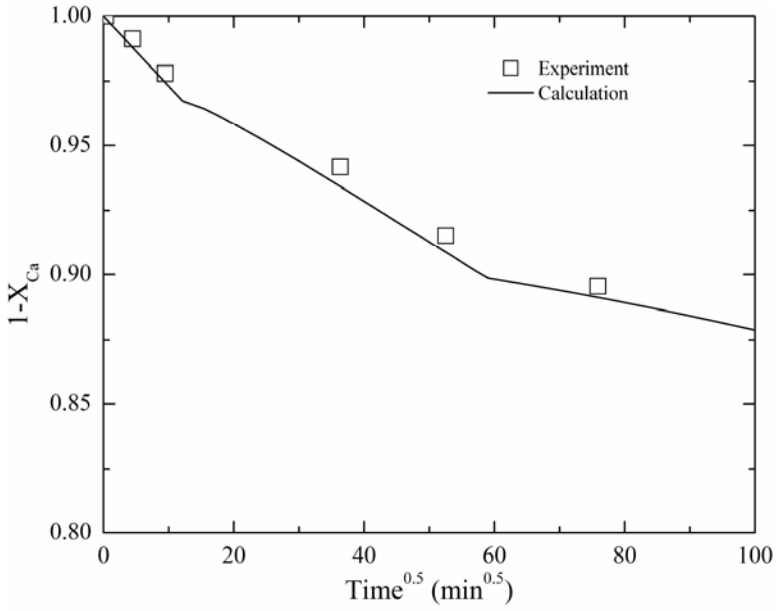

(a)

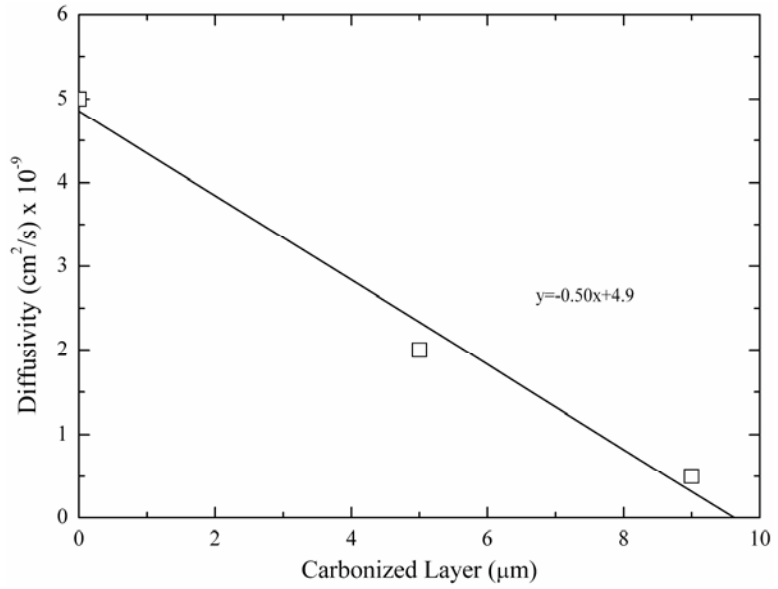

(b)

Fig. 9—(a) Comparison of calculated and experimental data for the carbonization of Slag #1 with 0.5 mm average particle diameter and (b) dependence of diffusivity on thickness of carbonized layer.

Finally, data for the rate of Ca leaching were compared to data for the rate of Ca carbonization for the same slag. In both cases, some calcium from the slag reacted with the aqueous solution, but the rate of these reactions differed significantly due to the

mechanisms and limiting steps involved. In the slag leaching test, Ca ions dissolved from the slag into the unsaturated aqueous solution. The limiting step was diffusion of calcium ions though the developed porous layer. An additional Ca leaching test was performed on Slag #2 (<200 μm), which had been partially carbonized preliminarily. Figure 10 compares the percentage of reacted Ca from slag (leached or carbonized) to reaction time, illustrating that slag carbonization proceeds slower than Ca leaching. The calcium carbonate product layer also inhibits the Ca leaching process. The experimental data and kinetic parameters obtained will be used to model an industrial prototype reactor that can be used to sequester carbon dioxide using steelmaking slag.

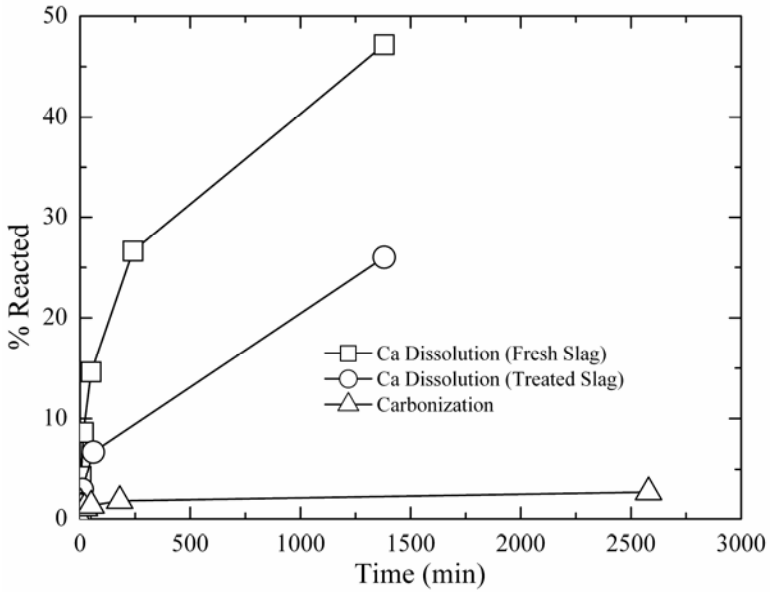

Fig. 10—Comparison of carbonized and leached Ca from fresh and stabilized LMF Slag #2 in aqueous solutions.

V. CONCLUSIONS

Carbon dioxide sequestration using steelmaking slag was studied in a three-phase, batch-system containing industrial slag, water, and CO_2 gas at ambient temperature and pressure. The reaction rates of aqueous Ca-leaching and direct carbonization were

quantified independently to yield the reaction parameters and rate-limiting mechanisms listed below.

1. The specific surface area of slag particles is increased by leaching or carbonization. Selective dissolution of the Ca-bearing phase results in increased surface porosity, while carbonization produces overlapping plates of $CaCO_3$ product layer to create a highly irregular surface.
2. Both Ca-leaching and carbonization were analyzed using the shrinking core model. The experimental data for both processes fit this model well after correction for effective particle size based on the measured specific surface area.
3. Analysis of Ca-leaching shows a linear proportionality to particle size during the initial stage (to 0.30 conversion), which supports a chemical reaction controlled model (CaO dissolution). The later stage of leaching is controlled by diffusion of the Ca^{2+} ions through the resulting porous surface layer, as shown by square-root proportionality of reaction time to particle size.
4. Increasing the leachate temperature from 20 to 60°C (at atmospheric pressure) initially enhanced the Ca-leaching rate but the terminal amount of Ca leached after 24 hours was nearly the same (47% versus 50%).
5. Carbonate conversion is heavily dependent on particle size and the reaction is limited by product layer diffusion. The calculated value of diffusivity decreased by an order of magnitude from the initial value of $5x10^{-9}$ cm^2/sec due to changing product layer density.
6. Carbonate conversion proceeds more slowly than leaching conversion, but both processes are inhibited by the calcium carbonate product layer.

VI. ACKNOWLEDGMENTS

This paper was prepared as an account of work sponsored by the U.S. Department of Energy, in cooperation with the American Iron and Steel Institute (AISI) and its participating companies, under Agreement DE-FC36-97ID13554. Such support does not constitute an endorsement by DOE or AISI of the views expressed in the article. The

authors also acknowledge the support of DOFASCO, Gallatin Steel, Hylsa, IPSCO, Mittal Steel, Praxair, Nucor, Timken Company, and US Steel.

VII. REFERENCES

1. U.S. Department of the Interior, U.S. Geological Survey, Minerals Information. http://minerals.usgs.gov/minerals/pubs/commodity/iron_&_steel_slag/, June 2005.
2. H.G. van Oss: U.S. Geological Survey Minerals Yearbook (2003): 69.1-69.3, June 2005, http://minerals.usgs.gov/minerals/pubs/commodity/iron_&_steel_slag/islagmyb03.pdf
3. National Slag Association, Steelmaking Slag [brochure], June 2005, http://www.nationalslagassoc.org/PDF_files/SSPremAgg.PDF
4. D.W. Lewis: National Slag Association. Report MF 182-6.
5. Missouri Department of Transportation, Standards and Specifications, June 2005, http://www.modot.org/business/standards_and_specs/nov2004specbook/Sec1002.pdf
6. P.S. Kandhal and G.L. Hoffman: Transportation Research Record, 1997, no. 1583, pp. 28-36.
7. K.S. Lackner: Annual Review of Energy and the Environment, 2002, vol. 27, pp. 193-232.
8. R.N.J. Comans and W.J.J. Huijgen: Proceedings of the 32nd International Geological Congress, Session G15.05, Florence, Italy, 23 August 2004.
9. W.J.J. Huijgen, G.-J Witkamp, and R.N.J. Comans: Environmental Science and Technology, 2005, vol. 39, no.24, pp. 9676-9682.
10. S. Eloneva, S. Teir, C.-J. Fogleholm, and R. Zevenhoven: Proceedings of the 4th Nordic Minisymposium on Carbon Dioxide Capture and Storage, 8-9 September 2005, Espoo, Finland.
11. J.K. Stolaroff, G.V. Lowry, and D.W. Keith: EOS Trans. AGU, vol. 84, no.46, Fall Meeting; 8-12 December 2003; San Francisco, CA, United States.
12. J.K. Stolaroff, G.V. Lowry, and D. W. Keith: Energy Conservation and Management, 2005, vol. 46, no. 5, pp. 687-699.
13. C.H. Rawlins, V.L. Richards, K.D. Peaslee, and S.N. Lekakh: Proceedings of the AISTech 2006 Conference, May 1-4, 2006; Cleveland, OH, U.S.
14. C.H. Rawlins, V.L. Richards, K.D. Peaslee, and S.N. Lekakh: Steel Times International, 2006, vol. 30, no. 7, pp. 25-26.
15. K.N. Han, Fundamental of Aqueous Metallurgy, Society for Mining, Metallurgy, and Exploration Inc., Littleton, CO, 2002, pp. 129-140.

3. Investigation of a Two-Stage Aqueous Reactor Design for Carbon Dioxide Sequestration Using Steelmaking Slag

S.N. Lekakh, D.G.C. Robertson, C.H. Rawlins, V.L. Richards, K.D. Peaslee

Department of Materials Science and Engineering
Missouri University of Science and Technology
Rolla, Missouri, USA 65401
Email: kpeaslee@mst.edu

Accepted for publication in Metallurgical and Materials Transactions B.

Hydrous carbonate sequestration of carbon dioxide using steelmaking slag was studied using a METSIM process model to analyze experimental data and determine reactor design parameters. Several operating scenarios of a two-stage system with water/slag contact in Reactor 1 and leachate/carbon dioxide contact in Reactor 2 were investigated. These scenarios included batch versus continuous processing and fresh water input versus water recirculation. The METSIM leaching and carbonation models were verified with results obtained from previous slag sequestration experiments. Fresh water additions to Reactor 1 allowed the highest leaching efficiency and resulted in excellent carbonation in Reactor 2, but a continuous system has a high water demand. Recirculation of the spent leachate minimizes the fresh water addition required, but inhibits the leaching process by producing a calcium carbonate product layer on the slag particles in Reactor 1. Increasing the slag surface area, slag/solution ratio, or reactor residence time partially overcomes product layer "blinding." Optimal residence times were defined for different process parameters and slag particle sizes.

I. INTRODUCTION

Steelmaking slag contains a high fraction of alkaline-earth oxides that exothermically form carbonates, making this material an excellent vehicle for capturing and sequestering carbon dioxide. This material has been shown to have the potential to sequester 35-45% of the carbon dioxide generated from electric arc furnace (EAF) production and 6-11% of the carbon dioxide generated from basic oxygen furnace (BOF) production.[1] Extraction of carbon dioxide from steel manufacturing offgas using steelmaking slag for geological sequestration was studied by quantifying the extent and rate of carbonate formation under near-atmospheric aqueous conditions.[2] Because the natural carbonate formation kinetics are very slow, fine grinding to increase slag surface area, increasing pCO_2, increasing temperature, and aqueous catalysis are being investigated to increase the reaction rate to a level suitable for industrial use.[3] The goal of this research is to design a reactor for aqueous-based carbonation of steelmaking slag.

Several research groups have investigated the design of an aqueous reactor system for sequestration of carbon dioxide using steelmaking slag. Huijgen et al.[4], Eloneva et

al.[5], and Stolaroff et al.[6] have worked with leaching and carbonation of steelmaking slag under various conditions. Each study found that the rate and extent of aqueous leaching and carbonation was inversely related to particle size as the primary factor, while pH, temperature, and pCO_2 had milder effects on Ca-conversion. In comparison with naturally occurring wollastonite ($CaSiO_3$), eleven times more carbon dioxide could be sequestered from steel slag at ambient temperature. Other consortia have actively researched methods of large-scale mineral-based carbon dioxide sequestration. O'Connor et al. conducted research in an effort to optimize the process conditions for direct aqueous carbonation of silicate minerals.[7-9] Activation of the minerals (serpentine or olivine) through attrition grinding or heat-treatment was necessary to achieve high levels of carbonation. Additions of $NaHCO_3$ and NaCl to the mineral suspension were found to catalyze the reaction significantly. Park et al. investigated carbonation of olivine and serpentine in a manner similar to the work of O'Connor et al.[10] Aqueous carbonation studies revealed that increasing reactor temperature, pCO_2, and $NaHCO_3$/NaCl concentration increased the carbonation rate. Fernandez et al. found that the reactivity of magnesite slurries for carbonation increases with decreasing particle size and increases with pCO_2, temperature, and solid-liquid ratio.[11]

The current study capitalizes on the findings of many of these researchers, as well as current experimental work, in modeling the design of a reactor for aqueous-based sequestration of carbon dioxide with steelmaking slag. The current process uses a two-stage system to decouple the competing leaching and carbonation mechanisms that may occur simultaneously in a one-stage reactor. The reaction rate of calcium leaching from slag into water and the direct carbonation of slag particles were investigated separately to understand the limiting mechanisms for the overall sequestration process. The main process parameters modeled in this investigation include particle size, reactor residence time, reaction time, and reactor flow sequencing.

II. REACTOR DESIGN AND MODELING PROCEDURE

A. Carbon Dioxide Sequestration Reactions

Carbon sequestration via an aqueous-based reaction of carbon dioxide in offgas with lime in steelmaking slag may follow several possible reactions steps. A list of the key competing reactions considered is given in Table I. The thermodynamic and kinetic parameters of aqueous carbon dioxide dissolution (reactions 1-4) and the reaction of carbonate and calcium ions to precipitate the carbonate (reaction 6) have been previously described.[12,15] Among these reactions, the rate controlling steps are carbon dioxide hydration (reaction 2) and carbonate precipitation (reaction 6).[15,16] However, compared to slag-solution reactions (solid-liquid type) the gas-liquid reactions are relatively rapid.[3]

In this study, experimental kinetic data of calcium leaching from slag (reaction 5) and direct carbonation of slag particles by dissolved carbon dioxide (reaction 7) were used in the process model. The solid-liquid reactions listed in Table I are shown in simplified form as a convenience for studying the kinetics of the overall process. The real processes involving slag are significantly more complicated, as most of the CaO is combined into complex oxide phases (i.e., Ca_2SiO_4 or $Ca_{12}Al_{14}O_{33}$).[2] The dissolution rate of metal oxides (e.g., Ca, Mg, Al, Si, Fe) depends on the degree of iconicity of the M-O bond.[12] For simplification in the current study, the calcium containing phases are designated as CaO, while the experimental leaching kinetic parameters were obtained from industrial steelmaking slags containing multiple mineral phases.[3] The actual mechanism of direct slag carbonation may take several different reaction paths. For simplicity of process modeling however, reaction 6 of Table I was used as the direct carbonation reaction method.

B. CO_2 Sequestration Reactor Design

The process design consists of two vessels connected by a pumped water stream, as shown in Figure 1. Each reactor vessel operates at ambient pressure and temperature. Water and slag particles are introduced into Reactor 1, wherein calcium ions are dissolved to form an alkaline leachate. The leachate is pumped to Reactor 2, through which gaseous carbon dioxide is bubbled. Carbon dioxide dissolves into the water to

form carbonic acid ions, which react with the calcium ions in solution or report to the surface of the slag particle. At the particle surface, several competing reactions take place to precipitate $CaCO_3$. This process design allows investigation of several system scenarios for optimizing carbon dioxide capture.

Table I. Reactions Occurring During Aqueous Slag-Carbon Dioxide Sequestration[4,12]

Description		Reaction
Carbon dioxide dissolution	(1)	$CO_{2(g)} \rightarrow CO_{2(aq)}$
	(2)	$CO_{2(aq)} + H_2O \rightarrow H_2CO_3$
	(3)	$H_2CO_3 \rightarrow H^+ + HCO_3^-$
	(4)	$HCO_3^- \rightarrow H^+ + CO_3^{2-}$
Calcium leaching	(5)	$CaO + H_2O \rightarrow Ca^{2+} + 2(OH^-)$
Carbonate precipitation	(6)	$Ca^{2+} + CO_3^{2-} \rightarrow CaCO_3$
Calcium oxide direct carbonization	(7)	$CaO + CO_{2(aq)} \rightarrow CaCO_3$

Scenario 1: Fresh water is supplied into Reactor 1 and the leachate containing calcium ions is pumped to Reactor 2, where calcium carbonate precipitates. The spent leachate (containing residual dissolved carbon dioxide) is discharged.

Scenario 2: The design is the same as Scenario 1, except that the water supplied to Reactor 1 is recirculated from Reactor 2 after complete degassing.

Scenario 3: Fresh water is supplied to Reactor 2 for saturation with carbon dioxide, and then the saturated water is pumped to Reactor 1 for direct reaction with slag. The spent water (containing residual dissolved carbon dioxide) is discarded.

Scenario 4: The water supplied to Reactor 1 is recirculated from Reactor 2 without degassing.

Experimental verification of the different scenarios was undertaken using a lab-scale apparatus consisting of two connected reactors (tanks). Recirculation of the aqueous stream took place both with and without partial degassing by argon bubbling. Reactor 1 contained two kg of slag mixed in 20 liters of water. The leachate was pumped at varying

rates to Reactor 2, which was sized with a two-liter volume. Bottle grade carbon dioxide was bubbled through a diffuser in the bottom of Reactor 2 to generate a fine gas bubbles distribution, which allowed intimate mixing of the gas and alkaline solution. A multi-channel pH meter was used to measure the pH level in both reactors. At the completion of each test, a sample of the slurry from Reactor 1 was filtered, dried, and analyzed for fraction carbonation, as described previously.[3] Kinetic data from this earlier work was used to develop a process model with METSIM (ver. 15.07) process simulation software.

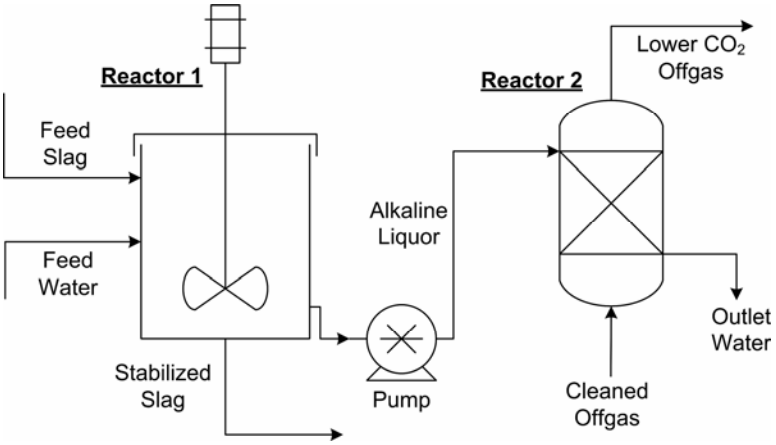

Fig. 1—Flow schematic of system for carbon dioxide sequestration with slag.

C. METSIM Modeling Procedure

An approach developed by Robertson for modeling the heterogeneous reaction kinetics of a non-steady-state process was used for the two-stage reactor system.[13] A block diagram of the METSIM model is shown in Figure 2. The computer model consists of two blocks representing Reactor 1 (Figure 2a) and Reactor 2 (Figure 2b) and connected by streams 15/17 and 20/12. In Reactor 1, the amount of input slag is defined by Stream 10, which connects the mixer and splitter pair A and C, respectively. In the same manner, the amount of aqueous solution is defined by Stream 2, which connects the mixer and splitter pair B and D, respectively. Slag leaching and direct carbonation reactions occur in splitters E and F, respectively. In Reactor 2, carbon dioxide gas (Stream 16) is mixed with the aqueous stream from Reactor 1 (Stream 12) in Mixer F,

while carbon dioxide dissolution to form carbonic acid ions takes place in Splitter G. Carbonic acid ions react with calcium ions in Splitter M, and precipitated calcium carbonate accumulates in the loop consisting of the mixer/splitter pair H/L.

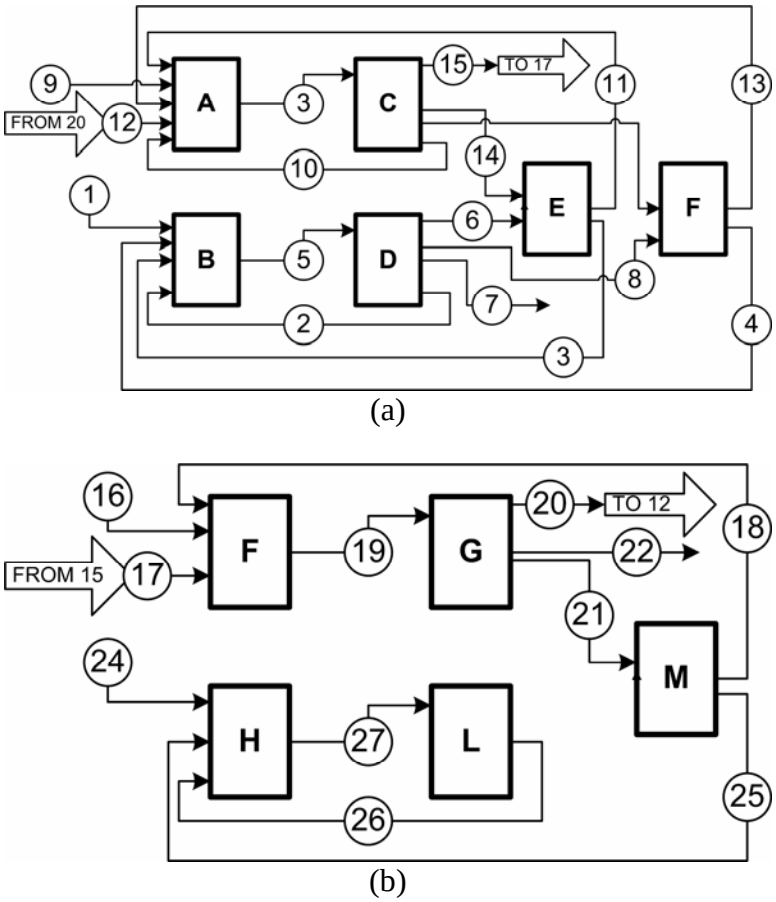

Fig. 2—Block diagrams of the METSIM model for (a) Reactor 1 and (b) Reactor 2, which are interconnected by streams 15/17 and 20/12.

This model allows the study of each scenario individually. For example, in Scenario 1 fresh water is supplied by Stream 9 to leach the slag in Reactor 1. The leached calcium ions are pumped by Stream 15/17 to Reactor 2, where precipitated calcium carbonate accumulates in Stream 26. The spent aqueous stream is discarded by Stream 22 without flowing back to Reactor 1. Alternatively, in Scenario 4 the aqueous solution is recirculated by streams 15/17 and 12/20 without fresh water input in Reactor 1 or

solution discharge from Reactor 2. The model was used to calculate both a non-steady-state batch type process in Reactor 1 with no fresh slag input from Stream 1 and no product discharge to Stream 7, and a steady-state continuous type process with fresh slag input and carbonate product output. Because the dissolution rate of carbon dioxide occurs more rapidly than slag leaching and carbonation, carbon dioxide dissolution was modeled using the known Henry constant with a reaction extent equal to one (equilibrium).[12]

D. Experimental Reaction Kinetics for METSIM Modeling

In the METSIM model, the reaction rate (F) is defined by Equation 1. The rate constant (K) is defined by the mass flow rate ($m_i/\Delta t$) from the mixer/splitter to the phase splitter, where the reaction occurs with the particular value of reaction extent (RE) at each time step (Δt). The experimentally measured kinetic parameters for leaching and carbonation from earlier work were used to evaluate the factors in Equation 1.[3]

$$F = K \times (RE) \tag{1}$$

Heterogeneous direct aqueous carbonation of slag particles was modeled for the batch case of Scenario 4 in order to validate the results with the experimental data. In this scenario, the reaction rate is limited by mass transfer through the carbonate product layer and decreases with time as a result of increasing thickness and density of carbonate layer.[3] The reaction rate expression increases in complexity because the porosity of the product layer decreases the core of unreacted slag (with radius r_c) in each particle (with initial radius R) shrinks. Therefore, a modified shrinking core model was used with the assumption that diffusivity (D) decreases as the reaction proceeded. This model is defined by Equations 2-5, where J_A (moles/m^2·s) is the flux of component A, dN_A/dt (moles/s) is the reaction rate, ρ_m (moles/m^3) is the molar density, and the parameter k (m/s) was chosen to fit the experimental data.[4]

$$-\frac{dN_A}{dt} = -4\pi r^2 J_A \tag{2}$$

$$J_A = -D\frac{dC_A}{dr} \tag{3}$$

$$dN_A = 4\pi\rho_m r_c^2 dr_c \tag{4}$$

$$D = D_0 - k(R - r_c) \tag{5}$$

In this system, Equation 2 is the reaction rate as a function of surface area and flux, Equation 3 is the diffusion flux as a function of diffusivity and concentration gradient, and Equation 4 is the mass balance of component A.[14] Equation 5 is the diffusivity as a function of carbonized layer thickness. This system of equations was solved numerically for three incremental time steps, each with changing diffusivity, to fit the experimental data for carbonation of ladle metallurgy furnace (LMF) slag with 49.9 wt.% CaO (Slag #2, 420-590 μm).[3] In Figure 3 the experimental results are compared to the modified shrinking core model using constant and decreasing diffusivity. Ca_C and Ca_S are the fractions of calcium carbonized and initial present in the slag, respectively.

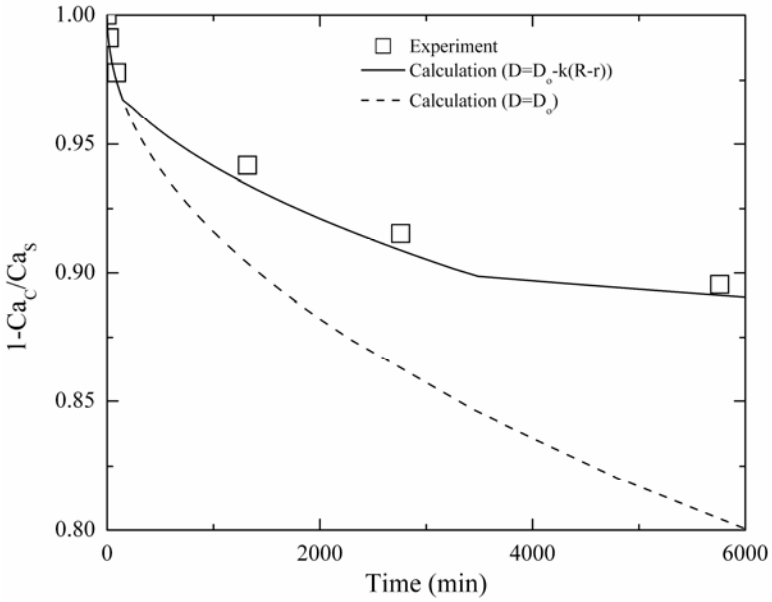

Fig. 3—Comparison of experimental data for slag carbonization with shrinking core model using constant ($D=D_0$) and decreasing ($D=D_0-k(R-r)$) diffusivity of the product layer for slag with 49.9 wt.% CaO and 420-590 μm particle size.

For application in the METSIM model, the experimental kinetics of the carbonation reaction was approximated to be a function of time (t), as shown in Equation 6. A factor of n=⅓ resulted in an appropriate fit for the reaction conversion (Ca_C/Ca_S) calculated from Equations 2-5 and the experimental data.

$$\ln\left(1-\frac{Ca_C}{Ca_S}\right) = f(t)^n \tag{6}$$

For direct carbonation (Figure 4), the experimental data was fit to Equations 7 and 8, where d is the particle diameter (mm), t is the time (min), and the coefficient A=0.0012 was taken from correlated experimental data (Figure 4b). Equation 8 is the first derivative form, which represents the reaction rate (F), and was the equation used in the METSIM model.

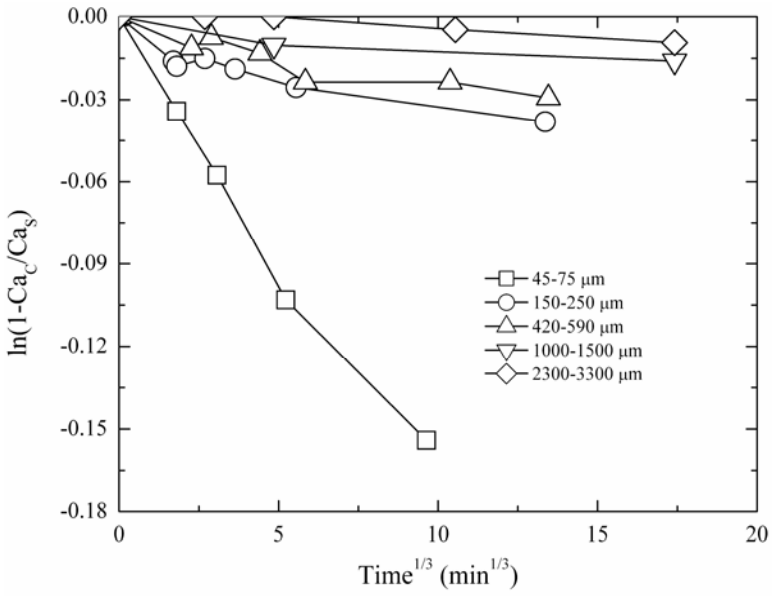

(a)

Fig. 4—Comparison of experimental data for slag carbonization with the parameters (a) $\ln(1-Ca_C/Ca_S)$ and (b) $d*\ln(1-Ca_C/Ca_S)$ versus $time^{1/3}$.

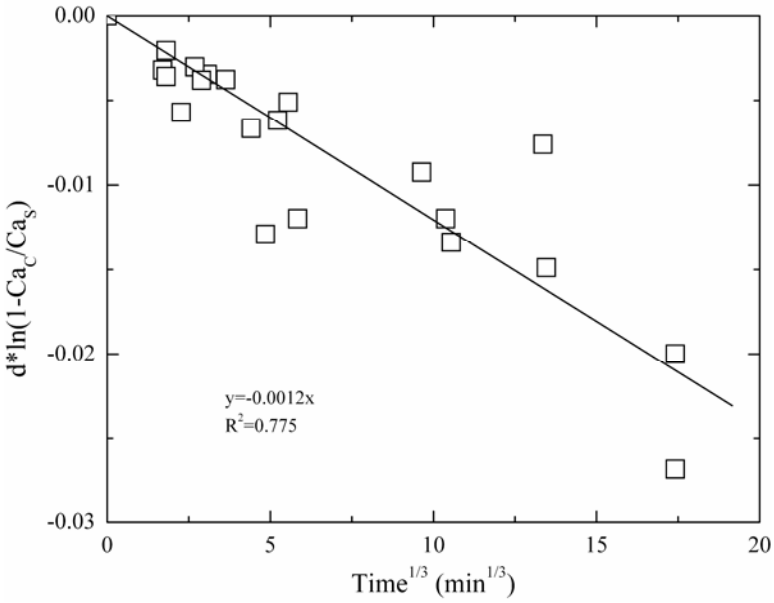

(b)

Fig. 4—Comparison of experimental data for slag carbonization with the parameters (a) $\ln(1-Ca_C/Ca_S)$ and (b) $d*\ln(1-Ca_C/Ca_S)$ versus $time^{1/3}$ (cont.).

$$Ca_C = Ca_S\left(1-\exp\left(-\frac{A}{d}t^{1/3}\right)\right) \tag{7}$$

$$F = \frac{dCa_C}{dt} = \frac{ACa_S}{3d}t^{-2/3}\exp\left(-\frac{A}{d}t^{1/3}\right) \tag{8}$$

A similar analysis of the calcium leaching process was undertaken using a set of reactions that corresponds to Scenario 1. The reaction rate changes during the leaching process because the initial chemical reaction limited mechanism is overtaken by diffusion through the porous surface layer developed during treatment.[3] The difference in Equation 9 between leaching and carbonation (Equation 8) arises from the necessity to take into account the solution volume V (cm^3), the calcium saturation level C_{sat} (wt. %) for solution in equilibrium with solid $Ca(OH)_2$, and the total surface area $S= 6W/\rho d$ (cm^2) of slag particles with diameter d (cm), density ρ (g/cm^3), and weight W (g) according to the batch test procedure. In Equation 9 C_D is the concentration of dissolved calcium in solution (wt.

%) and the coefficient *A*=0.0004 was taken from the correlation of experimental data shown in Figure 5. The extent of calcium leaching from slag depends on slag particle size and particle surface conditions. Calcium from fresh slag leached twice as fast than from the same slag in the carbonized condition.[3] Because leaching and carbonation may occur simultaneously in the Scenario 4 apparatus, the leaching reaction rate (Equation 9) was linked to the current slag carbonation level during each calculation step.

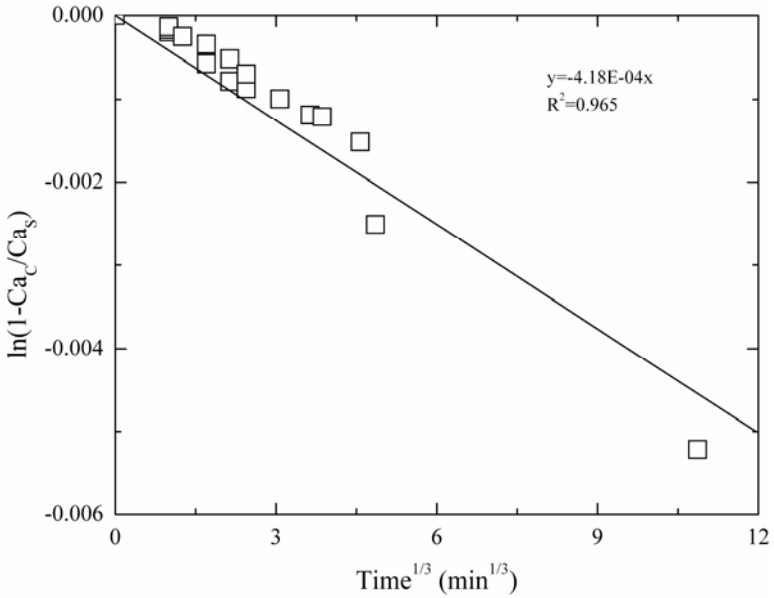

Fig. 5— Comparison of experimental data for slag leaching with the parameter $(1/S)*\ln(1-C_D/C_{sat})$ versus time$^{1/3}$.

$$F = \frac{dC_D}{dt} = \tfrac{1}{3}VAC_{sat}St^{-2/3}\exp\left(-ASt^{1/3}\right) \tag{9}$$

III. RESULTS AND DISCUSSION

A. Model Validation with a Batch Reactor

The METSIM model was first validated by comparing the calculated results with the experimental data obtained from the batch reactor tests in the previous work.[3] The calcium leaching experiments were performed in a batch type reactor under a protective

argon atmosphere with unsaturated aqueous solutions, which corresponds to Scenario 1 for Reactor 1. The METSIM modeling of the batch type reactor was conducted by disconnecting Reactor 1 from Reactor 2 and disregarding the feed streams. Figure 6 compares the calculated and experimental results for the concentration of calcium leached (C_D) from LMF Slag #2 (49.9 wt.% CaO) at two average particle sizes (60 µm and 200 µm). The calculated leaching results were in good agreement with the experimental data. Direct carbonation of the same slag was studied in a batch type reactor using an aqueous solution saturated by carbonic acid at one atmosphere pressure.[3] This process was modeled using batch type Reactor 1 connected to Reactor 2 with continuously flowing carbon dioxide gas saturating the aqueous solution. The transport of calcium ions from Reactor 1 to Reactor 2 was prohibited. This approach modeled the experimental conditions of Scenario 3. Figure 7 shows that the experimental results for the amount of calcium carbonized (Ca_C) were in good agreement with that predicted by the METSIM model for two different average particle sizes of LMF Slag #2 (60 µm and 2800 µm).

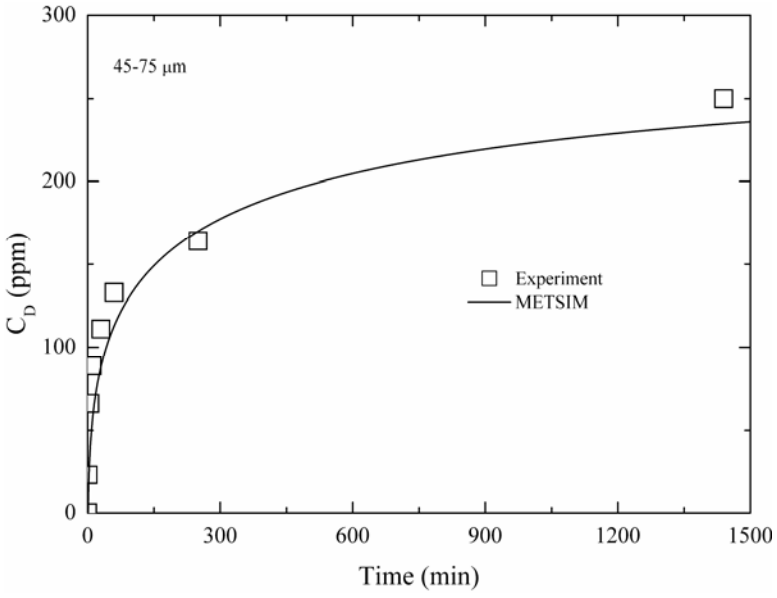

(a)

Fig. 6—Comparison of experimental and calculated concentration of leached calcium (C_D) for slag particles with (a) 60 µm and (b) 200 µm average diameter.

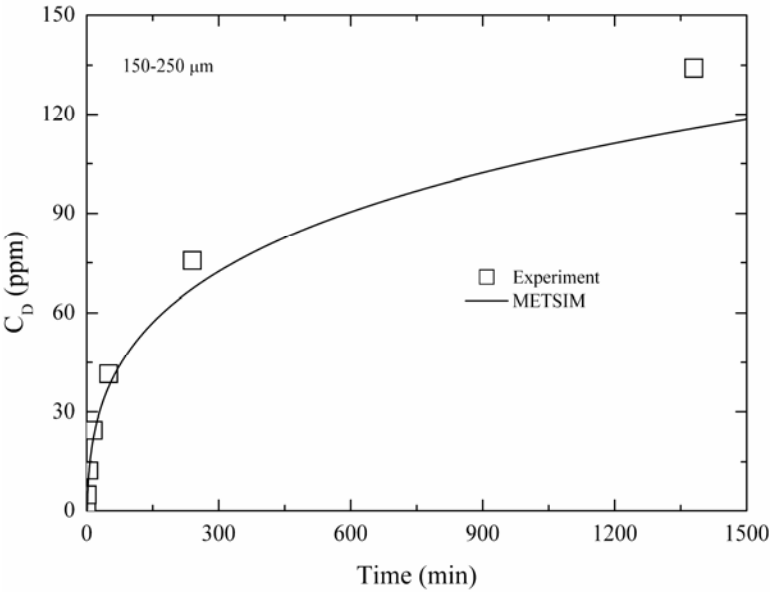

(b)

Fig. 6—Comparison of experimental and calculated concentration of leached calcium (C_D) for slag particles with (a) 60 μm and (b) 200 μm average diameter (cont.).

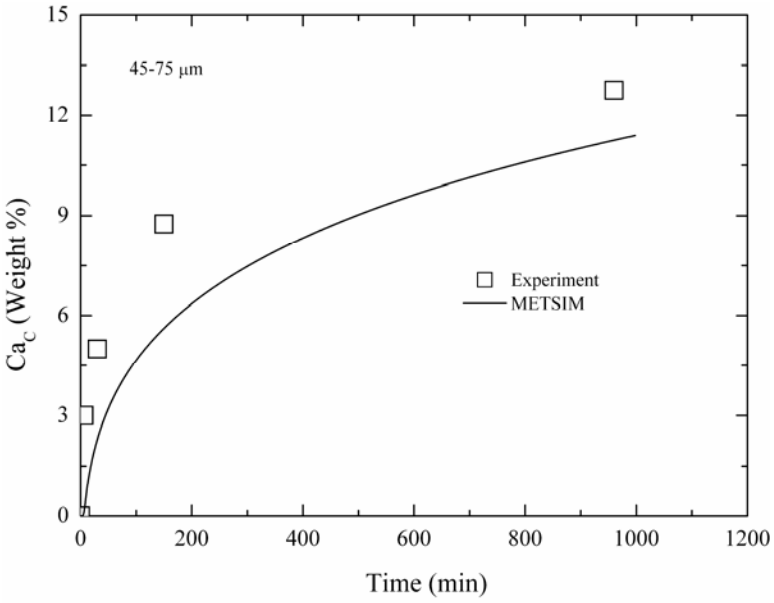

(a)

Fig. 7—Comparison of experimental and calculated results for slag carbonation (Ca_C) with (a) 60 μm and (b) 2800 μm average diameter particles.

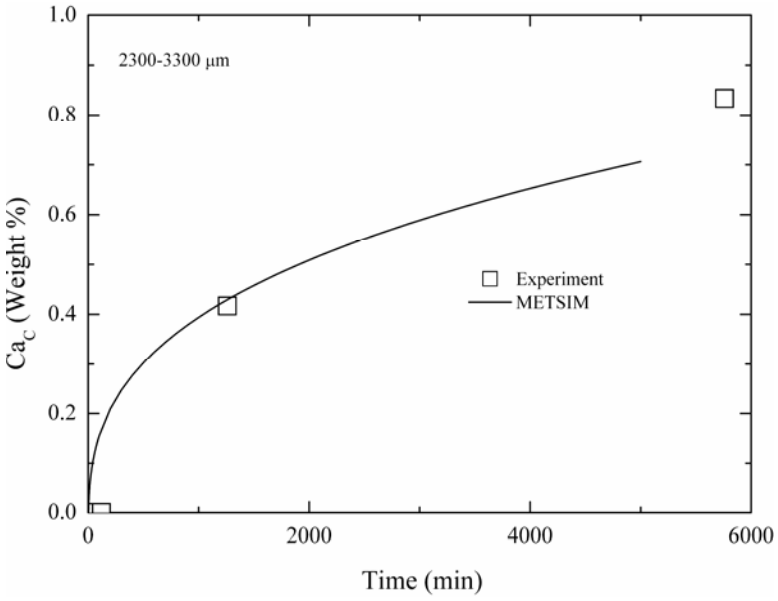

(b)

Fig. 7—Comparison of experimental and calculated results for slag carbonation (CaC) with (a) 60 μm and (b) 2800 μm average diameter particles (cont).

B. Model Validation with Experimental Two-Stage Reactor

The METSIM model was further validated by comparing the calculated results with the experimental data obtained from the two-stage reactor tests of the previous work.[3] Scenario 4 (a batch amount of slag with recirculated non-degassed water) was modeled and the results compared to the experimental data for slag carbonation. Calcium leaching and direct slag particle carbonation were monitored simultaneously in both reactors. Reactor 1 contained 200 g LMF slag (<3.2 mm) in 20 liters of water, while Reactor 2 contained two liters of solution, through which 1.5 g/min carbon dioxide was bubbled. A solution exchange rate of one liter per minute was used to transfer the fluid between the two reactors. The experimental procedure included soaking the slag in Reactor 1 for 20 minutes with solution recirculation and no carbon dioxide input into Reactor 2. During this time, the pH increased in both reactors as $Ca(OH)_2$ was formed. Shortly after introducing carbon dioxide into Reactor 2, the concentration of calcium ions in solution decreased, while the concentration of carbonic acid increased. The rate of pH decrease (Figure 8) depended on the solution residence time in Reactor 1 (20 minutes)

and Reactor 2 (2 min). When using ideal (equilibrium) carbon dioxide dissolution conditions in the Reactor 2 METSIM model, the pH neutralization time in Reactor 1 was shorter than experimentally measured. Reactor size and method of carbon dioxide injection may influence the gas dissolution efficiency because the bubbles of injected carbon dioxide may not completely dissolve in the two-liter volume of Reactor 2. Upon completion of the neutralization period, equilibrium approximation did not affect on the process model results.

The reaction was allowed to proceed for 20 hours, after which the product was dried, sieved, and analyzed for calcium carbonation. The prevailing reaction was direct slag particle carbonation in Reactor 1, while a minor amount of residual precipitated carbonates was found in Reactor 2. A similar result was achieved using the METSIM simulation. The model predicted carbonate precipitation in Reactor 2 immediately after introducing carbon dioxide, after which direct carbonation of the slag in Reactor 1 took predominance. As the particle size decreased, the amount of slag carbonate product increased, as shown in the model results in Figure 9a.

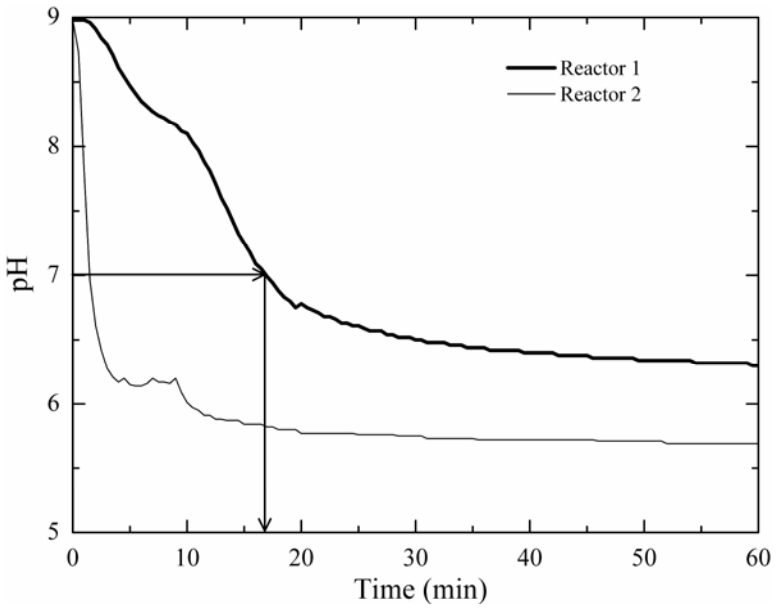

Fig. 8—Changing pH of aqueous solutions in reactors during carbonization (200 g of crushed <3.2 mm LMF Slag #2, 1.5 g/min flow rate carbon dioxide) based on start of carbon dioxide flow.

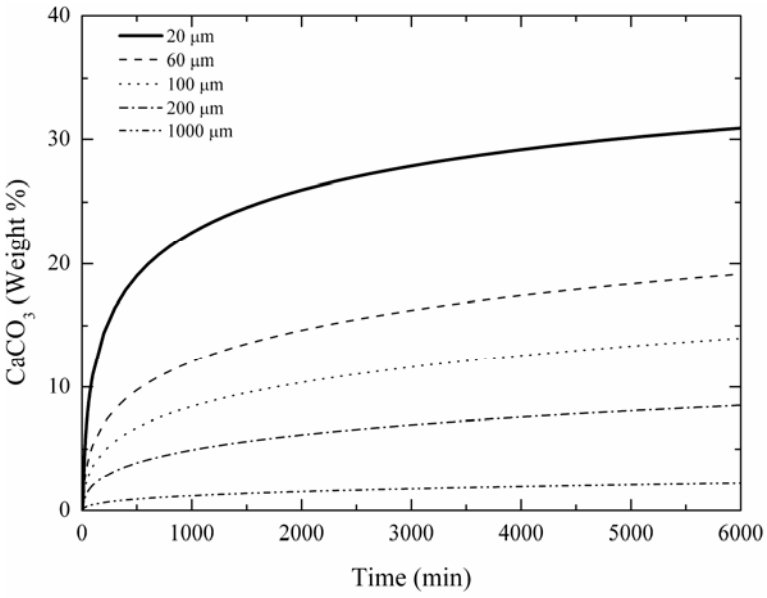

(a)

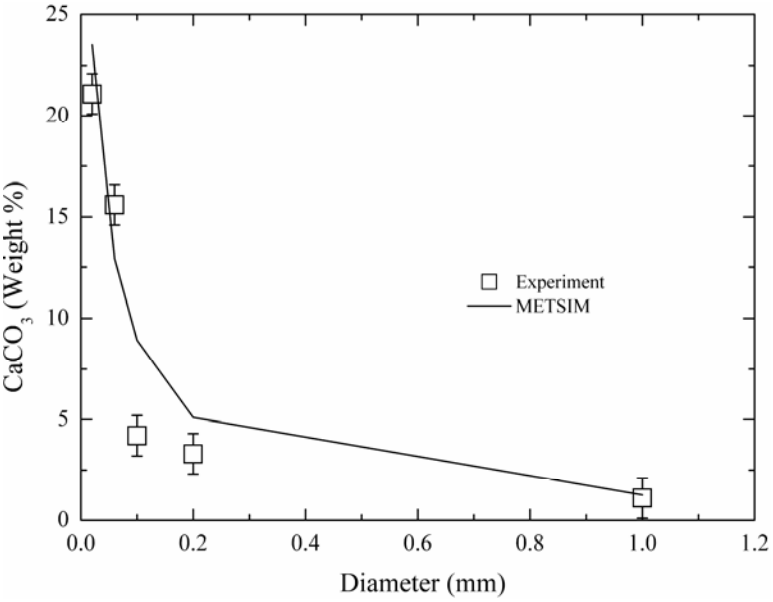

(b)

Fig.9—METSIM calculated kinetics of (a) LMF slag carbonation for several particle sizes and (b) comparison of calculated and experimentally measured calcium carbonate content after 20 hours reaction (cont.).

A 1000 µm particle size produced 2% $CaCO_3$ at 20 hours (1200 min), while decreasing the particle size by an order of magnitude to 100 µm produced 8% $CaCO_3$ at the same time. Decreasing the particle size another half order of magnitude to 20 µm

resulted in 23% $CaCO_3$. A comparison of the experimental results (Figure 9b) and modeled results (Figure 9a) for five particle sizes shows good agreement.

C. Industrial Process Modeling

The validated METSIM process model was used to study the four scenarios defined for the purpose of reactor flow schematic optimization.

Scenario 1: The goal of Scenario 1 was to analyze the influence of slag/solution ratio and solution residence time in Reactor 1 on the extent of leaching only. In this model, slag was leached in Reactor 1 and the alkaline leachate was carbonized in Reactor 2. LMF Slag #2 with 49.9 wt.% CaO and a monosize 200 μm distribution was used. During continuous operation, fresh water was input into Reactor 1, which contained a fixed amount of slag, while the spent leachate was discharged at the same rate from Reactor 2, with no water recirculated to Reactor 1. For comparison, a batch operation was studied using a fixed starting volume of water and slag in Reactor 1, with no water input or output.

The results from this scenario are presented in Figure 10. They show that increasing the slag/solution ratio and the solution residence time in Reactor 1 produced a higher concentration of calcium ions in solution. Increasing the slag/solution ratio with zero water throughput (i.e., in batch mode) provided a diminishing increase in calcium ions in solution due to saturation of the aqueous phase (Figure 10a). For example, increasing the slag solution ratio by an order of magnitude from 0.08% to 0.8% results in an increase of $Ca(OH)_2$ from 150 PPM to 950 PPM at 10 hours, while a further doubling of the slag/solution ratio to 1.6% results in a corresponding increase to 1100 PPM at the same time. To overcome saturation of the aqueous phase, the feed water throughput in Reactor 1 can be increased, which corresponds to a decrease in residence time (Figure 10b). At a fixed slag/solution ratio of 0.8%, a 5000 minute residence time approaches the response of a batch system, which has a theoretical infinite residence time. As the residence time decreases, the resulting solution becomes less saturated and at five minutes the leachate is under-saturated. While minimizing the solution saturation provides increased driving force for Ca dissolution, it also requires a significant increase in feed water. The total fraction of calcium leached from the slag (ordinate axis of Figure

10c) is equal to the concentration of calcium in solution multiplied by the solution volume. The optimal residence time is therefore a balance between maximizing the amount leached and minimizing fresh water input. For slag with 200 μm particle diameter and 0.8% slag/solution ratio, the optimal residence time is near one hour (Figure 10c).

Scenario 2: This scenario minimizes fresh water input into the system by recirculating the leachate from Reactor 2 to Reactor 1. However, for this scenario to work properly, the recirculated leachate must be fully degassed to prevent carbonic acid from reporting to Reactor 1. Preliminary experiments with degassing the leachate by argon bubbling showed that full leachate degassing is difficult to achieve and the residual content of carbonic acid will provide direct carbonation of the slag particles in Reactor 1. This problem is addressed in Scenario 4.

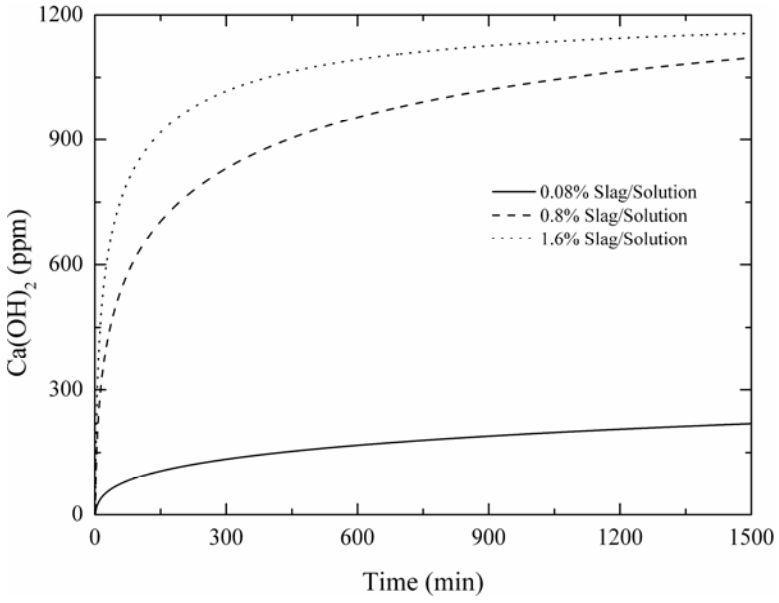

(a)

Fig. 10—Results of METSIM model for leaching LMF Slag #2 (200 μm diameter) at different slag/solution ratios in (a) batch mode and (b,c) increase of Ca leaching by fresh water input into mix-flow type Reactor 1 with different residence times.

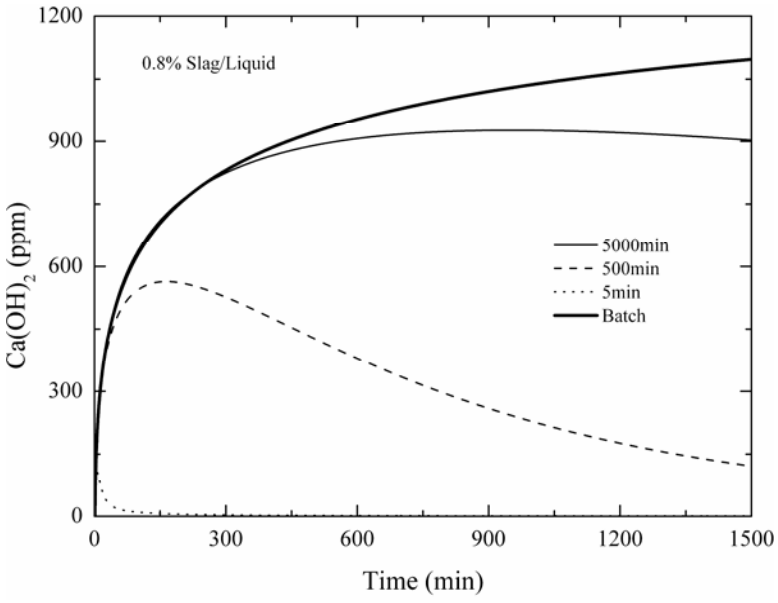

(b)

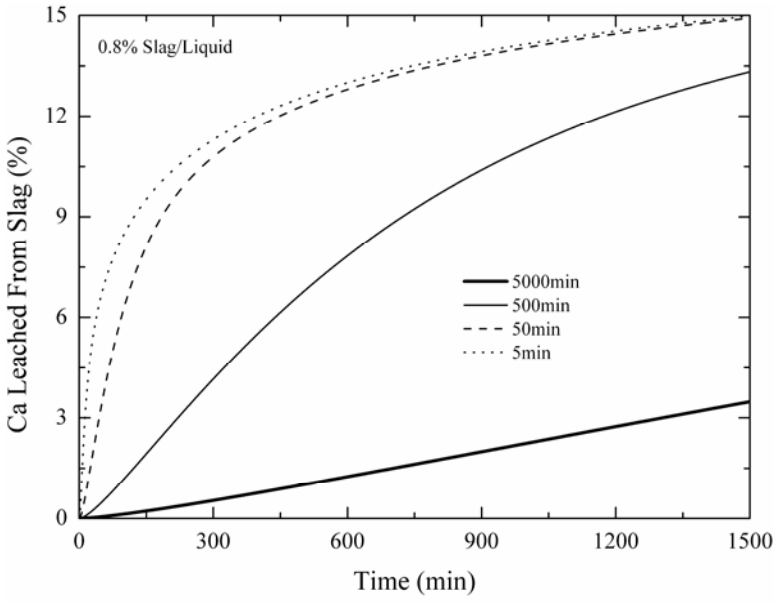

(c)

Fig. 10—Results of METSIM model for leaching LMF Slag #2 (200 µm diameter) at different slag/solution ratios in (a) batch mode and (b,c) increase of Ca leaching by fresh water input into mix-flow type Reactor 1 with different residence times.

Scenario 3: This scenario inputs fresh water into Reactor 2 for saturation with carbon dioxide, then pumps the saturated water to Reactor 1 for direct reaction with slag.

Because this scenario requires a significant quantity of fresh water input, it was not modeled in this analysis.

Scenario 4: For scale-up to an industrial process of carbon dioxide sequestration, continuous processing of slag through the system is desired. To meet this criteria, a steady-state METSIM model was set up to allow continuous feed of fresh slag to Reactor 1 at the same rate as carbonized product was discharged from Reactor 2. Carbon dioxide was introduced into Reactor 2 and the aqueous solution was recirculated from Reactor 2 to Reactor 1. As a first approximation, Reactor 1 was assumed to operate in back-mix mode with the composition of the discharged stream as an average for Reactor 1. The steady-state model was compared to a batch processing model both of which used fresh slag (LMF Slag #2 with 49.9 wt.% CaO).

In batch processing mode, the amount of slag carbonation increased steadily with reaction time, as shown in Figure 11a. At seven days (10,800 min.) of processing in batch mode, ~8% carbonation was achieved using 200 μm particles. In steady-state processing mode and with a constant amount of slag throughput, the overall amount of carbonation depended on Reactor 1 slag residence time and particle size (Figure 11b). A 200 μm particle at seven days residence time achieved ~8% carbonation, while a 20 μm particle achieved ~22.5% carbonation at the same residence time. Particle size is critical. A 1.0 mm particle achieved only ~2% carbonation at the same residence time. Increasing the slag residence time of Reactor 1 produces more carbonation. For a 200 μm particle, a two-day residence time enabled ~5% carbonation, while a twenty day residence time allowed ~12% carbonation. While increasing the slag residence time in Reactor 1 results in more carbonation, it also requires a larger reactor volume. Decreasing the slag residence time makes it possible to minimize the volume of Reactor 1, but results in a simultaneous decrease in the level of slag carbonation in the discharged product. A balance can be realized between particle size and reactor residence time. When working to achieve a specific amount of carbonation, reducing the slag particle size allows for reduction in reactor residence time.

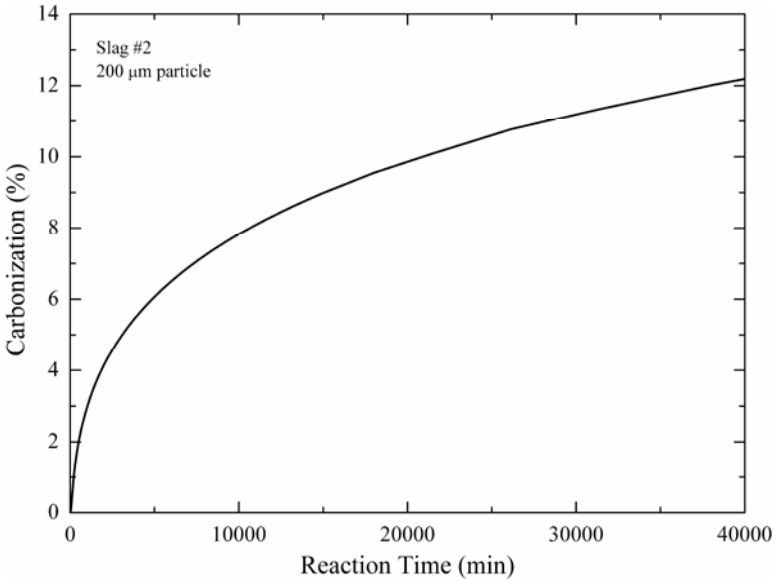

(a)

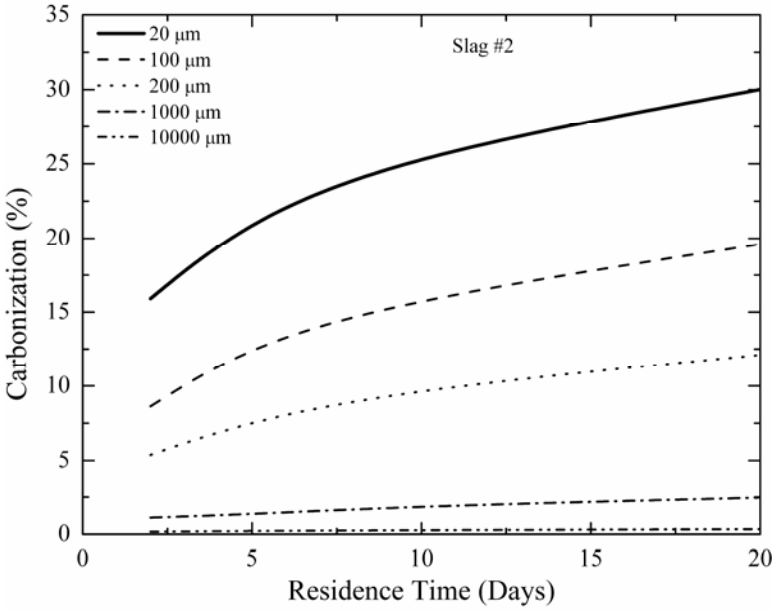

(b)

Fig. 11—Comparison of batch carbonization a 200 μm particle (a) and steady-state continuous carbonation (b) using varying particle size of LMF Slag #2 in Reactor 1.

IV. CONCLUSIONS

METSIM process simulation software was used to model several reactor design scenarios for hydrous carbonate sequestration of carbon dioxide using steelmaking slag.

A two-stage reactor design was modeled in batch and continuous modes. The process allowed the introduction of water and slag into the first reactor and carbon dioxide into the second reactor, along with the possibility of recirculating the solution. A comparison of the scenarios shows that continuous calcium leaching by fresh water in the first reactor has the advantage of preventing the formation of a carbonate product layer on the slag particles, which could reduce the leaching efficiency. However, the water requirement in a continuous system is much higher than a recirculated system. To minimize the fresh water make-up, the spent leachate from the second reactor can be recirculated to the first reactor. The main drawback of this system is that the residual absorbed carbon dioxide in the recirculated water results in the formation of a calcium carbonate layer on the slag particles, which inhibits leaching of calcium ions. The product layer blinding effect could be partially overcome by increasing the slag surface area (i.e., decreasing the particle size), and increasing the residence time in the first reactor. The METSIM model showed that these two factors greatly affected the amount of calcium carbonated. The METSIM model was shown to be a useful tool for designing and optimizing carbon dioxide sequestration reactor systems based on different slag fractions and compositions.

V. ACKNOWLEDGEMENTS

This paper was prepared as an account of work sponsored by the U.S. Department of Energy, in cooperation with the American Iron and Steel Institute (AISI) and its participating companies, under Agreement DE-FC36-97ID13554. Such support does not constitute an endorsement by DOE or AISI of the views expressed in the article. The authors also acknowledge the support of DOFASCO, Gallatin Steel, Hylsa, IPSCO, Mittal Steel, Praxair, Nucor, Timken Company, and US Steel.

VI. REFERENCES

1. C.H. Rawlins, V.L. Richards, K.D. Peaslee, and S.N. Lekakh: Steel Times Intern., 2006, vol. 30, no. 7, pp. 25-26.
2. C.H. Rawlins, V.L. Richards, K.D. Peaslee, and S.N. Lekakh: Proc. AISTech 2006 Conf., May 1-4, 2006; Cleveland, OH, U.S.

3. S.N. Lekakh, C.H. Rawlins, D.R. Robertson, V.L. Richards, and K.D. Peaslee: Metall. Mater. Trans. B (on-line), 2007.
4. W. Huijgen, G-J. Witkamp, and R.N.J. Comans: Environ. Sci. Technol., 2005, vol. 39, no. 24, pp. 9676-9682.
5. S. Eloneva, S. Teir, C.-J. Fogleholm, and R. Zevenhoven: Proc. 4th Nordic Minisymp. Carbon Dioxide Capture and Storage.
6. J.K. Stolaroff, G.V. Lowry, and D. W. Keith: Energy Conserv. Manag., 2005, vol. 46, no. 5, pp. 687-699.
7. W.K. O'Connor, R.P. Walters, D.C. Dahlin, G.E. Rush, D.N. Nilsen, and P.C. Turner: Proc. 26th Int. Tech. Conf. Coal Utiliz. Fuel Syst., 2001, pp. 765-776.
8. M.T., Ityokumbul, S. Chander, W.K. O'Connor, D.C. Dahlin, and S.J. Gerdemann: Proc. 18th Annu. Int. Pittsburgh Coal Conf., 2001, pp. 843-852.
9. L.R. Penner, S.J. Gerdemann, D.C. Dahlin, W.K. O'Connor, and D.N. Nilsen: Proc. 28th Int. Tech. Conf. Coal Utiliz. Fuel Syst, 2003, pp. 353-364.
10. A.-H. Park, R.A. Jadhav, and L.-S. Fan: Proc. Annu. Meet. AIChE, 2001, paper 257a.
11. A.I., Fernandez, J.M. Chimenos, M. Segarra, M.A. Fernández, and F. Espiell: Hydromet., 1999, vol. 53.2, pp. 155-167.
12. Luigi Marini: Geological Sequestration of Carbon Dioxide; Thermodynamics, Kinetics, and Reaction Path Modeling, Elsevier B.V., Amsterdam, The Netherlands, 2007, pp. 88-91.
13. D.G.C., Robertson: EPD Congr. 1995, Proc. Symp. TMS Annu. Meet., 1995, pp. 347-61.
14. Octave Levenspiel: Chemical Reaction Engineering, John Wiley & Sons, Hoboken, NJ, 1962, pp. 338-357.
15. G. Bond, J. Stringer, D. Brandvold. A. Simsek, M. Medina, and G. Egeland: Energy and Fuels, 2001, vol. 15, pp. 309-316.
16. Mirjafari, K. Asghari, and N. Mahinpey: Ind. Eng. Chem. Res., 2007, vol. 46, pp. 921-926.

4. Investigation of Carbonic Anhydrase Assisted Carbon Dioxide Sequestration Using Steelmaking Slag

C. Hank Rawlins, Simon N. Lekakh, Kent D. Peaslee, Von L. Richards

Missouri University of Science & Technology
Rolla, Missouri, U.S.A.
E-mail: kpeaslee@mst.edu

Prepared for publication in Hydrometallurgy.

ABSTRACT

Batch aqueous leaching and carbonation tests were conducted using industrial steelmaking slags to determine their rates and the effect of carbonic anhydrase enzyme as a catalyst. The amount of calcium leached is a strong function of particle surface area, which is a more important factor than calcium oxide content. Carbonic anhydrase did not affect the leaching rate. The extent of calcium leaching is expressed mathematically as a function of time and particle size. Carbonic anhydrase catalyzed the reaction between calcium oxide and carbon dioxide in water to achieve a neutralization time near the theoretical rate. Additionally, carbonic anhydrase modified the precipitate from an overlapping block structure to a dendritic morphology with a smaller average particle size because it accelerated particle nucleation more than particle growth. The rate of carbonation is a strong function of pH. Time controlled tests in which the pH dropped to ~6 resulted in a decreased amount of carbonate produced for a given time that was accelerated by carbonic anhydrase. pH controlled tests (>8.5) exhibited the highest rate of carbonation, even compared to previous testing. Because the leaching rate was ~50% faster than the carbonation rate, a further increase in the amount of carbonation may be realized by using carbonic anhydrase (but the pH must be maintained >10.33).

INTRODUCTION

Steelmaking slag contains high fractions of alkaline earth oxide based phases (i.e., CaO and MgO) that exothermically form carbonates. Thus, it is being considered as a means of permanent carbon dioxide sequestration. At current U.S. steel production rates, approximately 13-17 million tons/year of slag are generated from basic oxygen furnace (BOF), electric arc furnace (EAF), and ladle metallurgy furnace (LMF) processes.[1] BOF and EAF slag is used as high quality mineral aggregate or cement clinker, while LMF slag, produced at ~15% the rate of BOF and EAF slags, has limited use as blast furnace flux or acid mine neutralization with the majority going to landfill.[2] Based on slag's chemical nature and immediate availability as a co-product from steel production, the steel industry initiated a project to investigate hydrous carbonate formation in

steelmaking slag as a method of sequestering carbon dioxide emitted in steelmaking offgas.[3] The goal of this project is to determine the reactor parameters suitable for the design of an industrial system for treating steelmaking offgas with raw or minimally processed slag.

While, thermodynamically, slag can capture 6-11% of the carbon dioxide emitted by integrated mills and 35-45% emitted by mini-mills, the actual reaction kinetics are very slow and full equilibrium may not be reached at atmospheric conditions for 3-6 months.[4] Retardation of the carbonate formation reactions is caused by binding the alkaline earth oxides into complex oxide phases (i.e., Ca_2SiO_4, $Ca_{12}Al_{14}O_{33}$, and $MgFe_2O_4$) which reduces their activities, encapsulation of these complex oxides by inert phases (i.e., SiO_2 and Al_2O_3), and formation of a dense product layer (i.e., $CaCO_3$) upon initial carbonation that inhibits diffusion of the reacting species.[1] Therefore, the primary focus of this investigation is to improve the process kinetics of carbonate formation from the alkaline earth oxide phases.

Both physical and chemical methods of improving the reaction kinetics for large-scale mineral deposit based sequestration systems have been investigated. These efforts have primarily focused on geologic features containing serpentine, olivine, and wollastonite, but the results are directly applicable to slag based sequestration.[5-7] Physical methods include increasing temperature and/or carbon dioxide partial pressure to enhance diffusion rates, pre-treating particles through grinding or acid leaching to increase surface area, and exfoliation of the product layer by high shear/abrasive reactors. High-pressure high-temperature (HPHT) processes require autoclave-based reactors and are not feasible for large scale processing of commodity priced slag. Only grinding pre-treatment (with associated metal recovery) was deemed an appropriate physical method for improving the kinetic reaction rate.[2] Slag leaching and carbonation studies showed that particle size is a controlling factor for the conversion of calcium oxide in slag.[1] Physical methods alone cannot achieve industrial scale rates; therefore, improvements to the process chemistry are required. Chemical enhancements have primarily focused on aqueous based processing, which has a much higher inherent reaction rate than gas-solid reactions. Additives to the aqueous slurry include NaCl, $NaHCO_3$, citric acid, or EDTA.[5-8] These

additives have moderately improved the carbonation rates, but only when used in HPHT systems.

The current work seeks to investigate a catalytic additive for calcium carbonate precipitation in aqueous systems operating under atmospheric conditions. The use of purified carbonic anhydrase in a biomimetic-based industrial scale carbon dioxide sequestration process has been proposed by Bond et al.[9] Carbonic anhydrase is an enzyme found in animals, plants, algae, and bacteria that catalyzes a wide range of metabolic functions including respiration, photosynthesis, and calcium carbonate formation (in both avian shell and mollusk nacre). Carbonic anhydrase (CA) is of interest for sequestration as it catalyzes the reversible hydration of carbon dioxide at or near the diffusion-controlled limit. One molecule of the CA II (an isozyme of carbonic anhydrase) can hydrate $1.4x10^6$ molecules of CO_2 per second, which is equivalent to processing more than 2 million m^3/min of carbon dioxide (at atmospheric conditions) with one mole of CA II.

Bond et al. have focused on designing a system to sequester carbon dioxide emitted by large-scale thermal power plants. While purified carbonic anhydrase is available commercially (e.g., bovine erythrocytes carbonic anhydrase [BCA] from Sigma-Aldrich Co.), this form may be too cost prohibitive for industrial use. Bond et al. have identified less costly sources such as plant extracts[9] and bacterial overexpression[10]. The latter method can produce carbonic anhydrase at a rate similar to that used to produce inexpensive commercial detergent enzymes. Also, because carbonic anhydrase is water soluble, Bond et al. have focused on immobilizing the enzyme into chitosan-alginate beads that maintain accelerated carbonate formation through fifteen cycles, thus demonstrating an effective way to minimize enzyme loss.[11] BCA showed no denaturing up to 70°C in the presence of SO_x and NO_x contaminants at levels expected in normal power plant exhaust gas, so it should be sufficiently robust for industrial scale use.[12] In their system concept, Bond et al. have assumed a sufficient cation (i.e., Ca^{2+}) source is available for reaction with the hydrated carbon dioxide to form calcium carbonate. They have investigated seawater, well brines, and produced water (a byproduct of oil wells).[13] These water sources are feasible, but their low calcium ion concentrations require buffering (pH~8.5) to maintain high carbonate precipitation rates.

Carbonic anhydrase assisted slag-based carbon dioxide sequestration must be considered in both the rate of cation leaching from slag and the subsequent precipitation of calcium carbonate. Previous aqueous kinetic studies of slag showed that leaching occurs faster than carbonation, but both processes are inhibited by the calcium carbonate product layer.[1] The leaching rate is governed by the rate of calcium (complex) oxide dissolution and the tortuous porous surface layer of the slag particle. The dissolution rate may be increased with temperature and the porous layer effect may be reduced in proportion to particle size. Carbonic anhydrase has been shown to increase the release rate of Ca^{2+} from limestone by a factor of 11.7, so it may assist in cation release from slag particles.[14] The carbonation rate is governed by product layer diffusion, and any mechanism that can increase the diffusivity of the reacting species through this layer, or remove this layer to continually expose fresh surface, will improve the carbonation kinetics. As shown by Bond et al.[9-12] and Mirjafari et al.[15], carbonic anhydrase greatly improves the precipitation rate of calcium carbonate and thus, may affect the growth rate or morphology of the product layer on a slag particle during carbonation. This project investigates the role of carbonic anhydrase in assisting cation leaching or carbonate formation in an aqueous carbon dioxide sequestration system using steelmaking slag.

CARBONIC ANHYDRASE MECHANISM

Aqueous sequestration of carbon dioxide produces calcium carbonate through the reaction of calcium ions and aqueous carbon dioxide. First, gaseous carbon dioxide dissolves into water, as shown in Reaction 1, then aqueous carbon dioxide reacts with water to form carbonic acid, as shown in Reaction 2.

$$CO_{2(g)} \leftrightarrow CO_{2(aq)} \quad (1)$$

$$CO_{2(aq)} + H_2O \xrightarrow{k_2} H_2CO_3 \quad (2)$$

Carbonic acid dissociates into bicarbonate and carbonate ions, as shown in Reactions 3 and 4.

$$H_2CO_3 \xrightarrow{k_3} H^+ + HCO_3^- \quad (3)$$

$$HCO_3^- \rightarrow H^+ + CO_3^{2-} \quad (4)$$

Calcium carbonate is formed by a reaction between the resulting carbonate ions and calcium cations in solution. Because calcium carbonate is semi-soluble in water, it precipitates as shown in Reaction 5.

$$Ca^{2+} + CO_3^{2-} \leftrightarrow CaCO_3 \downarrow \quad (5)$$

In Reactions 1 through 5, the rate-controlling step of fixing gaseous carbon dioxide into carbonate ions is the hydration of carbon dioxide (Reaction 2).[9,15] The forward rate constant of Reaction 2 (k_2) is 0.062 s^{-1} at 25°C, whereas the formation of the bicarbonate ion (Reaction 3) is very rapid (k_3=8x10^6 s^{-1}), its rate being virtually diffusion controlled. Carbonic anhydrase catalyzes Reaction 2 to accelerate the precipitation of calcium carbonate.

The presence of carbonic anhydrase enzyme changes the mechanism of carbon dioxide hydration. Activation energies for hydrating carbon dioxide have values of 14.7 kJ/mol for hydration by H_2O and 6.0 kcal/mol for hydration by CA II, respectively.[9] The CA-catalyzed reaction pathway for the hydration of carbon dioxide in Reactions 6 through 8 replaces Reaction 2 above and significantly enhances the overall reaction rate. Carbonic anhydrase is a zinc metalloenzyme. In these reactions, E represents the enzyme and Zn the zinc ion at the enzyme active site.

$$E \cdot ZnH_2O \leftrightarrow EZnOH^- + H^+ \quad (6)$$

$$E \cdot ZnOH^- + CO_2 \leftrightarrow EZnHCO_3^- \quad (7)$$

$$E \cdot ZnHCO_3^- + H_2O \leftrightarrow EZnH_2O + HCO_3^- \quad (8)$$

The suggested enzyme operating mechanism for the catalysis of carbon dioxide hydration is the nucleophilic attack on the carbon atom by zinc-bound OH^- to produce bicarbonate, which is then displaced by a water molecule.[15]

MATERIAL CHARACTERIZATION AND EXPERIMENTAL PROCEDURE

Three industrial slag samples were selected for use in leaching and carbonation tests. Raw slag samples were collected from BOF, EAF, and LMF steelmaking facilities and stored in a sealed container with a desiccant until each test commenced. Physical and chemical characterization on each slag sample was undertaken in an effort to understand the nature of the starting material.

A portion of each slag sample was divided by splitting and then analyzed by x-ray fluorescence (XRF) for chemical composition and x-ray diffraction (XRD) for phase identification. Another portion was ground to <106 μm and analyzed by helium pycnometry to determine its true density. The grindability of each slag was measured as part of a separate study to determine the work index values for each slag sample.[2] Table 1 lists the results from the chemical and physical characterization analyses. The XRD results are discussed in subsequent sections.

Table 1. Chemical and Physical Properties of Steelmaking Slags Studied

	BOF	EAF	LMF
XRF Comp. (wt.%)			
CaO	40.9	35.9	50.0
SiO_2	12.9	9.9	4.3
FeO	21.7	28.0	6.3
MgO	12.0	10.1	4.5
Al_2O_3	5.2	9.2	32.3
MnO	4.7	4.3	0.9
Density (kg/m^3)	3614	3822	3069
Work Index (kWh/st)	21.4	19.9	13.8

Each slag contained a high fraction of calcium. Approximately one-half of the volume of the LMF slag was composed of lime containing phases. BOF and EAF slags contained a much higher fraction of iron oxide, which reflects their processing history. The turbulence of BOF and EAF processes results in more entrained iron oxide (and metallic iron) compared to LMF slag. This particular LMF slag had a very high alumina content, which resulted from the deoxidation process used at the mill from which it was collected. The higher iron oxide and manganese oxide levels in BOF and EAF slags lead to their greater density than LMF slag. Additionally, BOF and EAF slags require 40-50% more energy (kWh/st) for grinding than LMF slag. This greater energy requirement can also be correlated to the iron and manganese oxide contents.

Scanning electron microscopy (SEM) analysis was used to observe the slag surface morphology through the various test stages. As a baseline, slag particles obtained in the "raw" as-ground state were imaged after each grindability test. Figure 1 shows the surface structure of BOF, EAF, and LMF slag particles obtained from a 90-106 μm sieve fraction.

Particles of EAF and LMF slags show smooth surfaces characteristic of brittle fracture from a glassy material, while BOF slag shows a much more irregular surface that is covered with grinding debris. Similar surface features were observed for particles in the 150-212 μm and 500-600 μm fractions. The specific surface area of raw and leached samples was measured using Brunauer-Emmett-Teller (BET) analysis using nitrogen gas. The raw samples were washed with dehydration alcohol before the surface area analysis to remove any grinding debris. The specific surface area of the 90-106 μm fraction of LMF slag was 0.12 m^2/g. Those of the same size fractions of EAF and BOF slags were significantly higher at 0.29 m^2/g (134%) and 1.09 m^2/g (776%), respectively. The 150-212 μm and 500-600 μm size fractions showed similar corresponding increases in surface area, indicating that EAF and BOF slags have a much higher surface areas for leaching due to higher porosity. Supersonic oxygen jets blow on the surface of EAF and BOF slags, forming an emulsion, and entraining gas bubbles and liquid steel drops in the slag matrix, which results in solidified slag with high porosity and iron content. The ladle metallurgy process is more quiescent, typically employing argon bottom stirring, which leads to less gas and metal entrainment in the slag.

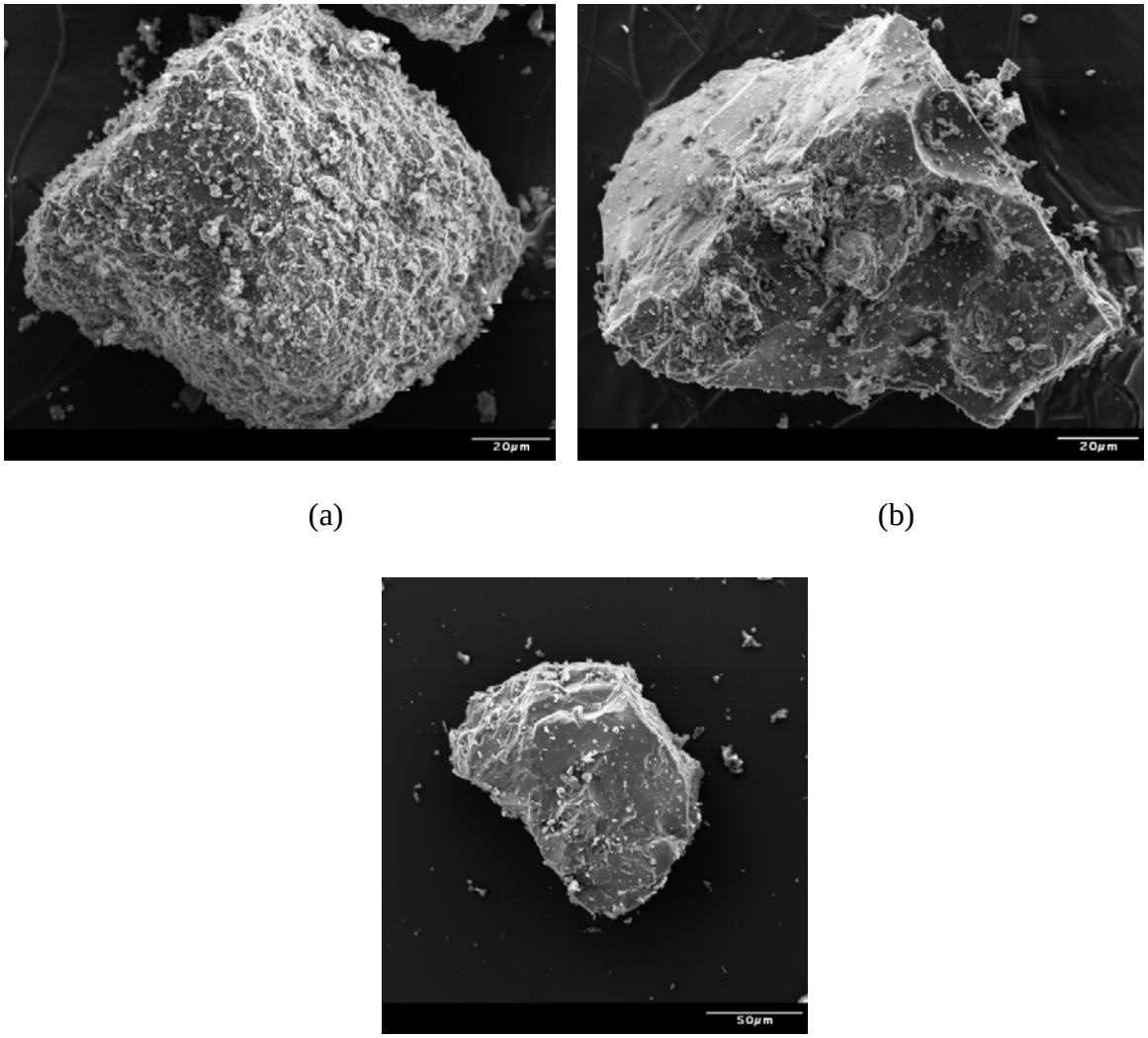

(a) (b)

(c)

Figure 1. SEM images of as-ground "raw" (a) BOF, (b) EAF, and (c) LMF slag particles obtained from 90-106 µm sieve fraction

Leaching studies were conducted using individual batch reactors. Each (ground) slag sample was sieved to obtain 45-53 µm, 90-106 µm, 150-212 µm, 500-600 µm, and 800-1180 µm size fractions. Seventy-five milligrams from each size fraction of each slag was added to a sterilized 50 ml polypropylene tube, which served as the leaching reactor. Fifty milliliters of distilled-deionized (DD) water (18.0 MΩ resistivity) was added to each reactor based on gravimetric analysis. For the initial LMF slag leaching tests (water only) 2 wt.% TES (2-[(2-hydroxy-1,1-bis(hydroxy-185-methyl)ethyl)amino]ethanesulfonic acid) pH buffer was added to the reactor. For LMF leaching tests with BCA and the BOF

and EAF tests, the amount of TES buffer was reduced to 1 wt.%. Each reactor was sealed, placed in a wrist-action shaker, and shaken for a prescribe period of time (1-1440 minutes) to prevent boundary layer concentration build-up of the leaching species. At the end of each test, a 10 ml aliquot was drawn off through a 0.45 μm filter using a syringe. The aliquot was placed into a separate 15 ml polypropylene sample tube to which 1 vol.% nitric acid was added to prevent metal precipitation. Each sample was analyzed using inductively coupled plasma optical emission spectroscopy (ICP-OES) to determine the calcium, magnesium, and iron concentrations. Method blanks containing DD water with TES buffer and nitric acid were prepared at each run for baseline metal measurement by ICP-OES. The ICP-OES was calibrated at 2, 20, 100, and 200 mg/L for each element (Ca, Mg, and Fe), and the results yielded a minimum detection limit of 0.3 mg/L and measurement error of 1%. Using the concentrations of Ca, Mg, and Fe in the original slag samples, the percent leached could be determined. For the leaching tests using BCA, a 10x stock solution of bovine erythrocyte carbonic anhydrase (Sigma-Aldrich Co.) was prepared using Tris-EDTA solution (2.5 mg BCA in 25 ml of TE). This solution was kept at 4°C until required for the leaching test. One milliliter of the stock solution was added to the 50 ml reactor, which produced a 66.6 nM concentration of BCA. This concentration matches that used by Bond et al. in their BCA studies.[9] Leached samples were analyzed for specific surface area using BET analysis and for morphology using SEM analysis.

Carbonation tests were conducted in a 500 ml spherical glass 3-hole flask placed on a mixing plate. For each test, 400 ml of water was added, into which argon or carbon dioxide gas was bubbled through a glass frit sparger introduced into the top hole. Separate pH and temperature probes were introduced through another entry hole, leaving the third-hole open for adding the powdered sample. Argon gas was bubbled through the water while a magnetic bar stirred the solution for ten minutes prior to the start of each test. Slag carbonation was conducted by adding 3000 mg of slag to the reactor. The slurry was mixed for five minutes with argon bubbling and the pH was measured continually. After five minutes of leaching, carbon dioxide was introduced through the sparger for a prescribed period of time (5-360 minutes). The slurry was mixed by the stir bar throughout the entire process. Upon completion of the reaction time, the sparger, pH

probe, and temperature probe were removed. The mixture was (vacuum) filtered through 11 μm paper and oven dried. The dried samples were placed into plastic bags and stored in a desiccant cabinet. Tests using 66.6 nM concentration of BCA were formed by adding 8 ml of 10x stock solution. A photograph of the test setup is shown in Figure 2.

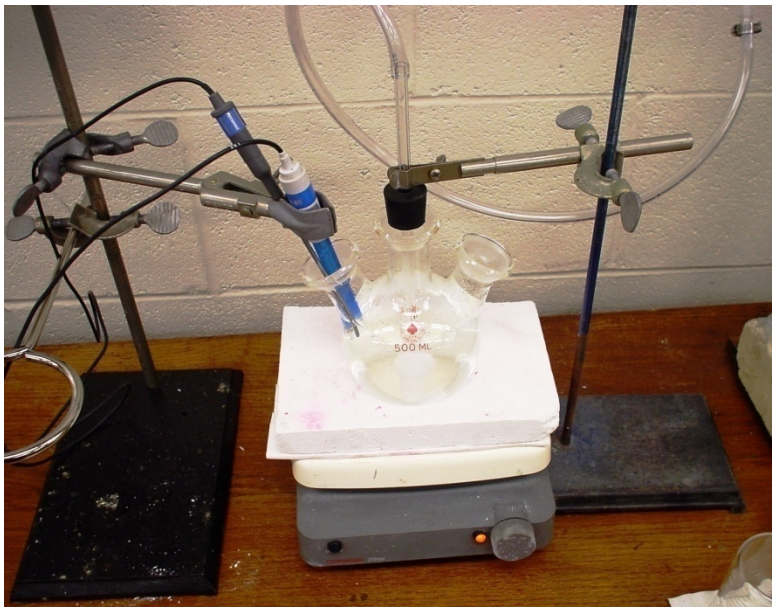

Figure 2. Carbonation test apparatus using 3-hole flask; pH and temperature probes at left and glass frit sparger for gas introduced at the top

Two sets of carbonation tests were conducted. The first set was time based and used no buffer in the solution. Tests ran for a prescribed time, regardless of the solution pH. As carbonate speciation is a function of pH, a second set of tests used a buffer to maintain an alkaline pH. The buffer used was CAPS (3-Cyclohexylamino-1-propanesulfonic acid) titrated with sodium hydroxide to an initial pH of 10.5. Instead of a prescribed test time, each test was conducted until the pH dropped to 8.5. Increasing the buffer concentration (0.0-0.200 M) allowed for longer test duration.

Carbonated samples were analyzed for surface morphology and composition using SEM and energy dispersive x-ray spectroscopy (EDS). The hydroxide and carbonate content of each carbonated sample was measured by thermogravimetric

analysis (TGA) in argon to 920°C. Weight loss at <600°C indicated hydroxide content, while weight loss >600°C indicated carbonate content.

Bond et al. recommends a spectrophotometric assay using the enzyme-mediated hydrolysis of para-nitrophenyl acetate (p-NPA) to monitor the activity of carbonic anhydrase.[12] As a first-order approximation, however, neutralization of CaO was used to measure the activity of the BCA 10x stock solution. This method used the same procedure as the carbonation tests, but only 300 mg of reagent grade CaO was added to the 400 ml of DD water. The solution was argon sparged and stirred for 15 minutes until all lime was dissolved. The pH was measured continually throughout the test. Carbon dioxide was introduced and the time to reach a pH of 7.0 (neutralization) was measured. This test was conducted in DD water only (0.0 nM BCA) and at four BCA concentrations (16.7, 33.3, 66.6, and 83.3 nM). The results are compared to the theoretical neutralization curve determined by FactSage™ Ver. 5.5 thermodynamic software in Figure 3.

Neutralization of the alkaline solution with no BCA took place in just under six minutes (356 seconds). A one-quarter dose (16.7 nM) of BCA resulted in neutralization 64% lower than the theoretical time (239 seconds). Increasing the concentration to 33.3 nM, 66.6 nM, and 83.3 nM concentrations resulted in neutralization times near the theoretical limit. These 0.5, 1.0, and 1.25 dosage rate concentrations resulted in neutralization times that were 3.5%, 2.3%, and 1.7% over the theoretical time, respectively. Based on these results, the stock solution of BCA was deemed active and the 66.6 nM concentration was chosen for all subsequent tests to correlate with the published data.

LEACHING RESULTS AND DISCUSSION

The three slag types all exhibited calcium leaching directly related to time and indirectly related to particle size. Figure 4 shows the calcium leaching curves for LMF slag at five particle sizes. The leaching of calcium provided the best straight-line proportionality on a log-normal scale.

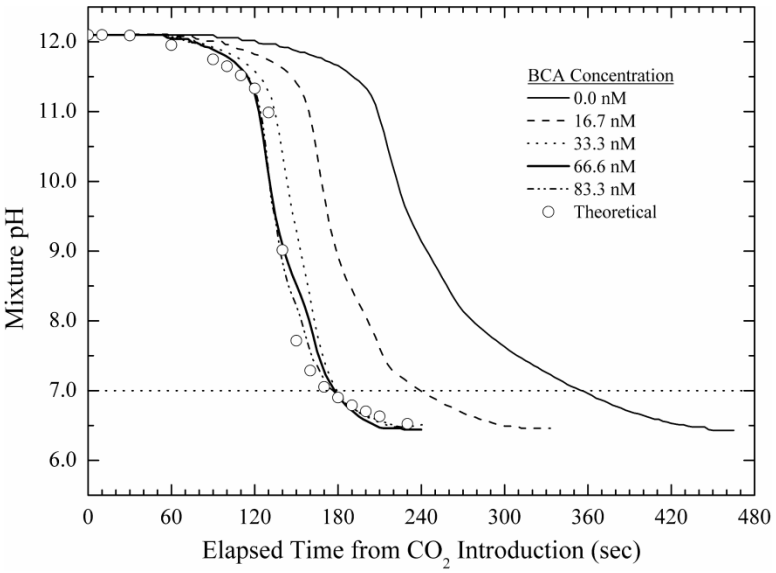

Figure 3. pH neutralization curves for CaO-CO_2-H_2O at varying concentrations of bovine carbonic anhydrase

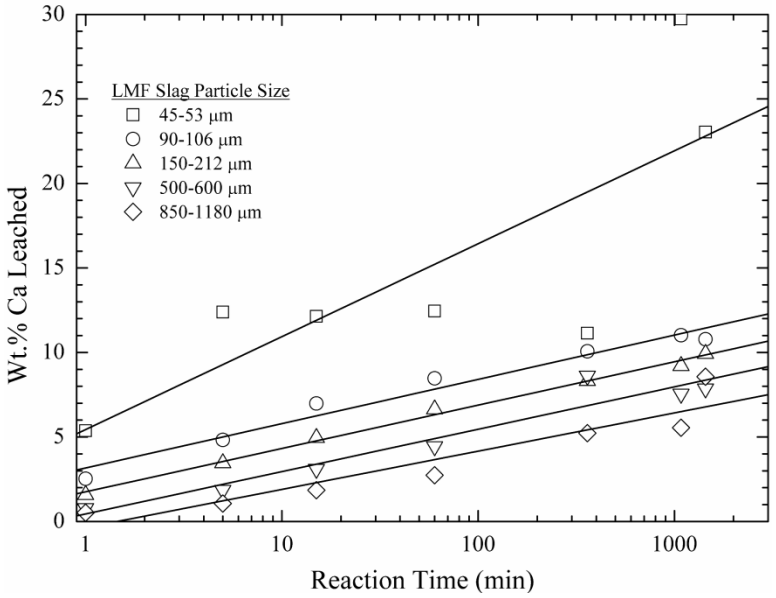

Figure 4. Calcium leaching from LMF slag with time at five particle size fractions

Curve fits of all particle size fractions >90 μm showed parallel proportionality with time. The overall amount leached with the >90 μm particles was low with a maximum of ~11% leached at 24 hours. The 45-53 μm size fraction exhibited a different slope of the proportionality and the interim points showed no change in leaching, but the

final point was much higher at 23-30% at 18-24 hours. Observation of the leached material showed that all particles >90 μm remained free flowing in the reactor, but the 45-53 μm particles had agglomerated together as a result of a chemical reaction. Because they had to be scraped from the reactor tube, these particles were not turbulently mixed to prevent boundary layer formation. Phase maps produced from EDS analysis of raw LMF slag particles (850-1180 μm fraction) showed equal distribution of 20-80 μm Fe and Ca rich regions. Magnesium was associated with the Fe while Si was associated with the Ca. Aluminum was located between the Fe and Ca rich regions. EDS analysis of the leached particles showed increased Al and Si concentrations in their respective regions. The same type of analysis on particles from the 45-53 μm fraction showed that the surface of the leached agglomerate contained mostly Al and Si with very little Fe, Ca, or Mg present.

Calcium leaching curves for three particle sizes of BOF and EAF slag are presented in Figure 5. Both slags show similar magnitude and proportionality of the amount of calcium leached by particle size. The overall amount of calcium leached is significantly higher than that exhibited by the LMF slag. These two slags showed five times the amount of calcium leached at 18 hours for the 90-106 μm size fraction than in the LMF slag.

While the BOF slag showed a greater amount of calcium leached in proportion to the amount of CaO present, than did the EAF slag (Table 1), both slags greatly surpassed the amount leached from LMF slag, which had the largest amount of calcium oxide. EDS analysis of leached BOF slag particles (90-106 μm fraction) showed alternating regions rich in Si and Mg and a high amount of Fe present throughout.

BCA added to the leaching solution had no affect on the amount of calcium leached from LMF slag (BCA was not tested with BOF or EAF slag). Figure 6 shows the calcium leaching curves for two particle size fractions (90-106 μm and 500-600 μm) of LMF slag with and without BCA in the leaching solution.

The amount of calcium leached under both conditions is nearly identical and no significant difference could be measured. The amount of Mg and Fe leached showed the same trend with no significant difference measured. Because BCA is a carbon dioxide active catalyst and leaching took place in the absence of this component, it had no effect on the leaching rate. The effect of BCA on the release of Ca^{2+} from limestone as reported

by Li et al.[14] is attributed to the carbonate present in the parent mineral. Carbonic anhydrase catalyzes Reaction 2 by replacing it with Reactions 6 through 8. These reactions reverse when gaseous carbon dioxide is absent. By means of this reverse reaction, carbon dioxide and calcium ions are released from the carbonate mineral. Because raw slag contains no carbonate material, BCA had no species on which to act rendering it inert in regards to Ca, Mg, or Fe leaching.

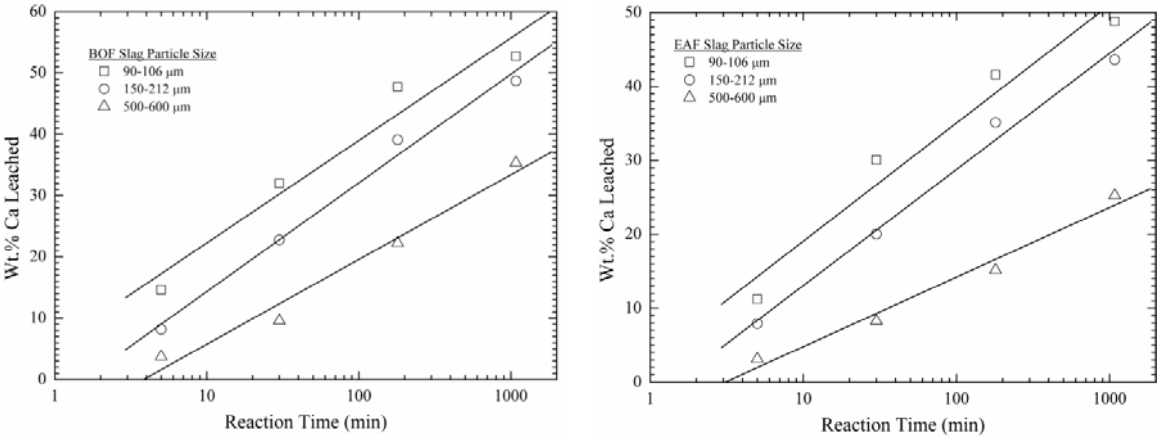

(a) (b)

Figure 5. Calcium leaching curves for (a) BOF and (b) EAF slags at three particle size fractions

Ca, Mg, and Fe leaching for the 90-106 μm fraction of LMF slag are compared in Figure 7. The leaching curves for Mg and Fe fit the best linear proportionality on a log-log scale.

The amounts of Mg and Fe leached showed very similar trends. Approximately 20% of each element was leached after 24 hours. Up to six hours, the amount of calcium leached on a percentage basis was higher than Mg or Fe. However, after six hours, the magnesium and iron leached at higher percentages than calcium. The other size fractions showed similar trends. LMF slag contained much lower fractions of magnesium and iron oxides than did BOF and EAF slags, yet the amount of Mg and Fe leached (on a percentage basis) was higher than calcium after six hours.

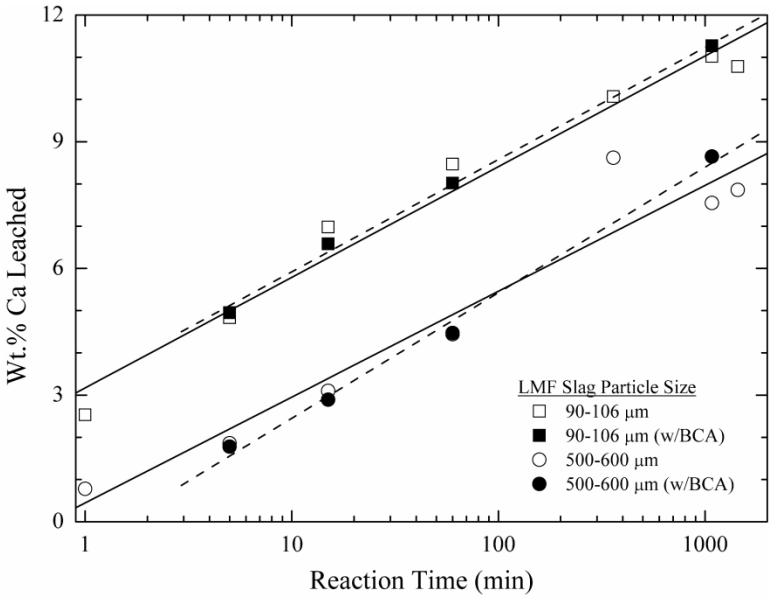

Figure 6. Calcium leaching from LMF slag with and without the addition of BCA to the leaching solution

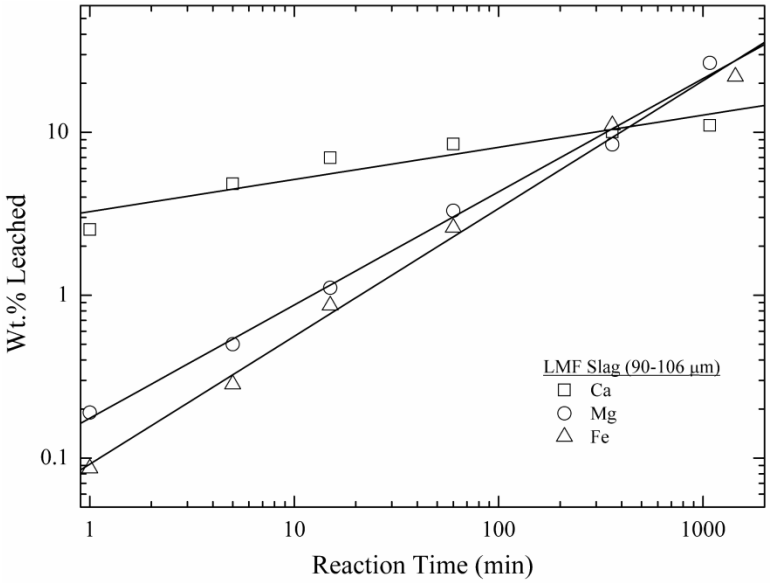

Figure 7. Leaching curve for Ca, Mg, and Fe from LMF slag particles in the 90-106 μm fraction

A possible explanation for the lower calcium leaching in LMF slag is that much of the calcium is bound as an inert complex oxide, while magnesium and iron are more available for dissolution. The high total fraction of calcium provides some free calcia,

which dissolves rapidly, providing an initial higher rate. As the free calcia is consumed, the resultant inert layer prevents further calcium leaching allowing magnesium and iron to dissolve even at lower concentrations.

BOF and EAF slags show very different magnesium and iron leaching relationships than those of LMF slag. Figure 8 shows the leaching curves for BOF and EAF slag particles in the 90-106 μm size fractions. The amount of calcium leached is significantly higher than LMF slag, as noted previously. The amount of Mg is lower than in LMF slag, even though BOF and EAF slags have a much higher starting fraction of these elements. The amount of magnesium leached at 18 hours for BOF slag was ~7%, which is one third that of LMF slag, while EAF slag barely reached 1% magnesium leaching after the same duration. The amount of iron leached by both slags was too low to report (<0.01%) at all times and all size fractions. While these values represent the percent of each element leached, the resulting concentration in solution will also depend on the amount initially present in the slag. BOF and EAF slags have two to three times the initial amount of MgO of LMF slag, so they may achieve the same concentration in solution even though the percentage leached is less.

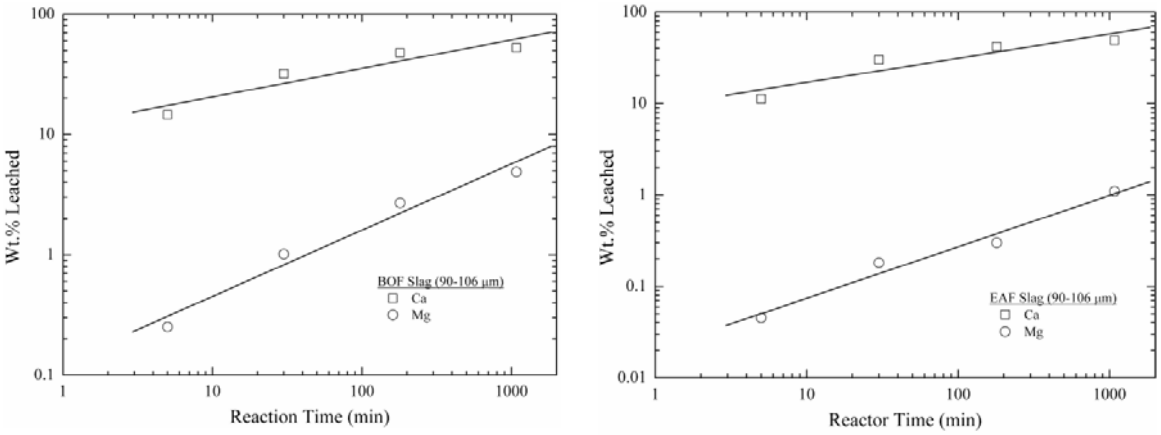

Figure 8. Calcium and magnesium leaching curves for the 90-106 μm size fraction of (a) BOF and (b) EAF slags

The difference between leaching amounts for BOF and EAF slag and LMF slag can be understood from their surface morphologies, specific surface areas, and phase

analyses. Surface morphology was observed through SEM analysis of the leached slag particles. Figure 9 shows particles from the 90-106 μm size fraction of BOF and EAF slag after 18 hours leaching and of LMF slag after 24 hours leaching.

The BOF slag particles show very deep, interconnected leaching pores extending up to 25% into the particle. EAF slag showed a high increase in surface porosity, but its pores were less connected and extended up to 10% into the particle. Leaching of LMF slag was more selective with some particles showing morphology similar to EAF slag and some particles showing no leaching at all. The distribution of leachable material was more extended and connected in BOF slag, while LMF slag contained a high fraction of inert material. EAF particle morphology fell between these two extremes. Table 2 shows the specific surface area for the raw and leached particles of the three slag samples at two size fractions. The increased porosity in the raw and leached particles is shown by specific surface area analysis. Raw BOF slag has approximately 9-10 times the specific surface area of LMF slag and up to four times the specific surface area after leaching. EAF slag specific surface area values lie closer to LMF slag before leaching and closer to BOF slag after leaching. The increased porosity of BOF and EAF slag leads to higher specific surface areas, which support a higher leaching rate than in LMF slag.

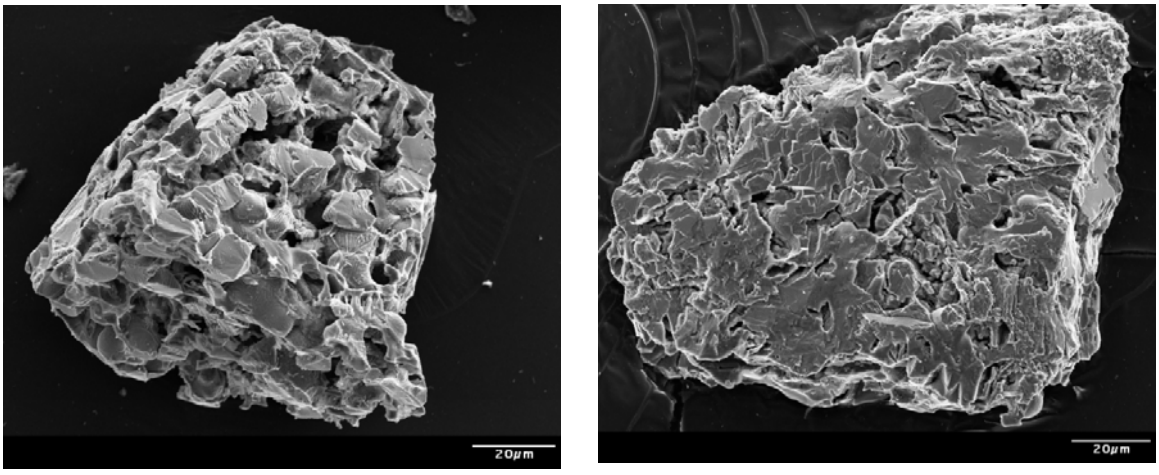

(a) (b)

Figure 9. Particles of (a) BOF and (b) EAF slag after 18 hours aqueous leaching, and (c) LMF slag after 24 hours leaching (all particles from the 90-106 μm size fraction)

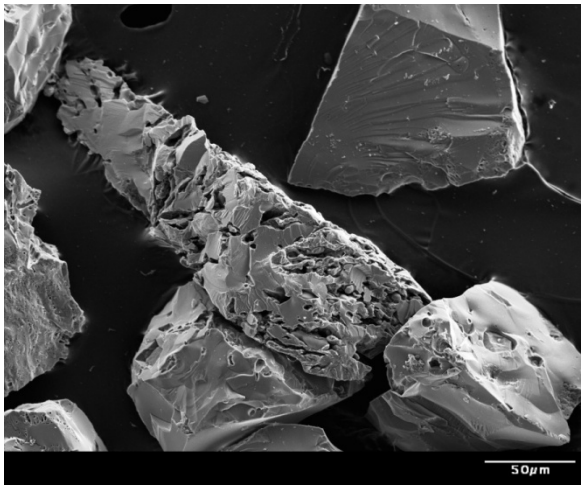

(c)

Figure 9. Particles of (a) BOF and (b) EAF slag after 18 hours aqueous leaching, and (c) LMF slag after 24 hours leaching (all particles from the 90-106 µm size fraction), (cont.)

Table 2. Effect of Leaching on Specific Surface Area

Specific Surface Area (m^2/g)	BOF	EAF	LMF
90-106 µm fraction			
Raw (post-grind)	1.09	0.292	0.125
Post-Leach	16.76	13.37	4.87
500-600 µm fraction			
Raw (post-grind)	0.997	0.145	0.086
Post-Leach	10.86	7.65	6.18

XRD analysis primarily identified complex oxide phases in the three slag samples. BOF slag contained Ca_2SiO_4, (Mg,Fe)O, and $Ca_2Al_2SiO_7$; EAF slag contained Ca_2SiO_4 and FeO; and LMF slag contained $Ca_{12}Al_{14}O_{33}$ and Al_2O_3. The calcium in BOF and EAF slags is primarily combined in a 2:1 ratio with silica ($2CaO{\cdot}SiO_2$), which is a short complex oxide with a relatively high degree of ionic bonding. The calcia in LMF slag is combined in a 12:7 ratio with alumina ($Ca_{12}Al_{14}O_{33}$), which is a more extensive complex oxide with a lower degree of ionic bonding. The lesser degree of ionicity reduces the calcium leachability in LMF slag. The combination of low specific surface

area and lower calcium bond iconicity results in an overall lower calcium-leaching rate for LMF slag.

The leaching curves for calcium all follow similar trends based on particle size and time, and can be approximated by a common function for each slag. The general approximation is shown in Equation 9 and the equation constants are given in Table 3. The weight percent of calcium leached (m_{Ca}) is a function of the particle diameter (d_p in μm) and time (t in minutes). The values A-D are equation constants for each slag type.

$$m_{Ca} = A\left(d_p\right)^B \left(t\right)^{C\left(d_p\right)^D} \tag{9}$$

Table 3. Calcium Leaching Constants for Equation 9

	A	B	C	D
BOF	1110.4	-0.997	0.0568	0.3228
EAF	642.27	-0.918	0.1029	0.2103
LMF	68.306	-0.66	0.046	0.302

CARBONATION RESULTS AND DISCUSSION

The first set of slag carbonation tests compared the neutralization time for the three slag samples at the same particle size range without solution buffering. Figure 10 shows the neutralization curves for the 90-106 μm size fractions of LMF, BOF, and EAF slags. In each test, the slag was allowed to leach for five minutes before carbon dioxide was introduced. The maximum pH values and neutralization times appear to trend opposite to that shown by the leaching results. LMF slag exhibited a higher initial pH than BOF or EAF slags, indicating that more Ca^{2+} was released during the initial five minutes of leaching. Also the neutralization time for LMF slag was 65-75% longer than the neutralization times of EAF and BOF slags indicating that more Ca^{2+} was released over a longer time. Based on the data obtained from this simple test, the results cannot be compared to the leaching test.

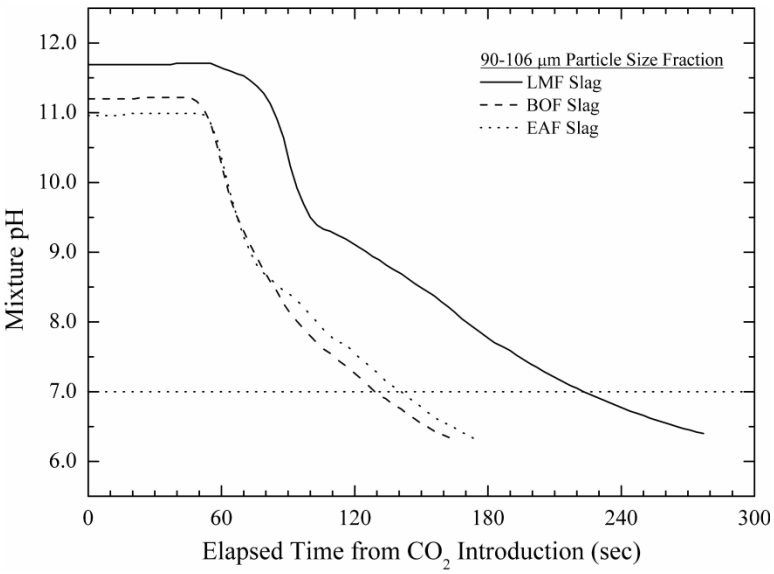

Figure 10. Neutralization curves for the 90-106 μm particle size fraction of LMF, BOF, and EAF slag

After the five-minute carbonation test, particles of each slag were analyzed in the SEM for surface morphology. Figure 11 shows the surface of particles from the 90-106 μm size fraction of BOF and LMF slags. The BOF particle (Figure 11a) shows small nucleates of a precipitating material distributed across its surface. EDS analysis indicates that the particles consist primarily of calcium. The difference between $Ca(OH)_2$ and $CaCO_3$ cannot be discerned because the particles are carbon coated. Figure 11b is a close-up of the LMF slag and shows the particles to be overlapping blocky plates of very narrow size distribution (2-3 μm). These particles were produced after introducing carbon dioxide into the aqueous leachate; therefore, it is assumed they are primarily formed from calcium carbonate.

Longer-term carbonation tests were conducted using BOF slag particles in the 90-106 μm size fraction. These tests were conducted for one and six hours with and without BCA added to the aqueous system. Figure 12 shows the early neutralization portion of the pH curve for the one-hour test. Carbon dioxide was bubbled into the mixture for a total of one hour but neutralization took place in a few minutes.

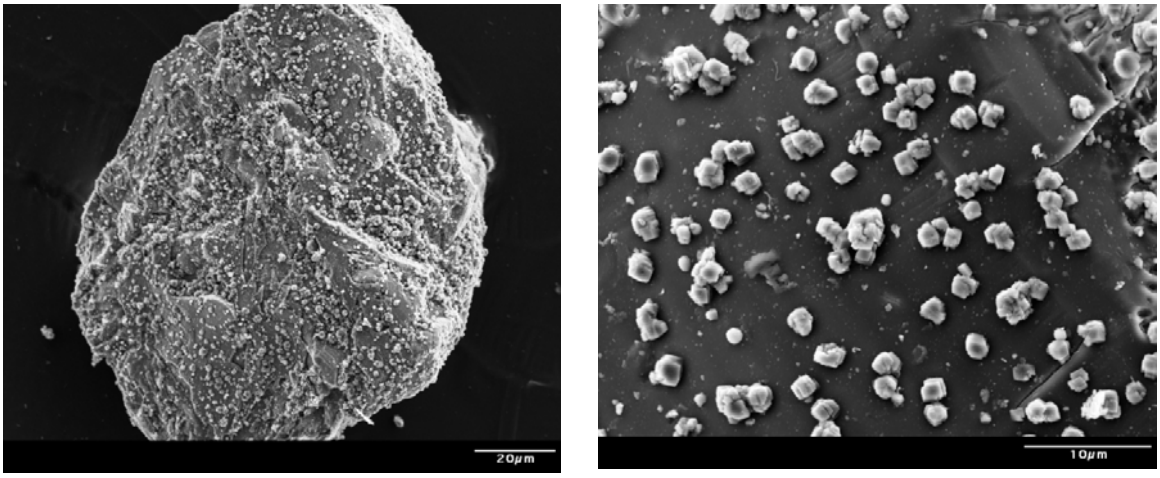

(a) (b)

Figure 11. Morphology of calcium carbonate formed on surface (a) BOF and (b) LMF slag particles after five minutes of carbonation (particles from 90-106 μm fraction)

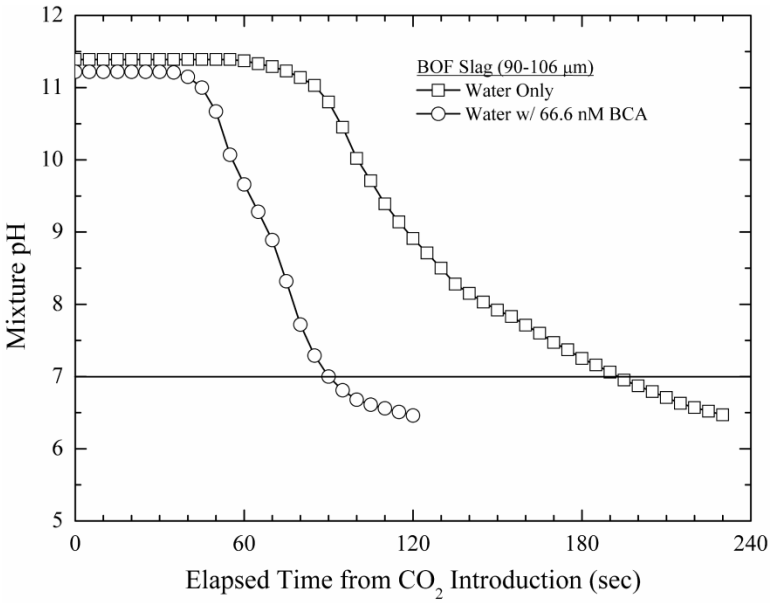

Figure 12. Neutralization curves for BOF slag (90-106 μm fraction) with and without BCA enzyme

BCA added to the aqueous mixture reduced the neutralization time by ~50% indicating that calcium was precipitating from solution faster. However, the terminal pH values were lower without BCA (pH=5.7) than with BCA (pH=6.0), indicating that,

overall, less calcium was precipitating into solution in the presence of the enzyme. Figure 13 shows SEM images of BOF slag particles (90-106 μm fraction) after one hour of carbonation.

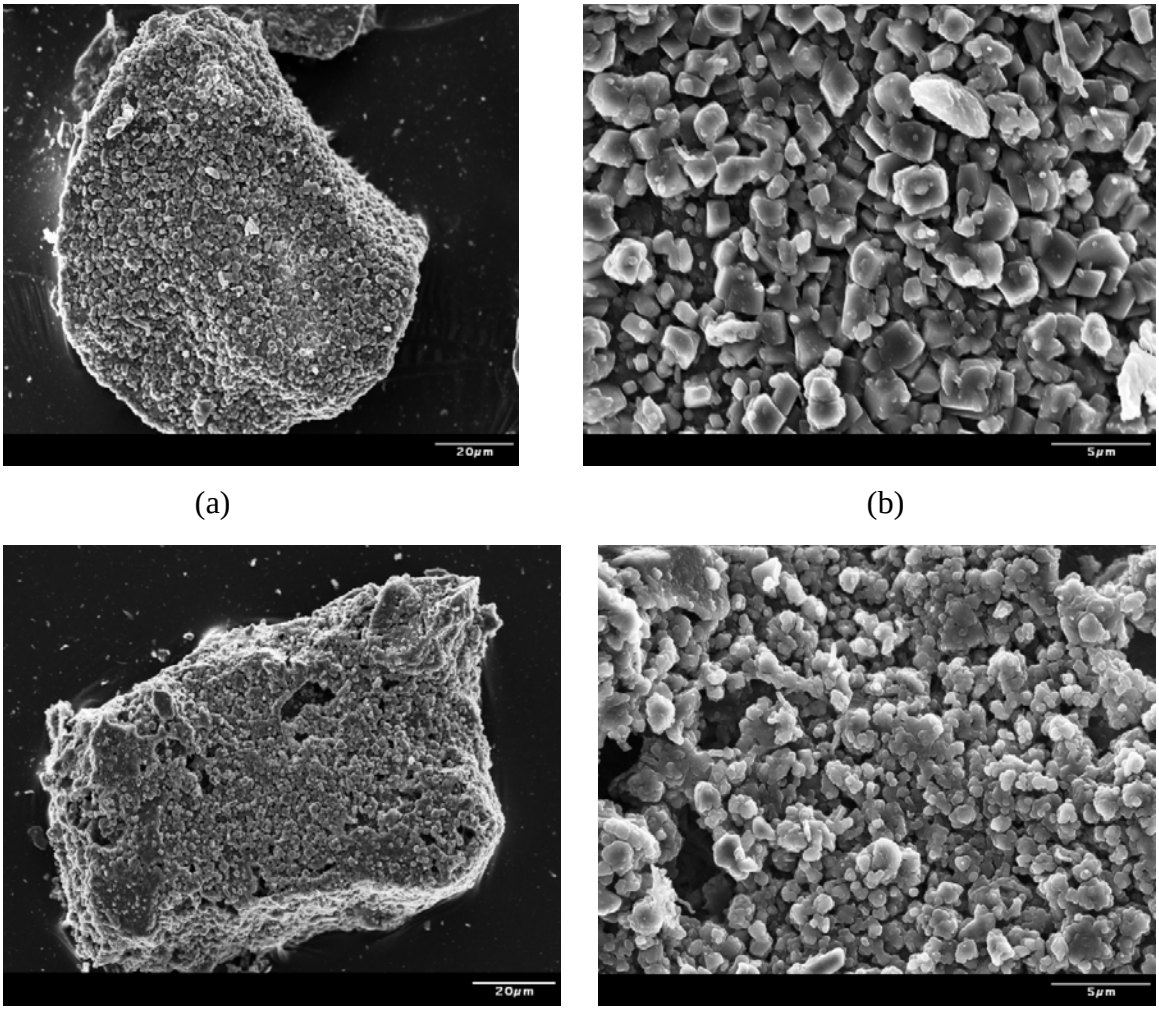

Figure 13. BOF slag particles (90-106 μm fraction) after one hour carbonation (a,b) without BCA and (c,d) with BCA added to the aqueous mixture

Figure 13a shows that, after one-hour carbonation without BCA, the slag particle was evenly coated with evenly sized granular precipitates that covered the particle with a regular spacing. Increasing the magnification (Figure 13b) revealed semi-blocky particles

with straight regular sides. Overlapping plates or ledges can be seen on some particles. The majority of the particles are 2-3 μm in diameter with some 0.5 μm particles scattered throughout. The morphology of the BCA-assisted precipitate coating (shown in Figure 13c) is less regular with granular particles that are heterogeneously distributed with several large pores indicating less even precipitate growth. Increased magnification (Figure 13d) showed the particles to be more dendritic in construction and less evenly distributed. While some 2 μm particles can be seen, most of the precipitates are <0.5 μm in diameter. BCA increased the rate of nucleation, resulting in a higher population of smaller nucleates. More nucleation events occurred on the existing precipitates, resulting in an irregular agglomeration of small nucleates as opposed to growth of the initial nucleating particles. The result should be a less dense precipitate layer containing interconnected pores. This morphology should allow continued carbonation as the layer thickens because the decreased structure density has a higher diffusion rate than does a fully dense product layer.

Thermogravimetric analysis was used to determine the amount of calcium hydroxide and calcium carbonate produced during the carbonation tests. Results of these tests are shown in Table 4.

Table 4. Carbonation Results with 90-106 μm Size Fraction Slag Particles

Slag Type	Reaction Time (min)	Water Only		W/ BCA	
		Wt.% Hydr.	Wt.% Carb.	Wt.% Hydr.	Wt.% Carb.
EAF	0 (raw)	0.71%	0.00%	0.71%	0.00%
EAF	5	0.70%	0.00%	-	-
LMF	0 (raw)	0.00%	0.04%	0.00%	0.04%
LMF	5	1.98%	0.24%	-	-
BOF	0 (raw)	3.20%	0.09%	3.20%	0.09%
BOF	5	1.02%	3.98%	-	-
BOF	60	1.75%	2.31%	1.94%	1.31%
BOF	360	2.90%	1.74%	4.78%	0.77%

The raw slag material contained varying amounts of hydroxide and carbonate. BOF slag started with the most hydroxide at 3.2 wt.%, while EAF slag had 0.71 wt.% and LMF slag had none. All of the slags had <0.1 wt.% carbonate in the raw state. Of the three slags, BOF slag had the most product material from handling and storage, showing it was the most reactive slag (corresponding to the leaching results). The EAF and LMF slags showed different results after the five-minute carbonation test. The hydroxide and carbonate amounts of EAF slag did not change, while both products increased for LMF slag. The results of the BOF test are the most intriguing. In the raw state the hydroxide amount was 3.2 wt.%, while the carbonate amount was near zero. After five minutes of the carbonation test, the hydroxide amount decreased to one-third the level, while the carbonate amount increased to nearly 4 wt.%. This result was more than twice the amount of carbonation achieved in previous carbonation tests with LMF and EAF slag at five minutes.[1] However, as the carbonation test proceeded to longer times the amount of hydroxide increased and the amount of carbonate decreased, contrary to the desired effect. These results were exaggerated with the use of BCA at each time. The most hydroxide and the least carbonate were achieved with BCA at six hours carbonation.

These results show the need for pH control when precipitating calcium carbonate. A significant portion of the five minute carbonation tests with the three slags took place at pH>7 (43% for BOF, 47% for EAF, and 74% for LMF). However, for the one and six hour tests, the slag (w/precipitate) was exposed to low pH (pH=5.7 for water only and pH=6.1 for BCA tests) for most of the test period (>97% of the time for the one hour test and >99.9% of the time for the six hour test). The carbonate ion is most abundant at pH>10.33 and is almost non-existent at ph<8.4, as shown in Figure 14, which illustrates the speciation of carbonate as a function of pH based on thermodynamic analysis.

As the carbonate ion is required to react with Ca^{2+} for calcium carbonate precipitation, allowing the pH to drop to the 5.7-6.1 level reduced the activity of this specie in the system to extremely low levels. At the pH range of 5.7-6.1, the most abundant carbonate specie is aqueous CO_2. Calcium carbonate is generated in the first few minutes of each carbonate test when the pH is high. As the pH drops, the carbonate species equilibrium shifts such that calcium carbonate species are robbed of CO_2 to maintain a high concentration of aqueous CO_2 in the system. Removing CO_2 from

calcium carbonate frees up the calcium, which then precipitates as calcium hydroxide. This effect is magnified with the use of BCA, which catalyzes the reversible carbon dioxide hydration reaction, thus increasing the rate at which CO_2 is robbed from calcium carbonate. To produce a large amount of calcium carbonate, the solution pH should be maintained at a value of at least 8.5.

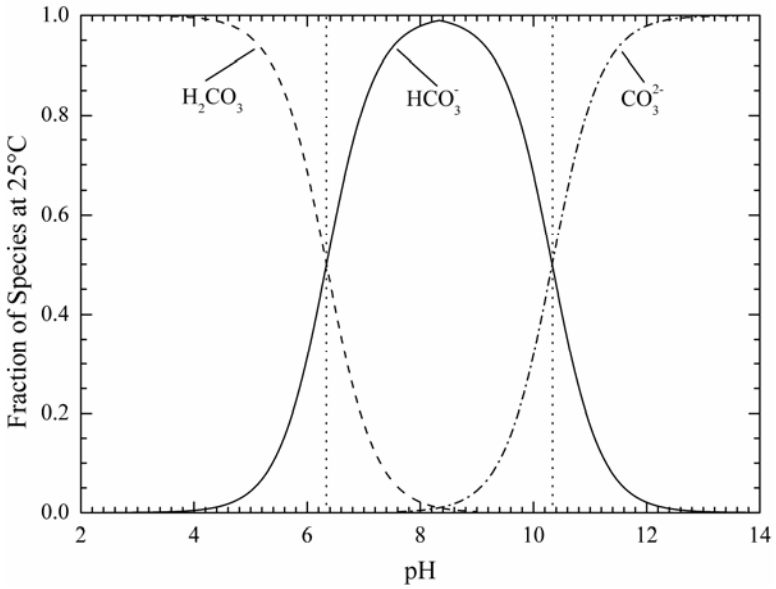

Figure 14. Predominance of carbonate species as a function of pH

The second set of carbonation tests was conducted to maintain a pH of above 8.5. A CAPS buffer was used to allow increased test length at higher pH. Several tests were conducted with and without BCA added. Figure 15 compares the carbonation results for BOF slag in water only, buffer, and buffer with BCA condition to EAF and LMF carbonation results from previous test work.

The water-only leaching results for BOF slag ("BOF, Water") from the time controlled tests show a decrease in carbonation due to low pH. The amounts of carbonation when the pH was kept >8.5 are shown as "BOF, Buffer" and "BOF, Buffer, BCA". Both sets of results show increasing carbonation with time and at a much higher magnitude than those of the time controlled tests. The highest amount of carbonation results from simple pH control without the BCA enzyme. Greater than 16% carbonation

was achieved in 13.25 minutes. Extrapolation of this rate yields 47% carbonation at 24 hours. The addition of BCA to the solution slightly decreased the amount of carbonation, but increased the amount of hydroxide formed. At 8.5 pH the carbonate ion is still present, but the bicarbonate ion is the dominant species. The effect of BCA is so rapid that it pulls the carbonate species towards equilibrium and begins to rob calcium carbonate even at 8.5 pH. To realize the full potential of the BCA enzyme in this system, a pH of at least 10.33 must be maintained. Comparing of the buffered test results to data from previous EAF and LMF carbonation tests[1] shows that a significantly higher amount of carbonation was achieved. These previous EAF and LMF tests were conducted at prescribed times and did not use pH buffer control, but a higher slag/water ratio (30 g slag/250 ml water) was used. This ratio produced a higher concentration of Ca^{2+} in solution, thus maintaining a higher pH for a longer time. For batch-based carbonation, the pH controlled method showed an increased carbonation rate of 5-6 times that of the previous tests (BOF slag versus EAF or LMF slag).

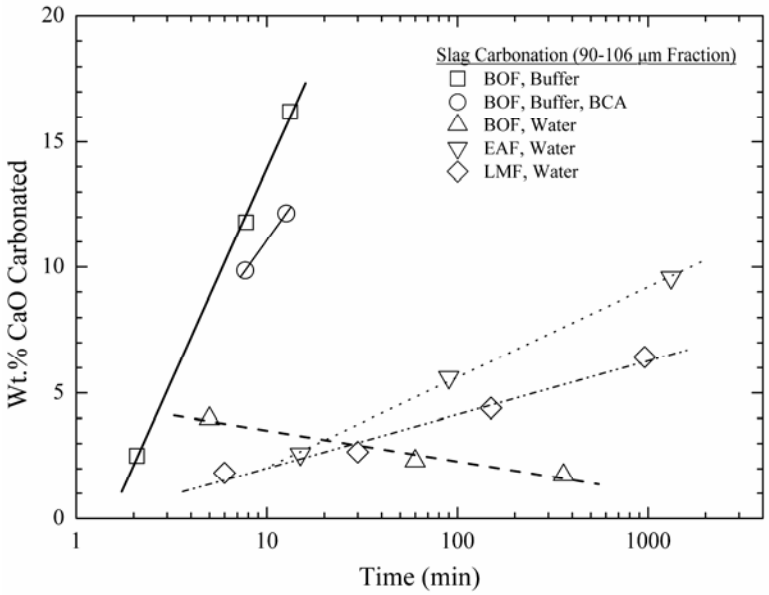

Figure 15. BOF slag carbonation results from time and pH controlled tests

The leaching rate of calcium from BOF slag is calculated using Equation 9, while the carbonation rate is shown in Figure 15. Leaching occurs approximately 50% faster

than carbonation (on a molar conversion basis) at a particle size of 100 μm. However, carbonation results in a product layer that retards the leaching process[2], so the leaching rate in a batch carbonation system will be less than in a two-stage system. According to the carbonation results, as long as the system pH stays above 8.5, the slag system can process 151 kg carbon dioxide per tonne of slag in a 24-hour period, which is 47% of the slag theoretical calcium carbonate capacity. The amount of carbon dioxide sequestered is 0.4% of that emitted per ton of steel produced for BOF production. As a first-order approximation, assuming the carbonation rate is proportional to leaching activity, the pH-controlled process should sequester 1.8% of the carbon dioxide emitted from EAF steelmaking. Under the same conditions, LMF slag can add another 0.1% and 0.6% to the sequestration amounts for BOF and EAF mills, respectively. In regards to slag stabilization, BOF and EAF slags will achieve approximately 50% stabilization in 24 hours, while LMF slag should reach the same amount in five days.

CONCLUSIONS

Tests conducted on steelmaking slags showed the rates and mechanisms underlying both aqueous leaching and carbonation processes, and the effect of carbonic anhydrase enzyme as a catalyst. The amount of calcium leached is a strong function of particle surface area, which is a more important factor than calcium oxide content. BOF slag exhibited a calcium-leaching rate of approximately five times the leaching rate of LMF slag even though it had 80% of the calcium content. This is because BOF slag had 8.7 times the specific surface area in its raw state. Like LMF slag, EAF showed an increase in calcium leached. Carbonic anhydrase did not affect the leaching rate because it only catalyzes reactions involving carbon dioxide. A low amount of magnesium was leached for all slags, and BOF/EAF slags showed negligible amounts of iron leached. The specific surface area increased from 15-40 times due to leaching, with BOF particles exhibiting the most extensive leaching depth. All leaching curves exhibited similar trends, and the extent of calcium leaching as a function of time and particle size can be expressed by a mathematical relationship.

Carbonic anhydrase catalyzed the reaction between calcium oxide and carbon dioxide in water to decrease neutralization time by 50%. A 66.6 nM concentration of BCA reduced the neutralization time to near the theoretical rate. Carbonic anhydrase modified the structure of the precipitating layer on the slag particles from an overlapping block structure to a dendritic morphology with smaller particles because carbonic anhydrase increased the nucleation rate of the precipitating particles at the expense of the particle growth. The rate of carbonation is a strong function of pH. Time controlled tests in which the pH dropped to ~six resulted in decreased carbonate production for a given time. This decrease was accelerated by carbonic anhydrase, which acts on the reversible hydration of carbon dioxide so it will pull the system rapidly towards equilibrium. Thus, if the pH drops to a level at which carbonate dissolution would be necessary to reach equilibrium, the enzyme will accelerate that dissolution. Tests in which the pH was maintained >8.5 exhibited the highest rate of carbonation. At the rate exhibited, 47 wt.% carbonation would be achieved by BOF slag at 100 μm particle size at 24 hours in a batch reactor. Because the leaching rate was found to be ~50% faster than the carbonation rate, a further increase in carbonation may be realized by using carbonic anhydrase (but the pH must be maintained >10.33).

ACKNOWLEDGMENTS

This paper was prepared as an account of work sponsored by the U.S. Department of Energy in cooperation with the American Iron and Steel Institute (AISI) and its participating companies under Agreement DE-FC36-97ID13554. Such support does not constitute an endorsement by DOE or AISI of the views expressed in the article.

REFERENCES

1. Lekakh, S.N., Rawlins, C.H., Robertson, D.R., Richards, V.L., and Peaslee, K.D., “Aqueous Leaching and Carbonization of Steelmaking Slag for Geological Sequestration of Carbon Dioxide,” Metallurgical and Materials Transactions B, (on-line) January 2008.
2. Rawlins, C.H., “Grindability Study of Steelmaking Slag for Size-by-Size Recovery of Free Metal,” SME Annual Meeting and Exhibit, Feb. 2008.

3. Rawlins, C.H., Richards, V.L., Peaslee, K.D., and Lekakh, S.N., "Sequestration of CO_2 from Steelmaking Offgas by Carbonate Formation with Slag," AISTech 2006 Proceedings, Vol. II, May 2006, pp. 1133-1144.
4. Rawlins, C.H., Richards, V.L., Peaslee, K.D., and Lekakh, S.N., "Steelmaking Slag as a Permanent Sequestration Sink for Carbon Dioxide," Steel Times International, Vol. 30, No. 7, October 2006, pp. 25-28.
5. O'Connor, W.K., R.P. Walters, D.C. Dahlin, G.E. Rush, D.N. Nilsen, P.C. Turner. "Carbon dioxide sequestration by direct aqueous mineral carbonation." In: Proceedings of the 26th International Technical Conference on Coal Utilization & Fuel Systems: Editor, B.A. Sakkestad. Gaithersburg, MD: Coal Technology Association, 2001, pp.765-776.
6. O'Connor, W. K., D.C. Dahlin, D.N. Nilsen, S.J. Gerdemann, G.E. Rush, L.R. Penner, R.P. Walters, P.C. Turner. "Continuing studies on direct aqueous mineral carbonation for CO_2 sequestration." In: Proceedings of the 27th International Technical Conference on Coal Utilization & Fuel Systems: Editor, B.A. Sakkestad. Gaithersburg, MD: Coal Technology Association, 2002, pp. 819-830.
7. Teir, S., S. Eloneva, R. Zevenhoven. "Production of precipitated calcium carbonate from calcium silicates and carbon dioxide," Energy Conversion and Management, Vol. 46, No. 18-19, 2005, pp. 2954-2979.
8. Lackner, K.S, "Carbonate chemistry for sequestering fossil carbon," Annual Review of Energy and the Environment, Vol. 27, 2002, pp. 193-232.
9. Bond, G.M., Egeland, G., Brandvold, D.K., Medina, M.G., Stringer, J., 1999. "CO_2 sequestration via a biomimetic approach," In: Proceedings of the Sessions and Symposia sponsored by the 1999 Extraction and Processing Division Congress. The Minerals, Metals, & Materials Society, Warrendale, Pennsylvania, U.S.A., pp. 763-781.
10. Medina, M.G., Bond, G.M., and S. Rogelj, "Comparison of carbonic anhydrase isozymes for use as a catalyst in carbon dioxide sequestration process," Proceedings of the 93rd Air & Waste Management Association Meeting and Exhibition, 2000, pp. 5996-6013.
11. Simsek-Ege, F.A., Bond, G.M., Stringer, J., "A biomimetic route to environmentally friendly CO_2 sequestration: catalyst immobilization," Electrochemical Society Proceedings, fall 2000, pp. 162-170.
12. Bond, G.M., Stringer, J., Brandvold, D.K., Simsek, F.A., Medina, M.-G., Egeland, G., "Development of integrated system for biomimetic CO_2 sequestration using the enzyme carbonic anhydrase," Energy & Fuels, Vol. 15, pp. 309-316.
13. Liu, N., Bond, G.M., Abel, A., McPherson, B.J., Stringer, J., "Biomimetic sequestration of CO_2 in carbonate form: role of produced waters and other brines," Fuel Processing Technology, Vol. 86, pp. 1615-1625.
14. Li, W., Yu, L.-J., Wu, Y., Pia, L.-P., Yuan, D.-X, "Enhancement of Ca^{2+} release from limestone by microbial extracellular carbonic anhydrase," Bioresource Technology, Vol. 98, pp. 950-953.
15. Mirjafari, P., Asghari, K., Mahinpey, N., "Investigating the application of enzyme carbonic anhydrase for CO_2 sequestration purposes," Industrial & Engineering Chemistry Research, Vol. 46, pp. 921-926.

5. Grindability Study of Steelmaking Slag for Size-by-size Recovery of Free Metal

C.H. Rawlins

Department of Materials Science and Engineering
Missouri University of Science and Technology
Rolla, Missouri
E-mail: kpeaslee@mst.edu

Published in the Proceedings of the 2008 SME Annual Meeting and Exhibit, and edited for this dissertation.

ABSTRACT

The total amount of ferrous slag generated in the U.S. is about one-third the amount of iron ore mined. Thus, ferrous slag can be considered a significant mineral body for processing. Steelmaking slag contains up to 30 wt.% metal, of which only the >25 mm fraction is commonly recovered. A grinding study was conducted on basic oxygen furnace (BOF), electric arc furnace (EAF), and ladle metallurgy furnace (LMF) slags using the Bond Work Index method to determine grindability to 106μm. Work Index values ranged from 13.8-24.9 kWh/ST, depending on slag type and composition. Steel particles were magnetically recovered from crushed and ground samples for size-by-size analysis, yielding up to 18 wt.% of the slag weight recovered as magnetic. The recovered material, as characterized by inert gas melting, was found to be 61-96 wt.% metallic.

INTRODUCTION

Slag is generated during each discrete state of iron and steel production, but steelmaking slag is generally characterized by a higher lime, iron oxide, and metallic iron content than slag produced from blast furnace iron. Total U.S. production of steelmaking slag ranges from 10-15 Mt.[1] This total correlates, per ton of steel produced, to 75-150 kg/t BOF slag, 65-80 kg/t EAF slag, and 15-20 kg/t LMF slag.[2] Steelmaking slag is currently sold at $3-4/t and is used in high quality mineral aggregate (asphaltic concrete, road/rail base, and surfaces), confined construction (fill), clinker feed, roofing, mineral wool, soil conditioning, iron making, and acid mine drainage neutralization.[1,3]

In 2005, a project entitled “Geological Sequestration of CO_2 by Hydrous Carbonate Formation in Steelmaking Slag” was initiated as part of the steel industry’s CO_2 sequestration breakthrough program.[4] Part of this study shows that to achieve CO_2 sequestration efficiency sufficient for industrial-scale use, grinding the slag <200 μm will provide sufficient surface area for rapid leaching of the alkaline-earth components and subsequent conversion to carbonates. To characterize the comminution energy for steelmaking slag, a separate study was conducted to determine the grindability of

steelmaking slag using the Bond Work Index method. Size-by-size separation of magnetic material from the ground slag was conducted as part of this study to include the value of the recovered metal into an overall cost model. This paper presents the results from the grinding study.

SLAG CHARACTERIZATION

Thirteen steelmaking slag samples were gathered from project partners for this study (8 EAF, 2 BOF, and 3 LMF). Chemical and physical characterization of these slags were undertaken to quantify their properties prior to grinding.

Table 1 lists the major elements (as oxides) as determined by X-ray fluorescence (XRF). A full listing of all the elements identified is shown in Table A-1 in the Appendix. The high mass fraction (40-55 wt.%) of alkaline-earth metal oxides (CaO and MgO) makes steelmaking slag attractive for CO_2 sequestration. Both CaO and MgO report to the slag from the (dolomite) lime added as a fluxing agent. Silica, alumina, and MnO result from the deoxidizing additions, while the high fraction of FeO in EAF/BOF slag comes from the oxidation of iron late in the decarburization process. The LMF process has stronger reducing conditions that result in a lower fraction of FeO.

Table 1. Average Slag Composition (as Oxides) from XRF

Element (wt.%)	EAF	BOF	LMF
# Samples→	(8)	(2)	(3)
CaO	32.44	40.71	49.43
MgO	11.20	12.90	6.23
FeO	26.85	21.68	5.61
SiO_2	13.95	11.65	12.96
Al_2O_3	8.29	5.93	21.26
MnO	5.37	4.59	1.06

Scanning electron microscopy (SEM) analysis of slag samples shows metallic iron particles distributed in an oxide-based matrix. Figure 1 shows a backscattered

electron image of an EAF slag particle. As determined by EDS, the matrix material (dark gray) is a mixture of $(Ca,Fe,Al,Si)_xO_y$ with a porous structure. Dispersed throughout the matrix are globules, stringer, and dendrites of metallic Fe (white) and Fe/Mn (light gray). Analysis of several samples suggests that a grind size of ~100 μm should be sufficient to expose the metallic fraction for separation.

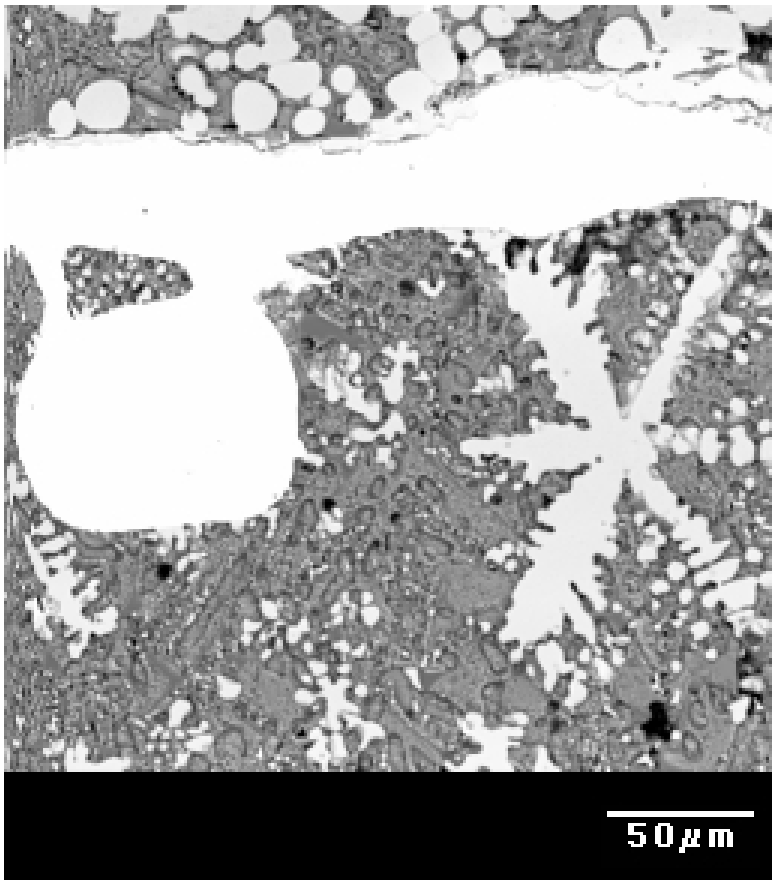

Figure 1. SEM backscattered electron image of EAF steelmaking slag. The dark gray matrix is a combination of oxides (Ca,Fe,Al,Si), while the distributed particles are free metallic steel (Fe or Fe-Mn).

Several key physical properties of the slag samples, as an average based on type, are listed in Table 2 and a full listing appears in Table A-2 in the Appendix. The as-received slags are dry with the EAF and LMF samples having less than 1% evaporable moisture. The BOF slag is higher at ~3%, which was a function of stockpile storage at the

generating site. The bulk and true densities of slag are higher than typical silica gangue minerals due to the high fraction of FeO and metallic Fe. Loss on ignition (LOI) results used to determine hydroxide/carbonate content were inconclusive because the free metallic Fe oxidized offsetting any weight loss, and actually resulted in weight gain for EAF and LMF samples. Figure 2 shows the particle size distribution (PSD) of five slag samples in the as-received condition as determined by sieve analysis. The d_{50} values ranged from 3-20 mm, with the top size of some samples ranging up to ~75 mm.

Table 2. Averaged Physical Properties of Slag

Property (# samples)	Evap. Moisture (wt.%)	Bulk Density (kg/m^3)	True Density (kg/m^3)	LOI @ 990°C (wt.%)
EAF (7)	0.91	1945.9	3826.2	-1.35
BOF (2)	3.38	2078.7	3580.9	0.57
LMF (3)	0.87	1688.1	2996.7	-0.58

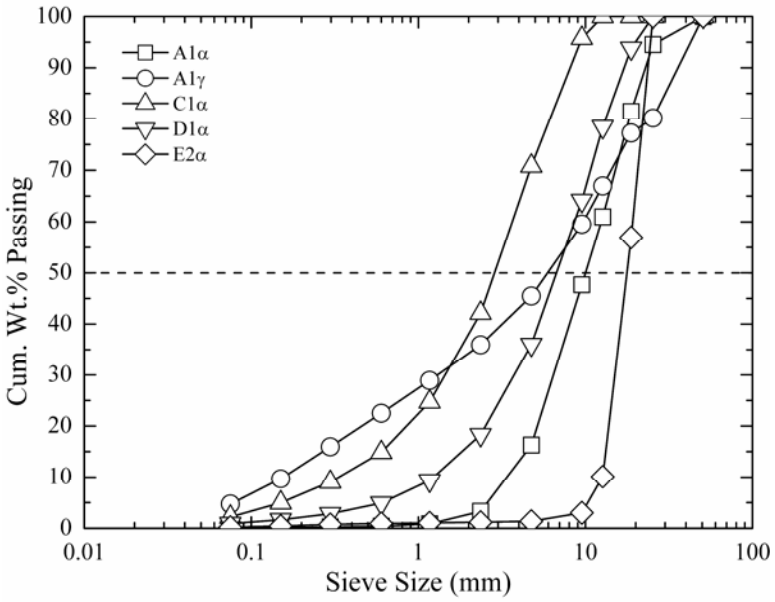

Figure 2. Particle size distribution of five raw (as-received) slag samples.

EXPERIMENTAL

The Bond closed-circuit ball mill test was used to determine the slag grindability. This type of test was chosen due to the availability of literature data for comparison and its applicability to mineral processing simulation software for subsequent analysis. To ensure a grind size of <200 μm for CO_2 sequestration and <100 μm for metal recovery, a test mesh size (P_1) of 106 μm was chosen.

The procedure listed in the SME Mineral Processing Handbook was followed for the experimental work.[5] A 12”x12” end-loading smooth mill was fabricated from a standard schedule pipe, as shown in Figure 3. The mill sets on a roller stand operating at 70-72 RPM. A counter measures the number of revolutions during each test period. The mill is charged with 285 balls at a size and number distribution given by the SME procedure.

Figure 3. 12”x12” end-loading (opposite face) smooth ball mill on stand for Bond closed-circuit grindability test.

The slag samples were prepared by crushing in a laboratory jaw and roll crusher until all slag particles passed 3360 μm (<6 mesh). PSD of the crushed slag as determined by sieve analysis is shown in Figure 4. Crushing the slag minimized the spread in PSD

between samples as evident by comparing the 80% passing feed size (F_{80}) for each sample. Metallic material from the crushed samples was separated using a 1.4 kgf (3 lb.) magnet. The crushed slag samples were further prepared by determining the packed bulk density, weight of feed that would occupy 700 ml, and calculating the ideal product period (IPP).

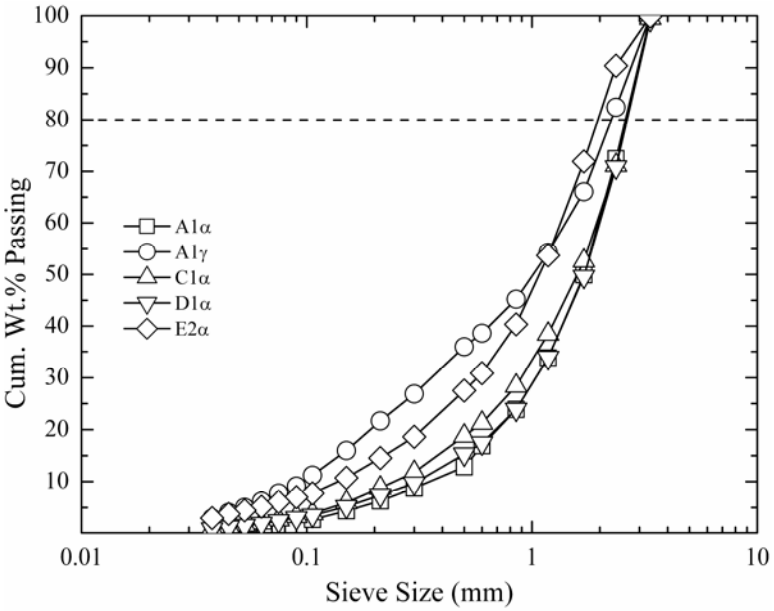

Figure 4. Particle size distribution of five slag samples after jaw/roll crushing <6 mesh (<3360 µm).

Ball mill grinding took place according to steps 7-20 listed in the SME procedure.[5] Each test took from 5-7 periods, and sieve analysis was conducted to determine the amount of product after each period. The procedure was repeated for each period until the net grams (of product) per revolution did not change significantly, which corresponded to a circulating load (C.L.) value of 250%. The data from the final two or three periods was averaged to obtain the corresponding percentage C.L. and net grams per revolution, which is the grindability value (G_{bp}). Sieve analysis of the material ground in the final period was used to determine the PSD of the undersize (product) and oversize (circulating load). From the plot of the product PSD, the 80% passing size (P_{80}) was

determined using a fifth-order polynomial curve fit and Solver in MS Excel®. The laboratory Work Index (W_{iB}) in kWh per short ton was calculated using Equation 1.

$$W_{iB} = \frac{44.5}{(P_1)^{0.23}(G_{bp})^{0.82}\left(\frac{10}{(P_{80})^{0.5}} - \frac{10}{(F_{80})^{0.5}}\right)} \quad (1)$$

Size-by-size magnetic fraction analysis was conducted on the product streams. For each sample, material from each of eleven size fractions in the circulating load and the complete product stream (<106 μm) was passed under a 1.4 kgf (3 lb.) magnet to separate the magnetic fraction. The separated material was then tested for quantification of the metallic content. The samples were placed in individual graphite crucibles and melted in an argon flooded (inert atmosphere) induction furnace. This method causes slag and metal to each form a discrete layer upon melting. These layers are then mechanically separated after cooling and the weight fraction metallic is determined. Figure 5 shows an example of the separated slag and metallic fractions.

Figure 5. Mechanical separation of slag (left) and metallic (right) fractions after inert induction melting and cooling.

RESULTS

Results from each grinding period for the ball mill test conducted on slag E2α are shown in Figure 6. The first period was conducted to obtain a baseline for the start of the

test. The grindability and C.L. results from this period deviate greatly from their ideal values as calculated from the IPP. In this case, the grindability and C.L. values were 0.31 g/rev and 972%, respectively. As the periods progressed, the grindability converged rapidly such that by the third period the value was within 9% of the final value. Seven periods were conducted with this slag. The grindability values of periods six and seven were within a few percentage points of each other signifying that the test reached steady state. The grindability and C.L. values for periods six and seven were averaged to provide values for the work index calculation. The values obtained were 0.90 g/rev and 250%, respectively. To obtain the P_{80} values, the PSD of the product was plotted, as shown in Figure 7, in comparison to the feed. The values of F_{80} and P_{80} for Slag E2α are 1934 μm and 89 μm, respectively. Using Equation 1, the work index value for Slag E2α was calculated to be 19.93 kWh/ST. In comparison, the work index for dolomite is 13.9 kWh/ST and for silica sand is 23.8 kWh/ST.[5]

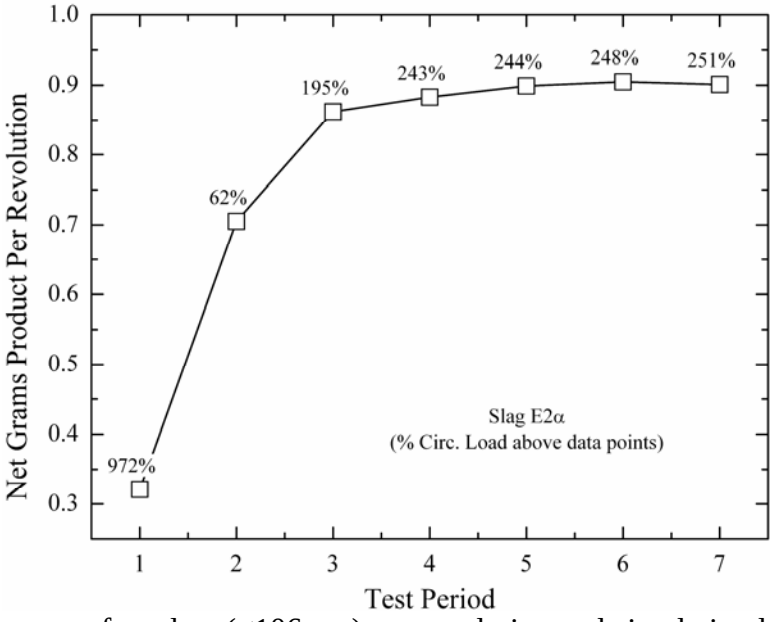

Figure 6. Net grams of product (<106 μm) per revolution and circulating load (%) values for each ball mill test period for Slag E2α.

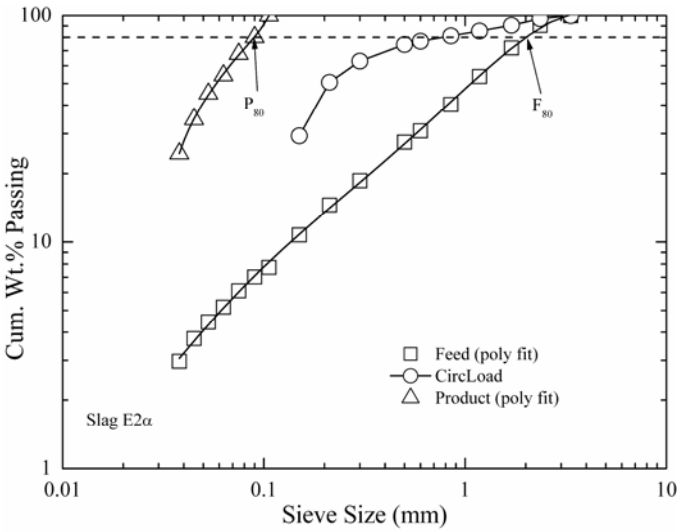

Figure 7. Particle size distribution of the feed, circulating load, and product for Slag E2α after period seven.

Tabulated results for the slags tested are listed in Table 3. The first two tests were stopped prematurely due to a misunderstanding of the test protocol, however, the W_{iB} value should be within a few percentage points of the final value.

Table 3. Results from Bond Work Index Test for Slag

Sample	C.L. (%)	Grind. (g/rev)	F_{80}	P_{80}	W_{iB} (kWh/ST)
A1α-EAF	240	0.83	2664	82	19.59
A1β-EAF	243	0.81	2818	86	20.30
A1γ-LMF	248	0.88	2228	88	19.84
B1α-BOF	245	0.78	2877	90	21.39
C1α-BOF	251	0.72	2702	90	22.99
D1α-EAF	248	0.71	2690	100	24.91
E1α-EAF	249	0.95	2339	81	17.51
E2α-EAF	250	0.90	1934	89	19.93
E1γ1-EAF	248	0.94	2672	80	17.36
E2β1-LMF	250	1.37	2218	88	13.80
E2γ1-EAF	249	0.73	2650	80	21.44
				EAF-Avg.	20.15
				BOF-Avg.	22.19
				LMF-Avg.	16.82
				Overall-Avg.	19.91

The work index values ranged from 13.8-24.9 kWh/ST, with an overall average of 19.91 kWh/ST. BOF slag had the highest average, with EAF slag next, then LMF slag exhibiting the lowest value. LMF slag has the highest amount of lime and lowest amount of FeO and free Fe, so it should be the easiest to grind based on the assumption grindability is proportional to hardness (Fe_xO_y has twice the hardness of CaO and MgO). The reason BOF slag ranks above EAF slag is unknown, but may be due to EAF slag's higher porosity (due to its foaming during the steel heat). An X-ray diffraction study of these slag samples is currently being conducted to quantify the phase fraction and may provide further insight into the ranking.

Size-by-size magnetic fraction results for Slag E2α are presented in Figure 8. These results are presented by size fraction and for the entire sample. All fractions >106 μm ranged from 14-21 wt.% magnetic, while the product fraction had less than 4 wt.% magnetic. Overall, 12.45 wt.% of the entire sample was magnetic, with 11.33 wt.% >106 μm, and 1.12% <106 μm. Thus, 91% of the magnetic particles were >106 μm, confirming that grinding to 106 μm should be sufficient to liberate the majority of the metallic fraction from the slag. A summary of results averaged from twelve slag samples are presented in Figure 9. For the overall average, >91 wt.% of the magnetic fraction is >106 μm. EAF slag had the lowest amount of material >106 μm (86.6%) due to fine steel droplet break-up generated during slag foaming. LMF slag had the largest amount >106 μm (95.6%), and when compared to EAF or BOF slag which use supersonic jets, it is produced using the least turbulent process, leading to less fine steel droplets generated and entrained into the slag. The overall average amount of magnetic fraction in slag liberated by grinding is 7.44 wt.%. This is the amount of material available after crushing to <3360 μm and magnetic separation. According to type, EAF and BOF slags have over twice the amount of magnetic material available for recovery than LMF slag. Details of the magnetically recoverable amount per slag sample after crushing and after grinding are presented in the Appendix in Table A-2.

The quality of the magnetically recoverable fraction is important in determining the valuation of the process. The metallic quantification process used was only moderately accurate because some of the samples did not stratify fully upon melting, making mechanical separation of the slag-steel phases difficult. In addition, some of the

samples were corrupted during melting due to offgas generation that led to splattering. Generally, the magnetic fraction after crushing, which consisted of 3-10 mm particles, melted cleaner and provided higher accuracy determination of the weight percent metallic. The magnetic fraction after grinding was a much finer powder, and several of the samples were contaminated due to splattering. The results presented in Table 5 are reasonably accurate (±5%).

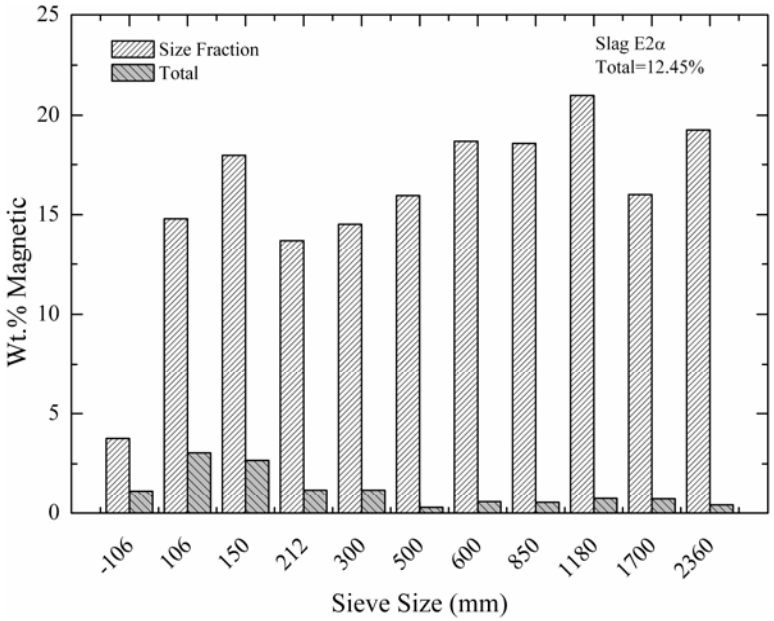

Figure 8. Size-by-size magnetic fraction results for Slag E2α.

The grade of the magnetic fraction after crushing is quite good with 89 wt.% of the material reporting as metallic. However, the grade of the magnetic fraction after grinding is less with 68 wt.% of the material reporting as magnetic. The lower grade is due to the higher surface area of the fine material, leading to a higher amount of oxidized iron, plus incomplete liberation as slag material is still bound to the magnetic particles. Based on the average amount of material recovered from magnetic separation during grinding (7.44 wt.%), the overall amount of metallic material recoverable from ground slag is estimated to be 5 wt.%. Using similar analysis yields an overall amount of metallic material recoverable from crushed slag of 1.2 wt.%.

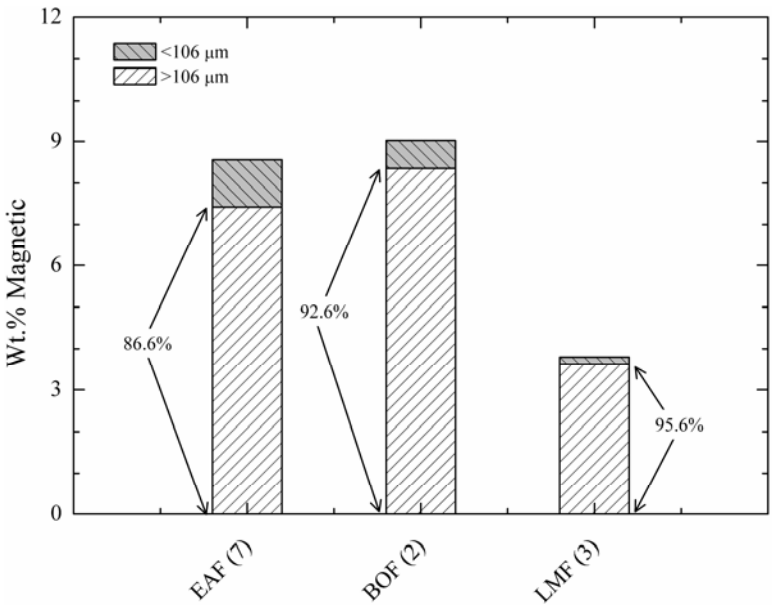

Figure 9. Weight percent magnetic material by slag type. Total bar height is total amount of magnetic material in each slag. Shaded regions represent the amount above or below 106 μm. Numbers to the side of each bar represent the percentage >106 μm.

Table 4. Metallic Content for Magnetic Fraction from Slag

Slag Type (# samples)	Magnetic Fraction Wt.% Metallic (post-crush)	Magnetic Fraction Wt.% Metallic (post-BWI)
EAF (6)	86%	61%
BOF (2)	88%	72%
LMF (3)	96%	72%
Average	89%	68%

CONCLUSIONS

The Bond closed-circuit ball mill method is labor intensive and generally requires about twenty man-hours per sample to produce final results. The primary source for error lies in the efficiency of product separation (e.g., screening) between each period and accurate determination of the F_{80} and P_{80} values. Multiple tests were not run on the same sample for comparison, but the final W_{iB} values lie in the expected range when compared to published values.

As an estimate for future (rapid) calculations, a comparison of density (bulk and true) to W_{iB} was made, but the results showed poor correlation. This is probably due to the slag's heterogeneity. Multiple density and work index tests on the same sample may lead to a closer fit. An alternate source for poor correlation may be caused by the free metallic content in the slag. Slag shows a much higher content of free metallic particles than most ores. The distributed steel particulates are not friable, so through this procedure any steel particles greater than the test size will remain in the circulating load (i.e. will not grind and report to the product, which is removed after each period). Therefore, an artificial mass of very dense particles will build up from period to period. Because only the oxide matrix is subject to crushing, segregation of the metal from the slag takes place. Analysis of the grinding results, after calculated removal of the non-friable particles, will be undertaken in future work to establish the W_{iB} for the matrix material in-absentia of the steel.

A cost analysis model that factors grinding energy into the slag-CO_2 sequestration process is being constructed. Reduction in slag particle size provides a more favorable reaction rate for industrial-scale CO_2 sequestration, but the tradeoff comes in form of the energy required to grind the slag. The energy required has a direct cost and an associated CO_2 generation amount, both of which have an economically quantifiable value. To offset these costs, the metal fraction can be recovered and returned to the steel mill for subsequent inclusion in the charge material, providing a cost credit. The results of this model will be published in future work.

ACKNOWLEDGMENTS

The author would like to acknowledge the support of Gallatin Steel, IPSCO, ArcelorMittal, Nucor, and US Steel for their support in supplying slag samples and analysis. Josh Noll, an undergraduate metallurgical engineering student at UMR, is also acknowledged for turning a sketch concept of the ball mill system design into physical reality.

REFERENCES

1. "Iron and Steel Slag Statistics and Information." Reston, VA, U.S.: U.S. Department of the Interior, U.S. Geological Survey, Minerals Information, June 2005, http://minerals.usgs.gov/minerals/pubs/commodity/iron_&_steel_slag/
2. "Steel slag: A premier construction aggregate." West Lawn, PA, U.S.: National Slag Association, June 2005, http://www.nationalslagassoc.org/PDF_files/SSPremAgg.PDF
3. van Oss, H.G. "Slag-iron and steel." U.S. Geological Survey Minerals Yearbook (2003): 69.1-69.3, June 2005, http://minerals.usgs.gov/minerals/pubs/commodity/iron_&_steel_slag/islagmyb03.pdf
4. C.H. Rawlins, V.L. Richards, K.D. Peaslee, and S.N. Lekakh. "Sequestration of CO_2 from Steelmaking Offgas by Carbonate Formation with Slag." In: Proceedings of the AISTech 2006 Conference, May 1-4, 2006; Cleveland, OH, U.S. Warrendale, PA, U.S.: Association for Iron and Steel Technology.
5. Society of Mining Engineers. SME Mineral Processing Handbook. Ed. N.L. Weiss. New York: American Institute of Mining, Metallurgical, and Petroleum Engineers, Inc., 1985.

APPENDIX

Table A-1. Slag Composition (as Oxides) from XRF Analysis

Elements (# samples)	EAF (8)		BOF (2)		LMF (3)	
	Avg. (wt.%)	Range (wt.%)	Avg. (wt.%)	Range (wt.%)	Avg. (wt.%)	Range (wt.%)
CaO	32.44	27.3-35.9	40.71	40.5-40.9	49.43	47-51.3
MgO	11.20	9.4-12.8	12.90	12.0-13.8	6.23	4.3-10
FeO	26.85	20.2-31.6	21.68	21.6-21.7	5.61	5.0-6.3
SiO_2	13.95	8.7-19.4	11.65	10.4-12.9	12.96	4.5-28.3
Al_2O_3	8.29	5.6-11.8	5.93	5.2-6.6	21.26	4.9-32.3
MnO	5.37	3.4-7.1	4.59	4.5-4.7	1.06	0.8-1.3
TiO_2	0.47	0.4-0.5	0.58	0.5-0.7	0.34	0.3-0.4
ZrO_2	0.07	0-0.2	0.18	0.1-0.3	0.20	0.20
Cr_2O_3	1.48	0.8-2.5	0.36	0.3-0.4	0.25	0.25
K_2O	0.05	0.05	B.L.	B.L.	0.01	0.01
Na_2O	B.L.	B.L.	B.L.	B.L.	0.01	0.01
S	0.34	0.1-0.9	0.11	0.11	1.33	1.0-1.6
P	0.30	0.2-0.6	0.43	0.4-0.5	0.08	0-0.2
C	0.23	0.1-0.3	0.53	0.4-0.7	0.38	0.38
Sr	B.L.	B.L.	B.L.	B.L.	B.L.	B.L.
F	0.65	0.3-0.9	0.33	0.33	1.66	1.66

Table A-2. Physical Properties of Slag Samples

Sample	Slag Type	Evap. Moisture (wt.%)	Bulk Density (kg/m^3)	True Density (kg/m^3)	LOI @ 990°C (wt.%)	Magnetic Fraction (wt.%)	
Method→		ASTM C566-97	ASTM C29M-97	Pycn.		>6 mesh post-crush	<6 mesh post-BWI
A1α	EAF	0.00	2014	4052	-1.7	0.32	3.83
A1β	EAF	1.14	1941	3881	-1.4	0.18	11.53
A1γ	LMF	2.59	1778	2900	3.3	0.53	2.61
B1α	BOF	2.52	2019	3614	0.8	0.76	12.08
C1α	BOF	4.25	2138	3548	0.3	0.18	5.95
D1α	EAF	1.56	2180	3697	-1.1	0.12	2.68
E1α	EAF	1.44	1795	3760	-1.7	0.27	5.21
E2α	EAF	0.41	1650	3822	-1.7	0.46	12.45
E1β-1	LMF	0.02	1438	3021	-3.2	5.08	4.77
E1γ-1	EAF	0.81	2167	3906	-1.2	3.28	6.30
E2β-1	LMF	0.00	1849	3069	-1.9	1.28	3.99
E2γ-1	EAF	1.03	1874	3665	-0.7	3.75	17.92
Average						1.23	7.44

6. Feasibility of Processing Steelmaking Slag for CO_2 Sequestration and Metal Recovery

C.H. Rawlins, K.D. Peaslee, V.L. Richards

Department of Materials Science and Engineering
Missouri University of Science and Technology
Rolla, Missouri, USA 65409
Email: kpeaslee@mst.edu

Accepted publication in AIST Transactions, and edited for this dissertation.

ABSTRACT

The feasibility of processing electric arc furnace (EAF), basic oxygen furnace (BOF), and ladle metallurgy furnace (LMF) slags for metal recovery and carbon dioxide sequestration was evaluated using a combination of grindability and sequestration tests on industrial slags and modeling studies using METSIM. Power consumption, slag-carbon dioxide capture, and metal recovery all increased inversely to grind size (P_{80}) within the range of 50 to 1000 μm. The optimum grind size was determined based on a calculated process net value using commodity indexes. EAF and BOF slags exhibited sharp maximum values at 110-120 μm, with a rapid decrease at larger or smaller sizes due to increased power consumption or decreased metal recovery. LMF slag exhibited much less sensitivity to grind size, with ~3% variation from its peak size of 370 μm over most of the studied range. All slags showed net positive carbon dioxide sequestration benefits based on slag capture and generation by the power supply source.

INTRODUCTION

Slag is a co-product from each distinct stage of ferrous liquid-metal processing. However, steelmaking slag contains higher calcium oxide, iron oxide, and metallic iron content than slag produced from blast furnace iron. Ranging from 10-15 million metric tons in U.S. production, steelmaking slag is a significant mineral resource to study for value optimization.[1] Currently, steelmaking slag is sold for $3-4/metric ton (tonne) for use in such applications as high quality mineral aggregate, construction fill, cement clinker feed, and ironmaking flux.[2] The use of slag as an agent for capturing carbon dioxide emissions has the potential of increasing its application and value.[3] Due to its high alkaline earth oxide content and immediate availability at the steel mill, steelmaking slag can serve as a unique source point mitigation for carbon dioxide sequestration.

To further investigate this hypothesis, a project was initiated in 2005 to study geological sequestration of carbon dioxide by hydrous carbonate formation in steelmaking slag.[3] The project goals include investigation of the kinetic mechanisms limiting the carbonation reaction rate and determination of process parameters necessary

to design an industrial-scale sequestration system. In this study, carbonate conversion was found to be strongly dependent on particle size.[4] Achieving suitable efficiency for industrial-scale carbon dioxide sequestration requires fine slag grinding, which provides sufficient surface area for rapid leaching of the alkaline-earth components and subsequent conversion to carbonates.[5]

Because mineral comminution is energy intensive, there are concerns that the energy required to grind the slag would exceed the carbon dioxide sequestration benefit in both direct cost and indirect generation (e.g., carbon dioxide emitted from the electric generation source). To accurately characterize the comminution energy for steelmaking slag, a separate study was conducted to determine the grindability of this slag using the Bond Work Index method.[6] This work index is a comminution parameter that expresses the resistance of a mineral to crushing or grinding and permits calculation of the power expended in these unit processes. Included as part of the study, size-by-size separation of the liberated magnetic fraction from the ground product allowed corresponding quantification of the separated material for metallic content (e.g., grade).

The current work seeks to assess the feasibility of grinding steelmaking slag for carbon dioxide sequestration and metal recovery. Slag comminution promotes carbonate conversion at a rate sufficient for industrial-scale sequestration, but the overall merit of the process is determined by a balance of the grinding costs (i.e., direct energy and indirect carbon dioxide generation) and benefits (i.e., improved carbon dioxide sequestration and metal recovery). Using three industrial slags (EAF, BOF, and LMF) at five grind sizes (50, 100, 200, 500, and 1000 μm) and results from the previous sequestration and grinding studies[4-6], these four factors were investigated. An accurate correlation was fit within the grind size range for each factor to yield the optimum grind size for each slag type.

SLAG COMMINUTION

Slag grinding research has primarily been conducted in the cement industries where granulated blast furnace slag is used as a clinker amendment. These efforts have focused on comparing various grinding processes to achieve a desired Blaine fineness,

but do not address steelmaking slag, metal recovery, or provide suitable data for estimating power consumption.[7-9] A study on metals recovery from slags found the density, resistance to impact, and Los Angeles abrasion test values for steel slag are higher than those of basalt or granite, but does not provide sufficient details to characterize the power consumption for steel slag grinding.[10] Published values for a slag Work Index are available, but are not delineated by type and the as-published inaccuracy is too high for the current calculations.[11]

Because detailed comminution data for steelmaking slag by type was not available, grindability measurements were conducted as part of the current project.[6] Using industrial samples of EAF, BOF, and LMF slags; Bond Work Index values (W_i) were obtained using a laboratory ball mill. The ball mill closed circuit test was chosen for its applicability to grind sizes as low as 500 mesh (25 μm). This grindability test is based on the Third Theory of Comminution, as shown in Equation 1.[12-13]

$$W = \frac{10W_i}{\sqrt{P_{80}}} - \frac{10W_i}{\sqrt{F_{80}}} \quad (1)$$

Work input (W) in kilowatt-hours per short ton (st) is a function of the work index (W_i) and particle diameter in microns, at which 80% passes in the product (P_{80}) and feed (F_{80}). Numerically, W_i is the kilowatt-hours per short ton required to reduce the material (slag) from a theoretical infinite feed size to 80% passing 100 μm. The W_i value has high portability as a standard for comparing comminution of minerals and for use in mineral processing sizing and simulation programs.

Based on slag characterization results, a target grind size (P_{80}) for the work index test was determined. Scanning electron microscopy (SEM)/backscatter electron (BSE) analysis of steelmaking slag samples indicated that a grind size of ~100 μm should be sufficient to liberate most of the metal particles.[6] Furthermore, carbon dioxide sequestration kinetic analysis and modeling showed that a particle size of 200 μm or less will provide sufficient reaction time for an industrial scale reactor.[5] Based on these observations, a target grind size of 106 μm (150 Tyler mesh) was chosen for the Bond

Work Index test . Size-by-size analysis of the ground material subsequently found that more than 90% of the metallic fraction is >106 μm.

The grindability experimental results enabled the development of a model for estimating the comminution power requirement. Figure 1 shows a schematic of the grinding model developed in METSIM (ver. 15.07), a commercially available metallurgical processing simulator. Raw slag undergoes primary size reduction in a cone crusher. For each slag type, the cone crusher size and settings remained constant regardless of the final product grind size. This allows the cone crusher to provide the same function in each case. The crushed slag is fed to a ball mill for grinding to the final product size. The mill is operated dry and sized based on a target P_{80} (i.e. 50, 100, 200, 500, and 1000 μm). An approximate 2:1 inside length to diameter ratio with 40 vol.% ball loading is used for the mill in each scenario. The top ball size varied from 50-75 mm, depending upon the target P_{80}. The ground product from the ball mill was passed across a single deck vibrating screen for topsize control, where the oversize material recirculates back to the ball mill feed and the undersize particles report to the product. The screen aperture was selected to provide ≤1 wt.% recirculation of topsize material to the ball mill feed. In this manner, the mill operates essentially in open circuit mode. Based on these mill-circuit operating parameters, the efficiency factors shown in Table 1 were applied to the calculated grinding power (work input) using Equation 1.[14]

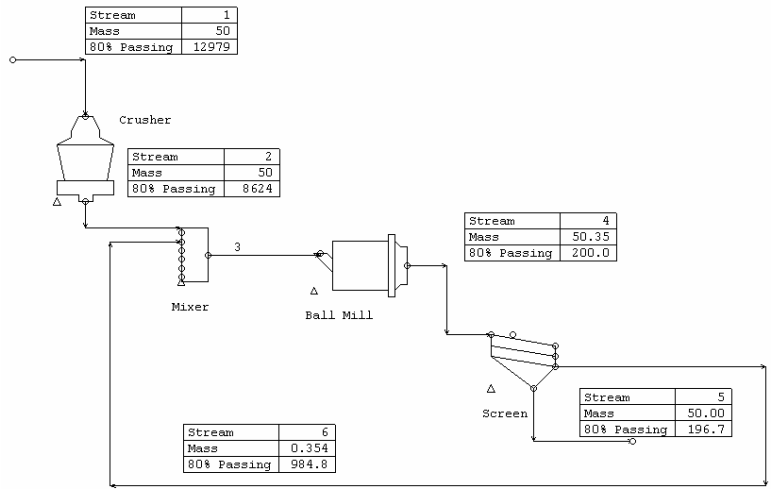

Figure 1. Schematic of METSIM grinding circuit use to calculate comminution energy

Details of the crusher, ball mill, and screen dimension and operating parameters are listed in Table A-1 in the Appendix. In this model, only the power draw of the cone crusher and ball mill are calculated. Power requirements for the vibrating screen and subsequent magnetic separation processes are minor compared to that of the comminution equipment.

Table 1. Efficiency Factors Applied to Calculated Grinding Power (W)[14]

Factor	Value
Dry Grinding (EF_1)	1.3
Open Circ. Grind, 80% Passing (EF_2)	1.2
Mill Diameter, *D* in meters (EF_3)	$(2.44/\ D)^{0.2}$
Oversized Feed (EF_4)	$\left[F_{80}/P_{80} + (W_i - 7)(F_{80} - F_o)/F_o\right]/(F_{80}/P_{80})$
	$F_o = 4000(13/W_i)^{0.5}$
Fineness of Grind (EF_5)	$(P_{80} + 10.3)/1.145P_{80}$

The slag parameters input to the model were obtained from characterization of the different slag types in previous work.[6] Table 2 lists the input slag parameters, while Figure 2 shows the feed particle size distribution (PSD), with all data obtained as an average from multiple samples (number of samples shown in parentheses). The density of slag is higher than that of typical silica gangue minerals due to the higher iron and iron oxide content. Work index values ranged from 13.8-24.8 kWh/st, with the average for each slag type listed in Table 2. LMF slag has the highest amount of lime and the lowest amount of iron oxide, so it should be the easiest to grind (based on a rule of mixture estimation using W_i for burnt limestone and hematite of 11.0 and 18.0, respectively).[11] The reason BOF slag ranks higher than EAF slag is unknown given EAF slag's higher iron oxide and lower calcium oxide content. Higher porosity in the EAF slag may provide an easier crack propagation path. Overall, slag has a higher work index than burnt limestone, hematite, or magnetite (19.2), and is comparable to silica sand (23.8).[11] The mass flow used in the simulation for EAF and BOF slag was 100,000 tonne/yr (50 tonne/hr), while that used for LMF slag was 25,000 tonne/yr (12.5 tonne/hr). These

values approximate slag production for a one million ton per year steel mill. Comparing the particle size distributions shows LMF slag to have the widest spread, the largest F_{80}, and the highest amount of fines (<100 μm). Overall, EAF slag has the largest particle size, with 47% passing 12.5 mm, compared to 67% passing for LMF slag and 80% passing for BOF slag. LMF slag has the highest amount of material already in the target P_{80} size range (50-1000 μm), while EAF slag has the least. While BOF slag has a higher work index, it has more material in the feed already in the product size range and a smaller topsize (compared to EAF slag), which may offset some of the energy consumption.

Table 2. Slag Physical Properties used in METSIM Grinding Model

Slag Type (# samples)	Density (kg/m^3)	W_i (kWh/st)	Mass Flow (tonne/hr)
EAF (7)	3826	20.15	50.0
BOF (2)	3581	22.19	50.0
LMF (3)	2997	16.82	12.5

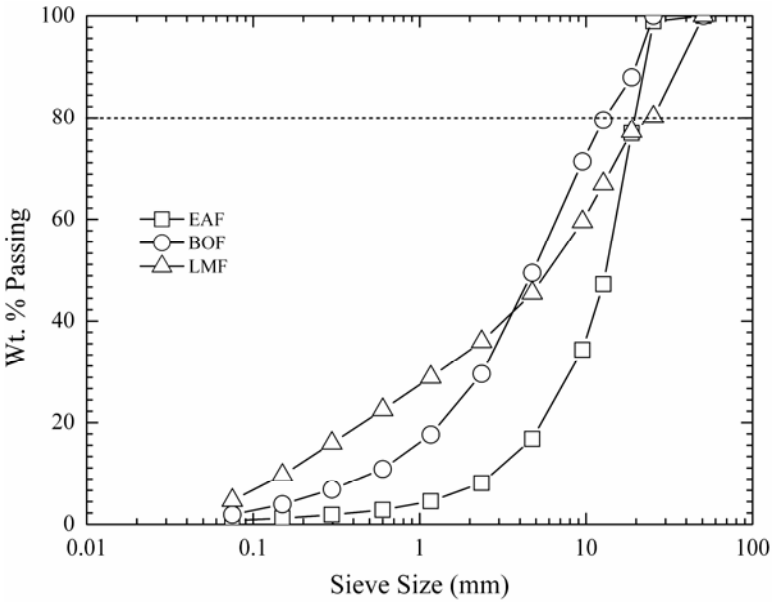

Figure 2. Feed stream particle size distribution of EAF, BOF, and LMF slags used in METSIM comminution model

The total comminution power required at each target grind size as estimated by the METSIM model is shown in Figure 3. This data is based on total mass throughput (Figure 3a), in which EAF and BOF slag are processed at four times the rate of LMF slag. Normalized mass throughput (Figure 3b) is the total power divided by mass flow rate. All slag types show increasing comminution power with decreasing P_{80}, which increases sharply below 200 μm. The crushing power draw ranges from 1-7% of the total power required, showing that slag grinding will be the controlling process for optimization (Table A-1). On a total mass throughput basis, EAF and BOF slag have similar power requirements with a 10% difference at 50 μm and a 3% difference at 1000 μm. On a normalized basis, the power draw follows the W_i values, descending from BOF to LMF, and the difference increases as the P_{80} decreases. The curves in Figure 3 were fit with the second order exponential decay given in Equation 2. This correlation yielded an R^2>0.999, indicating accurate interpolation within the P_{80} range modeled. The terms of this equation are detailed in the Appendix in Table A-2.

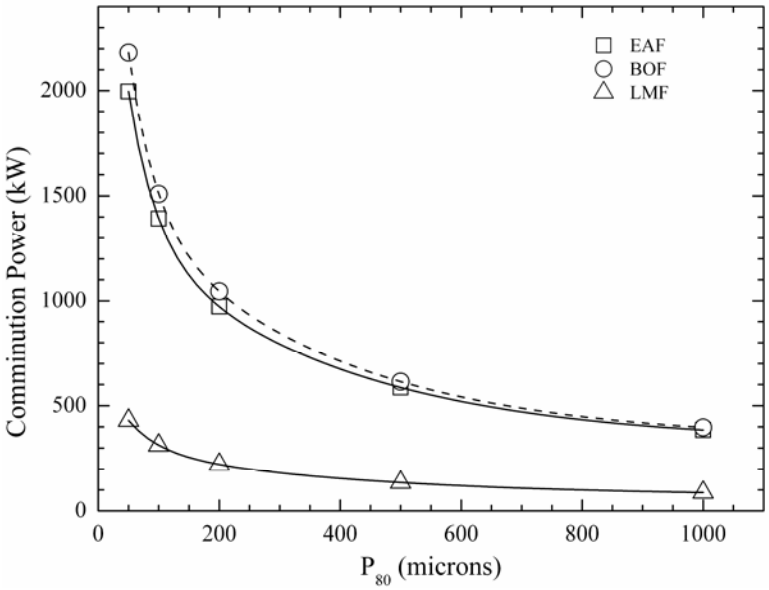

(a)

Figure 3. Total comminution power (crushing+grinding) versus P_{80} for three slag types based on (a) total mass throughput and (b) normalized mass throughput

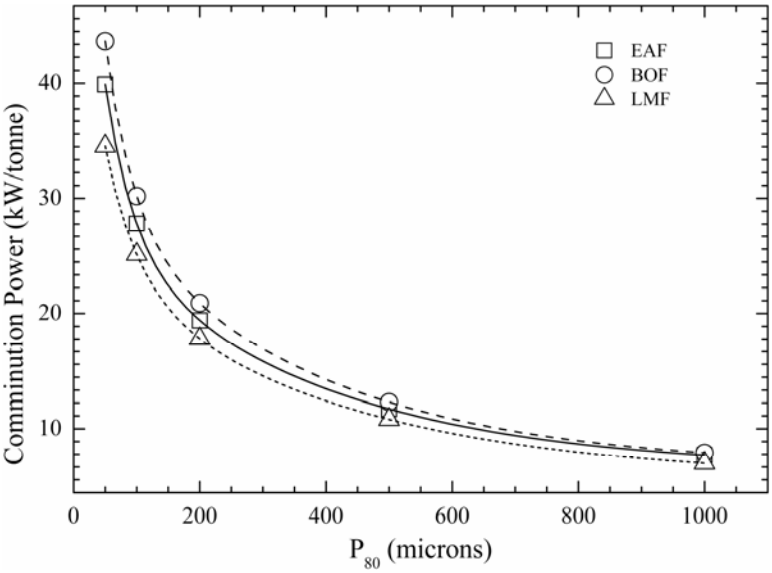

(b)

Figure 3. Total comminution power (crushing+grinding) versus P80 for three slag types based on (a) total mass throughput and (b) normalized mass throughput

$$y = y_o + A_1 e^{-P_{80}/t_1} + A_2 e^{-P_{80}/t_2} \quad (2)$$

The primary concerns about slag grinding have been the issues of power (electric) consumption and carbon dioxide generation (emission) at the electric supply source. Both terms can be quantified as input into an overall valuation model. The cost of electric power is published each month by the U.S. Department of Energy in *Electric Power Monthly* (EPM). The retail price for electricity in the industrial sector based on the October 2007 EPM publication (12 month rolling average ending July 2007) is used in the valuation model.[15] Conversion of energy consumption to carbon dioxide emissions is greatly dependent upon the energy source and varies by geographic region. The U.S. average, as published by the U.S. Environmental Protection Agency, of 0.704 kg carbon dioxide per kWh (considering power plant generation only, and not factoring transmission losses) can be applied to the comminution energy amount.[16] The total amount of carbon dioxide emitted by the consumption of comminution electricity will be factored into the section on sequestration as an offset (e.g., negative sequestration).

CARBON DIOXIDE SEQUESTRATION

Thermodynamically, carbon dioxide sequestration is a function of alkaline earth oxide content. In the slag sequestration study, the theoretical amount of carbon dioxide captured is calculated from the lime plus magnesia content.[3] While full thermodynamic conversion of these oxides to carbonates can result in significant capture potential (i.e., 9.0-11.2 kg carbon dioxide captured per tonne of liquid steel produced, which is 35-45% of that emitted from a mini-mill), the kinetic reaction rate limits the actual yield. The conversion rate is limited both by encapsulation of calcium and magnesium oxides by non-porous, non-reactive materials (i.e., silica, iron oxide, or alumina), and by locking of these oxides into less reactive phases (i.e., dicalcium silicate or calcium ferrite). The reaction rate can be significantly enhanced through particle size reduction and aqueous processing.[4] Particle size reduction increases the surface area of the slag particles to expose encapsulated reactive phases, thus greatly increasing the carbonate conversion rate. Aqueous processing allows for stepwise leaching of the alkaline phases and subsequent conversion of the leachate to carbonate. The two-step process minimizes carbonate product layer build-up on the slag particles, which inhibits further conversion.

Based on the size-by-size slag leaching and carbonization study, a two-stage reactor system was designed in METSIM to model industrial-scale slag sequestration.[5] Inputs to the model are the slag particle size distribution (produced from the METSIM grinding model) and slag chemical composition, which is listed in Table 3. In this model, only the calcium oxide fraction is considered for carbonation. The model simulates a two-stage continuous processing system where water in Reactor 1 leaches the alkaline components and the leachate is sent to Reactor 2 for precipitation of carbonated through reaction with bubbled carbon dioxide. The leachate water is continuously recirculated to minimize the feed water requirement, and the precipitated carbonate is deposited onto the slag particles in Reactor 1. Both reactors operate at atmospheric pressure and temperature for a total processing time of twenty days.

The two-stage sequestration METSIM model was first investigated using LMF slag at five particle sizes (20, 100, 200, 1000, and 10000 μm) that encompass the full distribution of particles produced by the grinding model. The resulting weight percent

carbonate ($CaCO_3$) at each particle size was fit to Equation 3, which is applied to the ground slag, and assumes that calcium oxide is evenly distributed amongst the particle sizes. A Harris power fit was used for particles <1 mm and a simple power fit for particles >1 mm, resulting in excellent data correlation (R^2>0.99). In Equation 3, C_i is the weight percent carbonation for particle size P_i (mm), and the terms *a*, *b*, and *c* are correlation coefficients.

Table 3. Slag Composition used in METSIM Sequestration Model

Oxides	EAF (8)	BOF (2)	LMF (3)
CaO	32.44	40.71	49.43
MgO	11.20	12.90	6.23
FeO	26.85	21.68	5.61
SiO_2	13.95	11.65	12.96
Al_2O_3	8.29	5.93	21.26
MnO	5.37	4.59	1.06

$$C_i = \left(a + bP_i^c\right)^{-1}, P_i < 1mm$$
$$C_i = aP_i^b, P_i < 1mm \quad (3)$$

The total amount of carbonation (wt.% $CaCO_3$) for each particle size distribution (*C*) is calculated by Equation 4, which sums the product of each particles weight percent carbonation (C_i) and the amount (wt.% retained) in each size fraction (n_i). Particle sizes ranged from 32-2870 μm in *i*=17 fractions.

$$C = \sum_i C_i \frac{n_i}{100} \quad (4)$$

The amount of carbon dioxide captured per hour ($\dot{c}$, kg/hr) is then determined as a function of the total carbonation (*C* in weight percent), the molecular weight fraction of CO_2 in $CaCO_3$, and the mass flow rate of slag (*m*, tonne/hr), as shown in Equation 5.

$$\dot{c} = \left(\frac{c}{100}\right)\frac{\dot{MW}_{CO2}}{MW_{CaCO3}}\left(\frac{m}{1000}\right) \quad (5)$$

The amount (kg/hr) of carbon dioxide captured by LMF slag for each P_{80} value was calculated directly from Equations 3-5. The same approach was used for EAF and BOF slag except that each C_i term in Equation 3 was multiplied by a composition factor reflecting these slags lower calcium oxide content. The composition factor is the fraction of calcium oxide in each slag based on the LMF slag composition (i.e., for EAF=32.44/49.43). The composition factor methodology was validated for both LMF and EAF slags in the METSIM sequestration model. Although the model was not validated with BOF slag, applying the composition modification factor is an appropriate first order approximation.

Figure 4 shows the resulting carbon dioxide balance for each slag. Each graph shows, for each grind size of each respective slag, the amount of carbon dioxide captured by that slag (as calculated from Equations 3-5), the amount of dioxide emitted by the electric supply source (as a negative sequestration value), and the net carbon dioxide sequestered.. All amounts are shown on a normalized scale that is obtained by dividing $\dot{c}$ by the respective slag mass flow rate. In each graph, the data for slag-carbon dioxide capture was fit to a second-order exponential decay (see Table A-2 in the Appendix) with an R^2>0.999, while the other two sets of points are connected by straight lines. The data for emission by power source can be fit to the preceding curve for the power consumed, and the net sequestered data is a sum of the other two lines. Both the EAF and BOF slags show similar profiles at slightly different magnitudes. The amount of carbon dioxide captured by the slag and the amount released by the power source both increase with decreasing P_{80}. The amount captured is approximately three-seven times the amount released, resulting in a net positive amount of carbon dioxide sequestered for all slags. For EAF and BOF slag, the net amount sequestered peaks at a P_{80}~100 μm. Below this size, the amount released from power consumption rises faster than the amount captured by the slag, resulting in a decrease in the net amount. Above this size, the increasing particle size hinders the capture rate, resulting in a decrease in the net amount

sequestered. LMF slag shows a positive net sequestration rate, but no peak within the range tested due to the low W_i yielding low power consumption, even at fine grind sizes.

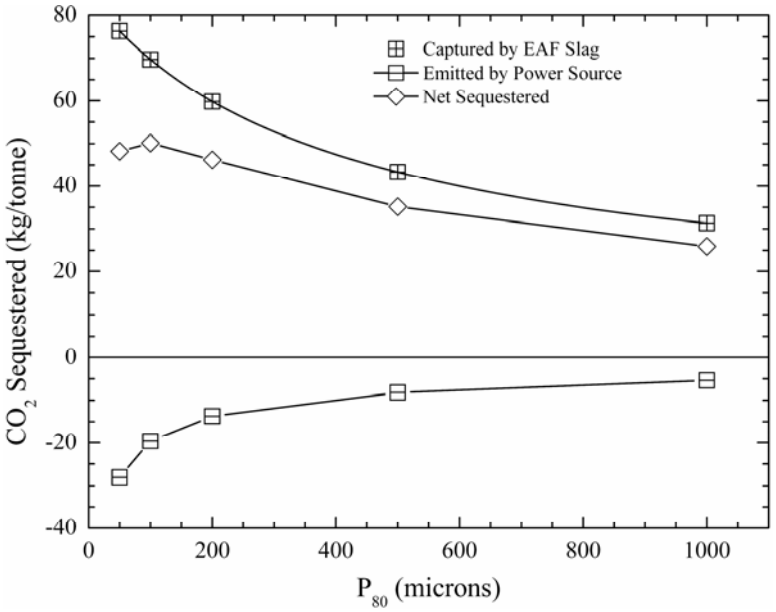

(a)

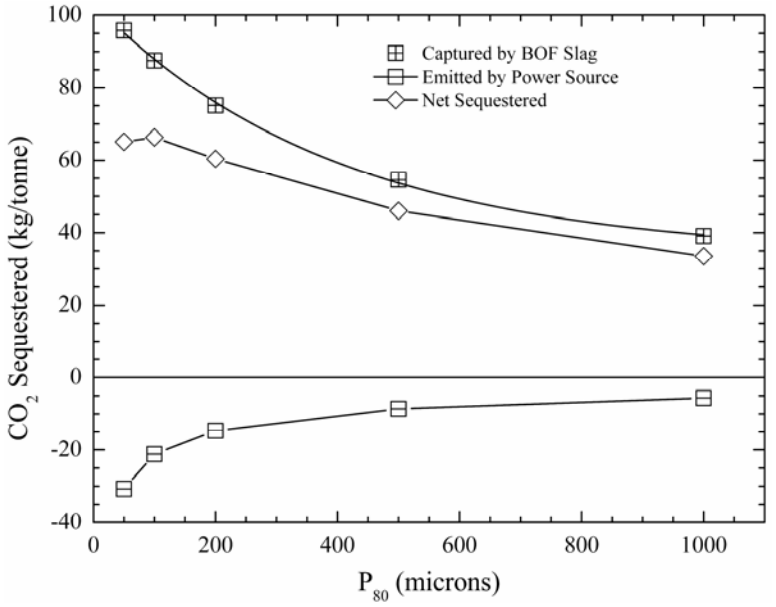

(b)

Figure 4. Net carbon dioxide sequestered (slag capture-power source emission) for (a) EAF, (b) BOF, and (c) LMF slags versus grind size (P80)

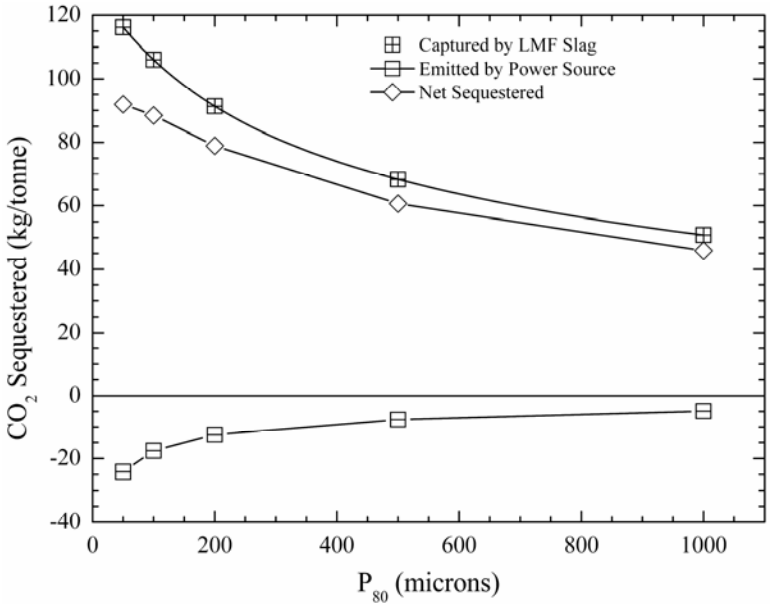

(c)

Figure 4. Net carbon dioxide sequestered (slag capture-power source emission) for (a) EAF, (b) BOF, and (c) LMF slags versus grind size (P_{80}) (cont.)

The theoretical amount of carbon dioxide captured by each slag is shown in Table 4 as a comparison to the peak values shown in Figure 4. While the predicted peak values are ~20% of the theoretical values due to the low kinetic reaction rate, the net amount of carbon dioxide sequestered is positive, indicating that slag grinding has positive environmental value. Work is ongoing to improve the kinetic reaction rate to increase the realized carbon dioxide sequestration rate.

Table 4. Comparison of Peak Theoretical and Actual Carbon Dioxide Sequestration

Net CO_2 Seq. (kg/tonne)	EAF	BOF	LMF
Theoretical	255	320	388
Peak from Figure 4	50	67	92

Sequestration values of carbon dioxide can be assigned through intercompany trading or open market exchange. For the valuation model, data from the Chicago

Climate Exchange (CCX), which trades in Carbon Financial Instrument (CFI) contracts, was used The October 2007 price is applied to each P_{80} value in Figure 4.[17]

METAL RECOVERY

The metal content of steelmaking slag was measured in the crushed product feeding the grindability test and in the ground product of the final period after the grindability test.[6] In preparation for the grindability test; all slags were crushed (jaw/roll) to pass through a 3.36 mm sieve. Magnetic material liberated from crushing (>3.36 mm) was separated and set aside for subsequent analysis. After each grindability test, the magnetic fraction was separated on a size-by-size basis into 10 fractions from 106-3360 μm, plus the <106 μm fraction as a whole. Figure 5 shows the particle size distribution of the magnetic fraction and Table 5 shows the total quantity of magnetic material in each slag. EAF and BOF slags have similar size distributions and total amounts of magnetic material, but EAF has slightly finer particles and more material that is magnetic in the finer fraction. LMF slag has a lower overall amount of magnetic material, but larger particle size. The more quiescent processing nature leading to less trapped metallic particles. Overall, ~90% of the magnetic particles were >106 μm, which aids in liberation and magnetic separation.

From the magnetic fraction separated after crushing and the fraction separated after grinding, the amount of steel trapped in the slag was determined by melt separation.[6] Because it was simpler to handling in the induction furnace, quantitative analysis was performed only on the total magnetic fraction separated after crushing (>3.36 mm) and the total magnetic fraction separated after grinding (<3.36 mm). The material from crushing stratified well upon melting and separated cleanly, leading to accurate determination of the weight fraction metallic. The post-ground powder magnetic fraction was less accurate because some of the sample did not fully stratify upon melting. Table 6 shows the weight percent metallic in each magnetic fraction analyzed. The grade of the magnetic fraction after crushing is very high at 86-96% metallic. However, the grade of the post-grind magnetic fraction is less at 61-72% metallic. This difference is due to the

higher surface area which results in a higher iron oxide content, and incomplete liberation from grinding, which leads to slag oxides remaining bound to the metallic particles.

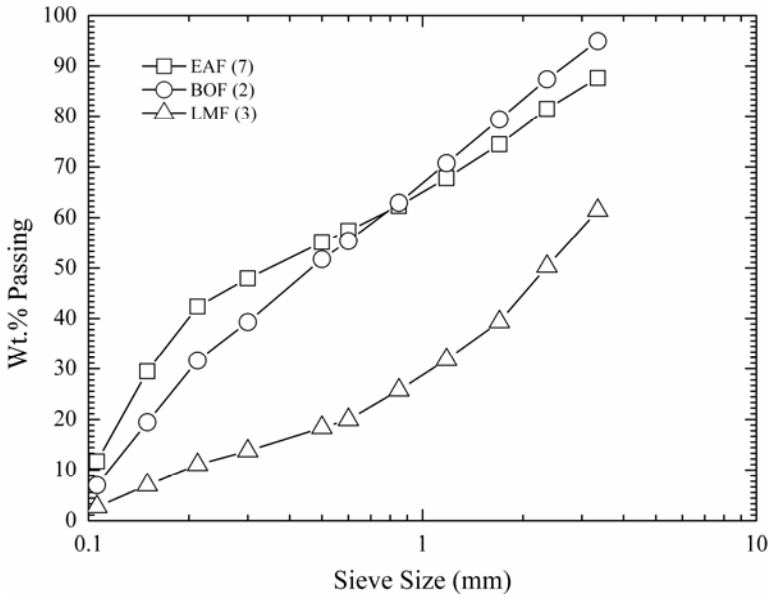

Figure 5. Particle size distribution of magnetic fraction in three types of steelmaking slags

Table 5. Quantity of Magnetic Material in Steelmaking Slag

Wt.% Magnetic	EAF	BOF	LMF
>106 μm	8.61	8.81	5.92
<106 μm	1.14	0.67	0.17
Total	9.75	9.48	6.09

Table 6. Metal Content of Magnetic Fraction in Slag

Wt.% Metallic	EAF	BOF	LMF
>3.36 mm	86.1	88.1	95.5
<3.36 mm	60.7	71.9	72.0

The amount of metallic material liberated from grinding is a function of individual size fraction magnetic content (Figure 5), the amount of slag in each size

fraction, and the metallic content of the magnetic fraction. The liberated magnetic fraction is first calculated according to Equation 6, where Φ_i is the weight percent of magnetic material liberated, B_i is the magnetic content in weight percent, and q_i is the weight percent passing, all of size fraction i. The amount of metal liberated at that size fraction (θ_i, weight percent) is given by Equation 7, which is the product of the weight percent magnetic material liberated and the metallic grade of that magnetic fraction (X_i). The total weight percent of magnetic material liberated (Φ) and corresponding amount of metallic material liberated (θ), are calculated by summing Equations 6 and 7 over the complete particle size range.

$$\Phi_i = B_i\left(\frac{q_i}{100}\right) \tag{6}$$

$$\Theta_i = \Phi_i\left(\frac{x_i}{100}\right) \tag{7}$$

The mass flow rate of liberated metal (S, tonne/hr) is given by Equation 8, where m is the mass flow rate of slag (tonne/hr) and β is the weight percent of magnetic material present in the slag. The mass flow rate is normalized to kg/tonne for comparison analysis.

$$S = m\left(\frac{\beta}{100}\right)\left(\frac{\Theta}{100}\right) \tag{9}$$

A plot of metal recovery (kg/tonne), normalized for each slag type, versus target grind size is shown in Figure 6. The results for the five P_{80} sizes studied are shown as individual points, which are then fit to a second-order exponential decay correlation with R^2>0.999 (terms are defined in Table A-2 in the Appendix). Both EAF and BOF slags show similar trends, in which metal recovery rapidly decreasing as P_{80} increases. The BOF slag trends at ~10-15% higher recovery than EAF slag over the entire range due to a higher amount of metal in the larger size fractions (Figure 5) and a higher quality of recovered magnetic fraction (Table 6), even though the overall amount of magnetic

material is lower (Table 5). Recovery of metal from LMF slag is less reliant on grind size (in the grind size range studied) because of the high content in the larger particle size fraction. On a normalized basis, more metal can be recovered from LMF slag than EAF slag at grind sizes >356 μm and BOF slag at grind sizes >770 μm.

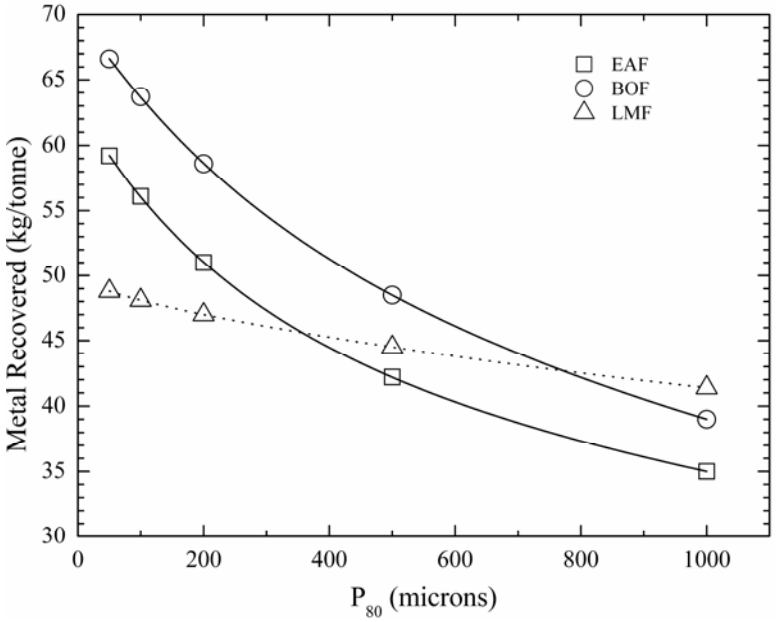

Figure 6. Amount of recovered metal liberated from steelmaking slag by target grind P_{80}

Valuation of the recovered metal is critical in determining the feasibility of slag grinding. While the metal in the particles should be similar in composition to other pit scrap, the smaller size of particles may require more handling and preparation as furnace feedstock. Recovered magnetic particles <1 mm may require briquetting to enable proper handling. In addition, the associated non-metallic materials (i.e., surface oxides and mechanically trapped slag) will take up space in the charge bucket without adding value to the melt. The recovered magnetic/metallic particles are treated as machine shop turnings, then devalued by 25% to estimate for particulate processing and reduced quality. The value used for machine shop turns is available through American Metals Market. The October 2007 monthly average, based on St. Louis, Missouri consumer purchase and converted to $/tonne, is used in the valuation model.[18]

VALUATION ANALYSIS

Valuation of the slag grinding process is determined through a cost analysis model. Input from the power consumption curve, carbon dioxide sequestration curve, and the metal recovery curve for each slag type are multiplied by their respective commodity prices given in Table 7, then summed to give the operating cost in $/hr. Dividing this result by the slag mass flow rate (*m*, tonne/hr) normalizes the values to provide the operating cost in $/tonne. Equation 9 shows the final expression applied to the P_{80} range from 50-1000 μm. All factors are shown in terms of operating cost hence the use of carbon dioxide generation (negative sequestration), and subtraction of metal recovery price. Equipment capital costs are not factored into this analysis. Peak P_{80} values for each curve were found by numerical analysis.

Table 7. Commodity Prices Used in Slag Grinding Valuation Model

	Electricity ($/kWh)	CO_2 Emissions ($/tonne)	Steel Scrap ($/tonne)
Basis	EPM[15] Industrial Sector July 2007 (12 month)	CCX[17] CFI Contract October 2007	AMM[18] St. Louis Consumer October 2007 Avg.
Cost	$0.0627	$1.90	$141.17

$$OperatingCost,\frac{\$}{hr}=\left(PowerConsumption,\frac{kW}{hr}\right)\left(ElectricCost,\frac{\$}{kWh}\right) \quad (10)$$

$$+\left(CO_2Generation,\frac{mt}{hr}\right)\left(CO_2Cost,\frac{\$}{mt}\right)-\left(Metal\,\mathrm{Recovered},\frac{mt}{hr}\right)\left(Scrap\,\mathrm{Price},\frac{\$}{mt}\right)$$

$$\left(OperatingCost,\frac{\$}{hr}\right)\left(\frac{1}{m},\frac{hr}{mt}\right)=NormalizedCost,\frac{\$}{mt}$$

The results of the cost analysis are presented in Figure 7, which shows net value normalized to $/tonne versus grind size (P_{80}). EAF and BOF slags show similar, nearly

parallel curves, with BOF slag at a ~15% higher net value than EAF slag. Both show similar peak P_{80} sizes (112 versus 122 μm), which indicates that maximum value is achieved by grinding both slags to similar sizes. The net value drops off sharply when P_{80} decreases to less than the peak value because rising power costs overtaking metal recovery. The net value also drops off at sizes larger than the peak P_{80} due to decreasing metal recovery. From peak size to largest P_{80}, the net value drops ~30%, indicating that accurate determination of metal content and distribution in each steel mill's slag is important in realizing the full potential of slag grinding for BOF and EAF slag. LMF slag has a peak at 369 μm and shows much less sensitivity to grind size. There is a sharp drop at sizes below 200 μm due to increased power consumption and negligible metal recovery, but from 200-1000 μm, the net value varied ~3%, indicating that the grind size is not that critical. For ease of handling the magnetic/metallic product, a larger grind size may be chosen for realization of nearly full net value. Grinding BOF slag below 700 μm or EAF slag below 300 μm provides more value than grinding LMF slag.

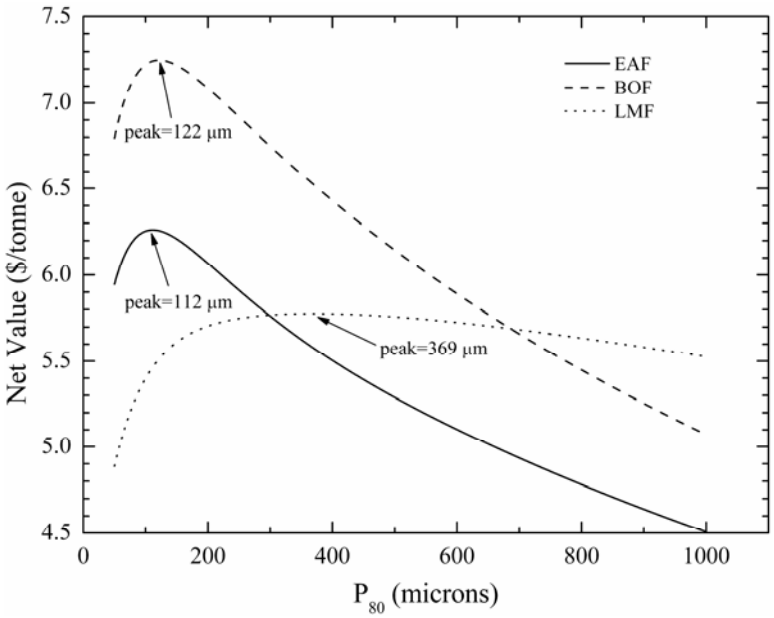

Figure 7. Net value from grinding versus P_{80} for steelmaking slags based on power consumption, carbon dioxide sequestration, and metal recovery

In terms of magnitude, the most significant factor in valuation is metal recovery, which accounts for 76-90% of the cost as P_{80} increases from 50-1000 μm. Power cost and carbon dioxide generation account for 23-9% and ~1%, respectively, over the same range. The peak P_{80} values decreases as scrap price increases or electricity cost decreases. Carbon dioxide credit/value is not a primary factor in direct economic valuation of the process as detailed. However, for environmental assessment this process does provide a net positive sequestration, which may have other benefits in addition to direct economic impact. Future emission regulations may also change the magnitude of the carbon dioxide sequestration term significantly.

CONCLUSIONS

The feasibility of processing EAF, BOF, and LMF slags for metal recovery and carbon dioxide sequestration was evaluated using a combination of grindability and sequestration tests on industrial slags, and modeling studies using METSIM. Slag comminution power consumption, associated carbon dioxide generation from the power supply source, carbon dioxide sequestration by the comminuted slag, and metal recovery from the comminuted slag were evaluated within a grind size P_{80} range of 50-1000 μm. Input data for the METSIM grinding and sequestration models came from experimental slag grindability tests, size-by-size metal recovery analysis, and aqueous carbon dioxide sequestration measurements. The results of this study yielded the following conclusions.

1. Power consumption increased with decreasing grind size for all slags, with the magnitude ranking a function of work index value. The values ranged from 6-8 kWh/tonne at 1000 μm to 35-45 kWh/tonne at 50 μm.
2. Slag-carbon dioxide capture increased with decreasing grind size for all slags and the overall amount captured was a function of calcium oxide content. After factoring in the carbon dioxide generated from the power supply source, all slags exhibited a positive net sequestration benefit, achieving a maximum of 50-90 kg carbon dioxide/tonne at ~100 μm.
3. Metal recovery increased with decreasing grind size and was a function of overall metal content and particle distribution. LMF slag showed much less sensitivity to

grind size than did EAF and BOF slags due to the higher metallic content in its larger size fraction.

4. Valuation analysis using commodity index data resulted in peak curves for all slags. EAF and BOF slags exhibited sharp maximum values at 112 μm and 122 μm, respectively, with rapid value decreases at larger or smaller sizes due to increased grinding cost or decreased metal recovery. LMF slag exhibited much less sensitivity to grind size, with ~3% variation from its peak size of 369 μm over most of the studied range.
5. In terms of fraction of the overall valuation, metal recovery is the most significant factor, with 3-10 times the magnitude of power consumption. Carbon dioxide credit/value is not a primary factor in direct economic valuation of the process as detailed.

This work is part of an overall study regarding geological sequestration by hydrous carbonate formation in steelmaking slag. Slag grinding was investigated because particle size was found to be a critical factor in accelerating the kinetic reaction rate.

ACKNOWLEDGEMENTS

This paper was prepared as an account of work sponsored by the U.S. Department of Energy, in cooperation with the American Iron and Steel Institute (AISI) and its participating companies, under Agreement DE-FC36-97ID13554. Such support does not constitute an endorsement by DOE or AISI of the views expressed in the article. The authors also acknowledge the support of ArcelorMittal Steel, Gallatin Steel, IPSCO, Nucor, and US Steel for their support in supplying slag samples and analysis.

REFERENCES

1. “Iron and Steel Slag Statistics and Information.” U.S. Department of the Interior, U.S. Geological Survey, Minerals Information, June 2005, http://minerals.usgs.gov/minerals/pubs/commodity/iron_&_steel_slag/
2. H.G. van Oss, “Slag-iron and steel.” U.S. Geological Survey Minerals Yearbook (2003): 69.1-69.3, June 2005, http://minerals.usgs.gov/minerals/pubs/commodity/iron_&_steel_slag/islagmyb03.pdf

3. C.H. Rawlins, V.L. Richards, K.D. Peaslee, and S.N. Lekakh. "Sequestration of CO_2 from Steelmaking Offgas by Carbonate Formation with Slag." In: *Proceedings of the AISTech 2006 Conference*, May 1-4, 2006; Cleveland, OH, U.S. Warrendale, PA, U.S.: Association for Iron and Steel Technology.
4. S.N. Lekakh, C.H. Rawlins, D.G.C. Robertson, V.L. Richards, and K.D. Peaslee, "Aqueous Leaching and Carbonization of Steelmaking Slag for Geological Sequestration of Carbon Dioxide," *Metallurgical and Materials Transactions B*, (on-line), Jan. 2008.
5. S.N. Lekakh, D.G.C. Robertson, C.H. Rawlins, V.L. Richards, and K.D. Peaslee, "Investigation of a Two-Stage Reactor for Carbon Dioxide Sequestration Using Steelmaking Slag," *Metallurgical and Materials Transactions B*, accepted for publication Feb. 2008.
6. C.H. Rawlins, "Grindability Study of Steelmaking Slag for Size-by-Size Recovery of Free Metal," submitted for *2008 SME Annual Meeting and Exhibit*, Feb. 2008.
7. D. Rose, "Granulated Blast Furnace Slag Grinding," *World Cement*, September 2000, pp. 49-52.
8. D. Longhurst, and M. Weihrauch, "Slag Grinding: Weighing Up the Options," *World Cement*, July 2001, pp. 123-126.
9. W. Stoiber, "Comminution Technology and Energy Consumption, Part 2," *Cement International*, Vol. 1, No. 6, 2003, pp. 90-97.
10. H. Shen, and E. Forssberg, "An overview of recovery of metals from slags," *Waste Management*, Vol. 23, 2003, pp. 933-949.
11. Society of Mining Engineers, *SME Mineral Processing Handbook*, Ed. N.L. Weiss. New York: American Institute of Mining, Metallurgical, and Petroleum Engineers, Inc., 1985, pp. 30-71.
12. F.C. Bond, "Crushing & Grinding Calculations Part I," *British Chemical Engineering*, Vol. 6, No. 6, June 1961, pp. 378-385.
13. F.C. Bond, "Crushing & Grinding Calculations Part II," *British Chemical Engineering*, Vol. 6, No. 8, August 1961, pp. 543-548.
14. C.A. Rowland, "Selection of Rod Mills, Ball Mills and Regrind Mills," *Mineral Processing Plant Design, Practice, and Control Proceedings, Volume 1*, Eds. A.L. Mular, D.N. Halbe, and D.J. Barratt. Littleton, Colorado: Society for Mining, Metallurgy, and Exploration, Inc., 2002, pp. 710-754.
15. "Electric Power Monthly October 2007, with Data for July 2007," Energy Information Administration, U.S. Department of Energy, p. 106, July 2007 http://www.eia.doe.gov/cneaf/electricity/epm/epm_sum.html.
16. "Useful Facts & Figures," Energy Star, U.S. Environmental Protection Agency & U.S. Department of Energy, July 2007 http://www.energystar.gov/index.cfm?c=energy_awareness.bus_energy_use.
17. Chicago Climate Exchange, July 2007, http://www.chicagoclimateexchange.com/
18. American Metals Market, July 2007, http://www.amm.com/

APPENDIX

Table A-1. Power and Dimension Parameters from Slag Grinding Circuit Model

P_{80} (μm)	Crusher Power Draw (kW)	Ball Mill Diameter (m)	Ball Mill Length (m)	Top Ball Size (mm)	Ball Mill Power Draw (kW)	Screen Aperture (mm)
EAF						
50	18.4	3.63	7.39	75	1977	1.5
100	18.4	3.32	6.30	65	1373	1.5
200	18.4	2.89	6.23	75	953	2.0
500	18.4	2.44	5.39	50	568	2.5
1000	18.4	2.14	4.66	50	367	3.5
BOF						
50	18.3	3.78	7.44	75	2163	1.5
100	18.3	3.32	6.70	75	1491	1.5
200	18.3	2.89	6.71	75	1026	2.0
500	18.3	2.55	5.13	65	595	2.5
1000	18.3	2.14	4.81	50	378	3.5
LMF						
50	6.9	2.24	4.63	50	423	1.0
100	6.9	1.98	4.63	50	306	1.0
200	6.9	1.83	3.88	50	215	1.0
500	6.9	1.52	3.52	50	128	1.5
1000	6.9	1.37	2.79	50	81	2.5

Table A-2. Terms from Second Order Decay Correlation

$$y = y_o + A_1 e^{-P_{80}/t_1} + A_2 e^{-P_{80}/t_2}$$

y	y_o	A_1	t_1	A_2	t_2
Power (kW/hr)					
EAF	321.8	1104	349.6	2137	45.81
BOF	333.7	1241	336.1	2385	44.65
LMF	70.13	387	51.82	243.1	380.6
Slag-CO_2 Capture (kg/tonne)					
EAF	21.90	46.21	627.0	16.38	149.7
BOF	33.73	34.78	395.6	34.78	404.9
LMF	29.68	66.36	871.8	33.19	151.5
Metal Recovered (tonne/hr)					
EAF	1.117	1.391	1256	0.643	208.5
BOF	0.561	0.908	339.8	2.029	2414
LMF	0.376	0.097	1065	0.142	3497

SECTION

3. CONCLUSIONS

This dissertation begins the investigation of carbon dioxide sequestration using steelmaking slag. It is my hope that steel producers will use this information to make informed and accurate decisions regarding more thorough utilization of their slag co-product. The following concepts are the key findings from this research project.

1. A slag-carbon dioxide reactor should be installed directly after the baghouse, with a maximum operating temperature <300°C. The gas composition at this point will average 4-5% carbon dioxide, with a maximum content <15%.

2. Carbonation reaction rate is primarily governed by particle size, which is the governing factor for surface area. Grinding can be used to decrease the particle size, and is itself carbon dioxide sequestration net positive (i.e., more CO_2 is sequestered by the slag than is released from the energy source). The cost for grinding can be recouped by recovering the liberated metal particles. The critical grind size (e.g., size at which maximum economic return is realized) for BOF and EAF slags is between 100-150 μm, while LMF has a larger critical grind size at 350-400 μm.

3. Aqueous processing proceeds much faster than dry processing. An aqueous-based system allows calcium to be leached from the slag particle, then react with carbon dioxide in solution to form calcium carbonate, while a dry system can only form calcium carbonate on the particle surface. The dense product layer forms a barrier that inhibits carbonation by decreasing diffusivity of the reacting ions. This same effect can take place in a batch aqueous system where the calcium carbonate precipitates on the slag particle surface; however, a continuous system allows separate leaching and carbonation to occur.

4. Leaching occurs faster than carbonation, and both processes are described by the shrinking core model. A minimum pH of 8.5 is critical to realize fast carbonation rates, while carbonic anhydrase enzyme will catalyze the reaction at pH>10.33. The best results achieved in this project show 47% of the theoretical amount of carbonation can be achieved at 24 hours in a reactor using 100 μm slag. This amount is equal to 0.5% and 2.4% of the carbon dioxide emitted by integrated and mini-mills, respectively.

APPENDIX A.
SLAG CHARACTERIZATION RESULTS

Table A.1. Elemental Analysis of EAF Slags as Determined by XRF (Wt.%)

Elements (as oxides)	A1α	A1β	D1α	D1β	E1α	E2α	E1γ-1	E2γ-1
Slag Type	EAF	EAF	EAF	EAF	EAF	EAF	EAF	EAF
CaO	27.34	31.22	33.02	34.49	31.91	35.86	32.08	33.59
MgO	10.55	11.61	10.98	11.76	12.85	10.13	9.41	12.31
FeO	30.05	24.96	27.93	25.76	20.20	27.98	26.36	31.59
SiO_2	14.84	13.86	12.43	15.08	17.32	9.93	19.41	8.72
Al_2O_3	7.02	8.61	8.74	5.56	6.79	9.22	8.56	11.81
MnO	6.51	6.07	3.98	4.85	7.07	4.29	6.76	3.40
TiO_2	0.39	0.42	0.50	0.55	0.49	0.49	0.45	0.43
ZrO_2	B.L.	0.03	B.L.	B.L.	0.16	0.02	-	-
Cr_2O_3	2.48	1.98	0.87	0.78	1.62	0.95	2.24	0.96
K_2O	0.05	B.L.	B.L.	B.L.	B.L.	B.L.	-	-
Na_2O	B.L.	B.L.	B.L.	B.L.	B.L.	B.L.	-	-
S	0.16	0.27	0.21	0.08	0.22	0.30	0.57	0.90
P	0.16	0.16	0.25	0.32	0.18	0.28	0.47	0.59
C	0.11	0.26	0.22	B.L.	0.32	B.L.	-	-
Sr	B.L.	B.L.	B.L.	B.L.	B.L.	B.L.	-	-
F	0.33	0.54	0.87	0.75	0.86	0.55	-	-

B.L.=Below Limit

Table A.2. Elemental Analysis of BOF/LMF Slags as Determined by XRF (Wt.%)

Elements (as oxides)	A1γ	E1β-1	E2β-1	B1α	C1α
Slag Type	LMF	LMF	LMF	BOF	BOF
CaO	47.02	51.32	49.95	40.90	40.53
MgO	10.03	4.32	4.32	11.98	13.81
FeO	5.02	5.54	6.28	21.72	21.65
SiO_2	6.07	28.28	4.53	12.89	10.42
Al_2O_3	26.55	4.91	32.32	5.22	6.65
MnO	1.04	1.31	0.85	4.67	4.50
TiO_2	0.41	0.27	0.34	0.68	0.47
ZrO_2	0.20	-	-	0.08	0.28
Cr_2O_3	0.25	-	-	0.31	0.42
K_2O	B.L.	0.01	0.01	B.L.	B.L.
Na_2O	B.L.	0.02	0.01	B.L.	B.L.
S	1.35	1.60	1.03	0.12	0.11
P	0.02	0.22	0.01	0.42	0.45
C	0.38	-	-	0.67	0.40
Sr	B.L.	-	-	B.L.	B.L.
F	1.66	-	-	0.33	0.33

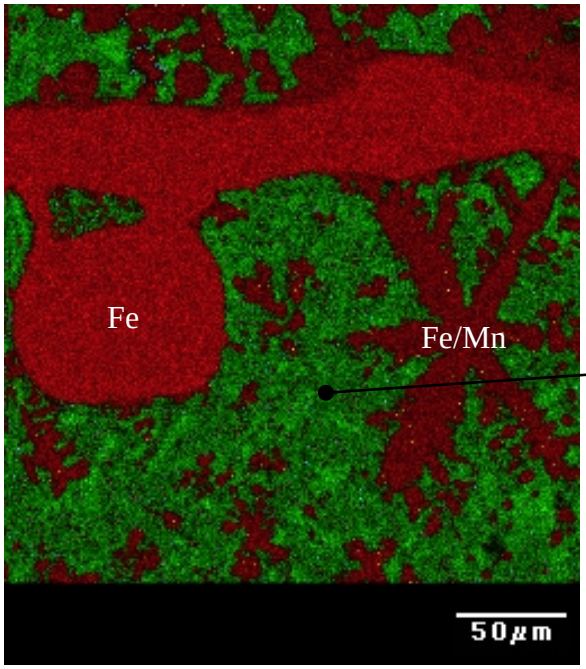

Figure A.1. EDS phase map and analysis of slag E1γ (EAF)

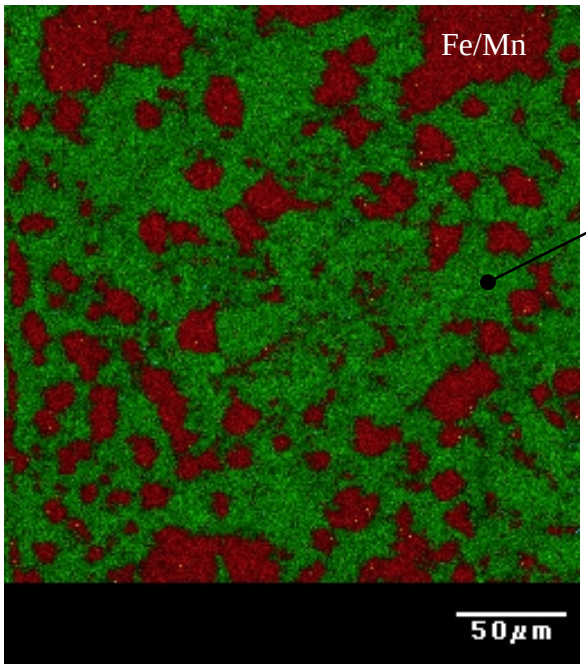

Figure A.2. EDS phase map and analysis of slag E1β (LMF)

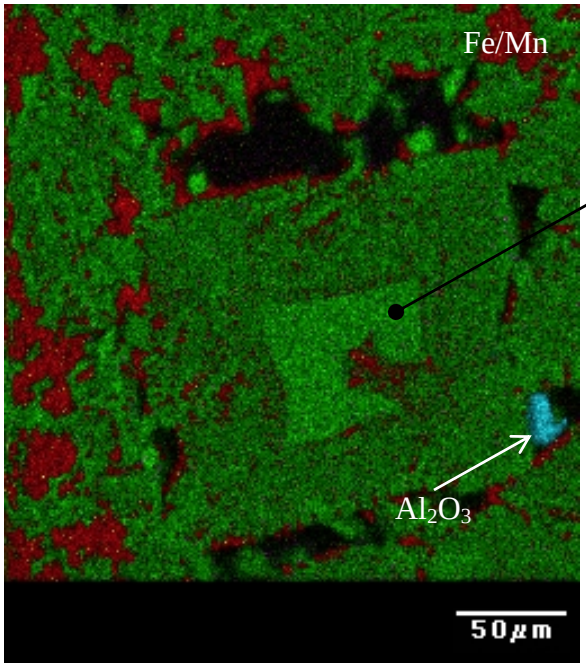

Figure A.3. EDS phase map and analysis of slag E2γ (EAF)

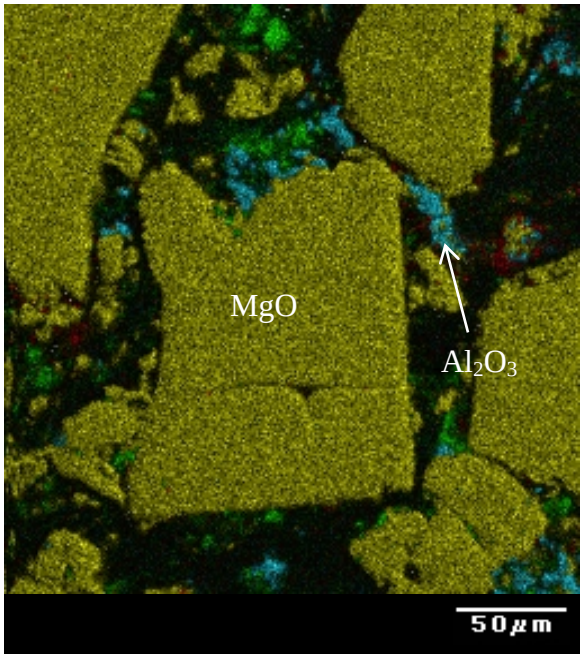

Figure A.4. EDS phase map and analysis of slag E2β (LMF)

APPENDIX B.
ANALYSIS OF THERMOGRAVIMETRIC REACTOR RESULTS

The data from Figure 2.7a can be analyzed by plotting the data on a log-log scale. Figure B.1 shows the carbonation of CaO in dry (Figure B.1a) and humidified (Figure B.1b) CO_2 from 200-500°C during a six-hour reaction time.

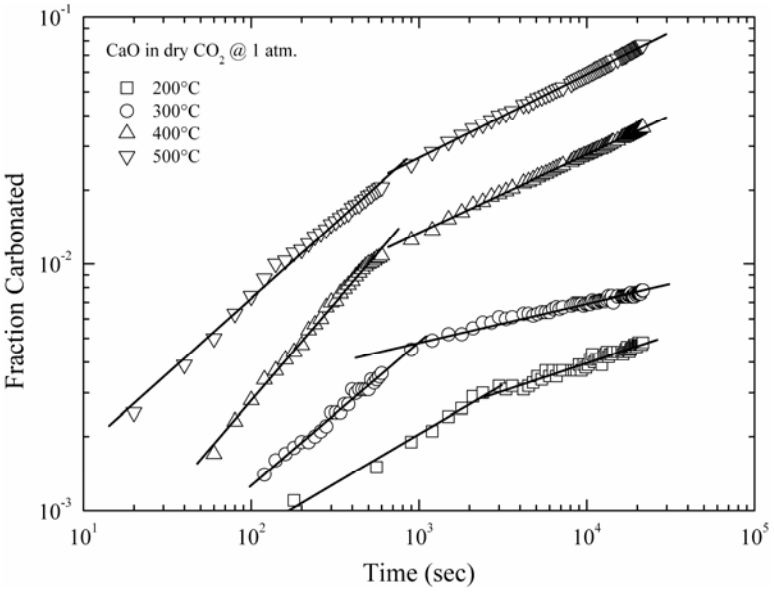

(a)

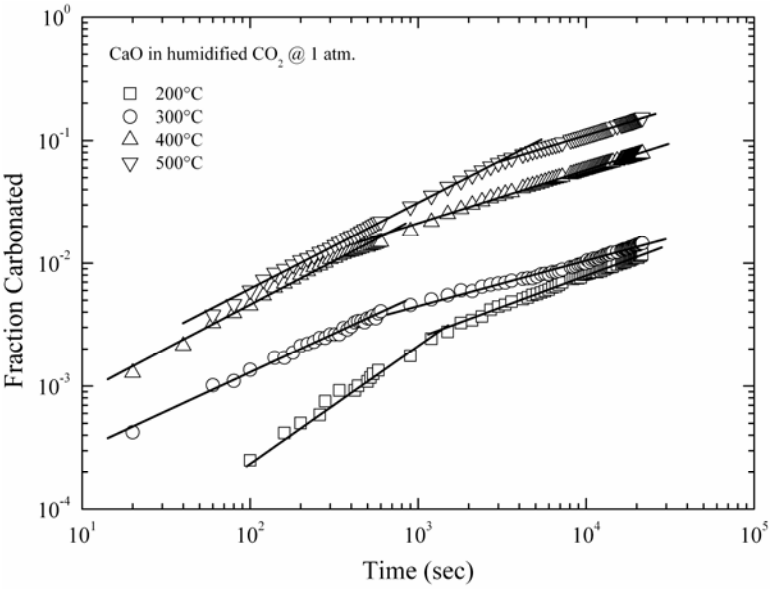

(b)

Figure B.1. Carbonation of CaO in (a) dry and (b) humidified gas streams (1 atm.)

Two distinct linear regions can be identified for each data set. An initial steep slope occurs from 100-200 seconds for the dry reaction and from 1000-2000 seconds for the humidified reaction. The slopes of each curve decrease after this time. Rapid carbonation takes place due to an initial mechanism, which is hypothesized to be the chemical reaction between CO_2 and the CaO at the surface of the test disc. After the initial CaO is consumed, diffusion of CO_2 through the $CaCO_3$ product layer must take place for the reaction to proceed. Carbonation therefore takes place at a slower rate, resulting in a decreased slope.

An Arrhenius analysis can be used to determine the activation energy of each mechanism. Figure B.2 shows a plot of 1/T (reaction temperature in Kelvin) versus ln(1/t), where t is the time in seconds to reach 0.3% carbonation for the first mechanism curve and 3.0% carbonation for the second mechanism curve. The slope of each curve yields the activation energy for each mechanism. The activation energy of the initial (chemical reaction) mechanism is 46.1 kJ/mole and 38.1 kJ/mole for the dry and humidified systems, respectively. The activation energy of the second (diffusion) mechanism is 121.5 kJ/mole and 63.9 kJ/mole for the dry and humidified systems, respectively.

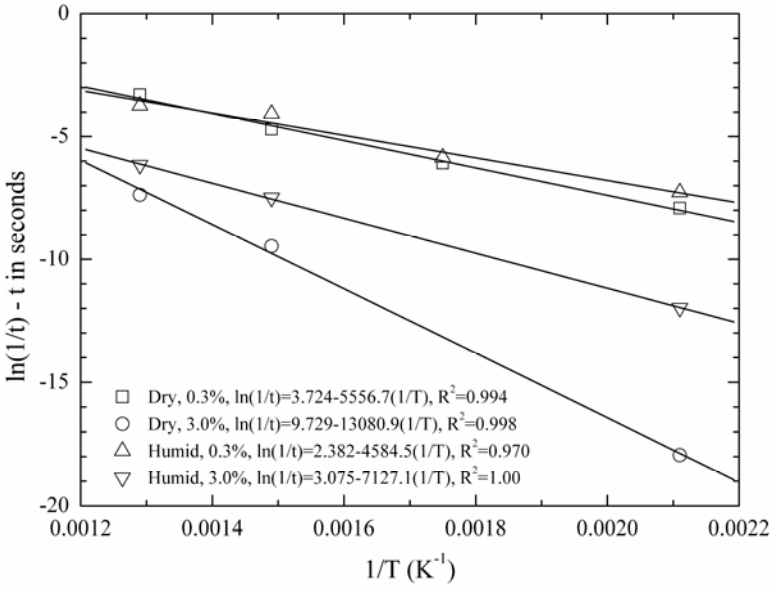

Figure B.2. Arrhenius plots determined from the CaO carbonation data

BIBLIOGRAPHY

[1] American Society for Testing and Materials. “D 5106-03 Steel Slag Aggregates for Bituminous Paving Mixtures.” *Annual Book of Standards* 04.03 (2004). West Conshohocken, PA, U.S.: American Society for Testing and Materials (ASTM).

[2] “Steel slag: A premier construction aggregate.” West Lawn, PA, U.S.: National Slag Association [brochure].

[3] van Oss, H.G. “Slag-iron and steel.” *U.S. Geological Survey Minerals Yearbook* (2003) 69.1-69.3.

[4] Ionescu, D., T.R. Meadowcroft, P.V. Barr. “Early-age hydration kinetics of steel slags.” *Advances in Cement Research* 13.1 (2001): 21-30.

[5] “Iron and Steel Slag Statistics and Information.” Reston, VA, U.S.: U.S. Department of the Interior, U.S. Geological Survey, Minerals Information.

[6] “Construction Sand and Gravel Statistics and Information.” Reston, VA, U.S.: U.S. Department of the Interior, U.S. Geological Survey, Minerals Information.

[7] “Slag Management (Our Services).” Surrey, UK: MultiServ (Division of Harsco).

[8] United States Steel. “The Making, Shaping, and Treating of Steel 10th Edition.” Ed. Lankford, W.T., N.L. Samways, R.F. Craven, H.E. McGannon. Pittsburgh, PA, U.S.: Herbick & Held, 1985. 333-338.

[9] Crawford, C.B., K.N. Burn. “Building damage from expansive steel slag backfill.” *Journal of the Soil Mechanics and Foundations Division, Proceedings of the American Society for Civil Engineers* 95.SM6 (1969): 1325-1334.

[10] Missouri (U.S.). Department of Transportation. “Section 1002: Aggregate for Asphaltic Concrete.” Jefferson City, MO, U.S.: Missouri Department of Transportation.

[11] Kandhal, P.S., G.L. Hoffman. “Evaluation of steel slag fine aggregate in hot-mix asphalt mixtures.” *Transportation Research Record* 1583 (1997): 28-36.

[12] Proctor, D. M., K.A. Fehling, E.C. Shay, J.L. Wittenborn, J.J. Green, C. Avent, R.D. Bigham, M. Connolly, B. Lee, T.O. Shepker, M.A. Zak. “Physical and chemical characteristics of blast furnace, basic oxygen basic furnace, and electric arc furnace steel industry slags.” *Environmental Science and Technology* 34.8 (2000): 1576-1582.

[13] “Runway project halted by recycled slag.” *Recycling Today Online*.

[14] Lewis D.W. “Properties and uses of iron and steel slags.” West Lawn, PA, U.S.: National Slag Association. Report MF 182-6.

[15] Emery, J. “Steel slag utilization in asphalt mixes.” West Lawn, PA, U.S.: National Slag Association. Report MF 186-1.

[16] Society of Mining Engineers. “SME Mineral Processing Handbook.” Ed. N.L. Weiss. New York: American Institute of Mining, Metallurgical, and Petroleum Engineers, Inc., 1985.

[17] Noureldin, A.S., R.S. McDaniel. “Performance evaluation of steel furnace slag-natural sand asphalt surface mixtures.” *Asphalt Paving Technology* 59 (1990): 276-303.

[18] Geiseler, J. “Steel slag – generation, processing, and utilization.” In: *Proceedings of the International Symposium on Resource Conservation and Environmental Technologies in Metallurgical Industries; 20-25 August 1994; Toronto, Ontario, Canada.* Editors: P. Mahant, C. Pickles, W-K. Lu. Montreal, Quebec, Canada: Canadian Institute of Mining, Metallurgy, and Petroleum; 1994. 87-95.

[19] “Steel slag unit weight standards.” Aliquippa, PA, U.S.: Beaver Valley Slag.

[20] Tsuchiya, K., T. Nagashima, T. Kawamoto, Y. Yamada. “Expansion characteristics of slags on water immersion test (Stabilization of LD converter slags by field aging-I)” *Transactions of the Iron and Steel Institute of Japan* 20.9 (1980): B-367.

[21] Tsuchiya, K., T. Nagashima, M. Fujishima, T. Kawamoto, T. Hinonishi, Y. Yamada. “Reduction of lumps of lime in slags (Stabilization of LD converter slags by field aging-II)” *Transactions of the Iron and Steel Institute of Japan* 20.9 (1980): B-368.

[22] American Society for Testing and Materials. “D 4792-00 Standard Test Method for Potential Expansion of Aggregates from Hydration Reactions.” *Annual Book of Standards* 04.03 (2004). West Conshohocken, PA, U.S.: American Society for Testing and Materials (ASTM).

[23] “Steel slag: A material of unusual ability, durability, and tenacity.” West Lawn, PA, U.S.: National Slag Association. Report MF 194-3.

[24] “Steel slag chemistry.” Aliquippa, PA, U.S.: Beaver Valley Slag.

[25] Sorentino, F., M. Giminez. “Mineralogy of modified steel slags.” In: *Proceedings of the 11th International Congress on the Chemistry of Cement (ICCC); 11-16 May 2003; Durban, South Africa.* Editors: G. Grieve and G. Owens. Midrand, Gauteng, South Africa: The Cement and Concrete Institute of South Africa. 2139-2147.

[26] "Mineralogy Applied to Steel Slag." Ijmuiden, The Netherlands: Corus RD&T Ceramic Research Centre.

[27] Monaco, A., W-K. Wu. "The effect of cooling conditions on the mineralogical characterization of steel slag." In: *Proceedings of the International Symposium on Resource Conservation and Environmental Technologies in Metallurgical Industries; 20-25 August 1994; Toronto, Ontario, Canada.* Editors: P. Mahant, C. Pickles, W-K. Lu. Montreal, Quebec, Canada: Canadian Institute of Mining, Metallurgy, and Petroleum; 1994. 107-116.

[28] Suito, H., Y. Hayashia, Y. Takahashi. "Mineralogical study of LD converter slags." *Tetsu to Hagne* 63.8 (1977): 1252-1259. (Japanese)

[29] Bradaskja, B., J. Triplat, M. Dobnikar, B. Mirtic. "Mineralogical characterization of steel-making slags." *Materiali in Tehnologije* 38.3-4 (2004): 205-208. (Slovenian)

[30] Luxán, M.P., R. Sotolongo, F. Dorrego, E. Herrero. "Characteristics of the slags produced in the fusion of scrap steel by electric arc furnace." *Cement and Concrete Research* 30 (2000): 517-519.

[31] FactSage. Version 5.5. Centre for Research in Computational Thermochemistry, École Polytechnique, Montreal, Quebec, Canada. 2004.

[32] Tennis, P.D., H.M. Jennings. "A model for two types of calcium silicate hydrate in the microstructure of Portland cement pastes." *Cement and Concrete Research* 30 (2000): 855-863.

[33] Robie, R.A., B.S. Hemingway, J.R. Fisher, Eds. *Thermodynamic properties of minerals and related substances at 298.15 K and 1 Bar (10^5 Pascals) pressure and higher temperatures*. United States Department of the Interior; U.S. Geological Survey; Bulletin 1452. 1984.

[34] Lea, F.M. *The Chemistry of Cement and Concrete, 3rd Ed*. New York: Chemical Publishing Company, 1971.

[35] Bentz, D.P. "A three dimensional cement hydration and microstructure program. I. Hydration rate, heat of hydration, and chemical shrinkage." Gaithersburg, MD, U.S.: U.S. Department of Commerce; National Institute of Standards and Technology. Report NISTIR 5756. 1995.

[36] Fujii, K., W. Kondo. "Estimation of thermochemical data for calcium silicate hydrate (C-S-H)." *Journal of the American Ceramic Society* 66 (1983): C220-221.

[37] Barin, I., F. Sauert, E. Schultze-Rhonhof, W.S. Sheng. *Thermochemical data of pure substances*. New York: VCH Publishers, 1989.

[38] Mu, J., D.D. Perlmutter. “Thermal decomposition of carbonates, carboxylates, oxalates, acetates, formates, and hydroxides.” *Thermochimica Acta* 49.2-3 (1981): 207-18.

[39] Lackner, K.S., C.H. Wendt, D.P. Butt, E.L. Joyce, D.H. Sharp. “Carbon dioxide disposal in carbonate minerals.” *Energy* 20.11 (1995): 1153-70.

[40] Butt, D.P., K.S. Lackner, C.H. Wendt, R. Vaidya, D.L. Pile, Y. Park, T. Holesinger, D.M. Harradine, K. Nomura. “The kinetics of binding carbon dioxide in magnesium carbonate.” In: *Proceedings of the 23rd International Technical Conference on Coal Utilization & Fuel Systems; 9-13 March 1998; Clearwater, FL, United States.* Editor, B.A. Sakkestad. Gaithersburg, MD: Coal Technology Association; 1998. 583-591.

[41] Chen, J.J., J.J. Thomas, H.F.W. Taylor, H.M. Jennings. “Solubility and structure of calcium silicate hydrate.” *Cement and Concrete Research* 34 (2004): 1499-1519.

[42] Taggart, A.F. “Handbook of Mineral Dressing, Ores and Industrial Minerals.” New York: John Wiley & Sons, Inc., 1945.

[43] Kelleher, I.J., S.A.T. Redfern. “Hydrous calcium magnesium carbonate, a possible precursor to the formation of sedimentary dolomite.” *Molecular Simulation* 28.6-7 (2002): 557-572.

[44] Goto, S., K. Suenaga, T. Kado, M. Fukuhara. “Calcium silicate carbonation products.” *Journal of the American Ceramic Society* 78.11 (1995): 2867-72.

[45] Zevenhoven, R., J. Kohlmann, A.B. Mukherjee. “Direct dry mineral carbonation for CO_2 emissions reduction in Finland.” In: *Proceedings of the 27th International Technical Conference on Coal Utilization & Fuel Systems; 4-7 March 2002; Clearwater, FL, United States.* Editor, B.A. Sakkestad. Gaithersburg, MD: Coal Technology Association; 2002. 743-754.

[46] Fitzgerald, F. “Global warming: a cool view.” *Ironmaking and Steelmaking* 31.3 (2004): 191-191-198.

[47] Lackner, K.S. “Carbonate chemistry for sequestering fossil carbon.” *Annual Review of Energy and the Environment* 27 (2002): 193-232.

[48] Broecker, W.S., T. Takahashi. “Neutralization of fossil fuel carbon dioxide by marine calcium carbonate.” *Marine Science* 6 (1977): 213-41.

[49] “Carbon dioxide storage rocks!” Environmental Technology Directorate at PNNL.

[50] Lackner, K.S., D.P. Butt, C.H. Wendt. “Magnesite disposal of carbon dioxide.” In: *Proceedings of the 22nd International Technical Conference on Coal Utilization & Fuel Systems; 16-19 March 1997; Clearwater, FL, United States.* Editor, B.A. Sakkestad. Gaithersburg, MD: Coal Technology Association; 1997. 419-430.

[51] Butt, D.P., K.S. Lackner, C.H. Wendt, S.D. Conzone, H. Kung, Y.-C. Lu, J.K. Bremser. “Kinetics of thermal dehydroxylation and carbonation of magnesium hydroxide.” *Journal of the American Ceramic Society* 79.7 (1996): 1892-1898.

[52] Park, A.-H, R.A. Jadhav, L.-S. Fan. “CO_2 mineral sequestration through carbonation of Mg-bearing minerals.” In: *Proceedings of the Annual Meeting of AIChE, Session 257-Risk Assessment and Management; 4-9 November 2001; Reno, NV, United States.* New York, NY: American Institute of Chemical Engineers; 2001. Paper 257a.

[53] Kuchta, M.E. “Mineral carbonation: activation of serpentine minerals for enhanced CO_2 sequestration.” [M.S. thesis]. The Pennsylvania State University, USA. 2003.

[54] Maroto-Valer, M.M., M.E. Kuchta, Y. Zhang, J.M. Andrésen. “Integrated carbonation: a novel concept to develop a CO_2 sequestration module for power plants.” In: *Proceedings of the 6th International Conference on Greenhouse Gas Control Technologies; 1-4 October 2002; Kyoto, Japan.* Editors, John Gale and Yoichi Kaya. Oxford, UK: Elsevier Ltd.; 2003. 1729-1734.

[55] McKelvy, M.J., A.V.G. Chizmeshya, H. Bearat, R. Sharma, R.W. Carpenter. “Developing an atomic-level understanding to enhance CO_2 mineral sequestration reaction processes via materials and reaction engineering.” In: *Proceedings of the 17th Annual International Pittsburgh Coal Conference; 11-15 September 2000; Pittsburgh, PA, United States.* Pittsburgh, PA: University of Pittsburgh School of Engineering; 2000. 1161-1173.

[56] Abanades, J.C., E.J. Anthony, J. Wang, J.E. Oakey. “Fluidized Bed Combustion Systems Integrating CO_2 Capture with CaO.” *Environmental Science and Technology* 39.8 (2005): 2861-2866.

[57] Abanades, J.C., E.J. Anthony, D.Y. Lu, C. Salvador, D. Alvarez. “Capture of CO_2 from combustion gases in a fluidized bed of CaO.” *AIChE Journal* 50.7 (2004): 1614-1622.

[58] Abanades, J.C., D. Alvarez. “Conversion Limits in the Reaction of CO_2 with Lime.” *Energy & Fuels* 17.2 (2003): 308-315.

[59] Abanades, J.C. “The maximum capture efficiency of CO_2 using a carbonation/calcination cycle of $CaO/CaCO_3$.” *Chemical Engineering Journal* 90.3 (2002): 303-306.

[60] Abanades, J.C., J.E. Oakey, D. Alvarez, J. Hämäläinen. “Novel combustion cycles incorporating capture of CO_2 with CaO.” In: *Proceedings of the 6th International Conference on Greenhouse Gas Control Technologies; 1-4 October 2002; Kyoto, Japan.* Editors, John Gale and Yoichi Kaya. Oxford, UK: Elsevier Ltd.; 2003. 181-186.

[61] Alvarez, D., J.C. Abanades. “Pore-size and shape effects on the recarbonation performance of calcium oxide submitted to repeated calcination/recarbonation cycles.” *Energy & Fuels* 19.1 (2005): 270-278.

[62] Salvador, C., D. Lu, E.J. Anthony, J.C. Abanades. Enhancement of CaO for CO_2 capture in an FBC environment.” *Chemical Engineering Journal* 96.1-3 (2003): 187-195.

[63] Baker, E.H. “The calcium oxide-carbon dioxide system in the pressure range 1-300 atmospheres.” *Journal of the Chemical Society* (1962): 464-470.

[64] Fernandez, A. I.; J.M. Chimenos, M. Segarra, M.A. Fernández, F. Espiell. “Kinetic study of carbonation of MgO slurries.” *Hydrometallurgy* 53.2 (1999): 155-167.

[65] Berger, R. L., W.A. Klemm. “Accelerated curing of cementitious systems by carbon dioxide. II. Hydraulic calcium silicates and aluminates.” *Cement and Concrete Research* 2.6 (1972): 647-52.

[66] Berger, R. L., J.F. Young, K. Leung. “Acceleration of hydration of calcium silicates by carbon dioxide treatment.” *Nature Physical Science* 240.97 (1972): 16-18.

[67] Young, J. F., R.L. Berger, J. Breese. “Accelerated curing of compacted calcium silicate mortars on exposure to CO_2.” *Journal of the American Ceramic Society* 57.9 (1974): 394-7.

[68] Bukowski, J. M., R.L. Berger. “Reactivity and strength development of carbon dioxide activated non-hydraulic calcium silicates.” *Cement and Concrete Research* 9.1 (1979): 57-68.

[69] Goodbrake, C. J., J.F. Young, R.L. Berger. “Reaction of beta-dicalcium silicate and tricalcium silicate with carbon dioxide and water vapor.” *Journal of the American Ceramic Society* 62.3-4 (1979): 168-71.

[70] Goodbrake, C. J., J.F. Young, R.L. Berger. “Kinetics of the reaction of β-C_2S and C_3S with CO_2 and water vapor. Reply.” *Journal of the American Ceramic Society* 63.1-2 (1980): 114-115.

[71] Golomb, D.S. “Carbon dioxide/limestone/water emulsion for ocean and geologic sequestration of CO_2.” In: *Proceedings of the 6th International Conference on Greenhouse Gas Control Technologies; 1-4 October 2002; Kyoto, Japan.* Editors, John Gale and Yoichi Kaya. Oxford, UK: Elsevier Ltd.; 2003. 683-688.

[72] “Combining mineral and geological sequestration using TecEco Tec and Eco-Cements and TecEco Tec-Kiln technology.” Glenorchy, Tasmania, Australia: TecEco Pty. Ltd.

[73] Bond, G.M., J. Stringer, D.K. Brandvold, F.A. Simsek, M.-G. Medina, G. Egeland. “Development of integrated system for biomimetic CO_2 sequestration using the enzyme carbonic anhydrase.” *American Chemical Society, Division of Fuel Chemistry* 45.4 (2000): 713-717.

[74] Medina, M.-G., G.M. Bond, S. Rogelj. “Comparison of carbonic anhydrase isozymes for use as a catalyst in carbon sequestration process.” In: *Proceedings of the Air & Waste Management Association’s 93rd Annual Meeting & Exhibition; 18-22 June 2000; Salt Lake City, UT, U.S.* Pittsburgh, PA., U.S.: Air & Waste Management Association; 2000. 5996-6013.

[75] Simsek-Ege, F.A., G.M. Bond, J. Stringer. “A biomimetic route to environmentally friendly CO_2 sequestration: catalyst immobilization.” *Electrochemical Society Proceedings* 2000-20 (2001): 162-170.

[76] Bond, G.M., M.-G. Medina, J. Stringer, F.A. Simsek-Ege. “CO_2 capture from coal-fired utility generation plant exhausts, and sequestration by a biomimetic route based on enzymatic catalysis-current status.” In: *Proceedings of the 1st National Conference on Carbon Sequestration; 14-17 May 2001; Washington, DC, USA.* Washington, DC, USA, U.S. Department of Energy, National Energy Technology Laboratory.

[77] Huijgen, W.J.J., R.N.J. Comans. “Carbon dioxide sequestration by mineral carbonation: literature review.” Petten, The Netherlands: Energy Research Centre of the Netherlands (ECN); February 2003. ECN-C—03-016.

[78] Comans, R.N.J., W.J.J. Huijgen. “Carbonation of alkaline waste materials and its application to mineral CO_2-sequestration.” In: *Proceedings of the 32nd International Geological Congress, Session G15.05; Florence, Italy; 23 August 2004.* Petten, The Netherlands: Energy Research Centre of the Netherlands (ECN); March 2005. ECN-RX—05-0088..

[79] Huijgen, W.J.J., R.N.J. Comans, G.J. Witkamp. “CO_2 sequestration by mineral carbonation.” *Poster presented at the 4th Netherlands Process Technology Symposium (NPS4); 26-27 October 2004; Veldhoven, The Netherlands.* The Netherlands: Energy Research Centre of the Netherlands (ECN); March 2005. ECN-RX—05-089.

[80] Huijgen, W., G.J. Witkamp, R. Comans. "Mineral CO_2 sequestration in alkaline solid residues." Petten, The Netherlands: Energy Research Centre of the Netherlands (ECN); December 2004. ECN-RX—04-079.

[81] Huijgen, W.J.J., G.-J Witkamp, R.N.J. Comans. "Mineral CO_2 sequestration by steel slag carbonation." *Environmental Science and Technology* 39.24 (2005): 9676-9682.

[82] Eloneva, S., S. Teir, C.-J. Fogleholm, R. Zevenhoven. "Carbonation of slags from iron-and steel industry." In: *Proceedings of the 4th Nordic Minisymposium on Carbon Dioxide Capture and Storage; 8-9 September 2005; Espoo, Finland*. Otaniemi, Espoo, Finland: Laboratory of Energy, Engineering and Environmental Protection; Helsinki University of Technology. 1-14.

[83] Stolaroff, J.K., G.V. Lowry, D.W. Keith. "CO_2 extraction from ambient air using alkali-metal hydroxide solutions derived from concrete waste and steel slag." In: *EOS Trans. AGU, 84(46), Fall Meeting; 8-12 December 2003; San Francisco, CA, United States*. Washington, DC: American Geophysical Union. Abstract GC32A-0207.

[84] Lowry, G.V., J. Stolaroff, D. Keith. "CO_2 extraction from ambient air using alkali-metal hydroxide solutions: niche markets to industrial scale implementation." *Preprints of Papers - American Chemical Society, Division of Fuel Chemistry* 49.1 (2004): 362-363.

[85] Stolaroff, J.K., G.V. Lowry, D.W. Keith. "Using CaO- and MgO-rich industrial waste streams for carbon sequestration." *Energy Conversion and Management* 46.5 (2005): 687-699.

[86] Lowry, G.V. "Carbon management: geochemical CO_2 sequestration using industrial wastes." Pittsburgh, PA, U.S.: Carnegie Mellon Civil and Environmental Engineering web page.

[87] Johnson, D. C., C.L. MacLeod, P.J. Carey, C.D. Hills. "Solidification of stainless steel slag by accelerated carbonation." *Environmental Technology* 24.6 (2003): 671-678.

[88] Sweeney, R. E. H., C.D. Hills, N.R. Buenfeld. "Investigation into the carbonation of stabilized/solidified synthetic waste." *Environmental Technology* 19.9 (1998): 893-902.

[89] Johnson, D.C. "Accelerated carbonation of waste calcium silicate materials." *SCI Lecture Papers Series* 108 (2000): 1-10.

[90] Johnson, D. C., C.L. MacLeod, C.D. Hills. "Acid neutralisation capacity of accelerated carbonated stainless steel slag." *Environmental Technology* 24.5 (2003): 545-551.

[91] Fernández Bertos, M., S.J.R. Simons, C.D. Hills, P.J. Carey. "A review of accelerated carbonation technology in the treatment of cement-based materials and sequestration of CO_2." *Journal of Hazardous Materials* 112.3 (2004): 193-205.

[92] Isoo, T., T. Takahashi, M. Fukuhara. "Using carbonated steelmaking slag blocks to help reduce CO_2." *American Ceramic Society Bulletin* 80.1 (2001): 73-75.

[93] Isoo, T., T. Takahasi, N. Okamoto, M. Fukuhara. "Development of large steelmaking slag blocks using a new carbonation process." *Advances in Cement Research* 12.3 (2000): 97-101.

[94] Takahashi, T., M. Fukuhara. "Production of steelmaking slag blocks by carbon dioxide and their durability in the sea." *Key Engineering Materials* 206-213(7^{th} Conference of the European Ceramic Society) (2002): 879-882.

[95] Rawlins, C.H., Richards, V.L., Peaslee, K.D., and Lekakh, S.N., "Sequestration of CO_2 from Steelmaking Offgas by Carbonate Formation with Slag," *AISTech 2006 Proceedings*, Vol. II, May 2006, pp. 1133-1144.

[96] Rawlins, C.H., Richards, V.L., Peaslee, K.D., and Lekakh, S.N., "Steelmaking Slag as a Permanent Sequestration Sink for Carbon Dioxide," *Steel Times International*, Vol. 30, No. 7, October 2006, pp. 25-28.

[97] Lekakh, S.N., Rawlins, C.H., Robertson, D.R., Richards, V.L., and Peaslee, K.D., "Aqueous Leaching and Carbonization of Steelmaking Slag for Geological Sequestration of Carbon Dioxide," *Metallurgical and Materials Transactions B*, (on-line) January 2008.

[98] Lekakh, S.N., Robertson, D.G.C., Rawlins, C.H., Richards, V.L., and Peaslee, K.D., "Investigation of a Two-Stage Reactor Carbon Dioxide Sequestration Using Steelmaking Slag," *Metallurgical and Materials Transactions B*, accepted for publication February 2008.

[99] Bond, G.M., J. Stringer, D.K. Brandvold, F.A. Simsek, M.-G. Medina, G. Egeland. "Development of integrated system for biomimetic CO_2 sequestration using the enzyme carbonic anhydrase." American Chemical Society, Division of Fuel Chemistry 45.4 (2000): 713-717.

[100] Rawlins, C.H., "Grindability Study of Steelmaking Slag for Size-by-Size Recovery of Free Metal," *SME Annual Meeting and Exhibit*, Feb. 2008.

[101] Rawlins, C.H., Peaslee, K.D., and Richards, V.L., "Feasibility of Processing Steelmaking Slag for CO_2 Sequestration and Metal Recovery," *AIST Transactions*, accepted for publication February 2008.

VITA

Charles Henry Rawlins was born November 5, 1968 in Town & Country, Missouri. He attended the University of Missouri-Rolla from 1986 to 1992 and received a B.S. in Metallurgical Engineering (May 1991) and M.S. in Metallurgical Engineering (December 1992). During his undergraduate education, he worked at various metallurgical intern positions, including T.S.D. Incorporated, GM Central Foundry, U.S.S. Research Center, and Johannesburg Consolidated Investments in South Africa.

Upon graduation, he began full-time work with Krebs Engineers in Menlo Park, CA conducting hydrocyclone research. During that time, he married his college sweetheart (Kristi Heinemann, B.S. Metallurgical Engineering 1994). In 1995, he was transferred to Krebs Petroleum Technologies to help start the oil and gas division in Houston, TX. Serving in product and project development, he helped grow the company until its sale to Baker Hughes in May 1998. He then transferred to Kvaerner Process Systems in Houston, TX to serve as the technology manager. During the next three and a half years with Kvaerner, Hank spent 18 months with a Kvaerner/Dresser-Rand joint venture in Wellsville, NY to develop multiphase turbines. While on that assignment, he received a professional engineer license in metallurgical engineering. In September 2002, he left the oil and gas industry to work for FuelCell Energy, Inc. in Danbury, CT as their international project manager.

In June 2005, after thirteen years of corporate work he decided to pursue his heart's goal and returned to full-time graduate school at the University of Missouri-Rolla. He was a GAANN Fellow in the Materials Science and Engineering department and studied slag-based carbon dioxide sequestration. He received his Ph.D. in Metallurgical Engineering from the Missouri University of Science and Technology in May 2008 under Dr. Kent D. Peaslee.